State, Parameter, and Unknown Input Estimation Problems in Active Automotive Safety Applications

A DISSERTATION
SUBMITTED TO THE FACULTY OF THE GRADUATE SCHOOL
OF THE UNIVERSITY OF MINNESOTA
BY

Gridsada Phanomchoeng

IN PARTIAL FULFILLMENT OF THE REQUIREMENTS
FOR THE DEGREE OF
DOCTOR OF PHILOSOPHY

Professor Rajesh Rajamani

September 2011

Acknowledgements

Firstly, the author would like to thank Professor Rajesh Rajamani, the author's advisor, for many helpful comments and suggestions and his review which have contributed to the clearness of this research. This research could not have been completed without his enthusiasm, knowledge, motivation, patience, and support. The author feels lucky and honored to work for such a wonderful advisor.

Besides the author's advisor, the author would like to thank the members of the thesis committee, Professor Demoz Gebre-Egziabher, Professor Zongxuan Sun, Professor Tryphon Georgiou, and Professor Yiyuan Zhao for their time, encouragement, and insightful comments.

The author also thanks Lee Alexander for his assistance. Without his design and manufacturing skills, it would have been very difficult to setup the scaled vehicle experiments. The author also learned about wireless and controller hardware from him.

The author thanks his labmates who have helped him at various times on his work: Dr. Shyam Sivaramakrishnan, Dr. Krishna Vijayaraghavan, Peng Peng, Sean Pruden, Dr. Hwa Soo Kim, Dr. Gurkan Erdogan, Matthew Hildebrand, Kalpesh Singal, Shan Hu, Saber Taghvaeeyan, and Garrett Nelson.

Also, the author thanks his friends at the University of Minnesota: Dr. Chayut Piromsombat for reminding him about graduate school requirements and procedures, and Dr. Pongstorn Maidee for giving him much good advice on programming.

Lastly, the author would like to thank his family: his parents, Chaiyot Phanomchoeng and Krongtong Phanomchoeng, for supporting his life, his sister and brother in law, Gridtiya Phanomchoeng and Nattapol Pornsalnuwat, for helping him with everything during his life in the United States.

Abstract

A variety of driver assistance systems such as traction control, electronic stability control (ESC), rollover prevention and lane departure avoidance systems are being developed by automotive manufacturers to reduce driver burden, partially automate normal driving operations, and reduce accidents.

The effectiveness of these driver assistance systems can be significant enhanced if the real-time values of several vehicle parameters and state variables, namely tire-road friction coefficient, slip angle, roll angle, and rollover index, can be known. Since there are no inexpensive sensors available to measure these variables, it is necessary to estimate them. However, due to the significant nonlinear dynamics in a vehicle, due to unknown and changing plant parameters, and due to the presence of unknown input disturbances, the design of estimation algorithms for this application is challenging.

This dissertation develops a new approach to observer design for nonlinear systems in which the nonlinearity has a globally (or locally) bounded Jacobian. The developed approach utilizes a modified version of the mean value theorem to express the nonlinearity in the estimation error dynamics as a convex combination of known matrices with time varying coefficients. The observer gains are then obtained by solving linear matrix inequalities (LMIs). A number of illustrative examples are presented to show that the developed approach is less conservative and more useful than the standard Lipschitz assumption based nonlinear observer. The developed nonlinear observer is utilized for estimation of slip angle, longitudinal vehicle velocity, and vehicle roll angle.

In order to predict and prevent vehicle rollovers in tripped situations, it is necessary to estimate the vertical tire forces in the presence of unknown road disturbance inputs. An approach to estimate unknown disturbance inputs in nonlinear systems using dynamic model inversion and a modified version of the mean value theorem is presented. The developed theory is used to estimate vertical tire forces and predict tripped rollovers in situations involving road bumps, potholes, and lateral unknown force inputs.

To estimate the tire-road friction coefficients at each individual tire of the vehicle, algorithms to estimate longitudinal forces and slip ratios at each tire are proposed. Subsequently, tire-road friction coefficients are obtained using recursive least squares parameter estimators that exploit the relationship between longitudinal force and slip ratio at each tire.

The developed approaches are evaluated through simulations with industry standard software, CARSIM, with experimental tests on a Volvo XC90 sport utility vehicle and with experimental tests on a $1/8^{th}$ scaled vehicle. The simulation and experimental results show that the developed approaches can reliably estimate the vehicle parameters and state variables needed for effective ESC and rollover prevention applications.

Table of Contents

Contents

List of Tables

List of Figures

Citations of Published Work

Some portions of this thesis have appeared in the following publications:

1) G. Phanomchoeng, R. Rajamani, and D. Piyabongkarn, "Nonlinear Observer for Bounded Jacobian Systems, with Applications to Automotive Slip Angle Estimation", *IEEE Transactions on Automatic Control*, vol. 56, no. 5, pp. 1163-1170, May 2011.
2) G. Phanomchoeng, R. Rajamani, and J. Hourdos, "Directional Sound for Long Distance Auditory Warnings From a HighwayConstruction Work Zone", *IEEE Transactions on Vehicular Technology*, Volume: 59, Issue: 5, pp. 2266-2276, 2010.
3) R. Rajamani, D. Piyabongkarn, J.Y. Lew, K. Yi and G. Phanomchoeng, "Tire Road Friction Coefficient Estimation - Real-Time Estimation Methods for Active Automotive Safety Applications", *IEEE Control Systems Magazine*, vol. 30, no. 4, pp. 54-69, August 2010.
4) G. Phanomchoeng, S. Sivaramakrishnan, R. Rajamani, and A. Gopinath, "Development of a wireless angle sensor based on the directional radiation pattern of antennas", *Measurement Science and Technology*, Volume 20, Issue 6, pp. 065202, 2009.
5) R. Rajamani, G. Phanomchoeng, D. Piyabongkarn, and J.Y. Lew, "Algorithms for Real-Time Estimation of Individual Wheel Tire-Road Friction Coefficients", *IEEE/ASME Transactions on Mechatronics*, Volume: pp, Issue: 99, pp. 1-13, 2011.
6) G. Phanomchoeng, R. Rajamani and L. Alexander, "New Rollover Index for Detection of Tripped and Un-Tripped Rollovers", submitted to *IEEE Transactions on Industrial Electronics*.
7) G. Phanomchoeng, and R. Rajamani, "Real-Time Estimation of Automotive Roll Angle with Nonlinear Observer", submitted to *International Journal of Control*.
8) G. Phanomchoeng, R. Rajamani, "Real-Time Estimation of Rollover Index with a Novel Unknown Inputs Nonlinear Observer", submitted to *IEEE Transactions on Automatic Control*.
9) G. Phanomchoeng, and R. Rajamani, "New Rollover Index for Detection of Tripped and Un-Tripped Rollovers", Proceedings of *the 50th IEEE Conference on Decision and Control and European Control Conference*, Orlando, FL, December 2011.

10) G. Phanomchoeng, R. Rajamani, and D. Piyabongkarn, “Real-Time Estimation of Automotive Slip Angle with Nonlinear Observer”, Proceedings of *2011 American Control Conference*, San Francisco, CA, 2011.

11) G. Phanomchoeng, R. Rajamani, “The Bounded Jacobian Approach to Nonlinear Observer Design”, Proceedings of *2010 American Control Conference*, Baltimore, Maryland, USA, 2010.

12) G. Phanomchoeng, R. Rajamani, “Observer Design for Lipschitz Nonlinear Systems Using Riccati Equations”, Proceedings of *2010 American Control Conference*, Baltimore, Maryland, USA, 2010.

Chapter 1

1. INTRODUCTION

The number of automobiles is increasing worldwide. The Bureau of Transportation Statistics of the U.S. Department of Transportation showed that in the United State there were 215 million vehicles registered in 1998 and there were 260 million vehicles in 2008. During the decade, the number of vehicles increased by almost 20%. Also, it was estimated that over 600 million vehicles were used in the world in 2005. In 2007, there were about 806 million vehicles in the world. The number of vehicles is increasing rapidly.

The increasing worldwide use of automobiles has brought an increase in total numbers of accidents. Based on 2005 Fatality Analysis Reporting Systems (FARS) and 2000-2005 National Automotive Sampling System (NASS) Crashworthiness Data System (CDS), there were 34,680 fatalities reported and over 2.4 million serious non-fatal crashes in the United States [**1**]. Moreover, World Health Organization (WHO) recorded that an estimated 1.2 million people were killed in road crashes and as many as 50 million were injured around the world in 2004 [**2**]. These fatalities and injuries were associated with single-vehicle crashes, multi-vehicle crashes, and rollovers. Also, the information indicates that, while a variety of factors contribute to accidents, over 90% of all accidents are related to human error.

The high number of accidents and their root cause in human error has motivated the need to develop active safety control systems. A variety of driver assistance systems such as electronic stability control (ESC), rollover prevention, lane departure avoidance systems, collision avoidance systems, and adaptive cruise control (ACC) are being developed to reduce driver burden, partially automate normal driving operations, and reduce accidents.

The National Highway Traffic Safety Administration (NHTSA) has studied the accident statistics of many active assistance systems that have potentiality to reduce the number of fatalities and accidents. Their study shows that ESC is highly effective in preventing

driver loss of control and rollover crashes. Based on the crash data of FARS [**1**], NHTSA estimates that ESC systems will reduce single-vehicle crashes of passenger cars by 34 percent and single-vehicle crashes of sport utility vehicles (SUVs) by 59 percent, with a much greater drop in rollover crashes. ESC has the potential to prevent 71 percent and 84 percent of passenger car rollovers and SUV rollovers respectively. Moreover, NHTSA estimates that the installation of ESC will save 5,300 to 9,600 lives and prevent 156,000 to 238,000 injuries in all types of crashes per year. Therefore, the US government has passed a new federal rule that enforces manufacturers to install ESC in all new vehicles from 2012 [**1**].

1.1. Electronic Stability Control

Electronic Stability Control (ESC) is an active safety system that prevents vehicles from spinning, drifting out, and rolling over. It has been developed and commercialized by many automotive manufacturers. ESC also has been known by other names such as yaw stability control (YSC), vehicle stability assist (VSA), vehicle stability control (VSC), electronic stability program (ESP), and direct yaw control (DYC).

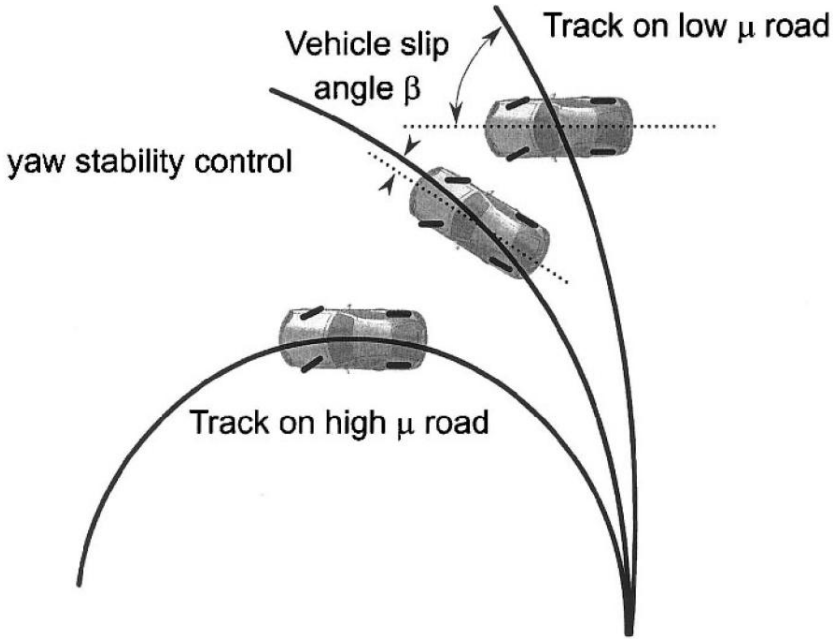

Figure 1-1 The functioning of an electronic stability control system [3**].**

Figure 1-1 shows the primarily function of an electronic stability control system. In the figure, the lower curve represents the vehicle trajectory that the vehicle would normally follow in response to a driver steering input. This case happens when the road is dry and has a high tire-road friction coefficient. The high friction coefficient is able to provide enough lateral force to keep the vehicle following the curved road. If the road has a small friction coefficient or the vehicle speed is too fast, then the vehicle would not be able to follow the nominal trajectory required by the driver. In this case, the vehicle would travel on a trajectory of larger radius as shown in the upper curve of Figure 1-1. The middle curve of Figure 1-1 shows the case that ESC might bring the trajectory closer to the nominal motion expected by the driver. The function of ESC is to try restoring the yaw rate of the vehicle to the nominal motion expected by the drive. However, if the friction coefficient is too small, ESC might not be able to achieve the nominal motion. It might only make the vehicle yaw rate closer to the expected yaw rate [**3**].

There are three types of ESC systems [**3**].

1. **Differential Braking Systems:** The yaw moment is controlled by utilizing the ABS brake system on the vehicle to apply differential braking between the right and left wheels. This technology has received the most attention from researchers and has been implemented on several commercial vehicles.
2. **Steer-by-Wire Systems:** The yaw moment of the vehicle is adjusted by modifying the driver's steering angle input and adding a correction steering angle to the wheels. This technology has received attention mostly from academic researchers.
3. **Active Torque Distribution Systems:** The yaw moment is controlled by utilizing active differentials and all-wheel drive technology to independently control the drive torque distributed to each wheel. Thus this technology can provide active control both of traction and yaw moment. These have received interest in the recent past and are starting to become available on commercial cars.

The objective of these types of ESC systems is to achieve either yaw rate tracking or slip angle tracking, or a combination of both. Many stability control systems use yaw rate for

feedback to ensure that the actual yaw rate tracks a desired yaw rate determined by the driver's steering input [**3**]. However, in the case that the road surface has low friction, it is possible that the actual yaw rate tracks the desired yaw rate but the vehicle still has significant skidding. This is because when the slip angle is too high, the ability of tires to generate lateral forces is reduced. The performance of the vehicle control is also reduced. So, it is also useful to control the vehicle slip angle to prevent this situation, in addition to controlling yaw rate [**3**], [**4**], [**5**].

To control the slip angle and yaw rate, the control law described in [**3**], [**6**], and [**7**] shows that it is necessary to know slip angle, slip angle derivative, and front and rear tire road fiction coefficients, μ, to compute a control law. However, there are no inexpensive sensors that can directly measure these variables. These variables must be estimated and used for feedback.

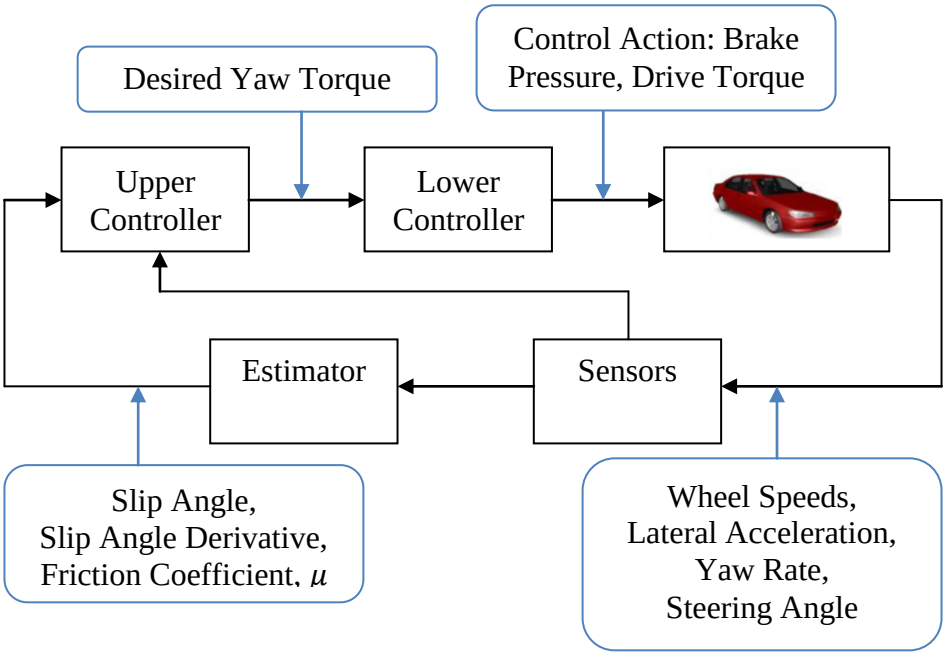

Figure 1-2 Structure of electronic stability control system.

The structure of an ESC system is shown in Figure 1-2. The objective of the upper controller is to ensure yaw stability control and assumes that any desired yaw torque can be commanded. The upper controller uses measurements from wheel speed sensors, an accelerometer sensor, a gyroscope, and a steering sensor. Also, it uses the slip angle, slip

angle derivative, and front and rear lateral tire forces from an estimator. The lower controller ensures that the desired yaw torque from the upper controller is obtained from the control action, namely the differential braking system or the drive torque distribution system.

There are no available sensors that can directly measure slip angle, slip angle derivative, and tire forces or friction coefficient, μ. Due to nonlinear vehicle dynamics and a number of unknown inputs, it is challenging to develop an approach for estimating slip angle and friction coefficient, μ, accurately.

1.2. Active Rollover Prevention

Rollovers occur in one of two ways, namely tripped or un-tripped [**8**]. The two types of rollovers are shown in Figure 1-3. A tripped rollover happens due to tripping from external inputs. An example of this rollover happens when a vehicle leaves the roadway and slides sideways, digging its tires into soft soil or striking an object such as a curb or guardrail. On the other hand, an un-tripped rollover happens due to high lateral acceleration from a sharp turn and without tripping. An example of un-tripped rollover is when a vehicle makes a collision avoidance maneuver or a cornering maneuver with high speed.

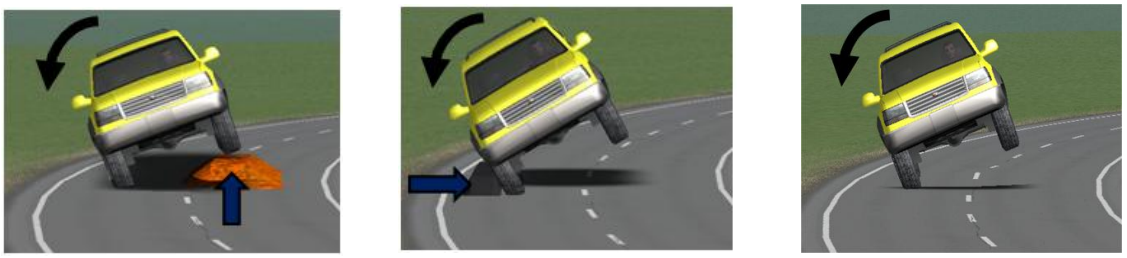

Rollover from vertical inputs

Roll from lateral inputs

a) Tripped Rollover b) Un-Tripped Rollover

Figure 1-3 Types of rollover.

Rollover accidents are seriously dangerous. According to NHTSA's records (http://www.safercar.gov), although there were nearly 11 million crashes in 2002, only 3% involved a rollover. However, there were more than 10,000 deaths in rollover crashes in 2002. Thus, rollovers caused nearly 33% of all deaths from passenger vehicle crashes.

In addition, NHTSA data also shows that 95% of single-vehicle rollovers are tripped while un-tripped rollover occurs less than 5% of the time.

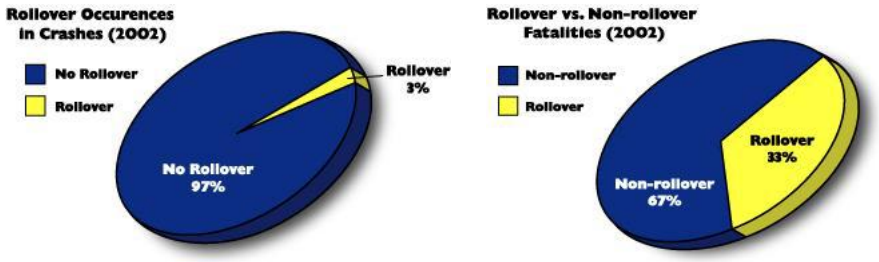

Figure 1-4 NHTSA Rollover Record (http://www.safercar.gov).

Active roll prevention is a vehicle stability system that prevents vehicles from un-tripped rollovers. (Note: There are no assistance systems available to prevent tripped rollovers.) It has been developed by some automotive manufacturers. Several types of active control systems can be used to prevent rollovers. The differential braking system has received the most attention from researchers to use for preventing rollovers by reducing the yaw rate of the vehicle and its speed. Thus, the vehicle propensity to rollover is reduced. Also, steer-by-wire systems and active suspensions can potentially be used to prevent rollovers.

In order to make these systems effective in their tasks, quick detection of the danger of vehicle rollover is necessary [**9**]. For this purpose, many researchers have developed a real-time index to indicate a danger of rollover. However, they have focused on developing an indicator only for un-tripped rollovers. There are no published papers that have studied how to detect vehicle rollovers for the tripped case. This dissertation will focus on developing a rollover index that can detect both tripped and un-tripped rollovers.

1.3. Thesis Objectives

Based on the motivation provided in the above sections, the specific objectives of this thesis are

1. Development of tire-road friction coefficient estimation algorithms that can estimate friction coefficients at each of the individual wheels of the vehicle,

2. Development of slip angle estimation algorithms that are applicable under a wide range of vehicle operating conditions and under unknown values of tire-road friction coefficient, μ,
3. Development of roll angle estimation algorithms that are applicable under a wide range of vehicle operating conditions for use in a rollover index,
4. Development of a rollover index that can reliably predict rollover for both tripped and un-tripped scenarios,
5. Experimental evaluation of all of the above estimation algorithms.

As discussed in the next section, development of the above estimation algorithms presents state, parameter and unknown input estimation problems for a highly nonlinear system. Thus, this dissertation also makes significant theoretical contributions to state estimation techniques for nonlinear systems.

1.4. Theoretical Contributions

A variety of nonlinear observers have been developed in this dissertation to deal with estimation problem in nonlinear systems. The developed nonlinear observer design techniques are

1. Nonlinear observer design for Lipschitz nonlinear systems,
2. Nonlinear observer design using a bounded Jacobian approach,
3. Nonlinear observer for systems with a nonlinear function in the measurement equation,
4. Nonlinear observer and unknown input estimation for bounded Jacobian nonlinear systems with unknown disturbance inputs.

The new nonlinear observer design techniques can be applied for many nonlinear systems and to several estimation problems in vehicle dynamics. These nonlinear observers will be presented in chapters 5, 6, 7, and 8.

Chapter 2

2. TECHNICAL CHALLENGES

There are several challenges in designing estimation algorithms for the tire-road friction coefficient, slip angle, roll angle, and rollover index estimation problems as discussed in section 1.3. The first major challenge is that the dynamics model of a vehicle is nonlinear when wide ranges of operating conditions are considered. So, the presence of a traditional linear observer cannot be used. The second challenge is due to an unknown and varying parameter, friction coefficient. This parameter needs to be indentified in real-time for state estimation. Also, an unknown disturbance input poses a significant challenge for the rollover index estimation problem in tripped rollovers.

2.1. Nonlinear Dynamics Due to Nonlinear Tire Models

Tire-road forces are important in vehicle dynamics and control because they are the only forces that a vehicle experiences from the ground. These forces significantly affect the lateral, longitudinal, yaw, and roll behavior of the vehicle. The maximum force that a tire can supply is determined by the maximum value of the tire-road friction coefficient for a given normal vertical load on the tire. For any given tire, the normalized traction force, ρ, is defined as

$$\rho = \frac{\sqrt{F_x^2 + F_y^2}}{F_z} \tag{2.1}$$

where F_x, F_y, and F_z are the longitudinal, lateral, and normal, that is, vertical, forces acting on the tire.

The normalized traction force, ρ, is typically a function of slip ratio, σ_x, slip angle, α, and the tire-road friction coefficient, μ. The tire road-friction coefficient, μ, on any given road surface is defined as the maximum value that ρ can achieve on that surface for any slip angle and slip ratio values. The value of the tire-road friction coefficient, μ, can vary between 0 and 1 depending on the type of road surface under consideration, such as icy, snow covered, gravel, dry asphalt, and others [**10**].

Experimental results have shown that longitudinal tire force for a given normal force, F_z, depends on the slip ratio, σ_x, and friction coefficient, μ, and the lateral tire force depends on the slip angle, α, and friction coefficient, μ. Figure 2-1 shows the longitudinal force vs. slip ratio relationship when assuming $F_y = 0$ and the lateral force vs. slip angle relationship when assuming $F_x = 0$ for a variety of road surfaces computed using a tire model. As the figures show, $\rho = \sqrt{F_x^2 + F_y^2}/F_z$ is an increasing function of slip ratio, σ_x, and slip angle, α, until a critical slip value, where ρ reaches a value equal to μ and then starts decreasing slowly.

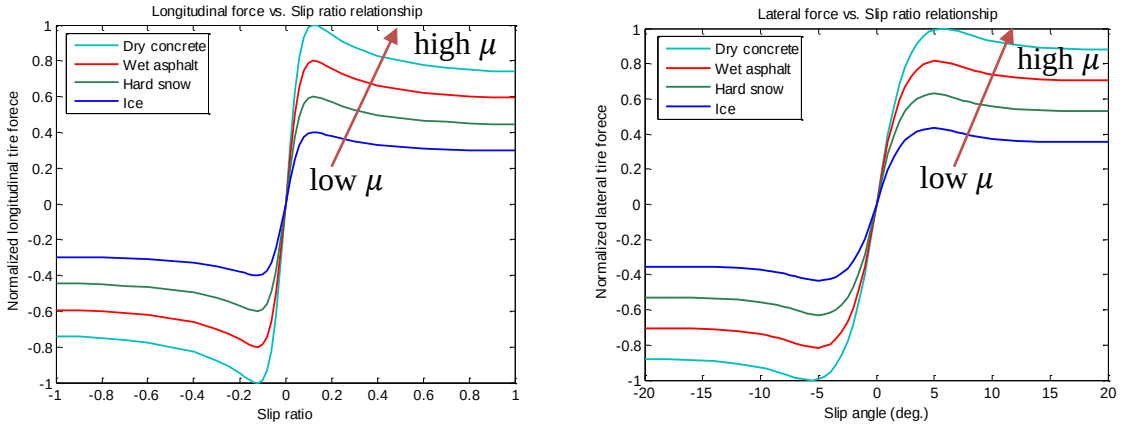

a) Longitudinal force vs. slip ratio ($F_y = 0$)

b) Lateral force vs. slip angle ($F_x = 0$)

Figure 2-1 Longitudinal and lateral tire force.

The slip ratio is defined as

$$\sigma_x = \frac{r_{eff}\omega_w - v_x}{\max\left(r_{eff}\omega_w, v_x\right)} \tag{2.2}$$

where r_{eff} is effective tire radius, ω_w is angular velocity of the wheel, and v_x is longitudinal velocity.

The tire slip angles are defined as

$$\alpha_f = \delta - \left(\frac{\dot{y} + ra}{v_x}\right), \qquad \alpha_r = -\left(\frac{\dot{y} - rb}{v_x}\right) \tag{2.3}$$

where α_f is front tire slip angle, α_r is rear tire slip angle, δ is steering wheel angle, $\dot{y}$ is lateral velocity, a and b are distance from c.g. to front and rear axis respectively.

The tire forces play an important role because vehicle models depend on tire forces. To describe the tire behavior shown in Figure 2-1a and Figure 2-1b, many researchers developed tire force models based on algebraic slip/force relationships. One of the most well-known tire models is known as the Magic Formula or Pacejka's model [**11**]. Another tire model proposed in [**12**] is Dugoff's tire model. Alternatively, [**3**] proposes a tire model for parabolic normal force distribution. All the previously developed models can reasonably describe tire behavior. However, they are highly nonlinear in the unknown parameters. Thus, they are not easy to use. An example of a lateral tire force model is presented in equation (2.4).

$$F_y = \mu F_z(3\theta\alpha - 3\theta^2\alpha^2 sgn(\alpha) + \theta^3\alpha^3) \tag{2.4}$$

where $\theta = \frac{4a_c^2 b_c k}{3\mu F_z}$, μ is tire-road friction coefficient, F_z is the vertical force on the tire, a_c is half-length of contact patch, b_c is half-width of contact patch, and k is isotropic stiffness of tire elements per unit area of the belt surface.

In control of the nominal motion of a vehicle during regular driving, linear tire models are used to describe vehicle dynamic models. The tire force of the linear model is assumed to be proportional to the appropriate slip variable. This type of model is valid only when slip ratio and slip angle are small. Thus, the linear tire force model is not effective to describe vehicle dynamic models when slip ratio and slip angle are large or the tire-road friction coefficient, μ, is small.

Consequently, to obtain an accurate vehicle dynamic model, it is necessary to use a nonlinear tire model to describe vehicle dynamics.

2.2. Unknown Parameter, Tire-Road Friction Coefficient, μ, Which Affects State Estimation

As described in the previous section, the accuracy of vehicle dynamic models depends on the tire force model. However, the tire force model includes the unknown parameter, tire-

road friction coefficient, μ, as shown in equation (2.4), that depends on the road surface condition. Without friction coefficient information, the state estimation cannot be done.

The knowledge of tire-road friction coefficient, μ, is extremely useful to many active vehicle safety control systems, including traction control, yaw stability control and roll-over prevention control systems. In particular, reliable estimation of the individual friction coefficients at each of the wheels of the vehicle will enable both traction and stability control systems to provide optimum drive torque and/or brake inputs to the individual wheels so as maximize traction, reduce skid and enhance stability. Many research papers in literature on stability control have also proposed the explicit use of friction coefficient information in calculations of desired yaw rate and other control system variables [**13**], [**14**]. Another example is an adaptive cruise control system. The friction coefficient can be used to adjust the spacing headway that the adaptive cruise control vehicle should maintain.

However, no available sensor can directly measure the friction coefficient. A combination of expensive sensors and complex methods to measure the friction coefficient may be needed for the whole vehicle. Thus, many researchers have tried to develop algorithms to estimate only the average friction coefficient. This thesis focuses on development and experimental evaluation of algorithms for real-time estimation of tire-road friction coefficients at individual tires of the vehicle.

2.3. Rollover Index and Unknown Disturbance Inputs for Tripped Rollovers

The quick detection of the danger of a vehicle rollover is necessary for initiating a rollover prevention action. To detect vehicle rollover, the concept of a static rollover threshold or the static stability factor (SSF) [**15**] was studied and used first, but it is not effective for dynamic situations. After that the concept of a rollover index was introduced. Rollover Index is a real time variable used to detect wheel lift off conditions. Many researchers have tried to develop a rollover index to more accurately predict vehicle rollover for un-tripped rollovers. References [**16**] has used the concept of a rollover index based on Time-To-Rollover (TTR) to estimate the time until rollover

occurs. References [**9**], [**17**], and [**18**] have described a rollover index using a model-based roll angle estimator. Reference [**19**] has combined a rollover index with influential factors such as the vehicle's center of gravity and energy of rollover. Even though there are many types of rollover indices, they are derived from the same basic model as shown in Figure 2-2. The basic concept of the rollover index is described by equation (2.5).

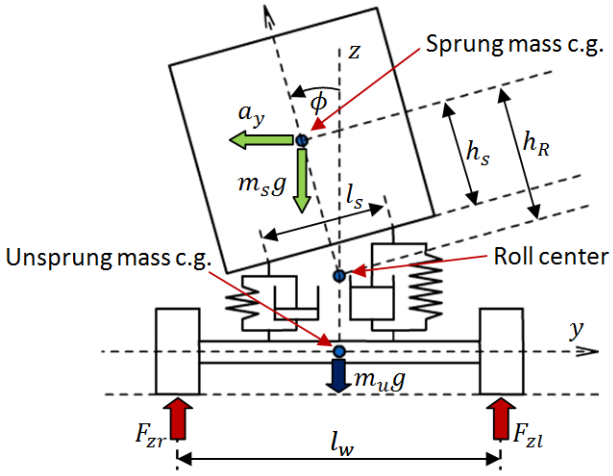

Figure 2-2 Un-tripped rollover model.

$$R = \frac{F_{zr} - F_{zl}}{F_{zr} - F_{zl}}, \qquad -1 \le R \le 1 \tag{2.5}$$

where F_{zr} and F_{zl} are the right and left vertical tire force of the vehicle respectively, m_u is unsprung mass, m_s is spung mass, a_y is lateral acceleration, ϕ is roll angle, and $\dot{\phi}$ is roll rate. A vehicle is considered to roll over when R equals 1 or -1. It should be noted that when a vehicle is traveling straight, F_{zr} equals to F_{zl} and $R = 0$.

The definition of R in equation (2.5) cannot be implemented in real-time because the vertical tire forces F_{zr} and F_{zl} cannot be measured. Using the 1-degree of freedom model in Figure 2-2, the summation and difference of tire forces $F_{zr} + F_{zl}$ and $F_{zr} - F_{zl}$ can be calculated. An implementable version of the rollover index R can then be calculated in terms of ϕ and a_y. Such an example of a traditional rollover index calculated using a one degree of freedom is shown below in equation (2.6).

$$R = \frac{F_{zr} - F_{zl}}{F_{zr} - F_{zl}} = \frac{2m_s a_y h_R}{mgl_w} + \frac{2m_s h_R tan\phi}{ml_w} \quad (2.6)$$

where $m = m_s + m_u$, h_R is c.g. height, m_u is unsprung mass, m_s is spung mass, a_y is lateral acceleration, and ϕ is roll angle.

This type of rollover index is used for detection un-tripped rollovers only. It is a function of lateral acceleration and roll angle as shown in equation (2.6). Some papers have proposed a rollover index that uses only lateral acceleration [**20**], [**21**], since roll angle is expensive to measure. The stability control with this rollover index may arbitrarily reduce lateral acceleration capability of the vehicle. Also, it still fails to detect rollovers when rollovers are induced by vertical road inputs or other external inputs.

In order to detect tripped rollovers, which happens due to tripping from external inputs, a new rollover index should include the influence of road and other external inputs. Figure 2-3 shows a vehicle rollover model that includes the influence of road inputs, z_{rr} and z_{rl}, and an unknown lateral force input, F_{lat}, at an arbitrary height, h_{lat}, from the roll center. The figure also shows the normal forces on the tires, F_{zr} and F_{zl}.

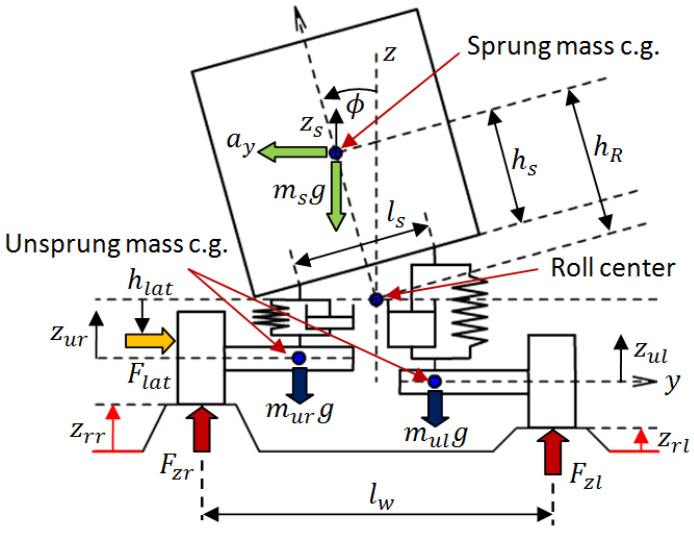

Figure 2-3 Un-tripped and tripped rollover model.

To derive a rollover index in this case, multi-degrees of freedom in the model are needed. When the influence of road inputs is included, the suspension forces are defined by

$$F_{sr} = -k\left(z_s - \frac{l_s}{2}sin\phi - z_{ur}\right) - d\left(\dot{z}_s - \frac{l_s}{2}\dot{\phi}cos\phi - \dot{z}_{ur}\right), \quad (2.7)$$

$$F_{sl} = -k\left(z_s + \frac{l_s}{2}sin\phi - z_{ul}\right) - d\left(\dot{z}_s + \frac{l_s}{2}\dot{\phi}cos\phi - \dot{z}_{ul}\right) \quad (2.8)$$

where k is suspension stiffness, d is suspension damping, z_{ur} and z_{ul} are left and right unsprung mass positions, and z_s is sprung mass position. z_s includes the static displacement due to weight and the vertical displacements due to road inputs.

The difference and the summation of F_{sr} and F_{sl} are given by

$$F_{sr} - F_{sl} = kl_s sin\phi + dl_s\dot{\phi}cos\phi + k(z_{ur} - z_{ul}) + d(\dot{z}_{ur} - \dot{z}_{ul}), \quad (2.9)$$

$$F_{sr} + F_{sl} = -2kz_s - 2d\dot{z}_s + k(z_{ur} + z_{ul}) + d(\dot{z}_{ur} + \dot{z}_{ul}). \quad (2.10)$$

With moment balance roll center, $F_{zr} - F_{zl}$ is given by

$$F_{zr} - F_{zl} = \frac{l_s}{l_w}(F_{sr} - F_{sl}) + \frac{2}{l_w}F_{lat}h_{lat} \quad (2.11)$$

Also, vertical force balance yields

$$\begin{aligned} F_{zr} + F_{zl} &= mg + F_{sr} + F_{sl} \\ F_{zr} + F_{zl} &= mg - 2kz_s - 2d\dot{z}_s + k(z_{ur} + z_{ul}) + d(\dot{z}_{ur} + \dot{z}_{ul}) \end{aligned} \quad (2.12)$$

Therefore, an example of the rollover index for tripped rollovers computed directly from the model of Figure 2-3 is given by

$$\begin{aligned} R = \frac{F_{zr} - F_{zl}}{F_{zr} + F_{zl}} = \frac{l_s}{l_w}\frac{kl_s sin\phi + dl_s\dot{\phi}cos\phi + k(z_{ur} - z_{ul}) + d(\dot{z}_{ur} - \dot{z}_{ul})}{(mg - 2kz_s - 2d\dot{z}_s + k(z_{ur} + z_{ul}) + d(\dot{z}_{ur} + \dot{z}_{ul}))} \\ + \frac{2}{l_w}\frac{F_{lat}h_{lat}}{(mg - 2kz_s - 2d\dot{z}_s + k(z_{ur} + z_{ul}) + d(\dot{z}_{ur} + \dot{z}_{ul}))} \end{aligned} \quad (2.13)$$

where left and right unsprung mass positions, z_{ur} and z_{ul}, depend on road inputs, z_{rr} and z_{rl}. The equations of motion of z_{ur} and z_{ul} are given by

$$m_{ur}\ddot{z}_{ur} = -F_{sr} + k_t(z_{ur} - z_{rr}) - m_{ur}g, \quad (2.14)$$

$$m_{ul}\ddot{z}_{ul} = -F_{sl} + k_t(z_{ul} - z_{rl}) - m_{ul}g \quad (2.15)$$

where k_t is the vertical tire stiffness, m_{ur} and m_{ul} are right unsprung mass and left unsprung mass, respectively.

In order to compute the rollover index in equation (2.13), many variables need to be measured. However, some variables such as unknown road inputs, vertical displacements of unsprung masses and sprung mass, and the unknown lateral force input cannot be directly measured by sensors. Therefore, it is necessary to develop an approach for estimating the new rollover index without knowing these variables.

Chapter 3

3. OUTLINE OF APPROACH TO RESEARCH

Chapters 1 and 2 show that there are many vehicle parameters, variables, and unknown inputs that need to be estimated in order to enhance automotive safety systems. Thus, the outline of the overall approach to the estimation problems will be presented in this chapter.

First, an outline of the algorithms to estimate friction coefficients for each individual wheel of the vehicle will be presented in section 3.1. Then, sections 3.2 and 3.3 describe the approach to estimate slip angle and roll angle, respectively. Lastly, the outline of the approach to develop a rollover index for tripped and un-tripped rollovers will be shown in section 3.4.

3.1. Estimation of Individual Wheel Tire-Road Friction Coefficients

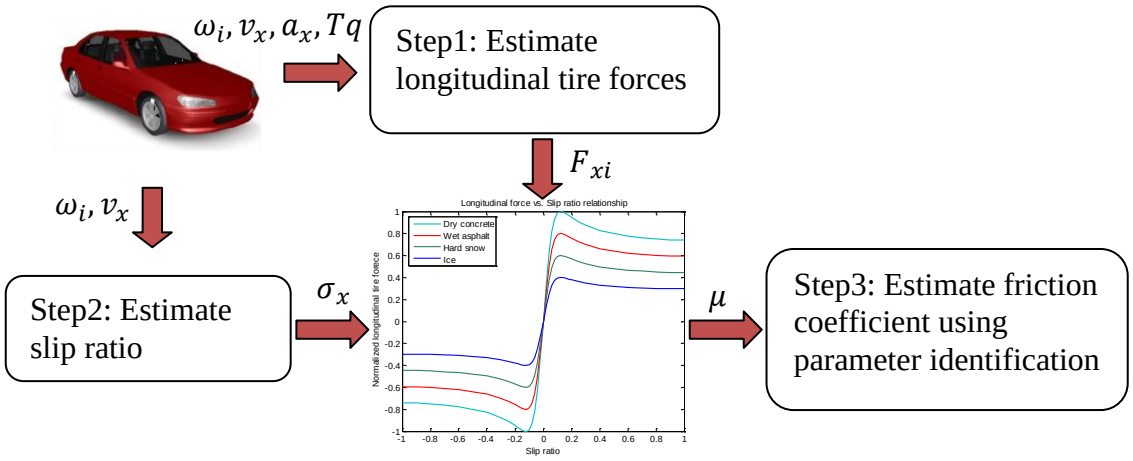

Figure 3-1 Schematic of the approach to individual wheel tire-road friction estimation.

The knowledge of the real-time tire-road friction coefficient can be extremely valuable for active safety applications, including traction control, yaw stability control and rollover prevention. So, this thesis develops algorithms to estimate friction coefficients for each individual wheel of the vehicle.

The overall approach used for individual wheel friction coefficient estimation consists of the following three steps:

1) Estimate the longitudinal tire force at each wheel.
2) Measure or estimate the longitudinal slip ratio at the wheel.
3) Use a recursive least squares parameter identification algorithm to calculate the tire-road friction coefficient.

Three different algorithms are considered for steps 1 and 2, based on the types of sensors available.

1) Using GPS and engine torque measurement
2) Using engine torque measurements and longitudinal accelerometer
3) Using GPS and longitudinal accelerometer

The wheel speeds are assumed to be available for all three algorithms. The details of individual wheel tire-road friction coefficient algorithms will be presented in chapter 4.

3.2. Slip Angle Estimation

Real-time knowledge of the slip angle in a vehicle is useful in many active vehicle safety applications, including yaw stability control, rollover prevention, and lane departure avoidance. Sensors to measure slip angle, including two-antenna GPS systems and optical sensors, are too expensive for ordinary automotive applications. So a nonlinear observer design technique is necessary for estimation of slip angle using inexpensive sensors normally available for yaw stability control applications.

The lateral dynamics of a vehicle can be written in a state space form described by

$$\begin{aligned} \dot{x} &= Ax + \Phi(x) + g(y,u), \\ y &= Cx + \Psi(x) \end{aligned} \tag{3.1}$$

where $x \in R^n$ is the state vector, $u \in R^p$ is the input vector, and $y \in R^m$ is the output measurement vector. $A \in R^{n\times n}$ and $C \in R^{m\times n}$ are appropriate matrices. The functions, $\Phi(x): R^n \to R^n$, $\Psi(x): R^n \to R^m$, and $g(y,u): R^m \times R^p \to R^n$ are nonlinear.

A nonlinear observer based on the above nonlinear vehicle model is desired to use for estimating slip angle. However, most available nonlinear observers in literature are designed for a nonlinear system with linear measurement equations. Moreover, the most commonly used techniques and applicable observer design methods are based on either linearization or on the assumption that the nonlinear system is Lipschitz. A major limitation of the existing results for Lipschitz nonlinear systems is that they work only for adequately small values of the Lipschitz constant. When the equivalent Lipschitz constant has to be chosen large due to the inherent non-Lipschitz nature of the nonlinearity (such as in the case of vehicle systems), most existing observer design results fail to provide a solution. Hence, a new nonlinear observer design technique is presented in chapter 7. Also, the details of the slip angle estimation algorithm will be presented in chapter 10.

3.3. Roll Angle Estimation

Rollover has become an important safety issue. Vehicles with their increased dimensions, high center of gravity and heavy weights are known to be high rollover risk vehicles. The measurement of roll angle of vehicle can be used in the computation of rollover index and to prevent rollover. The roll dynamic model of a vehicle is a model with complex nonlinearities. The roll dynamics of a vehicle can be written into the state space form as equation (3.2). A linear observer fails to guarantee the stability of the observer. To deal with the complex nonlinearities involved, we have developed a new nonlinear observer to estimate the roll angle [**22**]. The new observer design for this problem is presented in chapter 6 and the application of roll estimation is presented in chapters 9 and 11.

$$\begin{aligned} \dot{x} &= Ax + \Phi(x) + g(y,u), \\ y &= Cx \end{aligned} \tag{3.2}$$

where $x \in R^n$ is the state vector, $u \in R^p$ is the input vector, and $y \in R^m$ is the output measurement vector. $A \in R^{n\times n}$ and $C \in R^{m\times n}$ are appropriate matrices. The functions, $\Phi(x): R^n \to R^n$, and $g(y,u): R^m \times R^p \to R^n$ are nonlinear.

3.4. Tripped Rollover Index Estimation

In order to predict tripped and un-tripped rollovers as described in section 2.3, many variables need to be measured. However, some variables such as unknown road inputs,

vertical displacements of unsprung masses and sprung mass, and the unknown lateral force input cannot be directly measured by sensors. Therefore, algorithms to estimate the rollover index for tripped and un-tripped rollovers are developed.

Two different algorithms are considered based on the types of sensors available.

1) Using accelerometers, gyroscope, and suspension compression measurement
2) Using accelerometers, and roll angle measurement

The first algorithm is an approach to estimate unknown disturbance inputs in a nonlinear system using dynamic model inversion and a modified version of the mean value theorem. In this case, the vehicle dynamics involve both complex nonlinearities and unknown disturbance inputs. The dynamics of a vehicle in this case can be written into the state space form shown in equation (3.3). To deal with this type of system, a new unknown inputs nonlinear observer to estimate both unknown disturbance inputs and state variables has been developed. The developed observer design for this problem is presented in chapter 8. Then, the application of the unknown inputs nonlinear observer will be presented in chapter 12.

$$\begin{aligned} \dot{x} &= \bar{A}x + \eta(x,u) + \bar{B}\mu, \\ z &= \bar{E}x, \\ y &= Cx + \Psi(x) \end{aligned} \tag{3.3}$$

where $u \in R^P$ are the known control inputs, $\mu \in R^P$ are the unknown inputs, $y \in R^m$ and $z \in R^q$ are the output measurements. $\bar{A} \in R^{n\times n}$, $\bar{B} \in R^{n\times p}$, $\bar{E} \in R^{q\times n}$, and $C \in R^{m\times n}$ are appropriate matrices. The functions $\eta(x,u)\colon R^n \times R^p \to R^n$,and $\Psi(x)\colon R^n \to R^m$ are nonlinear.

The second algorithm relies on an algebraic formulation of the new rollover index. The new rollover index utilizes roll angle measurement and vertical accelerometers in addition to a lateral accelerometer and is able to predict rollover in spite of unknown external inputs acting on the system. The details of this new rollover index are also presented in chapter 12.

3.5. Conclusions

In order to deal with the problems as described in this chapter, algorithms for real-time estimation of individual wheel tire-road friction coefficients will be presented in chapter 4. Then chapters 5, 6, 7, and 8 present new nonlinear observer design techniques that can be applied for a large class of differentiable nonlinear systems. The new nonlinear observer design techniques can also be applied for the important vehicle estimation problems discussed in this dissertation such as longitudinal velocity estimation in chapter 9, slip angle estimation in chapter 10, roll angle estimation in chapter 11, and rollover index estimation for addressing un-tripped and tripped rollovers in chapter 12.

Chapter 4

4. ALGORITHMS FOR REAL-TIME ESTIMATION OF INDIVIDUAL WHEEL TIRE-ROAD FRICTION COEFFICIENTS

4.1. Summary

It has long been recognized in the automotive research community that knowledge of the real-time tire-road friction coefficient can be extremely valuable for active safety applications, including traction control, yaw stability control and rollover prevention. Previous research results in literature have focused on estimation of average friction coefficient for the vehicle or on average friction coefficient for both drive wheels of the vehicle. This section explores the development of algorithms for reliable estimation of friction coefficient at each individual wheel of the vehicle. Three different algorithms are proposed based on the types of sensors available. After estimation of slip ratio and tire force, the friction coefficient is identified using a recursive least squares parameter identification formulation. The observers include one that utilizes engine torque, brake torque and GPS measurements, one that utilizes torque measurements and an accelerometer and one that utilizes GPS measurements and an accelerometer. These algorithms are first evaluated in simulation and then evaluated experimentally on a Volvo XC90 sport utility vehicle. Experimental results demonstrate that friction coefficients at the individual wheels and road gradient can both be estimated reliably and quickly. Individual wheel friction measurements are expected to be more valuable for active safety systems than average friction measurements.

4.2. Introduction

The knowledge of tire-road friction coefficient can be extremely useful to many active vehicle safety control systems, including traction control, yaw stability control and roll-over prevention control systems. In particular, reliable estimation of the individual friction coefficients at each of the wheels of the vehicle will enable both traction and

stability control systems to provide optimum drive torque and/or brake inputs to the individual wheels so as maximize traction, reduce skid and enhance stability. Many research papers in literature on stability control have also proposed the explicit use of friction coefficient information in calculations of desired yaw rate and other control system variables [**13**], [**14**]. This dissertation focuses on development and experimental evaluation of algorithms for real-time estimation of tire-road friction coefficients at individual tires of the vehicle.

The tire-road friction coefficient at any tire of the vehicle is defined formally as follows. Let F_x, F_y, and F_z be the longitudinal, lateral, and normal forces acting on a tire. The normalized traction force for the tire, ρ, is defined as:

$$\rho = \frac{\sqrt{F_x^2 + F_y^2}}{F_z}. \tag{4.1}$$

If we consider only longitudinal motion of the vehicle and assume that the lateral force, F_y, can be neglected for the maneuver under consideration, then

$$\rho = \frac{F_x}{F_z}. \tag{4.2}$$

The normalized traction force, ρ, is typically a function of both slip ratio, σ_x, and the tire-road friction coefficient, μ. The tire road-friction coefficient, μ, on any given road surface is defined as the maximum value that ρ can achieve on that surface for any slip ratio value [**3**].

4.3. Longitudinal Vehicle Model

The vehicle model utilized consists of equations for the longitudinal motion of the vehicle, for the rotational dynamics of each wheel and for the relationship between tire forces, slip ratio and tire road friction coefficient.

The longitudinal dynamics can be represented as:

$$m\dot{v}_x = F_x - R_x - D_a v_x^2 + mgsin(\theta) \tag{4.3}$$

where v_x is the longitudinal speed, m is the mass of the vehicle, R_x is the rolling resistance, D_a is an aerodynamic drag parameter and θ is the road gradient. The total

longitudinal tire force is represented by F_x and F_x is the summation of the tire forces generated at all the 4 tires:

$$F_x = F_{xfl} + F_{xfr} + F_{xrl} + F_{xrr}. \quad (4.4)$$

Note that the first subscript in the tire force notation refers to the front or rear wheel while the second subscript refers to left or right wheel. In equation (4.3), the vehicle is assumed to be undergoing longitudinal motion only and the other degrees of freedom are ignored.

The rotational dynamics of each wheel is represented by

$$I_w \dot{\omega}_i = T_i^{dr} - T_i^{br} - r_{eff} F_{xi} \quad (4.5)$$

where the subscript $i = fl, fr, rl,$ and rr is used to separately represent the 4 wheels of the vehicle. T_i^{dr}, T_i^{br}, r_{eff} and F_{xi} represent the drive and brake torque delivered to the specific wheel, the effective radius of the tire and the longitudinal tire force of that specific wheel, respectively.

The longitudinal force generated at each tire is known to depend on the longitudinal slip ratio, the tire-road friction coefficient, and the normal force applied at the tire. Longitudinal slip ratio is defined as

$$\sigma_x = \frac{(r_{eff}\omega_w - v_x)}{v_x}, \text{ during braking} \quad (4.6)$$

$$\sigma_x = \frac{(r_{eff}\omega_w - v_x)}{r_{eff}\omega_w}, \text{ during acceleration} \quad (4.7)$$

The tire model utilized to represent the tire force is discussed further in section 4.4.2 of this chepter [**3**], [**12**].

4.4. Overall Approach to Individual Wheel Tire-Road Friction Estimation

4.4.1. Description of Approach

The overall approach used for individual wheel friction coefficient estimation consists of the following three steps:

1) Estimate the longitudinal tire force at the wheel.
2) Measure or estimate the longitudinal slip ratio at the wheel.
3) Use a recursive least squares parameter identification algorithm to calculate the tire-road friction coefficient.

Three different algorithms are considered for steps 1 and 2, based on the types of sensors available. Algorithm 1 relies on engine torque measurements and brake torque measurements available over the CAN bus of the vehicle and on absolute vehicle speed measured using a carrier-phase based GPS system. This is the simplest and most convenient algorithm to utilize. However, a GPS system is an expensive sensor and cannot always be utilized due to satellite drop-outs in urban environments. Algorithm 2 therefore utilizes engine torque and brake torque measurements and a longitudinal accelerometer for the estimation algorithm. Note that engine torque and brake torque signals are typically available over the CAN bus of newer vehicles and do not require any additional sensors at all for their measurement. Algorithm 3 takes yet another approach of assuming that engine torque measurements are not available and utilizes only a longitudinal accelerometer and GPS based vehicle speed measurement. All the three algorithms assume that wheel speed measurements are available.

In step 3, the friction coefficient at the tire is calculated based on the values of tire force and slip ratio obtained from steps 1 and 2. Step 3 is discussed further in the next three sub-sections.

4.4.2. Tire Model

Figure 4-1 shows the traction and braking force vs. slip ratio relationship for a variety of road surfaces computed using a tire model. As the figure shows, $\rho = F_x/F_z$ is an increasing function of slip ratio, σ_x, until a critical slip value, where ρ reaches a value equal to μ and then starts decreasing slowly.

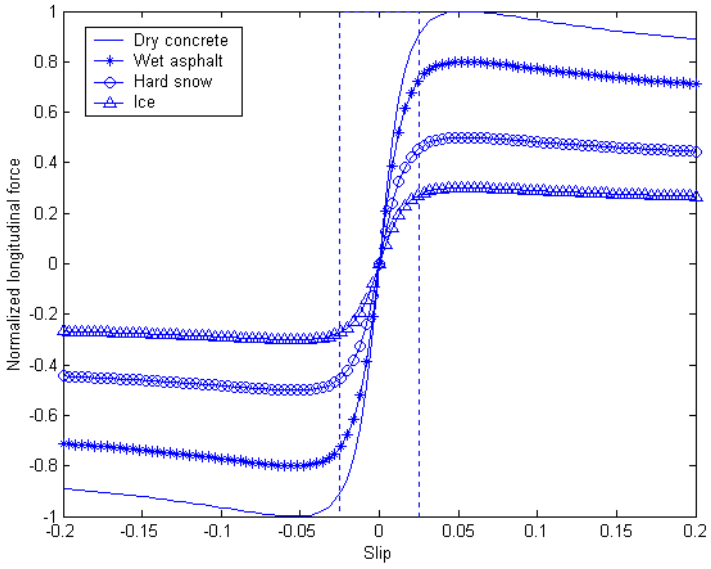

Figure 4-1 Longitudinal force vs. slip relationship.

From the above figure it is clear that if slip ratio and the normalized tire force are both available, then the tire-road friction coefficient can be calculated, except at very small slip ratios (< 0.005).

In the low-slip region (or the linear part of the tire force curves), the longitudinal force generated at an individual tire is proportional to its longitudinal slip for any given road surface and normal force. This relationship can be described as:

$$\rho = \frac{F_x}{F_z} = K\sigma_x \tag{4.8}$$

where K is the slip-slope, whose value changes with road surface conditions and can be directly used to predict the value of the friction coefficient, μ. Equation (4.8) holds for an individual tire.

The equation (4.8) can be rewritten in a standard parameter identification format as:

$$y(t) = \varphi^T(t)\theta(t) \tag{4.9}$$

where $y(t) = F_x/F_z$ is the system output, $\theta(t) = K$ is the unknown parameter, and $\varphi(t) = \sigma_x$ is the system input. The only unknown parameter, K, can be identified in real time using parameter identification approaches as will be addressed in the next section.

Once the slip-slope, K, is identified, it can be connected with the road surface condition or the maximum friction coefficient by a classification function.

Note that the above slip-slope based approach is for low slip ratios (linear part of the friction-slip curves) only. If the slip ratio is high, as in a hard braking situation, the tire works outside the linear relationship between normalized force and slip ratio and the slip-slope based method fails in this region. Fortunately, in the high slip region, the differences between the normalized longitudinal force values for different road surfaces are apparent enough to be able to classify the road surfaces based on this value. Thus, for the high slip region, the normalized force, ρ, can be directly used to classify the road surface friction level. The normalized force in this case can again be written in standard parameter identification form as $y(t) = \varphi^T(t)\theta(t)$, where $y(t) = F_x$ is the measured longitudinal force, $\theta(t) = \mu$ is the unknown parameter, and $\varphi^T(t) = F_z^T = F_z$ is the normal force.

4.4.3. Recursive Least-Squares (RLS) Identification [3]

The slip-slope model described in the previous section can be formulated in a parameter identification form as:

$$y(t) = \varphi^T(t)\theta(t) + e(t) \tag{4.10}$$

where $\theta(t)$ is the vector of estimated parameters, $\varphi(t)$ is the regression vector, $e(t)$ is the identification error between measured $y(t)$ and estimated value $\varphi^T(t)\theta(t)$.

The recursive least squares algorithm will be used in this dissertation to iteratively update the unknown parameter vector, $\theta(t)$, at each sampling time, using the past input and output data contained within the regression vector, $\varphi(t)$. The RLS algorithm updates the unknown parameters so as to minimize the sum of the squares of the modeling errors. The procedure of the RLS algorithm at each step t is as follows:

Step 1: Measure the system output, $y(t)$, and calculate the regression vector, $\varphi(t)$.

Step 2: Calculate the identification error, $e(t)$, which is the difference between system actual output at this sample and the predicted model output obtained from the estimated parameters in previous sample, $\theta(t-1)$, i.e.

$$e(t) = y(t) - \varphi^T(t)\theta(t-1) \tag{4.11}$$

Step 3: Calculate the update gain vector, $K(t)$, as

$$K(t) = \frac{P(t-1)\varphi(t)}{\lambda + \varphi^T(t)P(t-1)\varphi(t)} \tag{4.12}$$

and calculate the covariance matrix, $P(t)$, using

$$P(t) = \frac{1}{\lambda}\left[P(t-1) - \frac{P(t-1)\varphi(t)\varphi^T(t)P(t-1)}{\lambda + \varphi^T(t)P(t-1)\varphi(t)}\right]. \tag{4.13}$$

Step 4: Update the parameter estimate vector, $\theta(t)$, as

$$\theta(t) = \theta(t-1) + K(t)e(t). \tag{4.14}$$

The parameter, λ, in the above equations is called the forgetting factor, which is used to effectively reduce the influence of old data which may no longer be relevant to the model, and therefore prevent a covariance wind-up problem. This allows the parameter estimates to track changes in the process quickly. A typical value for λ is in the interval (0.9, 1).

4.4.4. Determination of the Normal Force

As seen from the friction coefficient estimation equation (4.8), the normal force plays an important role in determining the maximum force the tire can generate. For the same road surface and tire, the larger the normal force, the larger the longitudinal force could be. The mass of the vehicle contributes a major portion of the normal force, and the other forces acting on the vehicle during longitudinal maneuvers redistribute the normal forces between the tires [**3**].

If the vehicle is traveling in a straight line on level road, the normal forces at the front and rear tires can be calculated using a static force model of the vehicle as shown in Figure 4-2 [**23**]:

$$F_{zf} = \frac{mgL_r - ma_x h - D_a v_x^2 h_a}{L} \tag{4.15}$$

$$F_{zr} = \frac{mgL_f + ma_x h + D_a v_x^2 h_a}{L} \tag{4.16}$$

$$F_{zfl} = F_{zfr} = \frac{F_{zf}}{2}, F_{zrl} = F_{zrr} = \frac{F_{zr}}{2} \tag{4.17}$$

The vehicle mass, m, wheelbase, L, and L_f, L_r are measured and assumed to be constant.

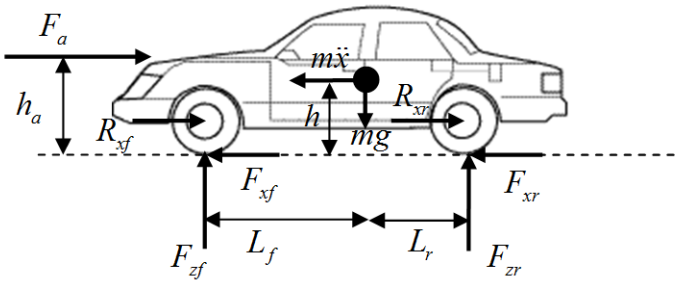

Figure 4-2 Vehicle longitudinal dynamics schematic diagram.

4.4.5. Calculation of Friction Coefficient

The estimated slip-slope varies with the road surface and is used to calculate tire road friction coefficient. Based on experimental data described later in the paper, the following linear equation is found to express the observer relationship between slip-slope and friction coefficient:

$$\mu = AK + C \tag{4.18}$$

where K is the slip-slope, $A = 0.026$ is the proportionality constant and $C = 0.047$ is a bias constant.

4.5. Friction Estimation Using GPS and Torque Measurements

For each wheel, the rotational dynamics is given by

$$I_w \dot{\omega} = T^{dr} - T^{br} - r_{eff} F_x \tag{4.19}$$

where the subscripts have been omitted for convenience. The same estimator and equations hold for all wheels. The following estimator which avoids the need to take derivatives of ω is proposed for estimating the longitudinal force, F_x.

$$I_w\dot{\hat{\omega}} = T^{dr} - T^{br} - r_{eff}\hat{F}_x + l\tilde{\omega}, \tag{4.20}$$

$$\dot{\hat{F}}_x = -\eta\tilde{\omega} \tag{4.21}$$

where $\tilde{\omega} = \omega - \hat{\omega}$ is the estimation error for wheel speed and $\tilde{F}_x = F_x - \hat{F}_x$ is the estimation error for tire force and η is a positive gain. The effective tire radius, r_{eff}, is assumed to be known. Subtracting equation (4.20) from equation (4.19), the estimation error dynamics are seen to be given by

$$I_w\dot{\tilde{\omega}} = -r_{eff}\tilde{F}_x - l\tilde{\omega} \tag{4.22}$$

or, after differentiation,

$$I_w\ddot{\tilde{\omega}} + l\dot{\tilde{\omega}} + r_{eff}\eta\tilde{\omega} = 0. \tag{4.23}$$

Thus with the observer gain l and η being positive, we have $\tilde{\omega} \to 0$, and $\dot{\tilde{\omega}} \to 0$. Since the estimation error dynamics are given by equation (4.22), it follows that $\tilde{F}_x \to 0$ as $t \to \infty$.

The proposed observer of equations (4.20) and (4.21) thus ensures stable estimation of the longitudinal tire force.

The slip ratio can be directly calculated using equations (4.6) and (4.7) in this algorithm, since vehicle speed is available from GPS and wheel speeds are also measured.

As described in section 4.4, once the longitudinal tire force and slip ratio have been estimated, the tire road coefficient can be estimated using a recursive least squares parameter identification technique.

4.5.1. Simulation Results

The proposed longitudinal force estimation algorithm is evaluated in simulations by implementing it in CARSIM, industry standard vehicle dynamics simulation software. The vehicle model from CARSIM chosen for this simulation is a D-Class sedan with default parameters ($m = 1530\ kg$, $I_w = 1\ kg.m^2$, $r_{eff} = 0.335\ m$). The D-Class sedan is a front wheel drive vehicle. The force distribution ratio between the front left and front right wheel is 0.5. It should be noted that while the longitudinal force estimation algorithm was developed using the simple model of equation (4.19), the simulations are being conducted using a high fidelity commercial vehicle dynamics model. At the

beginning of the simulation, the speed of the vehicle is kept constant at about 25.5 m/s. After that, the vehicle starts accelerating. The vehicle is accelerated to 33.5 m/s. The first row of Figure 4-3 shows the longitudinal speed and wheel speeds of this simulation. The engine torque and longitudinal acceleration are presented in the second row of Figure 4-3.

The comparison of the estimated longitudinal forces using the algorithm described in this section and simulated forces using the CARSIM software is presented in Figure 4-4. The results show that the estimated longitudinal forces are almost equal to the simulated forces. Also, those estimated forces converge very quickly to the simulated forces.

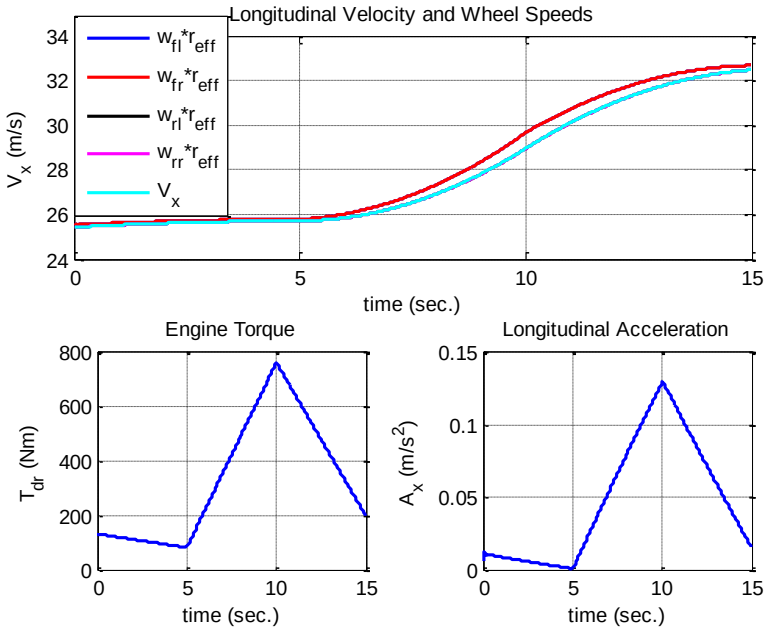

Figure 4-3 Longitudinal speed, wheel speeds, engine torque, and longitudinal acceleration.

Figure 4-3 also shows the relationship between the forces and engine torque. The shapes of the force curves are similar to the shape of the engine torque curve.

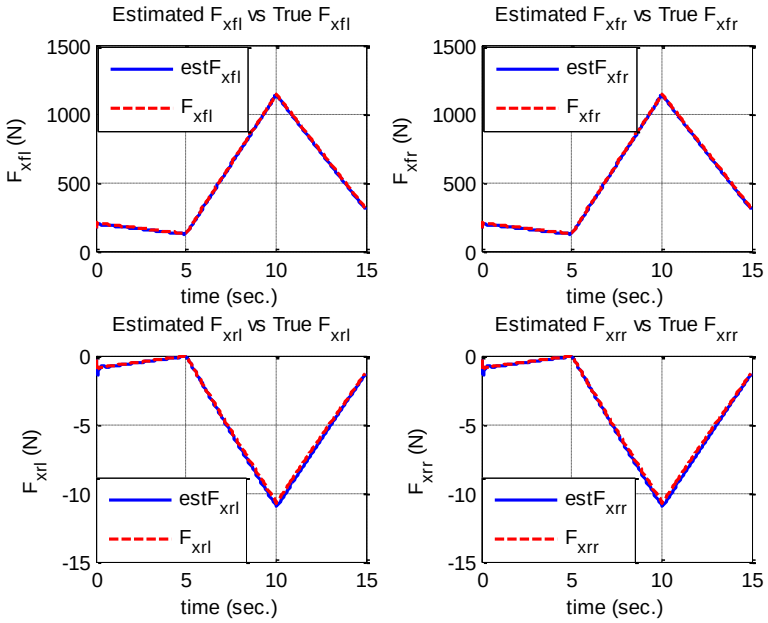

Figure 4-4 Estimated longitudinal forces vs true longitudinal forces.

An experimental evaluation of this longitudinal force estimation and tire-road friction coefficient estimation algorithm is presented in section 4.8 of this chapter.

4.6. Friction Estimation Using Torque Measurements and an Accelerometer

4.6.1. Using Torque Measurements and One Accelerometer

In this case the observer for estimation of longitudinal tire force remains the same as in section 4.5. However, an estimator is needed for estimation of longitudinal vehicle speed, since GPS measurements are no longer available. The longitudinal dynamics of the vehicle are

$$m\dot{v}_x = F_x - R_x - D_a v_x^2 + mgsin(\theta). \tag{4.24}$$

Note that the road gradient in equation (4.24) is unknown and must be estimated. The proposed observer for vehicle speed can be written as

$$m\dot{\hat{v}}_x = F_x - R_x - D_a \hat{v}_x^2 - me, \tag{4.25}$$

$$\dot{e} = -\frac{1}{\tau}e + \frac{1}{\tau}a_{meas} - \frac{1}{\tau}\dot{\hat{v}}_x. \tag{4.26}$$

where the longitudinal accelerometer measures both acceleration and a component of gravity due to road gradient and its measurement is given by

$$a_{meas} = \dot{v}_x - gsin(\theta). \tag{4.27}$$

Let $\tilde{v}_x = v_x - \hat{v}_x$ be the estimation error. The constant τ is a positive gain.

Claim: The observer given by equations (4.25) and (4.26) provides asymptotically stable estimates of both longitudinal vehicle speed and the road gradient angle, θ.

Proof:

First, by subtracting equation (4.25) from (4.24), we find

$$\dot{\tilde{v}}_x = -D_a\frac{(v_x^2 - \hat{v}_x^2)}{m} + [gsin(\theta) + e]. \tag{4.28}$$

Dynamics of e:

$$\begin{aligned}\dot{e} &= -\frac{1}{\tau}e + \frac{1}{\tau}a_{meas} - \frac{1}{\tau}\dot{\hat{v}}_x \\ &= -\frac{1}{\tau}e + \frac{1}{\tau}\left[-D_a\frac{(v_x^2 - \hat{v}_x^2)}{m} + [gsin(\theta) + e]\right] - \frac{1}{\tau}gsin(\theta) \\ &= -D_a\frac{(v_x^2 - \hat{v}_x^2)}{\tau m}\end{aligned} \tag{4.29}$$

Dynamics of $\tilde{v}_x$:

Substituting from equation (4.29) into equation (4.28)

$$m\dot{\tilde{v}}_x = -D_a(v_x^2 - \hat{v}_x^2) + mgsin(\theta) - \int\frac{D_a}{\tau}(v_x^2 - \hat{v}_x^2)dt \tag{4.30}$$

Note that $(v_x^2 - \hat{v}_x^2)$ can be written as $(v_x + \hat{v}_x)(v_x - \hat{v}_x)$ and that $(v_x + \hat{v}_x)$ is always positive. Equation (4.30) is therefore the same as the error dynamics of a PI controller with a constant disturbance input $mgsin(\theta)$. Hence $\tilde{v}_x \to 0$ as $t \to \infty$. Also $e \to -gsin(\theta)$ as $t \to \infty$.

The above observer is stable and leads to stable estimates of road gradient and vehicle speed. However, a disadvantage of the proposed observer is that the damping in the closed-loop estimation error dynamics is determined entirely by the aerodynamic drag parameter, D_a. This damping is typically low and leads to under-damped estimation dynamics.

4.7. Friction Estimation Using GPS and an Accelerometer

Since the longitudinal speed and wheel speeds are known, the longitudinal slip ratio can be calculated using equations (4.6) and (4.7). In the absence of engine and/or brake torque measurements, the following equations involving longitudinal vehicle dynamics and wheel rotational dynamics can be utilized to estimate the variables of drive torque, individual longitudinal tire forces and road gradient

$$m\dot{v}_x = \left(F_{xfl} + F_{xfr} + F_{xrl} + F_{xrr}\right) - R_x - D_a v_x^2 + mgsin(\theta), \tag{4.31}$$

$$I_w\dot{\omega}_{fl} = aT_q - r_{eff}F_{xfl}, \tag{4.32}$$

$$I_w\dot{\omega}_{fr} = bT_q - r_{eff}F_{xfr}, \tag{4.33}$$

$$I_w\dot{\omega}_{rl} = cT_q - r_{eff}F_{xrl}, \tag{4.34}$$

$$I_w\dot{\omega}_{rr} = dT_q - r_{eff}F_{xrr} \tag{4.35}$$

where T_q is total torque and can be due to engine or brake. a, b, c, and d are force distribution ratios used to determine the fraction of total torque, T_q, applied to each wheel. (Note: $a + b + c + d = 1$.) For example, $a = 0.5$, $b = 0.5$, and $c = d = 0$ for total torque of a front wheel drive vehicle.

Since the absolute vehicle speed, v_x, is measured using GPS and the corrected acceleration of the vehicle, $\dot{v}_x + gsin(\theta)$ is measured using a longitudinal accelerometer, there are five unknowns in the five equations (4.31)-(4.35). There can be solved to obtain F_{xfl}, F_{xfr}, F_{xrl}, and F_{xrr} and T_q. Road gradient can be calculated subsequently. A stable observer as described earlier in section 4.5 can also be designed for this purpose so as to avoid differentiation. The following estimator which avoids the need to take derivatives of ω is proposed for estimating the longitudinal force, F_x, and total torque, T_q.

$$\begin{bmatrix} \dot{\hat{v}}_x \\ \dot{\hat{\omega}}_i \\ \dot{\hat{F}}_{xi} \\ \dot{\hat{T}}_q \end{bmatrix} = \begin{bmatrix} 0 & 0 & p & 0 \\ 0 & 0 & r & q \\ 0 & 0 & 0 & 0 \\ 0 & 0 & 0 & 0 \end{bmatrix} \begin{bmatrix} \hat{v}_x \\ \hat{\omega}_i \\ \hat{F}_{xi} \\ \hat{T}_q \end{bmatrix} + \begin{bmatrix} -1 & -1 \\ 0 & 0 \\ 0 & 0 \end{bmatrix} \begin{bmatrix} D_a v_x^2/m \\ R_x/m \end{bmatrix} + K_a \left(\begin{bmatrix} \sum F \\ v_x \\ \omega_i \end{bmatrix} - \begin{bmatrix} 0 & 0 & s & 0 \\ 1 & 0 & 0 & 0 \\ 0 & 1 & 0 & 0 \end{bmatrix} \begin{bmatrix} \hat{v}_x \\ \hat{\omega}_i \\ \hat{F}_{xi} \\ \hat{T}_q \end{bmatrix} \right), \tag{4.36}$$

$$\sum F = m\dot{v}_x + R_x + D_a v_x^2 + mgsin(\theta), \tag{4.37}$$

where $\omega_i = [\omega_{fl} \quad \omega_{fr} \quad \omega_{rl} \quad \omega_{rr}]^T$, $\hat{\omega}_i = [\hat{\omega}_{fl} \quad \hat{\omega}_{fr} \quad \hat{\omega}_{rl} \quad \hat{\omega}_{rr}]^T$, $\hat{F}_i = \left[\hat{F}_{fl} \quad \hat{F}_{fr} \quad \hat{F}_{rl} \quad \hat{F}_{rr}\right]^T$, $p = \frac{1}{m}[1 \quad 1 \quad 1 \quad 1]$, $q = \frac{1}{I_w}[a \quad b \quad c \quad d]^T$, $r = -\frac{r_{eff}}{I_w} I_{4\times4}$, and $s = [1 \quad 1 \quad 1 \quad 1]$.

K_a is an observer gain matrix. Chosen so as to stabilize the error dynamics obtained by the difference between the state equation in equations (4.31)-(4.35) and the estimator dynamics in equations (4.36) and (4.37). The value of K_a is chosen based on desired locations of the closed-loop eigenvalues for this linear time invariant system. The effective tire radius, r_{eff}, is assumed to be known.

4.7.1. Simulation Results

Again, the performance of the observer will be evaluated by simulating the algorithm together with the CARSIM software. We use the same CARSIM vehicle model as described in section 4.5.1. However, in this section, only wheel speeds and acceleration will be used to estimate the longitudinal tire forces.

The comparison of the estimated longitudinal forces using the algorithm described in section 4.7 and actual forces using the CARSIM software is presented in Figure 4-6. The results show that the estimated longitudinal forces match the simulated forces very well. Also, those forces converge very quickly to the simulated forces. However, there are some minor errors in the rear wheel longitudinal forces. This may be due to model uncertainty.

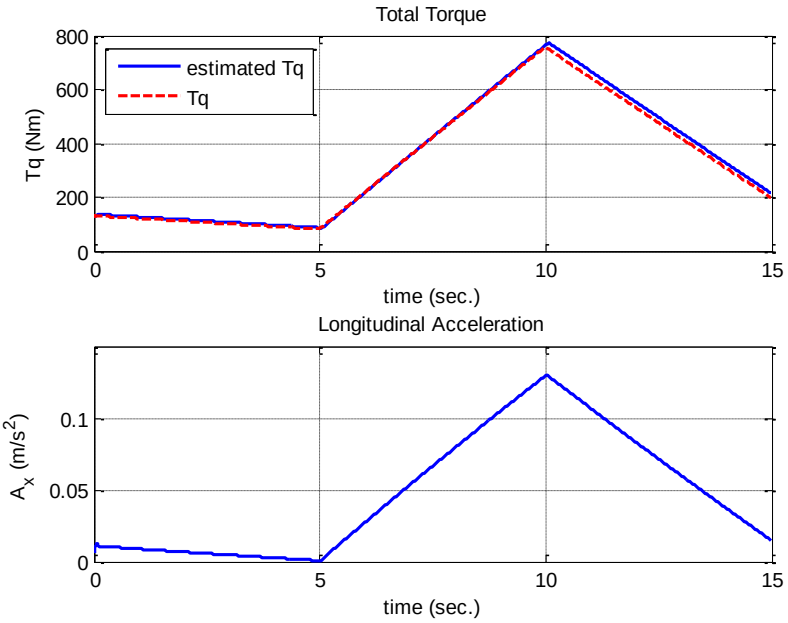

Figure 4-5 Estimated engine torque, and longitudinal acceleration.

The first row and second row of Figure 4-5 show the estimated engine torque and the longitudinal acceleration, respectively. Again, the minor errors in estimated engine torque may be due to model uncertainty.

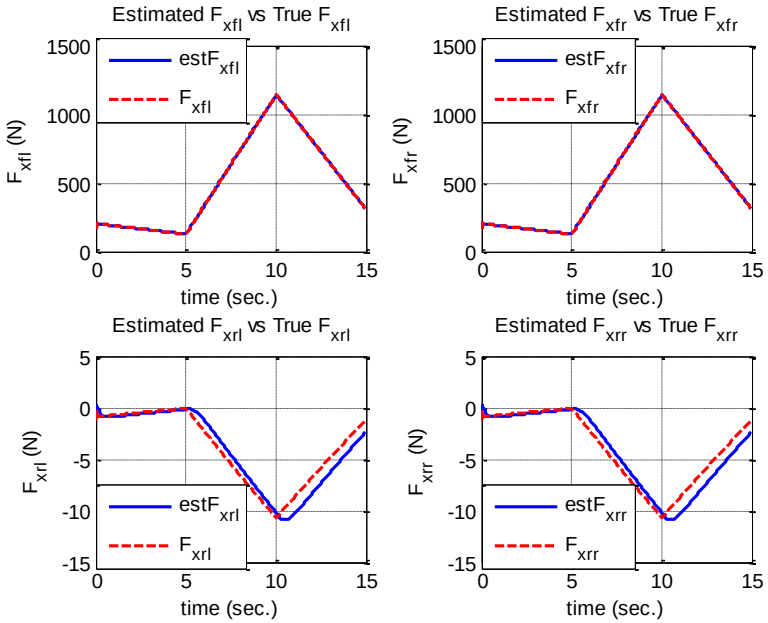

Figure 4-6 Estimated longitudinal forces vs true longitudinal forces.

After the longitudinal tire force and slip ratio have been estimated, then the tire road coefficient can be estimated using the algorithm in section 4.4.3.

4.8. Experimental Results

This section presents experimental evaluation of the estimation algorithms. In particular, evaluation of the longitudinal tire force estimation algorithm discussed in sections 4.5 and 4.7 and evaluation of the tire-road friction estimation algorithm discussed in section 4.4 are presented.

4.8.1. Test Vehicle and Experimental Set Up

The test vehicle used for the experimental evaluation is a Volvo XC90 sport utility vehicle. Vehicle testing was conducted at the Eaton Proving Ground in Marshall, Michigan. A MicroAutoBox from dSPACE is used for real-time data acquisition. A real-time GPS system, RT3000, from Oxford Technical Solutions is used to obtain absolute vehicle speed, slip angle and several other variables. The RT3000 is a full, six-axis inertial navigation system with integrated GPS and a Kalman filter that provides high frequency updates of the sensor bias, heading, and vehicle velocities. The GPS outputs were connected to the MicroAutoBox via CAN communication at the baud rate of 0.5 Mbits/sec. Engine torque, transmission gear ratio, wheel speeds and several other variables are obtained from the CAN bus signals already available on the CAN network of the Volvo XC90. The sampling time is set at 2 milliseconds. A photograph of the test vehicle is shown in Figure 4-7. Key vehicle parameters used in the estimation algorithms are $m = 2205$ kg, $D_a = 0.3693$, $I_w = 0.8$, and $r_{eff} = 0.3543$ m.

Figure 4-7 The Volvo XC90 test vehicle with GPS system.

4.8.2. Friction Estimation Using GPS and Torque Measurements

The longitudinal tire forces are estimated by algorithm described in section 4.5. In this test, the vehicle moves from a dry asphalt road to a gravel road surface. Consequently, a drop in friction coefficient occurs during the test. The drive torque which determines vehicle behavior during the test is shown in Figure 4-8b.

The estimated longitudinal tire forces for each wheel are shown in Figure 4-8a. Even though we do not know the true value of longitudinal tire forces, the estimated forces seem reasonable. The estimated forces of the front wheels agree roughly with the engine torque and longitudinal acceleration. Also, the estimated forces of the rear wheels are approximately zero as seen, because the vehicle used front wheel drive mode during the experiment.

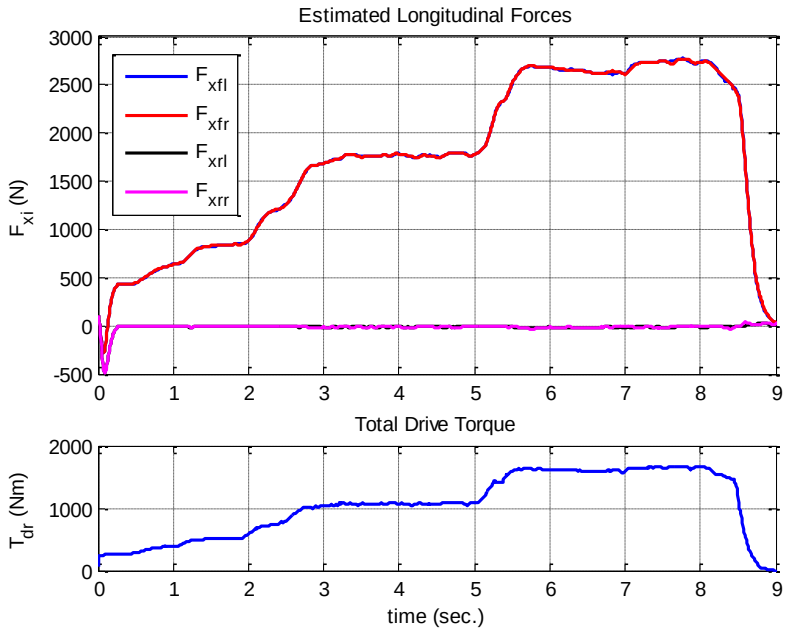

Figure 4-8 Drive torque and estimated longitudinal forces.

Figure 4-9 shows longitudinal speed, wheel speeds and acceleration. The change in friction coefficient occurred at about 6.5 seconds. At this point there is a jump in the front wheel speeds as seen in Figure 4-9.

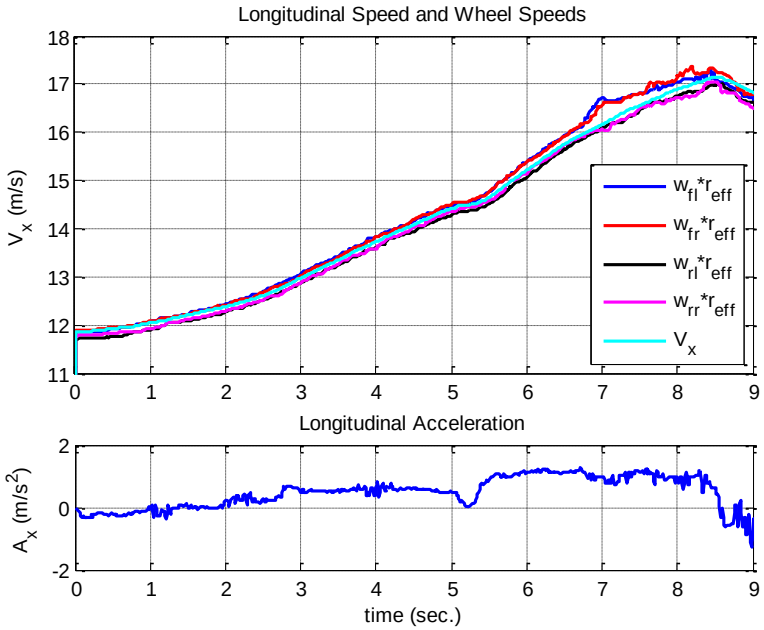

Figure 4-9 Longitudinal speed, wheel speeds, and longitudinal acceleration.

Next, we present the friction estimation experimental results. The friction coefficient is estimated using the algorithm as described in section 4.4. The system input is slip ratio computed by equation (4.6) or (4.7). The output is F_x/F_y. The normal force, F_z, is computed by equations (4.15) and (4.16). The longitudinal tire force is computed by algorithms in section 4.5.

The results of the friction estimation algorithm are shown in Figure 4-10. The first row of the figure presents the slip ratio vs normalized force of front left wheel and front right wheel. We do not show the slip ratio vs normalized force of rear left wheel and rear right wheel, since the vehicle is a front wheel drive vehicle. The longitudinal forces of rear wheels are approximately zero. The estimated slip slopes of front left wheel and front right wheel are presented in the second row of the figure. The figure shows that the estimated slip slopes of front left wheel and front right wheel converge from an initial guess value to the estimated slip slope value of about 32 for the first road surface and then converge to another estimated slip slope value of about 21 for the second road surface.

Using a linear relationship between the slip-slope and friction coefficient as described in section 4.4.5, the friction coefficient for the dry asphalt road is estimated to be 0.89 and for the gravel surface is estimated to be 0.56. It should be noted that the friction coefficient on dirt/gravel was found to vary between 0.5–0.7. However, the average value is distinctly different from that on dry asphalt and concrete.

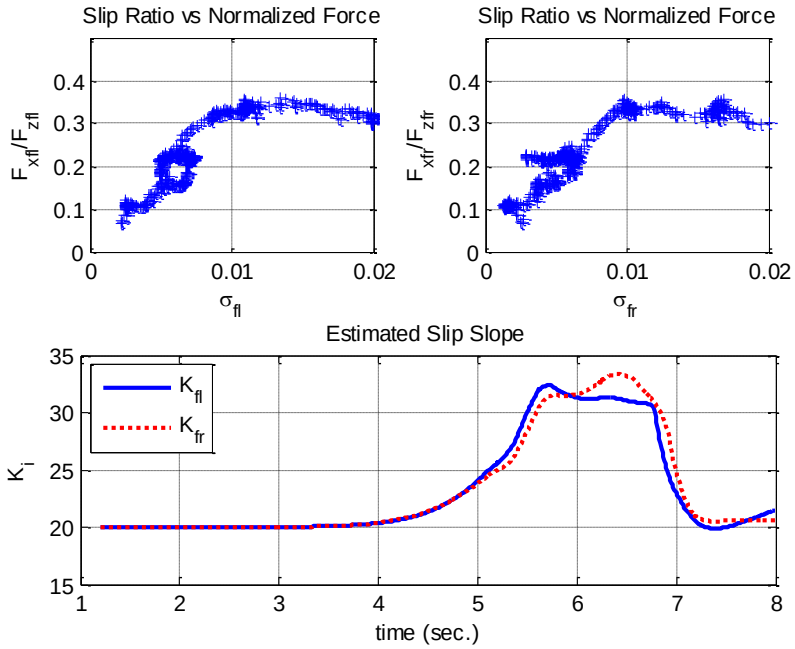

Figure 4-10 Step change in the friction coefficient experiment with acceleration during the transition.

4.8.3. Estimation Using GPS and an Accelerometer

In this section, the longitudinal tire forces are estimated by using wheel speeds and acceleration as described in section 4.7. In this test, the vehicle moved from a dry asphalt road surface to an icy surface. The vehicle decelerated due to braking during the road surface transition from asphalt to ice. The brake torque at the individual wheels were not measured and not available over the CAN bus of the vehicle. Hence the friction coefficient was estimated exclusively using GPS and accelerometer and wheel speed sensor signals.

The estimated longitudinal tire forces for each wheel and the estimated total brake torque are shown in Figure 4-11. The shape of the estimation force curves roughly tracks the

shape of the acceleration curves. Also if we compute total longitudinal tire force, the value of total forces is roughly close to the value of mass multiplied by acceleration after subtraction of drag force and rolling resistance force. The estimated forces therefore seem reasonable.

Figure 4-11 also shows that the longitudinal forces of the front wheels are larger than those of the rear wheels since the braking force distribution ratio between front and rear axles is 60:40.

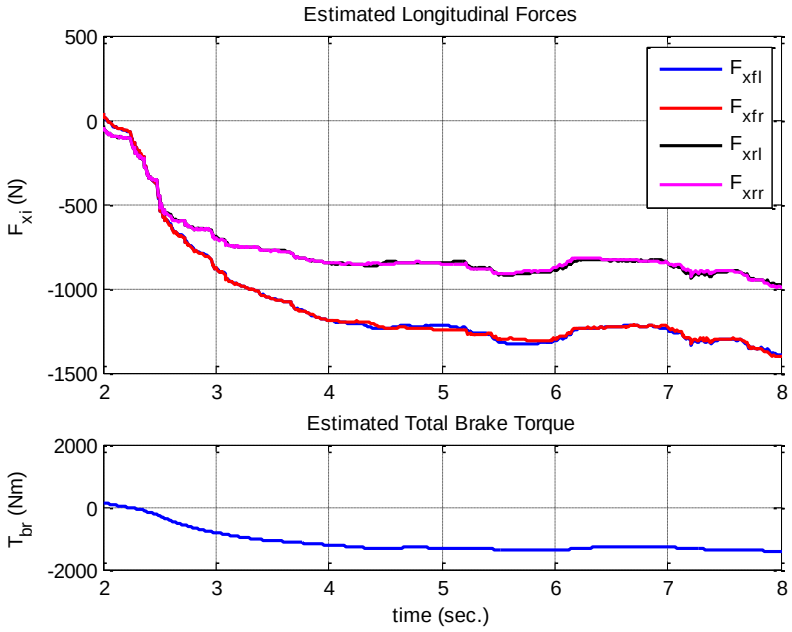

Figure 4-11 Estimated brake torque, and estimated longitudinal forces.

Figure 4-12 shows longitudinal speed, wheel speeds and acceleration. The change in friction coefficient occurred at about 4.5 seconds. At this point a dip in the front wheel speeds can be noticed.

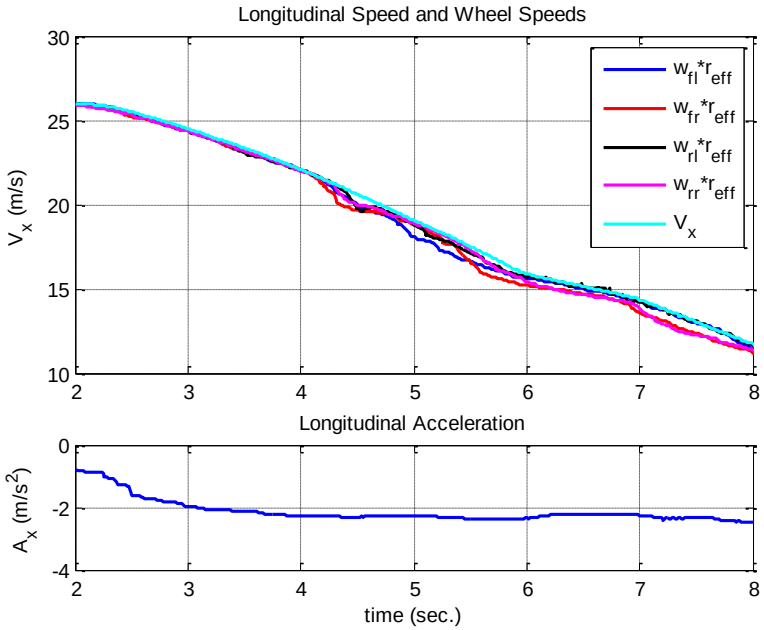

Figure 4-12 Longitudinal speed, wheel speeds, and longitudinal acceleration.

Next, the friction estimation experimental results will be evaluated by using algorithm as described in section 4.4.2.

Figure 4-13 presents the slip ratio vs normalized force for each wheel. The estimated slip slopes are presented in Figure 4-14.

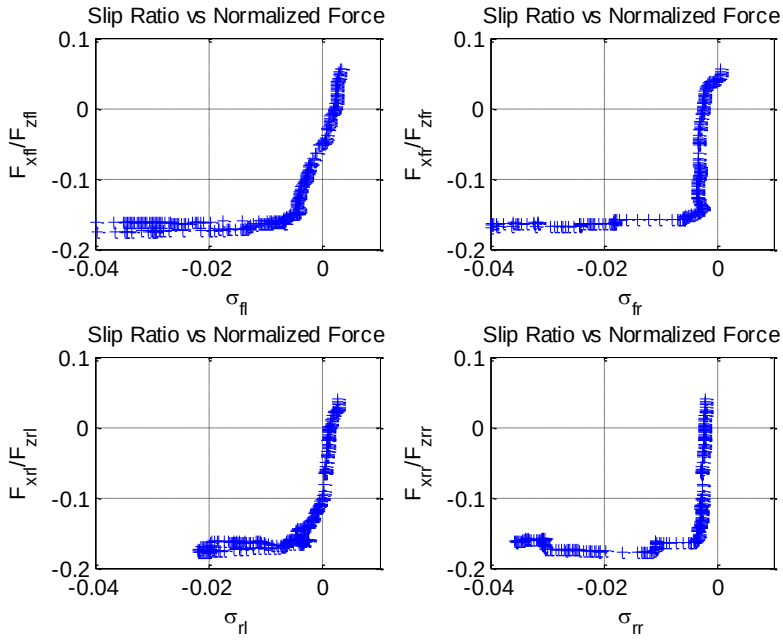

Figure 4-13 Step change in the friction coefficient experiment with deceleration during the transition.

4.8.4. Comparison of the Friction Coefficient Estimation Algorithms

Figure 4-14 shows that the estimated slip slopes of each wheel converges from the slip slope value of about 32.5 for the first road surface to the estimated slip slope value of about 5 for the second road surface. The estimated slip slopes of front wheels start to converge before the estimated slip slopes of the rear wheels. Thus the slip slopes can be reliably used to classify the friction coefficients of these 2 road surfaces.

Using the linear relationship between the slip-slope and friction coefficient described in section 4.8.4, the friction coefficient for the dry asphalt surface is seen to be approximately 0.89 and for ice to be 0.18.

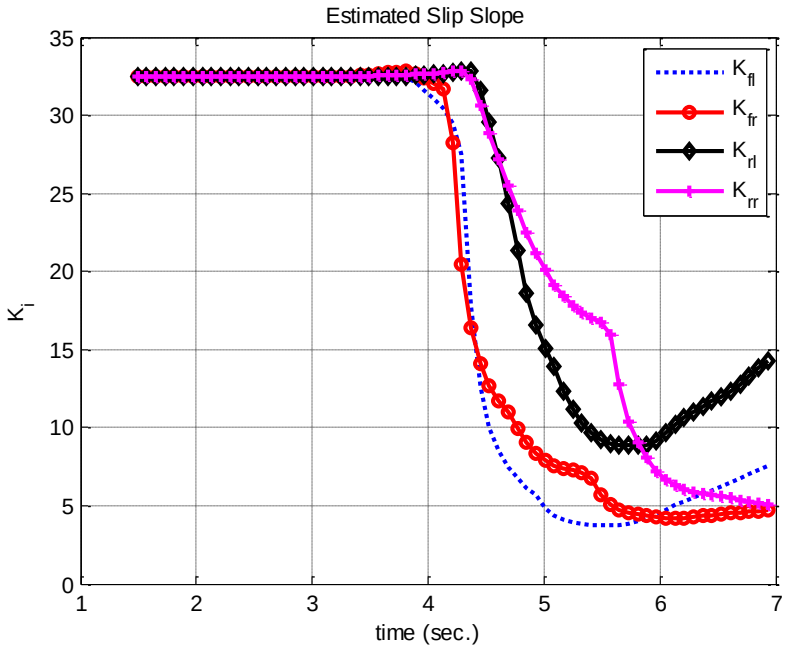

Figure 4-14 Step change in the friction coefficient experiment with deceleration during the transition.

The three friction coefficient estimation methods discussed in chapter 4 have different domains of applicability based on the set of sensors available for the estimation algorithm. However, Algorithm 2 (that utilizes torque measurements and an accelerometer) depends exclusively on aerodynamic drag to provide transient convergence. It is found to be unsuitable, since the aerodynamic drag coefficient is often not large enough to provide good transient performance. Between Algorithms 1 and 3, Algorithm 1 depends only on a wheel-level dynamic model. It involves a simpler computational algorithm and is found to be more accurate and to converge faster than Algorithm 3 which involves a vehicle-level fifth order dynamic model. For example, a comparison of the results in Figure 4-4 versus Figure 4-6 show that Algorithm 1 provides more accurate estimates of the longitudinal tire forces. However, wheel torque signal measurement may not be available in all applications, while GPS and accelerometer measurements could potentially be provided on all vehicles.

4.9. Sensitivity Analysis to Mass Change

4.9.1. Friction Estimation Algorithm Using GPS and Torque Measurements

The equations that include vehicle mass in the estimation algorithm are

$$F_{zf} = \frac{mgL_r - ma_x h - D_a v_x^2 h_a}{L}, \tag{4.38}$$

$$F_{zr} = \frac{mgL_f + ma_x h + D_a v_x^2 h_a}{L}. \tag{4.39}$$

Equations (4.38) and (4.39) are used to compute normal forces, F_{zi}. The longitudinal tire forces, F_{xi}, are computed by using the rotational dynamic equations. Subsequently, the normalized traction forces, μ, are computed:

$$\rho = \frac{F_x}{F_z} \tag{4.40}$$

The slip ratio depends on effective radius, longitudinal speed, and wheel speeds. The slip ratio is not sensitive to mass change.

To evaluate sensitivity to change in vehicle mass for this algorithm, the sensitivity of the normalized traction forces is first examined, followed by observing the sensitivity estimated slip slope to mass change.

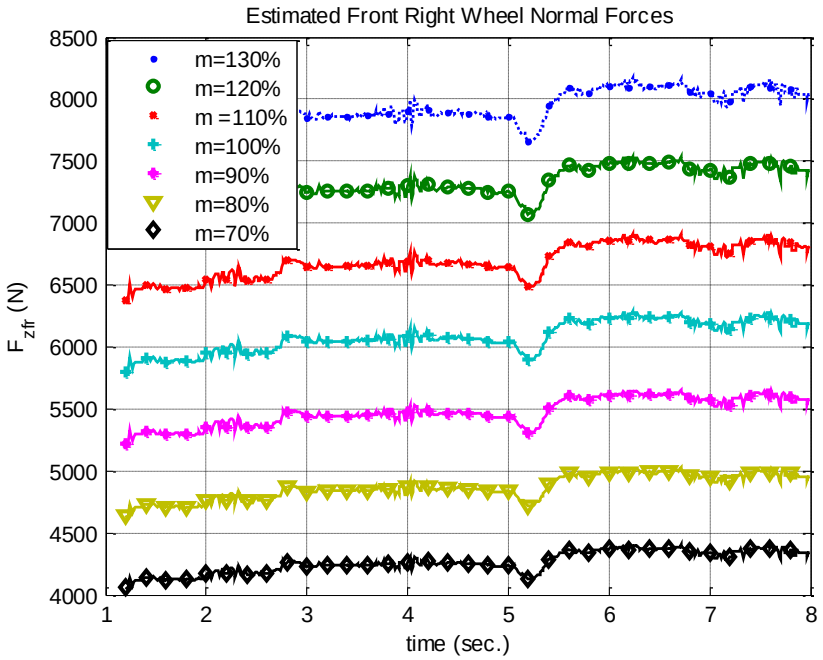

Figure 4-15 Estimate front right wheel normal forces.

Figure 4-15 shows the effect of mass change on normal forces. If a_x and D_a are neglected, the normal force is proportional to mass. The normal force increases when mass increases.

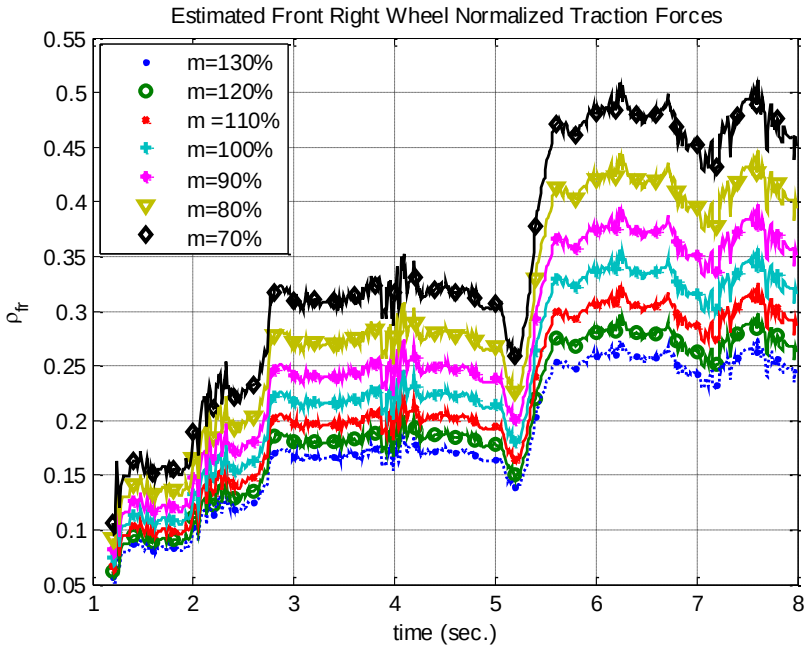

Figure 4-16 Estimated front right wheel normalized traction forces.

Figure 4-16 shows the effect of mass change on normalized traction forces. The normalized traction force is proportional to longitudinal tire force and inversely proportional to normal force. Since mass change affects only the normal force estimate in this algorithm, the normalized traction force changes when the normal force changes.

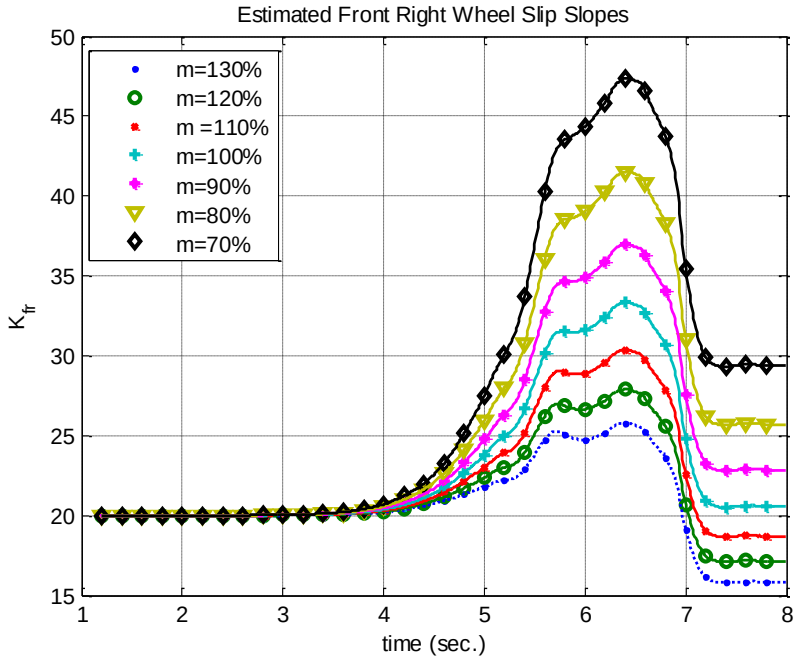

Figure 4-17 Estimated front right wheel slip slopes.

Figure 4-17 shows the effect of mass change on estimated slip slopes. The slip slope changes because the normalized traction forces change while the slip ratio values do not change. Thus this algorithm is seen to be very sensitive to mass change.

To improve the robustness of this algorithm, the value of vehicle mass could be updated in real-time. When the vehicle is first switched on, the vehicle mass can be estimated from Figure 4-17, assuming the road pavement is dry concrete and its friction coefficient is known. Subsequently, once the vehicle mass value has been updated, the algorithm will provide correct estimates of friction coefficient as the pavement surface changes.

4.9.2. Friction Estimation Algorithm Using GPS and an Accelerometer

The equations that include vehicle mass in the computation are

$$m\dot{v}_x = \left(F_{xfl} + F_{xfr} + F_{xrl} + F_{xrr}\right) - R_x - D_a v_x^2 + mgsin(\theta), \tag{4.41}$$

$$F_{zf} = \frac{mgL_r - ma_x h - D_a v_x^2 h_a}{L}, \tag{4.42}$$

$$F_{zr} = \frac{mgL_f + ma_x h + D_a v_x^2 h_a}{L}. \tag{4.43}$$

Equation (4.41) and the rotational dynamic equations are used to compute longitudinal tire forces. The normal forces, F_{zf} and F_{zr}, are computed from equations (4.42) and (4.43). Then the normalized traction forces, ρ, are computed. (The slip ratio does not depend on mass.)

To evaluate sensitivity of the estimation algorithm to mass change, first the sensitivity of the normalized traction forces is examined, followed by examining the sensitivity of the estimated slip slope.

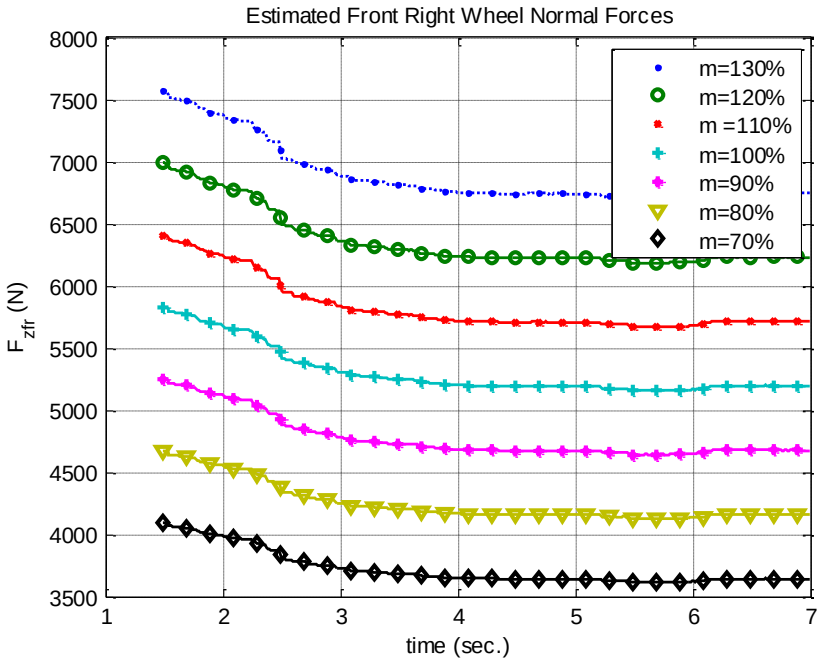

Figure 4-18 Estimate front right wheel normal forces.

Change in vehicle mass affects the normal forces, as shown in Figure 4-18.

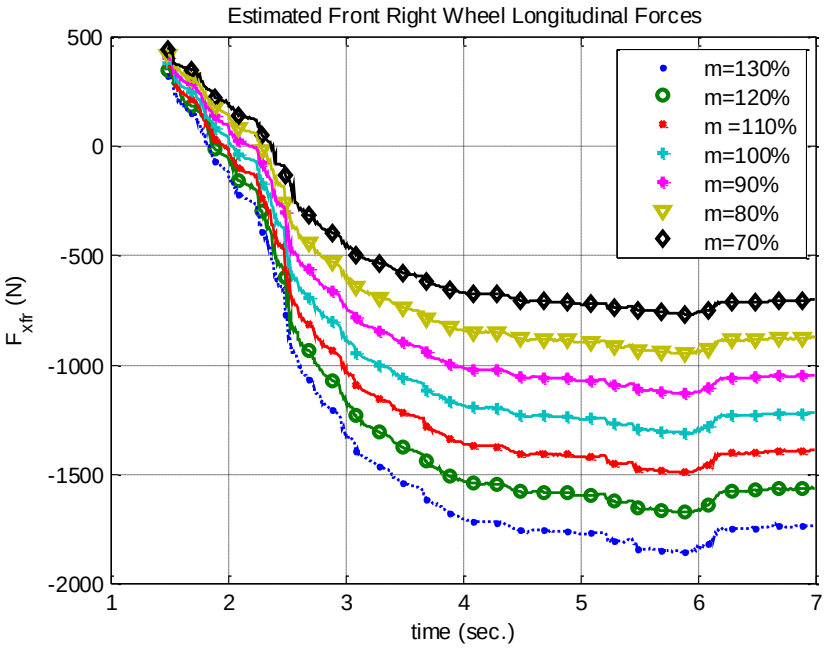

Figure 4-19 Estimated front right wheel longitudinal forces.

Figure 4-19 shows that mass change also affects the estimate of the longitudinal forces. If mass increases, the longitudinal forces will increase or if mass decreases, the normalized traction forces will decrease.

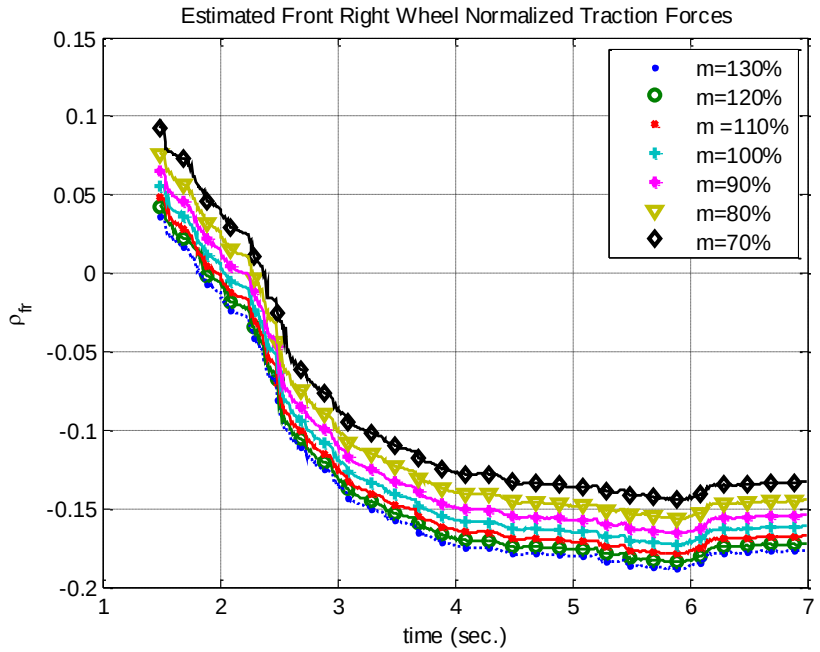

Figure 4-20 Estimated front right wheel normalized traction forces.

Figure 4-20 shows the effect of mass change on normalized traction forces. The normalized traction forces change only a little because when mass increases, longitudinal forces and normal forces both increase.

Since normalized traction forces change only a little, the slip slopes also change only a little. Figure 4-21 shows the effect of mass change on slip slopes. Thus, it can be concluded that this friction estimation algorithm is robust to changes in vehicle mass.

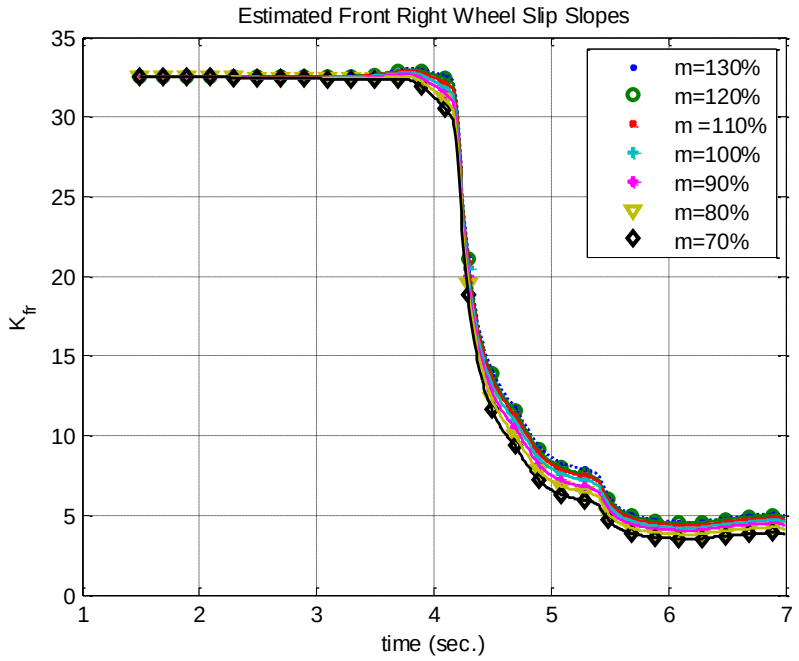

Figure 4-21 Estimated front right wheel slip slopes.

4.10. Conclusions

It has long been recognized in the automotive research community that knowledge of the real-time tire-road friction coefficient can be extremely valuable for active safety applications, including traction control, yaw stability control and rollover prevention. Previous research results in literature have focused on estimation of average friction coefficient for the vehicle or on average friction coefficient for both drive wheels of the vehicle. This dissertation is perhaps the first ever report to seriously undertake the

development of algorithms for reliable estimation of friction coefficient at each individual wheel of the vehicle.

Three different algorithms are proposed based on the types of sensors available – one that utilizes engine torque, brake torque and GPS measurements, one that utilizes torque measurements and an accelerometer and one that utilizes GPS measurements and an accelerometer. While GPS measurements are subject to long-time drop outs in urban environments, brake torque and engine torque signals may not be available on all cars. Thus, each of the three algorithms has different application domains.

The developed algorithms are first evaluated in simulation using industry standard simulation software CARSIM and then evaluated experimentally on a Volvo XC90 sport utility vehicle. Experimental results demonstrate that friction coefficients at the individual wheels and road gradient can both be estimated reliably. Individual wheel friction measurements are expected to be more valuable for active safety systems than average friction measurements.

Chapter 5

5. OBSERVER DESIGN FOR LIPSCHITZ NONLINEAR SYSTEMS USING RICCATI EQUATIONS

As described in Chapter 2, a nonlinear observer for a nonlinear system with complex nonlinearities is needed. Thus, four new nonlinear observers have been developed for this purpose. In this chapter, the nonlinear observer for Lipschitz nonlinear systems is presented.

5.1. Summary

This section presents a new observer design technique for Lipschitz nonlinear systems. Necessary and sufficient conditions for existence of a stable observer gain are developed using a S-Procedure Lemma. The developed condition is expressed in terms of the existence of a solution to an Algebraic Riccati Equation in one variable. Thus, the need to solve Linear Matrix Inequalities in multiple variables is eliminated. The advantage of the developed approach is that it is significantly less conservative than other previously published results for Lipschitz systems. It yields a stable observer for much larger Lipschitz constants than other techniques previously published in literature.

5.2. Introduction

For Linear Time Invariant (LTI) systems, the observer design problem is dual of the control system design problem. However, this is not the case for nonlinear systems. While the introduction of geometric techniques has led to great success in the development of controllers for nonlinear systems (Isidori, 1998, Khalil, 2001), it has not been possible to obtain results of wide applicability for state estimation. Early papers by Krener and Respondek (1985), Krener and Isidori (1983) and Xiao-Hua and Gao (1985) attempted to find a coordinate transformation so that the state estimation error dynamics were linear in the new coordinates. Necessary and sufficient conditions for the existence of such a coordinate transformation have been established but in practice are extremely difficult to satisfy.

There has been work by authors to propose observers for more specialized classes of nonlinear systems. These include results on observers for Lipschitz nonlinear systems (Thau, 1973, Kou, et. al., 1975, Raghavan and Hedrick 1992), results on sliding mode observers (Misawa, et. al., 1989), results for sector nonlinear systems (Arcak and Kokotovic, 2001), and results on observer based control for a fully linearizable nonlinear system (Esfandiari and Khalil (1992)). The extended Kalman Filter also continues to be used frequently as a deterministic observer for nonlinear systems (Reif and Unbehauen, 1996).

This section focuses on some new observer design results for the class of Lipschitz nonlinear systems. A major limitation of the existing results for Lipschitz nonlinear systems is that they work only for adequately small values of the Lipschitz constant. When the Lipschitz constant is large or when the equivalent Lipschitz constant has to be chosen large due to the non-Lipschitz nature of the nonlinearity, most existing observer design results fail to provide a solution. This section develops a solution methodology that works for significantly larger Lipschitz constants compared to exiting results. Furthermore, the methodology requires only an algebraic Riccati equation in one variable to be solved and does not require solving a multi-variable LMI problem. Thus the design procedure is easier to implement.

5.3. Problem Statement

This section presents an efficient methodology for designing observers for the class of nonlinear systems described by

$$\begin{aligned} \dot{x} &= Ax + Bu + \Phi(x,u), \\ y &= Cx \end{aligned} \tag{5.1}$$

where $x \in R^n$ is the state vector, $u \in R^p$ is the input vector, and $y \in R^m$ is the output measurement vector. $A \in R^{n\times n}$, $B \in R^{n\times p}$, and $C \in R^{m\times n}$ are appropriate matrices. The function $\Phi(x,u)$ is a Lipschitz nonlinearity with a Lipschitz constant, γ, i.e.

$$\|\Phi(x,u) - \Phi(\hat{x},u)\| \le \gamma\|x - \hat{x}\|, \qquad \forall x, \hat{x}, \qquad \gamma > 0 \tag{5.2}$$

To begin with, note that any nonlinear system of the form

$$\dot{x} = f(x,u) \tag{5.3}$$

can be expressed in the form of equation (5.1), as long as $f(x,u)$ is differentiable with respect to x. Further, many nonlinearities can be assumed to be Lipschitz, at least locally. For instance, the sinusoidal terms usually encountered in many problems in robotics are all globally Lipschitz. Even terms like x^2 can be regarded as Lipschitz provided we know that the operating range of x is bounded. Thus, the class of systems being considered in this dissertation is fairly general, with the linearity assumption being made only on the output vector, y.

The observer will be assumed to be of the form

$$\dot{\hat{x}} = A\hat{x} + Bu + \Phi(\hat{x},u) + L(y - C\hat{x}). \tag{5.4}$$

The estimation error dynamics are then seen to be given by

$$\dot{\tilde{x}} = (A - LC)\tilde{x} + \Phi(x,u) - \Phi(\hat{x},u) \tag{5.5}$$

where $\tilde{x} = x - \hat{x}$.

The Lyapunov function candidate for observer design is defined as

$$V = \tilde{x}^T P \tilde{x} \tag{5.6}$$

where $P > 0$ and $P \in R^{m \times n}$.

Its derivative is

$$\begin{aligned} \dot{V} = \tilde{x}^T[(A - LC)^T P + P(A - LC)]\tilde{x} + \tilde{x}^T P[\Phi(x,u) - \Phi(\hat{x},u)] \\ + [\Phi(x,u) - \Phi(\hat{x},u)]^T P \tilde{x}. \end{aligned} \tag{5.7}$$

This can be rewritten in matrix form as

$$\dot{V} = [\tilde{x}^T \quad \widetilde{\Phi}^T] \begin{bmatrix} (A - LC)^T P + P(A - LC) & P \\ P & 0 \end{bmatrix} \begin{bmatrix} \tilde{x} \\ \widetilde{\Phi} \end{bmatrix}. \tag{5.8}$$

where $\widetilde{\Phi} = \big(\Phi(x,u) - \Phi(\hat{x},u)\big)$.

5.4. Background Results

5.4.1. The S-Procedure Lemma

Lemma 1: The S-Procedure Lemma is as follows [**24**].

Let $V_0(x)$ and $V_1(x)$ be two arbitrary quadratic forms over R^n. Then $V_0(x) < 0$ for all $x \in R^n - \{0\}$ satisfying $V_1(x) \leq 0$ if and only if there exist $\varepsilon \geq 0$ such that

$$V_0(x) < \varepsilon V_1(x), \qquad \forall x \in R^n - \{0\}. \tag{5.9}$$

5.4.2. The Schur Inequality

Lemma 2: The Schur Inequality formula is as follows [**24**].

The linear matrix inequality (LMI)

$$\begin{bmatrix} Q & S \\ S^T & R \end{bmatrix} < 0, \qquad Q = Q^T, \qquad and\ R = R^T \tag{5.10}$$

is equivalent to one of the following conditions.

$$R < 0, \qquad Q - SR^{-1}S^T < 0 \tag{5.11}$$

or

$$Q < 0, \qquad R - S^T Q^{-1} S < 0 \tag{5.12}$$

5.5. Nonlinear Observer

5.5.1. Observer for Lipschitz Nonlinear Systems

Theorem 1: For the class of systems and observer forms described in equations (5.1)-(5.2) and (5.4), if an observer gain matrix can be chosen such that

$$\begin{bmatrix} (A - LC)^T P + P(A - LC) + \varepsilon\gamma^2 I & P \\ P & -\varepsilon I \end{bmatrix} < 0 \tag{5.13}$$

for some positive definite symmetric matrix P, then this choice of L leads to asymptotically stable estimates by the observer (5.4) for the system (5.1). Likewise, if there exists any symmetric positive definite matrix P such that the derivative of the

Lyapunov function, $\dot{V}$, in equation (5.8) is negative definite, then there also exists a matrix L such that equation (5.13) is satisfied. In this sense, equation (5.13) is both a necessary and sufficient condition for observer stability.

Proof: Suppose there exist matrices L and P which satisfy equation (5.13). Let this choice of L be used in the observer (5.4) for state estimation of the system given by (5.1).

Consider the traditional Lipschitz nonlinear system which satisfies

$$\|\Phi(x,u) - \Phi(\hat{x},u)\| \leq \gamma\|x - \hat{x}\|, \qquad \forall x, \hat{x}, \qquad \gamma > 0. \tag{5.14}$$

In this case, we find

$$[\Phi(x,u) - \Phi(\hat{x},u)]^T[\Phi(x,u) - \Phi(\hat{x},u)] \leq \gamma^2[x - \hat{x}]^T[x - \hat{x}]. \tag{5.15}$$

Hence

$$\begin{bmatrix}(x-\hat{x})^T & \left(\Phi(x,u) - \Phi(\hat{x},u)\right)^T\end{bmatrix}\begin{bmatrix}-\gamma^2 I & 0\\ 0 & I\end{bmatrix}\begin{bmatrix}(x-\hat{x})\\ \left(\Phi(x,u) - \Phi(\hat{x},u)\right)\end{bmatrix} \leq 0. \tag{5.16}$$

Thus the nonlinear function, $\Phi(x,u)$, satisfies an inequality of the type

$$\begin{bmatrix}(x-\hat{x})^T & \left(\Phi(x,u) - \Phi(\hat{x},u)\right)^T\end{bmatrix}M\begin{bmatrix}(x-\hat{x})\\ \left(\Phi(x,u) - \Phi(\hat{x},u)\right)\end{bmatrix} \leq 0 \tag{5.17}$$

where $M \in R^{2n\times 2n}$ is a symmetric matrix and is given by

$$M = \begin{bmatrix}-\gamma^2 I & 0\\ 0 & I\end{bmatrix}. \tag{5.18}$$

Applying the S-Procedure Lemma to equations (5.8) and (5.17), we find $\dot{V} < 0$ if and only if there exist $\varepsilon \geq 0$ such that

$$\begin{bmatrix}(A-LC)^T P + P(A-LC) & P\\ P & 0\end{bmatrix} - \varepsilon M < 0. \tag{5.19}$$

Hence the necessary and sufficient condition for observer design in this case is given by $\exists \varepsilon \geq 0$ such that

$$\begin{bmatrix}(A-LC)^T P + P(A-LC) + \varepsilon\gamma^2 I & P\\ P & -\varepsilon I\end{bmatrix} < 0. \tag{5.20}$$

Less Conservative Lipschitz Condition

It is possible to write equation (5.14) in the matrix form defined as

$$\|\Phi(x,u) - \Phi(\hat{x},u)\| \leq \|G(x-\hat{x})\|, \qquad \forall x, \hat{x}. \tag{5.21}$$

Note that the matrix G in this case could be a sparsely populated matrix. Hence $\|G(x-\hat{x})\|$ can be much smaller than the constant $\gamma\|x-\hat{x}\|$ used earlier in equation (5.2) for the same nonlinear function.

Illustrative Example for Less Conservative Lipschitz Condition

Let $\Phi(x,u)$ given by

$$\Phi(x,u) = \begin{bmatrix} 2\sin(x_1) \\ 0 \end{bmatrix}. \tag{5.22}$$

Then, apply the traditional Lipschitz condition for equation (5.22).

$$\left\| \begin{bmatrix} 2\sin(x_1) - 2\sin(\hat{x}_1) \\ 0 \end{bmatrix} \right\| \leq 2 \left\| \begin{bmatrix} x_1 - \hat{x}_1 \\ x_2 - \hat{x}_2 \end{bmatrix} \right\|, \qquad \forall x, \hat{x} \tag{5.23}$$

$$\sqrt{(2\sin(x_1) - 2\sin(\hat{x}_1))^2} \leq 2\sqrt{(x_1-\hat{x}_1)^2 + (x_2-\hat{x}_2)^2} \tag{5.24}$$

Next, apply the Less Conservative Lipschitz Condition for equation (5.22)

$$\left\| \begin{bmatrix} 2\sin(x_1) - 2\sin(\hat{x}_1) \\ 0 \end{bmatrix} \right\| \leq \left\| \begin{bmatrix} 2 & 0 \\ 0 & 0 \end{bmatrix} \begin{bmatrix} x_1 - \hat{x}_1 \\ x_2 - \hat{x}_2 \end{bmatrix} \right\|, \qquad \forall x, \hat{x} \tag{5.25}$$

$$\sqrt{(2\sin(x_1) - 2\sin(\hat{x}_1))^2} \leq 2\sqrt{(x_1-\hat{x}_1)^2} \tag{5.26}$$

It is clear that

$$2\sqrt{(x_1-\hat{x}_1)^2} \leq 2\sqrt{(x_1-\hat{x}_1)^2 + (x_2-\hat{x}_2)^2}. \tag{5.27}$$

Thus the bound (5.21) is less conservative than the bound (5.2).

The result brings us to the corollary to theorem 1.

Corollary to Theorem 1: For the class of systems and observer forms described in equations (5.1), (5.4) and (5.21), if an observer gain matrix *L* can be chosen such that

$$\begin{bmatrix} (A-LC)^T P + P(A-LC) + \varepsilon G^T G & P \\ P & -\varepsilon I \end{bmatrix} < 0 \tag{5.28}$$

for some positive definite symmetric matrix P, then this choice of L leads to asymptotically stable estimates by the observer (5.4) for the system (5.1).

The proof of the Corollary follows along the same lines as the proof of theorem 1, except for the definition of the Lipschitz condition. In this case, we use the Less Conservative Lipschitz condition.

5.5.2. Reformulation of Observer Design Using Riccati Equations

Equations (5.13) and (5.28) are LMIs involving two unknown matrices L and P. This equation can be replaced by a Riccati inequality in just one variable P. A necessary and sufficient condition in term of the existence of a solution to a Riccati inequality can be obtained. The following theorem summarizes the result.

Theorem 2: There exists an observer of the type given by equation (5.4) for the system given by equations (5.1) such that the error dynamics are quadratically stabilized if and only if there exist $\varepsilon > 0$ and $\beta \in R$ such that the following Riccati inequality has a symmetric positive definite solution P:

$$A^T P + PA + \varepsilon G^T G + \frac{1}{\varepsilon} PP - \beta^2 C^T C < 0 \tag{5.29}$$

The observer gain can then be chosen as

$$L = \frac{\beta^2}{2} P^{-1} C^T. \tag{5.30}$$

Proof: Applying the Schur Inequality (Lemma 2) to equation (5.28), the necessary and sufficient condition for observer design is

$$(A - LC)^T P + P(A - LC) + \varepsilon G^T G + \frac{1}{\varepsilon} PP < 0. \tag{5.31}$$

This can be re-written as

$$A^T P + PA + \varepsilon G^T G + \frac{1}{\varepsilon} PP - C^T L^T P - PLC < 0. \tag{5.32}$$

Note that equation (5.32) implies for all $\tilde{x}$ such that $C\tilde{x} = 0$, we must have $\tilde{x}^T \left(A^T P + PA + \varepsilon G^T G + \frac{1}{\varepsilon} PP \right) \tilde{x} < 0$. It also therefore follows that there must $\beta \in R$ sufficiently large such that $\tilde{x}^T \left(A^T P + PA + \varepsilon G^T G + \frac{1}{\varepsilon} PP \right) \tilde{x} - \beta^2 \tilde{x}^T C^T C \tilde{x} < 0$ for all $\tilde{x}(t)$.

Equation (5.29) is therefore a necessary condition. The fact that equation (5.29) is a sufficient condition can be proved as follows:

Let there exist a positive definite solution P to equation (5.29). Let the observer gain be chosen as

$$L = \frac{\beta^2}{2} P^{-1} C^T. \tag{5.33}$$

Then equation (5.29) can be rewritten as

$$A^T P + PA + \varepsilon G^T G + \frac{1}{\varepsilon} PP - C^T L^T P - PLC < 0 \tag{5.34}$$

which is the same as equation (5.32), thus proving the result.

5.6. Notes on Computation of *P* and *L*

5.6.1. Solution of LMI Inequality for *P* and *L*

The previous section has shown the necessary and sufficient conditions for observer design. The observer design by using theorems 1-2 needs to search for P and L to satisfy inequality (5.13) or (5.28). Solving the inequality by a numerical method would be an obvious approach. However, the inequalities (5.13) and (5.28) seem to be noncovex because each involves the product of the two variables P and L. Therefore, a simple change of variables that separates L from P needs to be made. Expand (5.13) to obtain

$$\begin{bmatrix} A^T P + PA - C^T L^T P - PLC + \varepsilon\gamma^2 I & P \\ P & -\varepsilon I \end{bmatrix} < 0, \qquad P > 0. \tag{5.35}$$

Now let $Y = PL$. Then the inequality (5.13) becomes

$$\begin{bmatrix} A^T P + PA - C^T Y^T - YC + \varepsilon\gamma^2 I & P \\ P & -\varepsilon I \end{bmatrix} < 0, \qquad P > 0. \tag{5.36}$$

Searching for P and L satisfying (5.13) is equivalent to searching for P and L satisfying (5.36). Once a feasible set of P and Y is found, L can be computed as $L = P^{-1}Y$. Note that $P > 0$ (or equivalently P is invertible) and that there is always a one to one mapping from Y to L for a given P.

In the same way, we can apply the change of variables to inequality (5.28). Then the inequality (5.28) become

$$\begin{bmatrix} A^T P + PA - C^T Y^T - YC + \varepsilon G^T G & P \\ P & -\varepsilon I \end{bmatrix} < 0, \qquad P > 0. \tag{5.37}$$

Hence, for a given ε and γ or G, the inequality (5.36), or (5.37), is affine with respect to its two variables P and Y. The corresponding feasibility problem can be solved using many standard convex optimization techniques or the MATLAB LMI control toolbox.

5.6.2. Solution of Algebraic Riccati Equation for *P* and *L*

The observer design by using theorem 2 involves solving for one unknown matrix, P, by providing ε, G, and β. Since P is the only unknown, it is easier to solve the Riccati inequality equation than to solve a LMI inequality.

Equation (5.29) can be modified as follows. Assume

$$A^T P + PA + \varepsilon G^T G + \frac{1}{\varepsilon} PP - \beta^2 C^T C = -\mu I < 0 \tag{5.38}$$

where $\mu > 0$, μ is a small value.

$$A^T P + PA + \varepsilon G^T G + \frac{1}{\varepsilon} PP - \beta^2 C^T C + \mu I = 0 \tag{5.39}$$

For give ε, G, β, and μ, the Riccati equality (5.39) can be easily solved. This equation may be solved with the MATLAB command "are":

$$X = ARE(a, b, c) \tag{5.40}$$

This returns the stabilizing solution (if it exists) to the continuous-time Riccati equation:

$$a'X + Xa - XbX + c = 0 \tag{5.41}$$

with b being symmetric and nonnegative definite and c being symmetric.

Rearrange the equation (5.39) to appropriate equation (5.41).

$$\underbrace{(-A^T)}_{a} P + P \underbrace{(-A)}_{a} - P \underbrace{(\frac{1}{\varepsilon} I)}_{b} P + \underbrace{(-\varepsilon G^T G + \beta^2 C^T C - \mu I)}_{c} = 0 \tag{5.42}$$

The Matlab function can now be used to find the solution.

5.7. Example Problems

5.7.1. Dynamic Model for a Flexible Link Robot

Consider a one link manipulator with revolute joints actuated by a DC motor. The elasticity of the joint can be well-modeled by a linear tensional spring [**25**]. The elastic coupling of the motor shaft to the link introduces an additional degree of freedom. The states of this system are motor position and velocity, and the link position and velocity.

The corresponding state-space model is

$$\begin{aligned} \dot{\theta}_m &= \omega_m \\ \dot{\omega}_m &= \frac{k}{J_m}(\theta_1 - \theta_m) - \frac{B}{J_m}\omega_m + \frac{K_\tau}{J_m}u \\ \dot{\theta}_1 &= \omega_1 \\ \dot{\omega}_1 &= -\frac{k}{J_1}(\theta_1 - \theta_m) - \frac{mgh}{J_1}\sin(\theta_1). \end{aligned} \tag{5.43}$$

with J_m being the inertia of the motor; J_1 the inertia of the link; θ_m the angular rotation of the motor; θ_1 the angular position of the link; ω_m the angular velocity of the motor; and ω_1 the angular velocity of the link.

Thus the system dynamics are nonlinear and of the form

$$\begin{aligned} \dot{x} &= Ax + Bu + \Phi(x), \\ y &= Cx \end{aligned} \tag{5.44}$$

where $x = [\theta_m \quad \omega_m \quad \theta_1 \quad \omega_1]^T$.

$$\begin{aligned} A &= \begin{bmatrix} 0 & 1 & 0 & 0 \\ -48.6 & -1.25 & 48.6 & 0 \\ 0 & 0 & 0 & 1 \\ 19.5 & 0 & -19.5 & 0 \end{bmatrix}, \qquad B = \begin{bmatrix} 0 \\ 21.6 \\ 0 \\ 0 \end{bmatrix}, \\ \Phi(x) &= \begin{bmatrix} 0 \\ 0 \\ 0 \\ -3.33\sin(x_3) \end{bmatrix}, \qquad C = \begin{bmatrix} 1 & 0 & 0 & 0 \\ 0 & 1 & 0 & 0 \end{bmatrix} \end{aligned} \tag{5.45}$$

The value of the Lipschitz constant for this system is $\gamma = 3.33$. The above parameters for the system are typical and have been taken from Spong [**25**].

Reference [**25**] presents a nonlinear I/O linearizing control law for this system. The control law guarantees closed-loop stability and tracking of any desired trajectory by the robotic link. However, this control law requires measurement of all the states. Physically, one can measure the motor position and velocity, but the measurement of the other states is non-trivial.

5.7.2. Observer Design for a Flexible Link Robot

In this section we present an observer for the above robotic system with guaranteed convergence of the state estimates.

Using Corollary to Theorem 1 on LMI based solution with $\varepsilon = 1$, an observer gain is found to be

$$L = \begin{bmatrix} 4.8710 & 2.7729 \\ 0.9774 & 60.2442 \\ 5.4689 & 12.8094 \\ 4.1360 & -13.1102 \end{bmatrix}. \tag{5.46}$$

The eigenvalues of $(A - LC)$ are

$$eig(A - LC) = \begin{bmatrix} -50.7854 \\ -9.5417 \\ -5.0855 \\ -0.9525 \end{bmatrix}. \tag{5.47}$$

Thus, the eigenvalues are well damped in this case. The response will show no transient oscillations. However, there is one small eigenvalue. So the estimated state will converge slowly to the actual state.

The robotic system with the above observer gain matrix was simulated under an open-loop excitation with being a sinusoid at 1 Hz. Figure 5-1 shows a comparison of actual and estimated link angular position. The actual system has an initial condition equal to 1 radian while the observer starts from an initial value of zero. Figure 5-2 shows actual and observer estimated link angular velocities. Both the estimated states converge to the correct values.

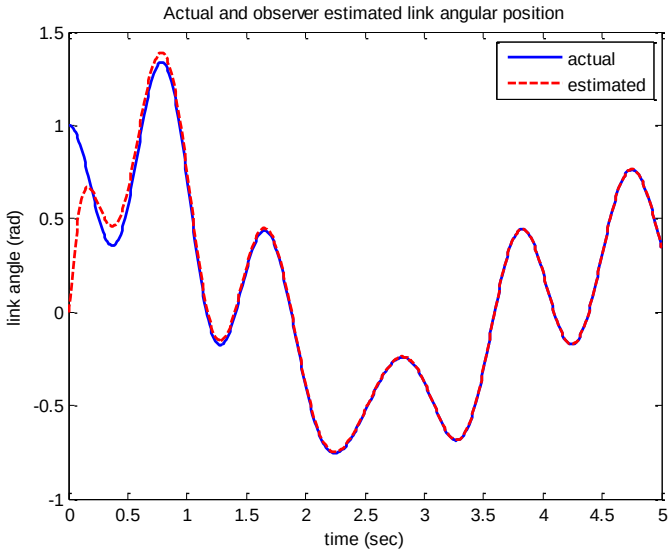

Figure 5-1 Actual and observer estimated link angular position (Corollary to Theorem 1).

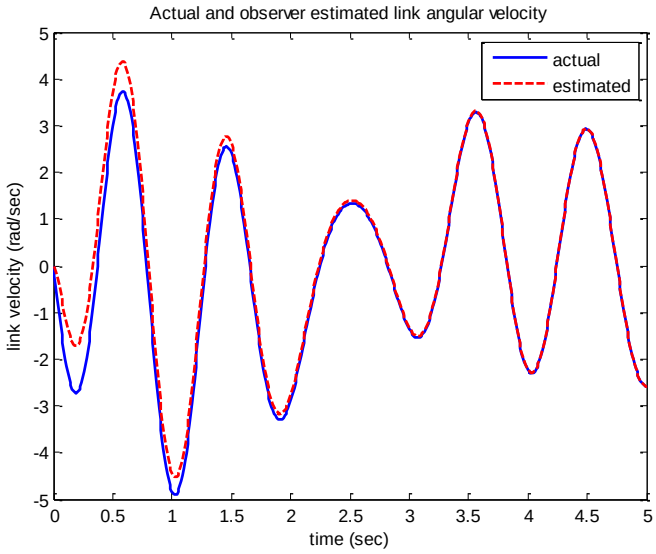

Figure 5-2 Actual and observer estimated link angular velocity (Corollary to Theorem 1).

Using theorem 2 on the Riccati based solution with $\varepsilon = 1$ and $\beta = 180$, an observer gain matrix is found to be

$$L = \begin{bmatrix} 78.9814 & -9.2259 \\ -9.2259 & 112.9897 \\ 10.0309 & 91.3947 \\ 14.2679 & 51.5085 \end{bmatrix}. \tag{5.48}$$

The eigenvalues of $(A - LC)$ are

$$eig(A - LC) = \begin{bmatrix} -71.6615 \\ -65.4807 + 34.5212i \\ -65.4807 - 34.5212i \\ -1.0914 \end{bmatrix}. \quad (5.49)$$

Thus, the eigenvalues have lower damping in this case. However, the overall eigenvalues are large. So the estimated states rapidly converge to the actual state and transient oscillations are not present. The transient performance is better than the previous LMI solution.

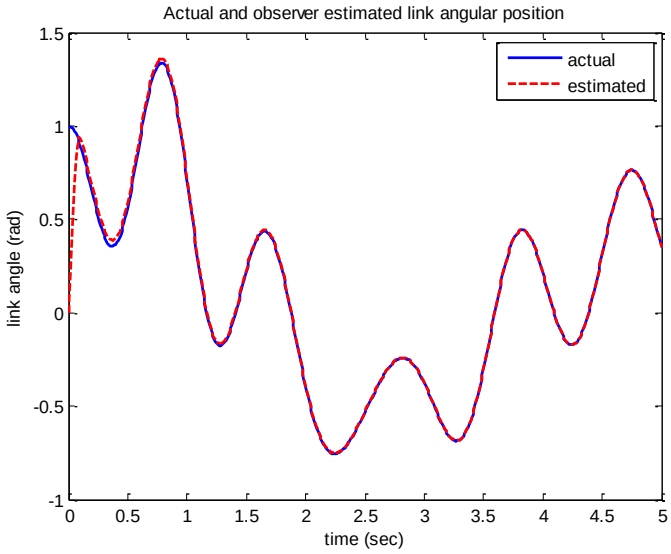

Figure 5-3 Actual and observer estimated link angular position (theorem 2).

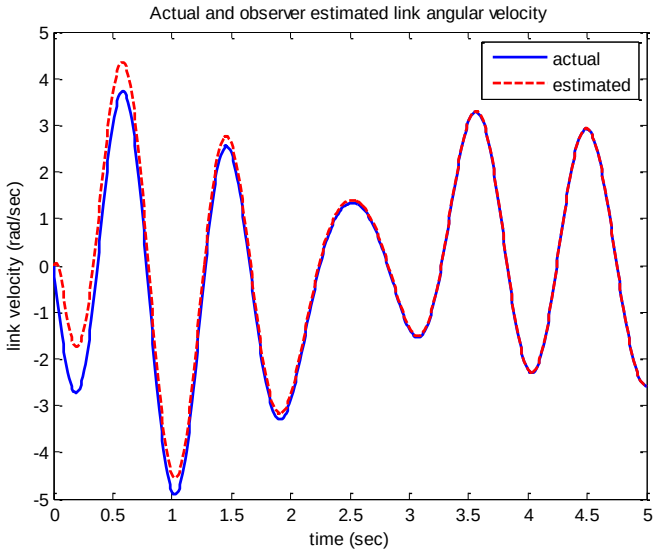

Figure 5-4 Actual and observer estimated link angular velocity (theorem 2).

5.7.3. Comparison of Observer Design Techniques

This section will compare observer design techniques in term of how conservative they are. We will examine which observer design techniques can deal with a larger Lipshitz constant. The problem in section 5.7.1 is reconsidered and we will keep the same plant equations. However, the nonlinearity will be scaled to increase the value of the Lipschitz constant for this system until the observer can no longer solve the problem when the Lipschitz constant is too large.

First, we find an observer gain by Theorem 1 which needs the solution of LMI Inequalities. Then, we use Theorem 2 to find an observer gain matrix by solving the corresponding Algebraic Riccati equation. Finally, the traditional standard LMI observer [**24**] as described below is used to find an observer gain matrix for comparison.

Standard LMI Observer

For the class of systems and observer forms described in equations (5.1) and (5.4), if an observer gain matrix can be chosen such that

$$\begin{bmatrix} (A-LC)^T P + P(A-LC) + I & P \\ P & -I/\gamma^2 \end{bmatrix} < 0 \qquad (5.50)$$

for some positive definite symmetric matrix P, then this choice of L leads to asymptotically stable estimates by the observer (5.4) for the system (5.1).

Table 5-1: Comparison of maximum Lipschitz constant for various observer design techniques

Method	Corollary to Theorem 1	Theorem 2	Standard LMI Observer
γ_{max}	48.5	48.4	0.99

Table 5-1 shows that the observer design techniques from corollary to theorem 1, and from theorem 2 can deal with a larger Lipshitz constant. They can solve the problem with a Lipshitz constant up to 48.4. On the other hand, the standard LMI observer can deal with the problem only for values of Lipshitz constant up to 0.99. Thus, the new observer design techniques are significantly less conservative than the traditional LMI technique.

5.8. Conclusions

This section presented a new observer design technique for Lipschitz nonlinear systems. Necessary and sufficient conditions for existence of a stable observer gain were developed using a S-Procedure Lemma. The developed condition was then expressed in terms of the existence of a solution to an Algebraic Riccati Equation in one variable. Thus, the need to solve Linear Matrix Inequalities in multiple variables was eliminated. The advantage of the developed approach is that it is significantly less conservative than other previously published results for Lipschitz systems. Using an illustrative example of a flexible joint robot, the developed observer design technique was found to yield a stable observer for much larger Lipschitz constants than a traditional LMI design technique.

Chapter 6

6. THE BOUNDED JACOBIAN APPROACH TO NONLINEAR OBSERVER DESIGN

As described earlier, a nonlinear observer for a nonlinear system with complex nonlinearities is needed. Thus, four new nonlinear observers have been developed for this purpose. In this chapter, the nonlinear observer using a bounded Jacobian approach is presented.

6.1. Summary

This chapter presents a new observer design technique for a nonlinear system with a globally (or locally) bounded Jacobian. The approach utilized is to use the mean value theorem to express the nonlinear error introductions as a convex combination of known matrices with time varying coefficients. The observer gains are then obtained by solving linear matrix inequalities (LMIs). The developed approach can enable observer design for a large class of differentiable nonlinear systems. Its advantage is that it enables easy observer design for a much wider range of operating conditions compared to linear or Lipschitz observer design methods. The developed theory is used successfully in the design of observers for vehicle systems involving complex nonlinearities. The use of the observer design technique is illustrated for estimation of longitudinal vehicle velocity in chapter 9 and roll angle in chapter 11. The performance of the new observer is shown to be clearly superior to that of a standard Lipschitz observer.

6.2. Introduction

This section focuses on a new observer design result for a nonlinear system with a locally or globally bounded Jacobian. A major limitation of the existing results for Lipschitz nonlinear systems is that they work only for adequately small values of the Lipschitz constant. When the equivalent Lipschitz constant has to be chosen large due to the inherent non-Lipschitz nature of the nonlinearity (such as in the case of aerointroduction drag force in vehicle systems), most existing observer design results fail to provide a

solution. This section develops a solution methodology that works well without requiring a small Lipschitz constant bound for the nonlinear function. The basic idea in this section is to use the mean value theorem (McLeod (1965) and Korobkov (2001)) to express the nonlinear error introductions as a convex combination of values of the derivatives of the nonlinear function. The observer gain guaranteeing the convergence of the proposed observer is easily computed by LMIs.

6.3. Problem Statement for Nonlinear Observer

This section presents an efficient methodology for designing observers for the class of nonlinear systems described by

$$\begin{aligned} \dot{x} &= Ax + \Phi(x) + g(y,u) \\ y &= Cx \end{aligned} \tag{6.1}$$

where $x \in R^n$ is the state vector, $u \in R^p$ is the input vector, and $y \in R^m$ is the output measurement vector. $A \in R^{n\times n}$ and $C \in R^{m\times n}$ are appropriate matrices. The functions $\Phi(x): R^n \to R^n$, and $g(y,u): R^m \times R^p \to R^n$ are nonlinear. In additional, $\Phi(x)$ is assumed to be differentiable.

The observer will be assumed to be of the form,

$$\dot{\hat{x}} = A\hat{x} + \Phi(\hat{x}) + g(y,u) + L(y - C\hat{x}). \tag{6.2}$$

The estimation error introductions are then seen to be given by

$$\begin{aligned} \dot{\tilde{x}} &= (A - LC)\tilde{x} + \big(\Phi(x) - \Phi(\hat{x})\big) \\ \dot{\tilde{x}} &= (A - LC)\tilde{x} + \widetilde{\Phi} \end{aligned} \tag{6.3}$$

where $\tilde{x} = x - \hat{x}$, $\widetilde{\Phi} = \Phi(x) - \Phi(\hat{x})$.

Let the Lyapunov function candidate for observer design be defined as

$$V = \tilde{x}^T P \tilde{x} \tag{6.4}$$

where $P > 0$ and $P \in R^{n\times n}$.

Then, its derivative is

$$\dot{V} = \tilde{x}^T[(A-LC)^T P + P(A-LC)]\tilde{x} + \tilde{x}^T P\tilde{\Phi} + \tilde{\Phi}^T P\tilde{x}. \quad (6.5)$$

6.4. Mean Value Theorem for Bounded Jacobian Systems

In this sub-section, we present a mathematical tools which are used subsequently to develop the observer gain in the next section. First, we present the scalar mean value theorem and the mean value theorem for vector functions. Then, we define the canonical basis for writing a vector function with a composition form. Lastly, we present a new modified form of the mean value theorem for vector functions.

Lemma 1: Scalar Mean Value Theorem

Let $f(x): R \to R$ be a function continuous on $[a,b] \subset R$ and differentiable on (a,b). For $x_1, x_2 \in [a,b,]$, there exist numbers $c \in (a,b)$ such that

$$f(x_2) - f(x_1) = \left.\frac{df}{dx}\right|_{x=c} \times (x_2 - x_1). \quad (6.6)$$

The equation (6.6) can also be rewritten as

$$f(x_2) - f(x_1) = \left(\delta_1 \left.\frac{df}{dx}\right|_{x=c_1} + \delta_2 \left.\frac{df}{dx}\right|_{x=c_1}\right)(x_2 - x_1), \quad \delta_1, \delta_2 > 0, \quad \delta_1 + \delta_2 = 1 \quad (6.7)$$

where $c_1, c_2 \in (a,b)$ and δ_1 and δ_2 are parameters that vary with the value of x_1 and x_2. The proof of this lemma is presented in [**26**].

Lemma 2: Mean Value Theorem for a Vector Function, [**27**]

Let $f(x): R^n \to R^n$ be a function continuous on $[a,b] \in R^n$ and differentiable on a convex hull of the set (a,b) with a Lipschitz continuous gradient ∇f. For $s_1, s_2 \in [a,b]$, there exists $c \in (a,b)$ such that

$$f(s_2) - f(s_1) = \nabla f(c)(s_2 - s_1). \quad (6.8)$$

However, we cannot directly use the mean value theorem of equation (6.8), since c is a varying parameter that continuously changes with the values of s_1 and s_2. Thus $\nabla f(c)$ is an unknown and changing matrix. We need to modify the mean value theorem before it can be utilized.

Lemma 3: Canonical Basis, [**28**]

Let a vector function be defined by:

$$f(x): R^n \to R^q. \tag{6.9}$$

Then,

$$f(x) = \left[f_1(x), f_2(x), \dots, f_q(x)\right]^T \tag{6.10}$$

where $f_i(x): R^n \to R$ is the i[th] component of $f(x)$ and $x \in R^n$.

Let the canonical basis of the vectorial space R^s for all $s \geq 1$ defined by:

$$E_s = \{e_s(i) | e_s(i) = (0, \dots, 0, 1, 0, \dots, 0)^T, \qquad i = 1, 2, \dots, s\}. \tag{6.11}$$

The vectorial space R^q is generated by the canonical basis E_q. Therefore, $f(x)$ can be written as:

$$f(x) = \sum_{i=1}^{q} e_q(i) f_i(x). \tag{6.12}$$

Now, we are ready to state and prove a modified form of the mean value theorem for a vector function.

Theorem 3: Modified Mean Value Theorem for a Vector Function

Let $f(x): R^n \to R^n$ be a function continuous on $[a, b] \in R^n$ and differentiable on convex hull of the set (a, b). For $s_1, s_2 \in [a, b]$, there exist δ_{ij}^{max} and δ_{ij}^{min} for $i = 1, \dots, n$ and $j = 1, \dots, n$ such that:

$$f(s_2) - f(s_1) = \left[\left(\sum_{i,j=1}^{n,n} H_{ij}^{max} \delta_{ij}^{max}\right) + \left(\sum_{i,j=1}^{n,n} H_{ij}^{min} \delta_{ij}^{min}\right)\right](s_2 - s_1), \qquad \delta_{ij}^{max}, \delta_{ij}^{min} \geq 0, \qquad \delta_{ij}^{max} + \delta_{ij}^{min} = 1 \tag{6.13}$$

where 1) $h_{ij}^{max} \geq max\left(\partial f_i / \partial x_j\right)$ and $h_{ij}^{min} \leq min\left(\partial f_i / \partial x_j\right)$ for $\forall x \in (a, b)$,

2) $H_{ij}^{max} = e_n(i) e_n^T(j) h_{ij}^{max}$ and $H_{ij}^{min} = e_n(i) e_n^T(j) h_{ij}^{min}$.

Proof: Lemma 2 shows that

$$f(s_2) - f(s_1) = \nabla f(c)(s_2 - s_1)$$
$$= \begin{bmatrix} \partial f_1/\partial x_1 & \partial f_1/\partial x_2 & \dots & \partial f_1/\partial x_n \\ \partial f_2/\partial x_1 & \partial f_2/\partial x_2 & \cdots & \partial f_2/\partial x_n \\ \vdots & \vdots & \vdots & \vdots \\ \partial f_n/\partial x_1 & \partial f_n/\partial x_2 & \cdots & \partial f_n/\partial x_n \end{bmatrix} ([s_2 - s_1]). \quad (6.14)$$

Lemma 1 shows that each derivative function can be replaced with a convex combination of 2 values of the derivative of the function. Hence, the derivative function, $\partial f_i(c)/\partial x_j$, can be replaced with

$$\frac{\partial f_i}{\partial x_j}(c) = \delta_{ij}^{max} \frac{\partial f_i}{\partial x_j}(\Omega) + \delta_{ij}^{min} \frac{\partial f_i}{\partial x_j}(\lambda), \quad \delta_{ij}^{max}, \delta_{ij}^{min} \geq 0, \qquad \delta_{ij}^{max} + \delta_{ij}^{min} = 1 \quad (6.15)$$

where $\Omega = (\Omega_1, \Omega_2, \dots, \Omega_n)$ and $\lambda = (\lambda_1, \lambda_2, \dots, \lambda_n)$. $c, \Omega, \lambda \in (a, b)$.

To satisfy lemma 1, the values of $\partial f_i(\Omega)/\partial x_j$ and $\partial f_i(\lambda)/\partial x_j$ need to be chosen such that

$$\frac{\partial f_i}{\partial x_j}(\Omega) = h_{ij}^{max} \geq max\left(\frac{\partial f_i}{\partial x_j}\right), \text{and } \frac{\partial f_i}{\partial x_j}(\lambda) = h_{ij}^{min} \leq min\left(\frac{\partial f_i}{\partial x_j}\right). \quad (6.16)$$

Note: One can easily show that if either $h_{ij}^{max} < max(df_i/dx_j)$ or $h_{ij}^{min} > min(df_i/dx_j)$ for $\forall x \in (a, b)$, then there are no $\delta_{ij}^{max}$and δ_{ij}^{min} that will satisfy equation (6.15) with the constraints $\delta_{ij}^{max}, \delta_{ij}^{min} \geq 0$ and $\delta_{ij}^{max} + \delta_{ij}^{min} = 1$.

Then, the equation (6.15) can be rewritten as

$$\frac{\partial f_i}{\partial x_j}(c) = \delta_{ij}^{max} h_{ij}^{max} + \delta_{ij}^{min} h_{ij}^{min}, \quad \delta_{ij}^{max}, \delta_{ij}^{min} \geq 0, \qquad \delta_{ij}^{max} + \delta_{ij}^{min} = 1 \quad (6.17)$$

where $h_{ij}^{max} \geq max(\partial f_i/\partial x_j)$ and $h_{ij}^{min} \leq min(\partial f_i/\partial x_j)$. Note: $\delta_{ij}^{max}, \delta_{ij}^{min}$ are parameters that vary with the value of s_1 and s_2. Hence, the equation (6.14) can be rewritten as

$$f(s_2)-f(s_1)=\begin{bmatrix}\delta_{11}^{max}h_{11}^{max} & \delta_{12}^{max}h_{12}^{max} & \dots & \delta_{1n}^{max}h_{1n}^{max}\\ \delta_{21}^{max}h_{21}^{max} & \delta_{22}^{max}h_{22}^{max} & \dots & \delta_{2n}^{max}h_{2n}^{max}\\ \vdots & \vdots & \vdots & \vdots\\ \delta_{n1}^{max}h_{n1}^{max} & \delta_{n2}^{max}h_{n2}^{max} & \dots & \delta_{nn}^{max}h_{nn}^{max}\end{bmatrix}([s_2-s_1])$$
$$+\begin{bmatrix}\delta_{11}^{min}h_{11}^{min} & \delta_{12}^{min}h_{12}^{min} & \dots & \delta_{1n}^{min}h_{1n}^{min}\\ \delta_{21}^{min}h_{21}^{min} & \delta_{22}^{min}h_{22}^{min} & \dots & \delta_{2n}^{min}h_{2n}^{min}\\ \vdots & \vdots & \vdots & \vdots\\ \delta_{n1}^{min}h_{n1}^{min} & \delta_{n2}^{min}h_{n2}^{min} & \dots & \delta_{nn}^{min}h_{nn}^{min}\end{bmatrix}([s_2-s_1]). \tag{6.18}$$

Use the canonical basis from lemma 3. Then $f(s_2)-f(s_1)$ can be written as

$$f(s_2)-f(s_1)=\left[\left(\sum_{i,j=1}^{n,n}H_{ij}^{max}\delta_{ij}^{max}\right)+\left(\sum_{i,j=1}^{n,n}H_{ij}^{min}\delta_{ij}^{min}\right)\right](s_2-s_1),$$
$$\delta_{ij}^{max},\delta_{ij}^{min}\geq 0,\qquad \delta_{ij}^{max}+\delta_{ij}^{min}=1 \tag{6.19}$$

where $H_{ij}^{max}=e_n(i)e_n^T(j)h_{ij}^{max}$ and $H_{ij}^{min}=e_n(i)e_n^T(j)h_{ij}^{min}$.

Illustrative Example for Theorem 3

The following is a 2 dimensional example of the application of the mean value theorem for a higher-dimensional function. Let $f(s)\colon R^2\to R^2$ be define by:

$$f(s)=[f_1(s)\quad f_2(s)]^T. \tag{6.20}$$

If we set $s_1=[s_{11},s_{12}]^T$ and $s_2=[s_{21},s_{22}]^T$, then

$$f(s_2)-f(s_1)=\nabla f(c)(s_2-s_1)$$
$$=\begin{bmatrix}\begin{bmatrix}max\left(\frac{\partial f_1}{\partial x_1}\right) & 0\\ 0 & 0\end{bmatrix}\delta_{11}^{max}+\begin{bmatrix}min\left(\frac{\partial f_1}{\partial x_1}\right) & 0\\ 0 & 0\end{bmatrix}\delta_{11}^{min}\\ +\begin{bmatrix}0 & max\left(\frac{\partial f_1}{\partial x_2}\right)\\ 0 & 0\end{bmatrix}\delta_{12}^{max}+\begin{bmatrix}0 & min\left(\frac{\partial f_1}{\partial x_2}\right)\\ 0 & 0\end{bmatrix}\delta_{12}^{min}\\ +\begin{bmatrix}0 & 0\\ max\left(\frac{\partial f_2}{\partial x_1}\right) & 0\end{bmatrix}\delta_{21}^{max}+\begin{bmatrix}0 & 0\\ min\left(\frac{\partial f_2}{\partial x_1}\right) & 0\end{bmatrix}\delta_{21}^{min}\\ +\begin{bmatrix}0 & 0\\ 0 & max\left(\frac{\partial f_2}{\partial x_2}\right)\end{bmatrix}\delta_{22}^{max}+\begin{bmatrix}0 & 0\\ 0 & min\left(\frac{\partial f_2}{\partial x_2}\right)\end{bmatrix}\delta_{22}^{min}\end{bmatrix}$$
$$\times\left(\begin{bmatrix}s_{21}\\ s_{22}\end{bmatrix}-\begin{bmatrix}s_{11}\\ s_{12}\end{bmatrix}\right) \tag{6.21}$$

or

$$f(s_2) - f(s_1) = \begin{bmatrix} H_{11}^{max}\delta_{11}^{max} + H_{11}^{min}\delta_{11}^{min} \\ +H_{12}^{max}\delta_{12}^{max} + H_{12}^{min}\delta_{12}^{min} \\ +H_{21}^{max}\delta_{21}^{max} + H_{21}^{min}\delta_{21}^{min} \\ +H_{22}^{max}\delta_{22}^{max} + H_{22}^{min}\delta_{22}^{min} \end{bmatrix} \times \left(\begin{bmatrix} s_{21} \\ s_{22} \end{bmatrix} - \begin{bmatrix} s_{11} \\ s_{12} \end{bmatrix} \right), \qquad (6.22)$$
$$\delta_{ij}^{max}, \delta_{ij}^{min} \geq 0, \qquad \delta_{ij}^{max} + \delta_{ij}^{min} = 1$$

where $H_{ij}^{max} = e_n(i)e_n^T(j)h_{ij}^{max}$, $H_{ij}^{min} = e_n(i)e_n^T(j)h_{ij}^{min}$, $h_{ij}^{max} \geq max\left(\partial f_i/\partial x_j\right)$ and $h_{ij}^{min} \leq min\left(\partial f_i/\partial x_j\right)$.

6.5. Nonlinear Observer

Theorem 4: Bounded Jacobian Observer for General Problems [**22**]

For the class of systems and observer forms described in equations (6.1) and (6.2), if an observer gain matrix L can be chosen such that

$$\begin{gathered} P\left(A + \bar{H}_{ij}^{max}\right) + \left(A + \bar{H}_{ij}^{max}\right)^T P - C^T L^T P - PLC < 0 \\ P\left(A + \bar{H}_{ij}^{min}\right) + \left(A + \bar{H}_{ij}^{min}\right)^T P - C^T L^T P - PLC < 0 \\ P > 0 \\ \forall i = 1, \dots, n \text{ , and } \forall j = 1, \dots, n \end{gathered} \qquad (6.23)$$

where 1) $h_{ij}^{max} \geq max\left(\partial \Phi_i/\partial x_j\right)$ and $h_{ij}^{min} \leq min\left(\partial \Phi_i/\partial x_j\right)$,

2) $H_{ij}^{max} = e_n(i)e_n^T(j)h_{ij}^{max}$ and $H_{ij}^{min} = e_n(i)e_n^T(j)h_{ij}^{min}$,

3) $z_H = n \times n$ is the state scaling factor, n being dimension of the state vector,

4) $\bar{H}_{ij}^{max} = z_H H_{ij}^{max}$ and $\bar{H}_{ij}^{min} = z_H H_{ij}^{min}$,

then this choice of L leads to asymptotically stable estimates by the observer (6.2) for the system (6.1).

Proof: The derivative of the Lyapunov function is

$$\dot{V} = \tilde{x}^T[(A - LC)^T P + P(A - LC)]\tilde{x} + \tilde{x}^T P\tilde{\Phi} + \tilde{\Phi}^T P\tilde{x}. \qquad (6.24)$$

The nonlinear terms can be rewritten using theorem 3 as

$$\tilde{\Phi} = [\Phi(x) - \Phi(\hat{x})\,]$$
$$= \left[\left(\sum_{i,j=1}^{n,n} H_{ij}^{max}\delta_{ij}^{max}\right) + \left(\sum_{i,j=1}^{n,n} H_{ij}^{min}\delta_{ij}^{min}\right)\right][x - \hat{x}], \tag{6.25}$$
$$\delta_{ij}^{max}, \delta_{ij}^{min} \geq 0, \qquad \delta_{ij}^{max} + \delta_{ij}^{min} = 1.$$

To simplify the form of the final result, we need to scale $\sum_{i,j=1}^{n,n}\left(\delta_{ij}^{max} + \delta_{ij}^{min}\right)$ to one. In the general problem, if all the terms in $\partial\Phi_i/\partial x_j$ are to be considered and not zero, then the scaling factors, z_H is computed by

$$\sum_{i,j=1}^{n,n}\left(\delta_{ij}^{max} + \delta_{ij}^{min}\right) = n \times n = z_H, \quad \frac{\sum_{i,j=1}^{n,n}\left(\delta_{ij}^{max} + \delta_{ij}^{min}\right)}{z_H} = 1 \tag{6.26}$$

Rewrite equation (6.25) as

$$\tilde{\Phi} = \left[\left(\sum_{i,j=1}^{n,n} \bar{H}_{ij}^{max}\bar{\delta}_{ij}^{max}\right) + \left(\sum_{i,j=1}^{n,n} \bar{H}_{ij}^{min}\bar{\delta}_{ij}^{min}\right)\right][x - \hat{x}],$$
$$\bar{\delta}_{ij}^{max}, \bar{\delta}_{ij}^{min} \geq 0, \bar{\delta}_{ij}^{max} + \bar{\delta}_{ij}^{min} = 1/z_H, \sum_{i,j=1}^{n,n}\left(\bar{\delta}_{ij}^{max} + \bar{\delta}_{ij}^{min}\right) = 1, \tag{6.27}$$

where 1) $\bar{H}_{ij}^{max} = z_H H_{ij}^{max}$ and $\bar{H}_{ij}^{min} = z_H H_{ij}^{min}$,

2) $\bar{\delta}_{ij}^{max} = \delta_{ij}^{max}/z_H$ and $\bar{\delta}_{ij}^{min} = \delta_{ij}^{min}/z_H$.

Then, the derivative of the Lyapunov function becomes

$$\dot{V} = \tilde{x}^T \left[\begin{array}{c} (A-LC)^T P + P(A-LC) \\ + \left[\left(\sum_{i,j=1}^{n,n} \bar{H}_{ij}^{max}\bar{\delta}_{ij}^{max}\right)^{\mathrm{T}} + \left(\sum_{i,j=1}^{n,n} \bar{H}_{ij}^{min}\bar{\delta}_{ij}^{min}\right)^{\mathrm{T}}\right] P \\ + P\left[\left(\sum_{i,j=1}^{n,n} \bar{H}_{ij}^{max}\bar{\delta}_{ij}^{max}\right) + \left(\sum_{i,j=1}^{n,n} \bar{H}_{ij}^{min}\bar{\delta}_{ij}^{min}\right)\right] \end{array}\right] \tilde{x} \tag{6.28}$$

$$\dot{V} = \tilde{x}^T \begin{bmatrix} \left((A - LC) + \left(\sum_{i,j=1}^{n,n} \bar{H}_{ij}^{max} \bar{\delta}_{ij}^{max} \right) + \left(\sum_{i,j=1}^{n,n} \bar{H}_{ij}^{min} \bar{\delta}_{ij}^{min} \right) \right)^T P \\ + P \left((A - LC) + \left(\sum_{i,j=1}^{n,n} \bar{H}_{ij}^{max} \bar{\delta}_{ij}^{max} \right) + \left(\sum_{i,j=1}^{n,n} \bar{H}_{ij}^{min} \bar{\delta}_{ij}^{min} \right) \right) \end{bmatrix} \tilde{x} \tag{6.29}$$

Since $\sum_{i,j=1}^{n,n} \left(\bar{\delta}_{ij}^{max} + \bar{\delta}_{ij}^{min} \right) = 1$, equation (6.29) can be rewritten as

$$\dot{V} = \tilde{x}^T \begin{bmatrix} \sum_{i,j=1}^{n,n} \bar{\delta}_{ij}^{max} \{ (A - LC)^T P + \bar{H}_{ij}^{max^T} P \} \\ + \sum_{i,j=1}^{n,n} \bar{\delta}_{ij}^{min} \{ (A - LC)^T P + \bar{H}_{ij}^{min^T} P \} \\ + \sum_{i,j=1}^{n,n} \bar{\delta}_{ij}^{max} \{ P(A - LC) + P \bar{H}_{ij}^{max} \} \\ + \sum_{i,j=1}^{n,n} \bar{\delta}_{ij}^{min} \{ P(A - LC) + P \bar{H}_{ij}^{min} \} \end{bmatrix} \tilde{x}. \tag{6.30}$$

$$\dot{V} = \tilde{x}^T M \tilde{x} = \tilde{x}^T \begin{bmatrix} \sum_{i,j=1}^{n,n} \bar{\delta}_{ij}^{max} \{ \left(A + \bar{H}_{ij}^{max} - LC \right)^T P + P \left(A + \bar{H}_{ij}^{max} - LC \right) \} \\ + \sum_{i,j=1}^{n,n} \bar{\delta}_{ij}^{min} \{ \left(A + \bar{H}_{ij}^{min} - LC \right)^T P + P \left(A + \bar{H}_{ij}^{min} - LC \right) \} \end{bmatrix} \tilde{x}. \tag{6.31}$$

Hence we need

$$M < 0 \tag{6.32}$$

where $\bar{\delta}_{ij}^{max}$, $\bar{\delta}_{ij}^{min} \geq 0$. However, it is not possible to directly solve equation (6.32) for L and P because $\bar{\delta}_{ij}^{max}$, $\bar{\delta}_{ij}^{min}$ are time varying coefficients. Hence, we transform equation (6.32) to equations (6.33) and (6.34).

$$P \left(A + \bar{H}_{ij}^{max} \right) + \left(A + \bar{H}_{ij}^{max} \right)^T P - C^T L^T P - PLC < 0, \tag{6.33}$$

$$P \left(A + \bar{H}_{ij}^{min} \right) + \left(A + \bar{H}_{ij}^{min} \right)^T P - C^T L^T P - PLC < 0, \tag{6.34}$$

for $\forall i = 1, \dots, n$, and $\forall j = 1, \dots, n$.

Then if equation (6.33) and (6.34) satisfy the condition, equation (6.32) will automatically satisfy the condition.

Corollary to Theorem 4: Bounded Jacobian Observer for Specified Problems

For the class of systems and observer forms described in equations (6.1) and (6.2), if an observer gain matrix L can be chosen such that

$$\begin{gathered} P\left(A + \bar{H}_{ij}^{max}\right) + \left(A + \bar{H}_{ij}^{max}\right)^T P - C^T L^T P - PLC < 0 \\ P\left(A + \bar{H}_{ij}^{min}\right) + \left(A + \bar{H}_{ij}^{min}\right)^T P - C^T L^T P - PLC < 0 \\ P > 0 \\ \forall i = 1, \dots, n \text{ , and } \forall j = 1, \dots, n \end{gathered} \tag{6.35}$$

where 1) $h_{ij}^{max} \geq max\left(\partial \Phi_i / \partial x_j\right)$ and $h_{ij}^{min} \leq min\left(\partial \Phi_i / \partial x_j\right)$,

2) $H_{ij}^{max} = e_n(i) e_n^T(j) h_{ij}^{max}$ and $H_{ij}^{min} = e_n(i) e_n^T(j) h_{ij}^{min}$,

3) $\bar{z}_H = n \times n - w_H$ is the state scaling factor, n being dimension of the state vector, w_H being the number of terms in $\partial \Phi_i / \partial x_j$ that equals zero,

4) $\bar{H}_{ij}^{max} = \bar{z}_H H_{ij}^{max}$ and $\bar{H}_{ij}^{min} = \bar{z}_H H_{ij}^{min}$.

then this choice of L leads to asymptotically stable estimates by the observer (6.2) for the system (6.1).

Proof: The proof of the Corollary follows along the same lines as the proof of theorem 4, except for the definition of the scaling factor $\bar{z}_H$.

In the general problem, if all of terms in $\partial \Phi_i / \partial x_j$ are not zero, then $\sum_{i,j=1}^{n,n} \left(\delta_{ij}^{max} + \delta_{ij}^{min}\right) = n \times n = z_H$. However, if in some problem, there exist $\partial \Phi_i / \partial x_j = 0$, then $\sum_{i,j=1}^{n,n} \left(\delta_{ij}^{max} + \delta_{ij}^{min}\right)$ is less than z_H. We need to define new scaling factor, $\bar{z}_H$.

$$\sum_{i,j=1}^{n,n} \left(\delta_{ij}^{max} + \delta_{ij}^{min}\right) = n \times n - w_H = \bar{z}_H \tag{6.36}$$

where w_H is number of terms in $\partial\Phi_i/\partial x_j$ that equals zero. Now, we use $\bar{z}_H$ instead of z_H to complete the proof.

6.6. Conclusions

In this section, a new observer design technique is developed for a nonlinear system with a locally or globally bounded Jacobian. The approach is developed in order to deal with differentiable nonlinear systems. The observer gains can be obtained by solving LMIs. The developed theory is used successfully in the design of observers for vehicle systems involving complex nonlinearities. The use of the observer design technique is illustrated for estimation of longitudinal vehicle velocity in chapter 9 and roll angle in chapter 11. The performance of the new observer is shown to be clearly superior to that of a standard Lipschitz observer.

Chapter 7

7. THE EXTENDED BOUNDED JACOBIAN APPROACH TO OBSERVER DESIGN FOR NONLINEAR SYSTEMS WITH NONLINEAR MEASUREMENT EQUATION

As described earlier, a nonlinear observer for a nonlinear system with complex nonlinearities is needed. Thus, four new nonlinear observers have been developed for this purpose. In this chapter, the nonlinear observer for systems with a nonlinear function in the measurement equation is presented.

7.1. Summary

This chapter extends the result in the chapter 6 and presents another new observer design technique for a nonlinear system with a globally (or locally) bounded Jacobian. This observer also can be applied for a nonlinear system with nonlinear measurement model. The approach utilized is to use the mean value theorem to express the nonlinear error introductions as a convex combination of known matrices with time varying coefficients. The observer gains are then obtained by solving linear matrix inequalities (LMIs). The developed approach can enable observer design for a large class of differentiable nonlinear systems. Its advantage is that it enables easy observer design for a much wider range of operating conditions compared to linear or Lipschitz observer design methods. The developed theory is used successfully in the design of observers for vehicle systems involving complex nonlinearities. The use of the observer design technique is illustrated for estimation of body slip angle in chapter 10.

7.2. Problem Statement for Nonlinear Observer

This chapter presents an efficient methodology for designing observers for the class of nonlinear systems described by

$$\begin{aligned} \dot{x} &= Ax + \Phi(x) + g(y,u), \\ y &= Cx + \Psi(x) \end{aligned} \tag{7.1}$$

where $x \in R^n$ is the state vector, $u \in R^p$ is the input vector, and $y \in R^m$ is the output measurement vector. $A \in R^{n\times n}$ and $C \in R^{m\times n}$are appropriate matrices. The functions $\Phi(x): R^n \to R^n$, $\Psi(x): R^n \to R^m$, and $g(y,u): R^m \times R^p \to R^n$ are nonlinear. In addition, $\Phi(x)$ and $\Psi(x)$ are assumed to be differentiable.

The observer will be assumed to be of the form

$$\begin{aligned} \dot{\hat{x}} &= A\hat{x} + \Phi(\hat{x}) + g(y,u) + L(y - \hat{y}) \\ \hat{y} &= C\hat{x} + \Psi(\hat{x}). \end{aligned} \tag{7.2}$$

The estimation error introductions are then seen to be given by

$$\dot{\tilde{x}} = (A - LC)\tilde{x} + \widetilde{\Phi} - L\widetilde{\Psi} \tag{7.3}$$

where $\tilde{x} = x - \hat{x}$, $\widetilde{\Phi} = \Phi(x) - \Phi(\hat{x})$, and $\widetilde{\Psi} = \Psi(x) - \Psi(\hat{x})$.

Let the Lyapunov function candidate for observer design be defined as

$$V = \tilde{x}^T P \tilde{x}. \tag{7.4}$$

where $P > 0$ and $P \in R^{n\times n}$. Then, its derivative is

$$\dot{V} = \tilde{x}^T[(A - LC)^T P + P(A - LC)]\tilde{x} + \tilde{x}^T P\widetilde{\Phi} + \widetilde{\Phi}^{\mathrm{T}} P\tilde{x} - \tilde{x}^T PL\widetilde{\Psi} - \widetilde{\Psi}^{\mathrm{T}} L^T P\tilde{x}. \tag{7.5}$$

7.3. Mean Value Theorem for Bounded Jacobian Systems

The mathematical tools which are used subsequently to develop the observer gain in the next section are the same as one in the chapter 6 section 6.4. So, we will not repeat them again.

7.4. Nonlinear Observer

Theorem 5: Bounded Jacobian Observer for General Problem

For the class of systems and observer forms described in equations (7.1) and (7.2), if an observer gain matrix L can be chosen such that

$$\begin{gathered}
P\left(A+\bar{H}_{ij}^{max}\right)+\left(A+\bar{H}_{ij}^{max}\right)^{T}P-\left(C+\bar{G}_{kj}^{max}\right)^{T}L^{T}P-PL\left(C+\bar{G}_{kj}^{max}\right)<0\\
P\left(A+\bar{H}_{ij}^{max}\right)+\left(A+\bar{H}_{ij}^{max}\right)^{T}P-\left(C+\bar{G}_{kj}^{min}\right)^{T}L^{T}P-PL\left(C+\bar{G}_{kj}^{min}\right)<0\\
P\left(A+\bar{H}_{ij}^{min}\right)+\left(A+\bar{H}_{ij}^{min}\right)^{T}P-\left(C+\bar{G}_{kj}^{max}\right)^{T}L^{T}P-PL\left(C+\bar{G}_{kj}^{max}\right)<0\\
P\left(A+\bar{H}_{ij}^{min}\right)+\left(A+\bar{H}_{ij}^{min}\right)^{T}P-\left(C+\bar{G}_{kj}^{min}\right)^{T}L^{T}P-PL\left(C+\bar{G}_{kj}^{min}\right)<0\\
P>0\\
\forall i=1,\dots,n\,,\forall j=1,\dots,n \text{ and } \forall k=1,\dots,m
\end{gathered} \tag{7.6}$$

where 1) $h_{ij}^{max}\geq max\left(\partial\Phi_i/\partial x_j\right)$ and $h_{ij}^{min}\leq min\left(\partial\Phi_i/\partial x_j\right)$,

2) $H_{ij}^{max}=e_n(i)e_n^T(j)h_{ij}^{max}$ and $H_{ij}^{min}=e_n(i)e_n^T(j)h_{ij}^{min}$,

3) $z_H=n\times n$ is the state scaling factor, n being dimension of the state vector,

4) $\bar{H}_{ij}^{max}=z_H H_{ij}^{max}$ and $\bar{H}_{ij}^{min}=z_H H_{ij}^{min}$,

5) $g_{kj}^{max}\geq max\left(\partial\Psi_k/\partial x_j\right)$ and $g_{kj}^{min}\leq min\left(\partial\Psi_k/\partial x_j\right)$,

6) $G_{kj}^{max}=e_n(k)e_n^T(j)g_{kj}^{max}$ and $G_{kj}^{min}=e_n(k)e_n^T(j)g_{kj}^{min}$,

7) $z_G=m\times n$ is the output scaling factor, m being dimension of the output vector,

8) $\bar{G}_{kj}^{max}=z_G G_{kj}^{max}$ and $\bar{G}_{kj}^{min}=z_G G_{kj}^{min}$,

then this choice of L leads to asymptotically stable estimates by the observer (7.2) for the system (7.1).

Proof: The derivative of the Lyapunov function is

$$\dot{V}=\tilde{x}^T[(A-LC)^TP+P(A-LC)]\tilde{x}+\tilde{x}^TP\tilde{\Phi}+\tilde{\Phi}^{\mathrm{T}}P\tilde{x}-\tilde{x}^TPL\tilde{\Psi}-\tilde{\Psi}^{\mathrm{T}}L^TP\tilde{x}. \tag{7.7}$$

The nonlinear terms can be rewritten using theorem 3 as

$$\begin{aligned}
\tilde{\Phi}&=[\Phi(x)-\Phi(\hat{x})\,]\\
&=\left[\left(\sum_{i,j=1}^{n,n}H_{ij}^{max}\delta_{ij}^{max}\right)+\left(\sum_{i,j=1}^{n,n}H_{ij}^{min}\delta_{ij}^{min}\right)\right][x-\hat{x}], \qquad (7.8)\\
&\qquad \delta_{ij}^{max},\delta_{ij}^{min}\geq 0, \qquad \delta_{ij}^{max}+\delta_{ij}^{min}=1\\
\tilde{\Psi}&=[\Psi(x)-\Psi(\hat{x})\,] \qquad (7.9)
\end{aligned}$$

$$= \left[\left(\sum_{k,j=1}^{m,n} G_{kj}^{max}\gamma_{kj}^{max}\right) + \left(\sum_{k,j=1}^{m,n} G_{kj}^{min}\gamma_{kj}^{min}\right)\right][x - \hat{x}],$$

$$\gamma_{kj}^{max}, \gamma_{kj}^{min} \geq 0, \qquad \gamma_{kj}^{max} + \gamma_{kj}^{min} = 1$$

To simplify the form of the final result, we need to scale $\sum_{i,j=1}^{n,n}\left(\delta_{ij}^{max} + \delta_{ij}^{min}\right)$ and $\sum_{k,j=1}^{m,n}\left(\gamma_{kj}^{max} + \gamma_{kj}^{min}\right)$ to one. In the general problem, if all the terms in $\partial\Phi_i/\partial x_j$ and $\partial\Psi_k/\partial x_j$ are to be considered and not zero, then the scaling factors, z_H and z_G are computed by

$$\begin{aligned}
&\sum_{i,j=1}^{n,n}\left(\delta_{ij}^{max} + \delta_{ij}^{min}\right) = n \times n = z_H, \ \frac{\sum_{i,j=1}^{n,n}\left(\delta_{ij}^{max} + \delta_{ij}^{min}\right)}{z_H} = 1 \\
&\sum_{k,j=1}^{m,n}\left(\gamma_{kj}^{max} + \gamma_{kj}^{min}\right) = m \times n = z_G, \ \frac{\sum_{k,j=1}^{m,n}\left(\gamma_{kj}^{max} + \gamma_{kj}^{min}\right)}{z_G} = 1
\end{aligned} \tag{7.10}$$

Rewrite equation (7.8) and (7.9) as

$$\begin{aligned}
\widetilde{\Phi} &= \left[\left(\sum_{i,j=1}^{n,n} \bar{H}_{ij}^{max}\bar{\delta}_{ij}^{max}\right) + \left(\sum_{i,j=1}^{n,n} \bar{H}_{ij}^{min}\bar{\delta}_{ij}^{min}\right)\right][x - \hat{x}], \\
&\bar{\delta}_{ij}^{max}, \bar{\delta}_{ij}^{min} \geq 0, \bar{\delta}_{ij}^{max} + \bar{\delta}_{ij}^{min} = 1/z_H, \sum_{i,j=1}^{n,n}\left(\bar{\delta}_{ij}^{max} + \bar{\delta}_{ij}^{min}\right) = 1,
\end{aligned} \tag{7.11}$$

$$\begin{aligned}
\widetilde{\Psi} &= \left[\left(\sum_{k,j=1}^{m,n} \bar{G}_{kj}^{max}\bar{\gamma}_{kj}^{max}\right) + \left(\sum_{k,j=1}^{m,n} \bar{G}_{kj}^{min}\bar{\gamma}_{kj}^{min}\right)\right][x - \hat{x}], \\
&\bar{\gamma}_{kj}^{max}, \bar{\gamma}_{kj}^{min} \geq 0, \ \bar{\gamma}_{kj}^{max} + \bar{\gamma}_{kj}^{min} = 1/z_G, \sum_{k,j=1}^{m,n}\left(\bar{\gamma}_{kj}^{max} + \bar{\gamma}_{kj}^{min}\right) = 1
\end{aligned} \tag{7.12}$$

where 1) $\bar{H}_{ij}^{max} = z_H H_{ij}^{max}$ and $\bar{H}_{ij}^{min} = z_H H_{ij}^{min}$,

2) $\bar{\delta}_{ij}^{max} = \delta_{ij}^{max}/z_H$ and $\bar{\delta}_{ij}^{min} = \delta_{ij}^{min}/z_H$,

3) $\bar{G}_{kj}^{max} = z_G G_{kj}^{max}$ and $\bar{G}_{kj}^{min} = z_G G_{kj}^{min}$,

4) $\bar{\gamma}_{kj}^{max} = \gamma_{kj}^{max}/z_G$, and $\bar{\gamma}_{kj}^{min} = \gamma_{kj}^{min}/z_G$.

Then, the derivative of the Lyapunov function becomes

$$\dot{V} = \tilde{x}^T \begin{bmatrix} (A-LC)^T P + P(A-LC) \\ -\left[\left(\sum_{k,j=1}^{m,n} \bar{G}_{kj}^{max} \bar{\gamma}_{kj}^{max}\right)^{\mathrm{T}} + \left(\sum_{k,j=1}^{m,n} \bar{G}_{kj}^{min} \bar{\gamma}_{kj}^{min}\right)^{\mathrm{T}}\right] L^T P \\ -PL\left[\left(\sum_{k,j=1}^{m,n} \bar{G}_{kj}^{max} \bar{\gamma}_{kj}^{max}\right) + \left(\sum_{k,j=1}^{m,n} \bar{G}_{kj}^{min} \bar{\gamma}_{kj}^{min}\right)\right] \\ +\left[\left(\sum_{i,j=1}^{n,n} \bar{H}_{ij}^{max} \bar{\delta}_{ij}^{max}\right)^{\mathrm{T}} + \left(\sum_{i,j=1}^{n,n} \bar{H}_{ij}^{min} \bar{\delta}_{ij}^{min}\right)^{\mathrm{T}}\right] P \\ +P\left[\left(\sum_{i,j=1}^{n,n} \bar{H}_{ij}^{max} \bar{\delta}_{ij}^{max}\right) + \left(\sum_{i,j=1}^{n,n} \bar{H}_{ij}^{min} \bar{\delta}_{ij}^{min}\right)\right] \end{bmatrix} \tilde{x} \qquad (7.13)$$

Since $\sum_{i,j=1}^{n,n}\left(\bar{\delta}_{ij}^{max} + \bar{\delta}_{ij}^{min}\right) = 1$, equation (7.13) can be rewritten as

$$\dot{V} = \tilde{x}^T \begin{bmatrix} \sum_{i,j=1}^{n,n} \bar{\delta}_{ij}^{max} \{(A-LC)^T P + \bar{H}_{ij}^{max^T} P \\ -\left(\sum_{k,j=1}^{m,n} \bar{G}_{kj}^{max} \bar{\gamma}_{kj}^{max}\right)^{\mathrm{T}} L^T P - \left(\sum_{k,j=1}^{m,n} \bar{G}_{kj}^{min} \bar{\gamma}_{kj}^{min}\right)^{\mathrm{T}} L^T P\} \\ + \sum_{i,j=1}^{n,n} \bar{\delta}_{ij}^{min} \{(A-LC)^T P + \bar{H}_{ij}^{min^T} P \\ -\left(\sum_{k,j=1}^{m,n} \bar{G}_{kj}^{max} \bar{\gamma}_{kj}^{max}\right)^{\mathrm{T}} L^T P - \left(\sum_{k,j=1}^{m,n} \bar{G}_{kj}^{min} \bar{\gamma}_{kj}^{min}\right)^{\mathrm{T}} L^T P\} \\ + \sum_{i,j=1}^{n,n} \bar{\delta}_{ij}^{max} \{P(A-LC) + P\bar{H}_{ij}^{max} \\ -PL\left(\sum_{k,j=1}^{m,n} \bar{G}_{kj}^{max} \bar{\gamma}_{kj}^{max}\right) - PL\left(\sum_{k,j=1}^{m,n} \bar{G}_{kj}^{min} \bar{\gamma}_{kj}^{min}\right)\} \\ + \sum_{i,j=1}^{n,n} \bar{\delta}_{ij}^{min} \{P(A-LC) + P\bar{H}_{ij}^{min} \\ -PL\left(\sum_{k,j=1}^{m,n} \bar{G}_{kj}^{max} \bar{\gamma}_{kj}^{max}\right) - PL\left(\sum_{k,j=1}^{m,n} \bar{G}_{kj}^{min} \bar{\gamma}_{kj}^{min}\right)\} \end{bmatrix} \tilde{x}. \qquad (7.14)$$

$$\dot{V} = \tilde{x}^T M \tilde{x}$$

$$= \tilde{x}^T \left[\begin{array}{l} \sum_{i,j=1}^{n,n} \bar{\delta}_{ij}^{max} \{ (A-LC)^T P + \bar{H}_{ij}^{max^T} P + P(A-LC) + P\bar{H}_{ij}^{max} \\ \quad - \left(\sum_{k,j=1}^{m,n} \bar{G}_{kj}^{max} \bar{\gamma}_{kj}^{max} \right)^{\mathrm{T}} L^T P - \left(\sum_{k,j=1}^{m,n} \bar{G}_{kj}^{min} \bar{\gamma}_{kj}^{min} \right)^{\mathrm{T}} L^T P \\ \quad - PL \left(\sum_{k,j=1}^{m,n} \bar{G}_{kj}^{max} \bar{\gamma}_{kj}^{max} \right) - PL \left(\sum_{k,j=1}^{m,n} \bar{G}_{kj}^{min} \bar{\gamma}_{kj}^{min} \right) \} \\ + \sum_{i,j=1}^{n,n} \bar{\delta}_{ij}^{min} \{ (A-LC)^T P + \bar{H}_{ij}^{min^T} P + P(A-LC) + P\bar{H}_{ij}^{min} \\ \quad - \left(\sum_{k,j=1}^{m,n} \bar{G}_{kj}^{max} \bar{\gamma}_{kj}^{max} \right)^{\mathrm{T}} L^T P - \left(\sum_{k,j=1}^{m,n} \bar{G}_{kj}^{min} \bar{\gamma}_{kj}^{min} \right)^{\mathrm{T}} L^T P \\ \quad - PL \left(\sum_{k,j=1}^{m,n} \bar{G}_{kj}^{max} \bar{\gamma}_{kj}^{max} \right) - PL \left(\sum_{k,j=1}^{m,n} \bar{G}_{kj}^{min} \bar{\gamma}_{kj}^{min} \right) \} \end{array} \right] \tilde{x}. \tag{7.15}$$

Hence we need

$$M < 0 \tag{7.16}$$

where $\bar{\delta}_{ij}^{max}$, $\bar{\delta}_{ij}^{min} \geq 0$. However, it is not possible to directly solve equation (7.16) for L and P because $\bar{\delta}_{ij}^{max}$, $\bar{\delta}_{ij}^{min}$ are time varying coefficients. Hence, we transform equation (7.16) to equations (7.17) and (7.18).

$$\left[\left(\begin{array}{l} (A-LC)^T P + \bar{H}_{ij}^{max^T} P + P(A-LC) + P\bar{H}_{ij}^{max} \\ - \left(\sum_{k,j=1}^{m,n} \bar{G}_{kj}^{max} \bar{\gamma}_{kj}^{max} \right)^{\mathrm{T}} L^T P - \left(\sum_{k,j=1}^{m,n} \bar{G}_{kj}^{min} \bar{\gamma}_{kj}^{min} \right)^{\mathrm{T}} L^T P \\ - PL \left(\sum_{k,j=1}^{m,n} \bar{G}_{kj}^{max} \bar{\gamma}_{kj}^{max} \right) - PL \left(\sum_{k,j=1}^{m,n} \bar{G}_{kj}^{min} \bar{\gamma}_{kj}^{min} \right) \end{array} \right) \right] < 0 \tag{7.17}$$

$$\left[\begin{pmatrix} (A-LC)^T P + \bar{H}_{ij}^{min^T} P + P(A-LC) + P\bar{H}_{ij}^{min} \\ -\left(\sum_{k,j=1}^{m,n} \bar{G}_{kj}^{max} \bar{\gamma}_{kj}^{max}\right)^{\mathrm{T}} L^T P - \left(\sum_{k,j=1}^{m,n} \bar{G}_{kj}^{min} \bar{\gamma}_{kj}^{min}\right)^{\mathrm{T}} L^T P \\ -PL\left(\sum_{k,j=1}^{m,n} \bar{G}_{kj}^{max} \bar{\gamma}_{kj}^{max}\right) - PL\left(\sum_{k,j=1}^{m,n} \bar{G}_{kj}^{min} \bar{\gamma}_{kj}^{min}\right) \end{pmatrix}\right] < 0 \quad (7.18)$$

Since $\sum_{k,j=1}^{m,n}\left(\bar{\gamma}_{kj}^{max} + \bar{\gamma}_{kj}^{min}\right) = 1$, equation (7.17) and (7.18) can be rewritten as

$$\left[\begin{pmatrix} \sum_{k,j=1}^{m,n} \bar{\gamma}_{kj}^{max}\left(\left(A+\bar{H}_{ij}^{max}\right)^T P - C^{\mathrm{T}} L^T P - \bar{G}_{kj}^{max^T} L^T P\right) \\ + \sum_{k,j=1}^{m,n} \bar{\gamma}_{kj}^{min}\left(\left(A+\bar{H}_{ij}^{max}\right)^T P - C^{\mathrm{T}} L^T P - \bar{G}_{kj}^{min^T} L^T P\right) \\ + \sum_{k,j=1}^{m,n} \bar{\gamma}_{kj}^{max}\left(P\left(A+\bar{H}_{ij}^{max}\right) - PLC - PL\bar{G}_{kj}^{max}\right) \\ + \sum_{k,j=1}^{m,n} \bar{\gamma}_{kj}^{min}\left(P\left(A+\bar{H}_{ij}^{max}\right) - PLC - PL\bar{G}_{kj}^{min}\right) \end{pmatrix}\right] < 0 \quad (7.19)$$

$$\left[\begin{pmatrix} \sum_{k,j=1}^{m,n} \bar{\gamma}_{kj}^{max}\left(\left(A+\bar{H}_{ij}^{min}\right)^T P - C^{\mathrm{T}} L^T P - \bar{G}_{kj}^{max^T} L^T P\right) \\ + \sum_{k,j=1}^{m,n} \bar{\gamma}_{kj}^{min}\left(\left(A+\bar{H}_{ij}^{min}\right)^T P - C^{\mathrm{T}} L^T P - \bar{G}_{kj}^{min^T} L^T P\right) \\ + \sum_{k,j=1}^{m,n} \bar{\gamma}_{kj}^{max}\left(P\left(A+\bar{H}_{ij}^{min}\right) - PLC - PL\bar{G}_{kj}^{max}\right) \\ + \sum_{k,j=1}^{m,n} \bar{\gamma}_{kj}^{min}\left(P\left(A+\bar{H}_{ij}^{min}\right) - PLC - PL\bar{G}_{kj}^{min}\right) \end{pmatrix}\right] < 0 \quad (7.20)$$

where $\bar{\gamma}_{kj}^{max}, \bar{\gamma}_{kj}^{min} \geq 0$. Further, rearrange equation (7.19) and (7.20) as

$$\left[\begin{array}{l}\left(\begin{array}{l}\sum_{k,j=1}^{m,n}\bar{\gamma}_{kj}^{max}\{\left(A+\bar{H}_{ij}^{max}\right)^{T}P+P\left(A+\bar{H}_{ij}^{max}\right)\\ -C^{\mathrm{T}}L^{T}P-\bar{G}_{kj}^{max^{T}}L^{T}P-PLC-PL\bar{G}_{kj}^{max}\}\\ +\sum_{k,j=1}^{m,n}\bar{\gamma}_{kj}^{min}\{\left(A+\bar{H}_{ij}^{max}\right)^{T}P+P\left(A+\bar{H}_{ij}^{max}\right)\\ -C^{\mathrm{T}}L^{T}P-\bar{G}_{kj}^{min^{T}}L^{T}P-PLC-PL\bar{G}_{kj}^{min}\}\end{array}\right)\end{array}\right]<0 \quad (7.21)$$

$$\left[\begin{array}{l}\left(\begin{array}{l}\sum_{k,j=1}^{m,n}\bar{\gamma}_{kj}^{max}\{\left(A+\bar{H}_{ij}^{min}\right)^{T}P+P\left(A+\bar{H}_{ij}^{min}\right)\\ -C^{\mathrm{T}}L^{T}P-\bar{G}_{kj}^{max^{T}}L^{T}P-PLC-PL\bar{G}_{kj}^{max}\}\\ +\sum_{k,j=1}^{m,n}\bar{\gamma}_{kj}^{min}\{\left(A+\bar{H}_{ij}^{min}\right)^{T}P+P\left(A+\bar{H}_{ij}^{min}\right)\\ -C^{\mathrm{T}}L^{T}P-\bar{G}_{kj}^{min^{T}}L^{T}P-PLC-PL\bar{G}_{kj}^{min}\}\end{array}\right)\end{array}\right]<0 \quad (7.22)$$

However, it is still not possible to solve equation (7.19) and (7.20) for L and P because $\bar{\gamma}_{kj}^{max}, \bar{\gamma}_{kj}^{min}$ are time varying coefficients. Hence, to overcome this problem, we transform the problem in equations (7.19) and (7.20) to equations (7.23)-(7.26) which do not involve $\bar{\gamma}_{kj}^{max}$, and $\bar{\gamma}_{kj}^{min}$.

$$P\left(A+\bar{H}_{ij}^{max}\right)+\left(A+\bar{H}_{ij}^{max}\right)^{T}P-\left(C+\bar{G}_{kj}^{max}\right)^{T}L^{T}P-PL\left(C+\bar{G}_{kj}^{max}\right)<0, \quad (7.23)$$

$$P\left(A+\bar{H}_{ij}^{max}\right)+\left(A+\bar{H}_{ij}^{max}\right)^{T}P-\left(C+\bar{G}_{kj}^{min}\right)^{T}L^{T}P-PL\left(C+\bar{G}_{kj}^{min}\right)<0, \quad (7.24)$$

$$P\left(A+\bar{H}_{ij}^{min}\right)+\left(A+\bar{H}_{ij}^{min}\right)^{T}P-\left(C+\bar{G}_{kj}^{max}\right)^{T}L^{T}P-PL\left(C+\bar{G}_{kj}^{max}\right)<0, \quad (7.25)$$

$$P\left(A+\bar{H}_{ij}^{min}\right)+\left(A+\bar{H}_{ij}^{min}\right)^{T}P-\left(C+\bar{G}_{kj}^{min}\right)^{T}L^{T}P-PL\left(C+\bar{G}_{kj}^{min}\right)<0, \quad (7.26)$$

for $\forall i = 1, \dots, n$, $\forall j = 1, \dots, n$, and $\forall j = 1, \dots, m$.

If equation (7.23)-(7.26) is satisfied, then equation (7.16) is automatically satisfied.

Corollary to Theorem 5: Bounded Jacobian Observer for Specified Problems

For the class of systems and observer forms described in equations (7.1) and (7.2), if an observer gain matrix L can be chosen such that

$$
\begin{gathered}
P\left(A+\bar{H}_{ij}^{max}\right)+\left(A+\bar{H}_{ij}^{max}\right)^{T}P-\left(C+\bar{G}_{kj}^{max}\right)^{T}L^{T}P-PL\left(C+\bar{G}_{kj}^{max}\right)<0 \\
P\left(A+\bar{H}_{ij}^{max}\right)+\left(A+\bar{H}_{ij}^{max}\right)^{T}P-\left(C+\bar{G}_{kj}^{min}\right)^{T}L^{T}P-PL\left(C+\bar{G}_{kj}^{min}\right)<0 \\
P\left(A+\bar{H}_{ij}^{min}\right)+\left(A+\bar{H}_{ij}^{min}\right)^{T}P-\left(C+\bar{G}_{kj}^{max}\right)^{T}L^{T}P-PL\left(C+\bar{G}_{kj}^{max}\right)<0 \\
P\left(A+\bar{H}_{ij}^{min}\right)+\left(A+\bar{H}_{ij}^{min}\right)^{T}P-\left(C+\bar{G}_{kj}^{min}\right)^{T}L^{T}P-PL\left(C+\bar{G}_{kj}^{min}\right)<0 \\
P>0 \\
\forall i=1,\dots,n\,,\forall j=1,\dots,n \text{ and } \forall k=1,\dots,m
\end{gathered}
\tag{7.27}
$$

where 1) $h_{ij}^{max} \geq max\left(\partial\Phi_i/\partial x_j\right)$ and $h_{ij}^{min} \leq min\left(\partial\Phi_i/\partial x_j\right)$,

2) $H_{ij}^{max} = e_n(i)e_n^T(j)h_{ij}^{max}$ and $H_{ij}^{min} = e_n(i)e_n^T(j)h_{ij}^{min}$,

3) $\bar{z}_H = n \times n - w_H$ is the state scaling factor, n being dimension of the state vector, w_H being the number of terms in $\partial\Phi_i/\partial x_j$ that equals zero,

4) $\bar{H}_{ij}^{max} = \bar{z}_H H_{ij}^{max}$ and $\bar{H}_{ij}^{min} = \bar{z}_H H_{ij}^{min}$,

5) $g_{kj}^{max} \geq max\left(\partial\Psi_k/\partial x_j\right)$ and $g_{kj}^{min} \leq min\left(\partial\Psi_k/\partial x_j\right)$,

6) $G_{kj}^{max} = e_n(k)e_n^T(j)g_{kj}^{max}$ and $G_{kj}^{min} = e_n(k)e_n^T(j)g_{kj}^{min}$,

7) $\bar{z}_G = m \times n - w_G$, is the state scaling factor, m being dimension of the output vector, w_G being the number of terms in $\partial\Psi_i/\partial x_j$ that equals zero,

8) $\bar{G}_{kj}^{max} = \bar{z}_G G_{kj}^{max}$ and $\bar{G}_{kj}^{min} = \bar{z}_G G_{kj}^{min}$,

then this choice of L leads to asymptotically stable estimates by the observer (7.2) for the system (7.1).

Proof: The proof of the Corollary follows along the same lines as the proof of theorem 5, except for the definition of the scaling factor $\bar{z}_H$ and $\bar{z}_G$.

In the general problem, if all of terms in $\partial\Phi_i/\partial x_j$ are not zero, then $\sum_{i,j=1}^{n,n}\left(\delta_{ij}^{max} + \delta_{ij}^{min}\right) = n \times n = z_H$ or if all of terms in $\partial\Psi_k/\partial x_j$ are not zero, then $\sum_{k,j=1}^{m,n}\left(\gamma_{kj}^{max} + \gamma_{kj}^{min}\right) = m \times n = z_G$. However, in some problems, if there exist $\partial\Phi_i/\partial x_j = 0$ or $\partial\Psi_k/\partial x_j = 0$, then $\sum_{i,j=1}^{n,n}\left(\delta_{ij}^{max} + \delta_{ij}^{min}\right)$ is less than z_H or $\sum_{k,j=1}^{m,n}\left(\gamma_{kj}^{max} + \gamma_{kj}^{min}\right)$ is less that z_G. We can then to define new scaling factors, $\bar{z}_H$ and $\bar{z}_G$.

$$\sum_{i,j=1}^{n,n} \left(\delta_{ij}^{max} + \delta_{ij}^{min}\right) = n \times n - w_H = \bar{z}_H \tag{7.28}$$

$$\sum_{k,j=1}^{m,n} \left(\gamma_{kj}^{max} + \gamma_{kj}^{min}\right) = m \times n - w_G = \bar{z}_G \tag{7.29}$$

where w_H is the number of terms in $\partial\Phi_i/\partial x_j$ that equals zero and w_G is the number of terms in $\partial\Psi_k/\partial x_j$ that equals zero. Now, we use $\bar{z}_H$ and $\bar{z}_G$ instead of z_H and z_G can be used to complete the proof.

7.5. Conclusions

In this chapter, a new observer design technique is developed for a nonlinear system with a locally or globally bounded Jacobian. The approach is developed in order to deal with differentiable nonlinear systems. The observer gains can be obtained by solving LMIs. The developed theory is used successfully in the design of observers for vehicle systems involving complex nonlinearities. The use of the observer design technique is illustrated for estimation of body slip angle in chapter 9.

Chapter 8

8. NOVEL UNKNOWN INPUTS NONLINEAR OBSERVER

As described earlier, a nonlinear observer for a nonlinear system with complex nonlinearities is needed. Thus, four new nonlinear observers have been developed for this purpose. In this chapter, the nonlinear observer and unknown input estimation for bounded Jacobian nonlinear systems with unknown disturbance inputs is presented.

8.1. Summary

This chapter extends the result in chapter 6 and chapter 7 and presents a new observer design technique for an unknown inputs nonlinear system with a globally (or locally) bounded Jacobian. This observer can applied for an unknown inputs nonlinear system with nonlinear measurement model. The approach utilized is to use measurements and state estimation to express the unknown inputs and use the mean value theorem to express the nonlinear error dynamics as a convex combination of known matrices with time varying coefficients. The observer gains are then obtained by solving linear matrix inequalities (LMIs). The developed approach can enable observer design for a large class of differentiable nonlinear systems with a globally (or locally) bounded Jacobian. The developed theory is used successfully in the design of observers for vehicle systems involving complex nonlinearities and unknown inputs. The use of the observer design technique is illustrated for estimation of roll angle and rollover index in chapter 12.

8.2. Introduction

This section focuses on a new observer design result for an unknown inputs nonlinear system with a locally or globally bounded Jacobian. A major limitation of the existing results for Lipschitz nonlinear systems is that they work only for adequately small values of the Lipschitz constant. When the equivalent Lipschitz constant has to be chosen large due to the inherent non-Lipschitz nature of the nonlinearity (such as in the case of aerointroduction drag force in vehicle systems), most existing observer design results fail to provide a solution. This section develops a solution methodology that works well

without requiring a small Lipschitz constant bound for the nonlinear function. The basic idea in this section is to use measurements and state estimation to express the unknown inputs and use the mean value theorem (McLeod (1965) and Korobkov (2001)) to express the nonlinear error introductions as a convex combination of values of the derivatives of the nonlinear function. The observer gain guaranteeing the convergence of the proposed observer is easily computed by LMIs.

8.3. Problem Statement for Unknown Inputs Nonlinear Observer

This section presents an efficient methodology for designing observers for the class of nonlinear systems described by

$$\dot{x} = \bar{A}x + \eta(x,u) + \bar{B}\mu \tag{8.1}$$

$$z = Ex \tag{8.2}$$

$$y = Cx + \Psi(x) \tag{8.3}$$

where $u \in R^P$ are the known control inputs, $\mu \in R^P$ are the unknown inputs, $y \in R^m$ and $z \in R^q$ are the output measurements. $\bar{A} \in R^{n\times n}$, $\bar{B} \in R^{n\times p}$, $E \in R^{q\times n}$, and $C \in R^{m\times n}$ are appropriate matrices. The functions $\eta(x,u)$: $R^n \times R^p \to R^n$,and $\Psi(x)$: $R^n \to R^m$ are nonlinear. In addition, $\eta(x,u)$ and $\Psi(x)$ are assumed to be differentiable nonlinear functions with globally (or locally) bounded Jacobian.

The objective of this estimation problem is to quantitatively estimate the unknown inputs $\mu(t)$ and to estimate the state vector $x(t)$, given the output measurements $y(t)$ and $z(t)$. The approach to estimate unknown inputs will first be described in the section 8.4 and subsequently the nonlinear observer design technique will be described in the section 8.5.

The overall approach to the estimation problem is as follows:

1. The unknown inputs are estimated assuming that full state measurement is available. The algebraic relation between the unknown inputs, the states and outputs is developed.
2. Using the algebraic relation between the unknown inputs and states, a modified state introductions equations are developed which do not depend on the unknown inputs.

3. Stable observer design for the new modified nonlinear introductions ensures that the state and unknown inputs can both be estimated.

8.4. Unknown Input Estimation

To make the presentation easy to follow, we will consider single input nonlinear systems first. Then, we will extend the results to multi-inputs nonlinear systems.

8.4.1. Single Input Nonlinear Systems [29]

Consider equations (8.1)-(8.3) when $p = 1$ (p is number of unknown inputs, μ) and $q = 1$ (q is number of output measurements, z).

Let the relative degree from μ to z be r_μ. Hence

$$E\bar{A}^i\bar{B} = 0, \qquad 0 \le i < r_\mu - 1 \tag{8.4}$$

$$E\bar{A}^{r_\mu - 1}\bar{B} \neq 0. \tag{8.5}$$

Define the relative degree r_η from the nonlinear function $\eta(x,u)$ to z as the number of times the output z must be differentiated before the nonlinear function $\eta(x,u)$ is encountered. In order words, r_η is defined as a whole number such that

$$E\bar{A}^i\eta(x,u) = 0, \qquad 0 \le i < r_\eta - 1 \tag{8.6}$$

$$E\bar{A}^{r_\eta - 1}\eta(x,u) \neq 0. \tag{8.7}$$

Theorem 6: Let the relative degrees from the input r_μ and from the nonlinearity r_η be such that $r_\eta \ge r_\mu$. Then the estimated unknown input is given by

$$\hat{\mu} = (E\bar{A}^{r_\mu - 1}\bar{B})^{-1}\left[z_f^{(r_\mu)} - E\bar{A}^{r_\mu}x - E\bar{A}^{r_\mu - 1}\eta(x,u)\right], \tag{8.8}$$

where we assume that the state variables, x, are known, and the filtered derivatives of the output z are given by

$$\frac{d}{dt}\begin{bmatrix} z_f \\ \dot{z}_f \\ \vdots \\ z_f^{(r-1)} \end{bmatrix} = \begin{bmatrix} -\frac{1}{\tau} & 0 & 0 & 0 \\ -\frac{1}{\tau^2} & -\frac{1}{\tau} & \ddots & 0 \\ \ddots & \ddots & \ddots & 0 \\ -\frac{1}{\tau^{r-1}} & \cdots & -\frac{1}{\tau^2} & -\frac{1}{\tau} \end{bmatrix}\begin{bmatrix} z_f \\ \dot{z}_f \\ \vdots \\ z_f^{(r-1)} \end{bmatrix} + \begin{bmatrix} \frac{1}{\tau} \\ \frac{1}{\tau^2} \\ \vdots \\ \frac{1}{\tau^{r-1}} \end{bmatrix} z. \tag{8.9}$$

Proof: Since the relative degree of the system from the output z to the unknown input μ is r_μ, it follows that

$$z^{(r_\mu)} = (E\bar{A}^{r_\mu}x) + \left(E\bar{A}^{r_\mu-1}\eta(x,u)\right) + E\bar{A}^{r_\mu-1}\bar{B}\mu. \tag{8.10}$$

Since $E\bar{A}^{r_\mu-1}\bar{B} \neq 0$, it therefore follows that the unknown input is given by

$$\mu = (E\bar{A}^{r_\mu-1}\bar{B})^{-1}\left[z^{(r_\mu)} - E\bar{A}^{r_\mu}x - E\bar{A}^{r_\mu-1}\eta(x,u)\right] \tag{8.11}$$

Since z is measured but the r_μth derivative of the output z is not unavailable, we therefore use the following estimator for the unknown input.

$$\hat{\mu} = (E\bar{A}^{r_\mu-1}\bar{B})^{-1}\left[z_f^{(r_\mu)} - E\bar{A}^{r_\mu}x - E\bar{A}^{r_\mu-1}\eta(x,u)\right] \tag{8.12}$$

where $z_f^{(r)}$ is obtained from the r_μth order filter given in equation (8.9). Then, as the filter constant $\tau \to 0$, $\hat{\mu} \to \mu$ as $t \to \infty$.

8.4.2. Multi-Input Nonlinear System [30]

Consider equations (8.1)-(8.3) when $p > 1$ (p is number of unknown inputs) and $q > 1$ (q is number of output measurements, z).

Let the vector relative degree of the system from the outputs z to the input μ be $[r_{\mu 1} \quad r_{\mu 2} \quad \cdots \quad r_{\mu q}]$. Let the relative degree from each of the outputs to the nonlinearity be $r_{\eta 1}, r_{\eta 2}, \ldots, r_{\eta(q-1)}$ and $r_{\eta q}$. Assume that $r_{\eta 1} \geq r_{\mu 1}, r_{\eta 2} \geq r_{\mu 2}, \ldots, r_{\eta(q-1)} \geq r_{\mu q}$ and $r_{\eta q} \geq r_{\mu q}$. It follows that

$$z_i^{(r_{\mu i})} = (E_i\bar{A}^{r_{\mu i}}x) + \left(E_i\bar{A}^{r_{\mu i}-1}\eta(x,u)\right) + E_i\bar{A}^{r_{\mu i}-1}\bar{B}\mu, \qquad i = 1,2,\ldots,q \tag{8.13}$$

Hence

$$\begin{bmatrix} z_1^{r_{\mu 1}} \\ z_2^{r_{\mu 2}} \\ \vdots \\ z_q^{r_{\mu q}} \end{bmatrix} = \begin{bmatrix} E_1\bar{A}^{r_{\mu 1}}x \\ E_2\bar{A}^{r_{\mu 2}}x \\ \vdots \\ E_q\bar{A}^{r_{\mu q}}x \end{bmatrix} + \begin{bmatrix} E_1\bar{A}^{r_{\mu 1}-1} \\ E_2\bar{A}^{r_{\mu 2}-1} \\ \vdots \\ E_q\bar{A}^{r_{\mu q}-1} \end{bmatrix} \eta(x,u) + \begin{bmatrix} E_1\bar{A}^{r_{\mu 1}-1}\bar{B} \\ E_2\bar{A}^{r_{\mu 2}-1}\bar{B} \\ \vdots \\ E_q\bar{A}^{r_{\mu q}-1}\bar{B} \end{bmatrix} \mu. \tag{8.14}$$

It therefore follows that the unknown inputs are given by

$$\begin{bmatrix} \mu_1 \\ \mu_2 \\ \vdots \\ \mu_q \end{bmatrix} = \begin{bmatrix} E_1\bar{A}^{r_{\mu 1}-1}\bar{B} \\ E_2\bar{A}^{r_{\mu 2}-1}\bar{B} \\ \vdots \\ E_q\bar{A}^{r_{\mu q}-1}\bar{B} \end{bmatrix}^{-1} \left\{ \begin{bmatrix} z_1^{r_{\mu 1}} \\ z_2^{r_{\mu 2}} \\ \vdots \\ z_q^{r_{\mu q}} \end{bmatrix} - \begin{bmatrix} E_1\bar{A}^{r_{\mu 1}}x \\ E_2\bar{A}^{r_{\mu 2}}x \\ \vdots \\ E_q\bar{A}^{r_{\mu q}}x \end{bmatrix} - \begin{bmatrix} E_1\bar{A}^{r_{\mu 1}-1} \\ E_2\bar{A}^{r_{\mu 2}-1} \\ \vdots \\ E_q\bar{A}^{r_{\mu q}-1} \end{bmatrix} \eta(x,u) \right\}. \tag{8.15}$$

Theorem 7: The estimated unknown inputs are given by

$$\begin{bmatrix} \hat{\mu}_1 \\ \hat{\mu}_2 \\ \vdots \\ \hat{\mu}_q \end{bmatrix} = \begin{bmatrix} E_1\bar{A}^{r_{\mu 1}-1}\bar{B} \\ E_2\bar{A}^{r_{\mu 2}-1}\bar{B} \\ \vdots \\ E_q\bar{A}^{r_{\mu q}-1}\bar{B} \end{bmatrix}^{-1} \left\{ \begin{bmatrix} z_{1f}^{r_{\mu 1}} \\ z_{2f}^{r_{\mu 2}} \\ \vdots \\ z_{qf}^{r_{\mu q}} \end{bmatrix} - \begin{bmatrix} E_1\bar{A}^{r_{\mu 1}}x \\ E_2\bar{A}^{r_{\mu 2}}x \\ \vdots \\ E_q\bar{A}^{r_{\mu q}}x \end{bmatrix} - \begin{bmatrix} E_1\bar{A}^{r_{\mu 1}-1} \\ E_2\bar{A}^{r_{\mu 2}-1} \\ \vdots \\ E_q\bar{A}^{r_{\mu q}-1} \end{bmatrix} \eta(x,u) \right\} \tag{8.16}$$

where we assume that the state variables, x, are known and

$$\frac{d}{dt}\begin{bmatrix} z_{if} \\ \dot{z}_{if} \\ \vdots \\ z_{if}^{(r-1)} \end{bmatrix} = \begin{bmatrix} -\frac{1}{\tau} & 0 & 0 & 0 \\ -\frac{1}{\tau^2} & -\frac{1}{\tau} & \ddots & 0 \\ \ddots & \ddots & \ddots & 0 \\ -\frac{1}{\tau^{r-1}} & \cdots & -\frac{1}{\tau^2} & -\frac{1}{\tau} \end{bmatrix} \begin{bmatrix} z_{if} \\ \dot{z}_{if} \\ \vdots \\ z_{if}^{(r-1)} \end{bmatrix} + \begin{bmatrix} \frac{1}{\tau} \\ \frac{1}{\tau^2} \\ \vdots \\ \frac{1}{\tau^{r-1}} \end{bmatrix} z_i, \qquad i = 1,2,\dots,q \tag{8.17}$$

Proof: Follows along the same lines as the proof for Theorem 4.

8.5. Unknown Inputs Nonlinear Observer

In the section 8.4, we have shown that the estimated unknown inputs, $\hat{\mu}$, can be estimated by using equation (8.16). So, we can substitute the unknown inputs, μ, by using equation (8.16). Then, the new dynamic equation for the nonlinear system is given by

$$\dot{x} = \bar{A}x + \eta(x,u) + \bar{B}\begin{bmatrix} E_1\bar{A}^{r_{\mu 1}-1}\bar{B} \\ E_2\bar{A}^{r_{\mu 2}-1}\bar{B} \\ \vdots \\ E_q\bar{A}^{r_{\mu q}-1}\bar{B} \end{bmatrix}^{-1} \left\{ \begin{bmatrix} z_{1f}^{r_{\mu 1}} \\ z_{2f}^{r_{\mu 2}} \\ \vdots \\ z_{qf}^{r_{\mu q}} \end{bmatrix} - \begin{bmatrix} E_1\bar{A}^{r_{\mu 1}}x \\ E_2\bar{A}^{r_{\mu 2}}x \\ \vdots \\ E_q\bar{A}^{r_{\mu q}}x \end{bmatrix} - \begin{bmatrix} E_1\bar{A}^{r_{\mu 1}-1} \\ E_2\bar{A}^{r_{\mu 2}-1} \\ \vdots \\ E_q\bar{A}^{r_{\mu q}-1} \end{bmatrix} \eta(x,u) \right\} \tag{8.18}$$

Rearrange equation (8.18), as

$$\dot{x} = Ax + \Phi(x,u) + g(z_f),$$

$$A = \bar{A} - \bar{B}\begin{bmatrix} E_1\bar{A}^{r_{\mu 1}-1}\bar{B} \\ E_2\bar{A}^{r_{\mu 2}-1}\bar{B} \\ \vdots \\ E_q\bar{A}^{r_{\mu q}-1}\bar{B} \end{bmatrix}^{-1} \begin{bmatrix} E_1\bar{A}^{r_{\mu 1}} \\ E_2\bar{A}^{r_{\mu 2}} \\ \vdots \\ E_q\bar{A}^{r_{\mu q}} \end{bmatrix},$$

$$\Phi(x,u) = \eta(x,u) - \bar{B}\begin{bmatrix} E_1\bar{A}^{r_{\mu 1}-1}\bar{B} \\ E_2\bar{A}^{r_{\mu 2}-1}\bar{B} \\ \vdots \\ E_q\bar{A}^{r_{\mu q}-1}\bar{B} \end{bmatrix} \begin{bmatrix} E_1\bar{A}^{r_{\mu 1}-1} \\ E_2\bar{A}^{r_{\mu 2}-1} \\ \vdots \\ E_q\bar{A}^{r_{\mu q}-1} \end{bmatrix} \eta(x,u), \tag{8.19}$$

$$g(z_f) = \bar{B}\begin{bmatrix} E_1\bar{A}^{r_{\mu 1}-1}\bar{B} \\ E_2\bar{A}^{r_{\mu 2}-1}\bar{B} \\ \vdots \\ E_q\bar{A}^{r_{\mu q}-1}\bar{B} \end{bmatrix}^{-1} \begin{bmatrix} z_{1f}^{r_{\mu 1}} \\ z_{2f}^{r_{\mu 2}} \\ \vdots \\ z_{qf}^{r_{\mu q}} \end{bmatrix}$$

where z_f is the derivative of the output z.

8.5.1. Nonlinear Observer

We have substituted for the unknown inputs, μ by using equation (8.16). Now, we need to design a nonlinear observer for a nonlinear system described by

$$\begin{aligned} \dot{x} &= Ax + \Phi(x,u) + g(z_f), \\ y &= Cx + \Psi(x). \end{aligned} \tag{8.20}$$

Note: Φ and Ψ are assumed to be differentiable and z_f is the derivative of the output z.

The observer for this problem will be assumed to be of the form

$$\begin{aligned} \dot{\hat{x}} &= A\hat{x} + \Phi(\hat{x}) + g(y,u) + L(y - \hat{y}), \\ \hat{y} &= C\hat{x} + \Psi(\hat{x}). \end{aligned} \tag{8.21}$$

Since the nonlinear system described by equation (8.20) is the same as that described by equation (7.1) in chapter 7, we can directly apply Theorem 5 or Corollary to Theorem 5 to design an observer.

The Corollary to Theorem 5 will be repeated as follow:

Corollary to Theorem 5: Bounded Jacobian Observer for Specified Problems

For the class of systems and observer forms described in equations (8.20) and (8.21), if an observer gain matrix L can be chosen such that

$$\begin{gathered} P\left(A+\bar{H}_{ij}^{max}\right)+\left(A+\bar{H}_{ij}^{max}\right)^{T}P-\left(C+\bar{G}_{kj}^{max}\right)^{T}L^{T}P-PL\left(C+\bar{G}_{kj}^{max}\right)<0 \\ P\left(A+\bar{H}_{ij}^{max}\right)+\left(A+\bar{H}_{ij}^{max}\right)^{T}P-\left(C+\bar{G}_{kj}^{min}\right)^{T}L^{T}P-PL\left(C+\bar{G}_{kj}^{min}\right)<0 \\ P\left(A+\bar{H}_{ij}^{min}\right)+\left(A+\bar{H}_{ij}^{min}\right)^{T}P-\left(C+\bar{G}_{kj}^{max}\right)^{T}L^{T}P-PL\left(C+\bar{G}_{kj}^{max}\right)<0 \\ P\left(A+\bar{H}_{ij}^{min}\right)+\left(A+\bar{H}_{ij}^{min}\right)^{T}P-\left(C+\bar{G}_{kj}^{min}\right)^{T}L^{T}P-PL\left(C+\bar{G}_{kj}^{min}\right)<0 \\ P>0 \\ \forall i=1,\dots,n\,,\forall j=1,\dots,n \text{ and } \forall k=1,\dots,m \end{gathered} \tag{8.22}$$

where 1) $h_{ij}^{max}\geq max\left(\partial\Phi_i/\partial x_j\right)$ and $h_{ij}^{min}\leq min\left(\partial\Phi_i/\partial x_j\right)$,

2) $H_{ij}^{max}=e_n(i)e_n^T(j)h_{ij}^{max}$ and $H_{ij}^{min}=e_n(i)e_n^T(j)h_{ij}^{min}$,

3) $\bar{z}_H=n\times n-w_H$ is the state scaling factor, n being dimension of the state vector, w_H being the number of terms in $\partial\Phi_i/\partial x_j$ that equals zero,

4) $\bar{H}_{ij}^{max}=\bar{z}_H H_{ij}^{max}$ and $\bar{H}_{ij}^{min}=\bar{z}_H H_{ij}^{min}$,

5) $g_{kj}^{max}\geq max\left(\partial\Psi_k/\partial x_j\right)$ and $g_{kj}^{min}\leq min\left(\partial\Psi_k/\partial x_j\right)$,

6) $G_{kj}^{max}=e_n(k)e_n^T(j)g_{kj}^{max}$ and $G_{kj}^{min}=e_n(k)e_n^T(j)g_{kj}^{min}$,

7) $\bar{z}_G=m\times n-w_G$, is the state scaling factor, m being dimension of the output vector, w_G being the number of terms in $\partial\Psi_i/\partial x_j$ that equals zero,

8) $\bar{G}_{kj}^{max}=\bar{z}_G G_{kj}^{max}$ and $\bar{G}_{kj}^{min}=\bar{z}_G G_{kj}^{min}$,

then this choice of L leads to asymptotically stable estimates by the observer (8.21) for the system (8.20).

8.6. Conclusions

In this chapter, a new observer design technique is developed for an unknown inputs nonlinear system with a locally or globally bounded Jacobian. The approach is developed in order to deal with differentiable nonlinear systems and unknown inputs. The observer gains can be obtained by solving LMIs. The developed theory is used successfully in the design of observers for vehicle systems involving complex nonlinearities. The use of the observer design technique is illustrated for estimation of roll angle and rollover index in chapter 12.

Chapter 9

9. APPLICATION OF NONLINEAR OBSERVER TO LONGITUDINAL VELOCITY ESTIMATION

9.1. Summary

The knowledge of longitudinal velocity can be useful to many active vehicle safety control systems such as anti-lock braking systems (ABS), yaw stability control and roll-over prevention control systems. This section illustrates the estimation of the longitudinal vehicle velocity by using the bounded jacobian approach in chapter 6. The results show that both the new and standard Lipschitz based observers can estimate the longitudinal velocity. However, the developed new observer is the more appropriate observer for this problem. This is because the aerodynamic force term, $-D_a\dot{x}^2$, is not Lipschitz. By using the developed theorem, it is possible to obtain observer gains which are smaller than those from a Lipschitz based observer. The small gains of the observer are good for estimating parameters because they will not enhance noise unlike the Lipshitz based observer. The performance of the new observer is clearly better than that of the standard Lipshitz observer.

9.2. Introduction

The knowledge of longitudinal velocity can be useful to many active vehicle safety control systems such as anti-lock braking systems (ABS), yaw stability control and roll-over prevention control systems. Longitudinal vehicle speed is often approximated from an average of the speed of the 4 wheels of the vehicle. While wheel speed can be measured, actual longitudinal vehicle speed itself cannot be easily measured. However, longitudinal vehicle speed can differ significantly from wheel speed during hard braking, slippery roads, etc. Hence an approximation of vehicle speed from wheel speed can lead to significant errors under these conditions. This section develops an observer to estimate longitudinal vehicle speed from measurement of wheel speed.

9.3. Longitudinal Vehicle Dynamics

The vehicle model consists of equations for the longitudinal motion of the vehicle, for the rotational dynamics of each wheel and for the relationship between tire forces, slip ratio and tire road friction coefficient [**3**], [**10**], [**22**], and [**31**].

The longitudinal dynamics can be represented as

$$m\dot{x} = F_x - R_x - D_a\dot{x}^2 \tag{9.1}$$

where $\dot{x}$ is the longitudinal speed, m is the mass of the vehicle, R_x is the rolling resistance, and D_a is an aerodynamic drag parameter. The total longitudinal tire force is represented by F_x.

$$F_x = F_{xf} + F_{xr} \tag{9.2}$$

where F_{xf} is front wheel longitudinal tire force and F_{xr} is rear wheel longitudinal tire force.

The rotational dynamics of front wheel and rear wheel are represented by

$$I_w\dot{\omega}_f = T_d - r_{eff}F_{xf}, \tag{9.3}$$

$$I_w\dot{\omega}_r = -r_{eff}F_{xr} \tag{9.4}$$

where ω_f and ω_r are angular velocity of front and rear wheel respectively. T_d represents the drive torque delivered to the front wheels. r_{eff} is the effective radius of the tire and I_w is wheel inertia.

The longitudinal force generated at tires is known to depend on the longitudinal slip ratio, the tire-road friction coefficient, and the normal force applied at the tire. Longitudinal slip ratio is defined as

$$\sigma_{xf} = \frac{r_{eff}\omega_f - \dot{x}}{\max\left(r_{eff}\omega_f, \dot{x}\right)}, \tag{9.5}$$

$$\sigma_{xr} = \frac{r_{eff}\omega_r - \dot{x}}{\max\left(r_{eff}\omega_r, \dot{x}\right)}. \tag{9.6}$$

The tire force in the small slip region can then be modeled as

$$F_{xf} = \lambda_f \sigma_{xf},\ F_{xr} = \lambda_r \sigma_{xr} \tag{9.7}$$

where λ_f and λ_r are called the longitudinal tire stiffness parameters of the front and rear tires respectively.

Assume we need to estimate longitudinal velocity, $\hat{\dot{x}}$, in the range 24-36 meters per second (or 54-80 mph) during positive acceleration. The measurements of system are the drive torque, T_d , wheel angular velocity, ω_f and ω_r. Then, it is reasonable to linearize equations (9.5) and (9.6). The modified equations of equations (9.5) and (9.6) are represented by

$$\sigma_{xf} = \frac{r_{eff}\omega_f - \dot{x}}{r_{eff}\omega_{fo}} \tag{9.8}$$

$$\sigma_{xr} = \frac{r_{eff}\omega_r - \dot{x}}{\dot{x}_0}\ or\ \sigma_{xr} = 0. \tag{9.9}$$

This approximation could be justified by the fact that $r_{eff}\omega_f$ and $\dot{x}$ are very close to each other and therefore $r_{eff}\omega_f - \dot{x}$ is small, while $r_{eff}\omega_{f0}$ is large and hence small changes in $r_{eff}\omega_{f0}$ would be negligible in the denominator while they would not be negligible in the numerator. Likewise, $r_{eff}\omega_r$ and $\dot{x}$ are almost equal during positive acceleration and $\dot{x}_0$ is large compared with $r_{eff}\omega_r - \dot{x}$. Then, F_{xr} is approximately zero.

Therefore, the observer is assumed to be of the form

$$\begin{aligned}\begin{bmatrix}\dot{\hat{x}}\\ \dot{\hat{\omega}}_f\end{bmatrix} &= \begin{bmatrix}-\dfrac{\lambda}{m(r_{eff}\omega_{f0})} & \dfrac{\lambda r_{eff}}{m(r_{eff}\omega_{f0})}\\ \dfrac{\lambda r_{eff}}{I_w(r_{eff}\omega_{f0})} & -\dfrac{\lambda r_{eff}^2}{I_w(r_{eff}\omega_{f0})}\end{bmatrix}\begin{bmatrix}\dot{\hat{x}}\\ \hat{\omega}_f\end{bmatrix} + \begin{bmatrix}0\\ 1/I_w\end{bmatrix}T_d\\ &+ \begin{bmatrix}-R_x/m\\ 0\end{bmatrix} + \begin{bmatrix}-D_a\dot{\hat{x}}^2\\ 0\end{bmatrix} + \begin{bmatrix}L_1\\ L_2\end{bmatrix}\left(y - [0 \quad 1]\begin{bmatrix}\dot{\hat{x}}\\ \hat{\omega}_f\end{bmatrix}\right)\\ y &= [0 \quad 1]\begin{bmatrix}\dot{x}\\ \omega_f\end{bmatrix}.\end{aligned} \tag{9.10}$$

9.4. Observer Design for Longitudinal Vehicle Motion

First, we will find observer gains by the developed theorem which needs to solve LMIs. Then, a standard observer [**24**] based on Lipschitz system based design is used to find

observer gains. The results and observer performance will be compared for the two types of observers.

For simulation, we will use a vehicle simulation (VS) model from CARSIM software runs within a Simulink model. The vehicle code is a D-Class, Sedan, with default parameters ($m = 1530\ kg$, $I_w = 2\ \ kg.m^2$, $r_{eff} = 0.335\ m$).

9.4.1. Observer Design Using the Corollary to Theorem 2 in Chapter 6

In this case, we would like to estimate longitudinal velocity in a range, $\dot{x} \in [24,36]$. Apply the corollary to theorem 2 in Chapter 6 for the problem.

In this case, $n = 2$.

$$\Phi(x) = \begin{bmatrix} -D_a\dot{x}^2 \\ 0 \end{bmatrix} \tag{9.11}$$

$$\frac{\partial \Phi_1}{\partial \dot{x}} = -2D_a\dot{x}, \qquad \frac{\partial \Phi_1}{\partial \omega_f} = 0 \tag{9.12}$$

$$\frac{\partial \Phi_2}{\partial \dot{x}} = 0, \qquad \frac{\partial \Phi_2}{\partial \omega_f} = 0 \tag{9.13}$$

Since $\frac{\partial \Phi_1}{\partial \omega_f} = \frac{\partial \Phi_2}{\partial \dot{x}} = \frac{\partial \Phi_2}{\partial \omega_f} = 0$, then the scaling factor is

$$\bar{z}_H = n \times n - w_H = 2 \times 2 - 3 = 1. \tag{9.14}$$

Next, find $\bar{H}_{ij}^{max}$ and $\bar{H}_{ij}^{min}$.

$$\bar{H}_{11}^{max} = \begin{bmatrix} -16 & 0 \\ 0 & 0 \end{bmatrix}, \qquad \bar{H}_{11}^{min} = \begin{bmatrix} -27 & 0 \\ 0 & 0 \end{bmatrix} \tag{9.15}$$

$$\bar{H}_{12}^{max} = \bar{H}_{12}^{min} = \bar{H}_{21}^{max} = \bar{H}_{21}^{min} = \bar{H}_{22}^{max} = \bar{H}_{22}^{min} = \begin{bmatrix} 0 & 0 \\ 0 & 0 \end{bmatrix} \tag{9.16}$$

Now, we are ready to solve equation (6.35) for observer gain. Observer gains are defined by Table 9-1.

Table 9-1 Observer gain schedule from the developed nonlinear observer

$r_{eff}\omega$	$r_{eff}\omega_0$	L
$24 \le r_{eff}\omega \le 28$	26	$[0.5149 \quad 2.8749]^T$

$28 \le r_{eff}\omega \le 32$	30	$[0.5556 \quad 2.9409]^T$
$32 \le r_{eff}\omega \le 26$	34	$[0.4810 \quad 2.6522]^T$

9.4.2. Standard Lipschitz Based Observer [24]

The class of nonlinear systems described by

$$\begin{aligned} \dot{x} &= Ax + \Phi(x) + g(y,u) \\ y &= Cx \end{aligned} \tag{9.17}$$

where $x \in R^n$ is the state vector, $u \in R^p$ is the input vector, and $y \in R^m$ is the output measurement vector. $A \in R^{n\times n}$ and $C \in R^{m\times n}$ are appropriate matrices. The functions $\Phi(x): R^n \to R^n$, and $g(y,u): R^m \times R^p \to R^n$ are nonlinear.

The observer form is given by:

$$\dot{\hat{x}} = A\hat{x} + \Phi(\hat{x}) + g(y,u) + L(y - C\hat{x}) \tag{9.18}$$

Lipschitz condition is given by:

$$\|\Phi(x,u) - \Phi(\hat{x},u)\| \le \gamma\|x - \hat{x}\|, \qquad \forall x, \hat{x}, \qquad \gamma > 0 \tag{9.19}$$

For the class of systems and observer forms described in equations (9.17), (9.18) and (9.19), if an observer gain matrix can be chosen such that

$$\begin{bmatrix} (A-LC)^T P + P(A-LC) + I & P \\ P & -I/\gamma^2 \end{bmatrix} < 0 \tag{9.20}$$

for some positive definite symmetric matrix P, then this choice of L leads to asymptotically stable estimates by the observer (9.18) for the system (9.17).

Apply the Lipschitz condition. We can show that

$$\left\| \begin{bmatrix} -D_a\dot{x}^2 + D_a\dot{\hat{x}}^2 \\ 0 \end{bmatrix} \right\| \le \begin{bmatrix} \gamma & 0 \\ 0 & \gamma \end{bmatrix} \left\| \begin{bmatrix} x - \hat{x} \\ 0 \end{bmatrix} \right\| \tag{9.21}$$

$$D_a\left\|\left(\dot{x}^2 + \dot{\hat{x}}^2\right)\right\| \le \gamma\|x - \hat{x}\| \tag{9.22}$$

$$\gamma \ge D_a\left\|\dot{x}_{max} + \dot{\hat{x}}_{max}\right\|. \tag{9.23}$$

The maximum longitudinal velocity is 36 meters per second and D_a is 0.3686. Then, the Lipschitz constant, γ, is 27.

For the Lipschitz constant, $\gamma = 27$, observer gains are defined by Table 9-2.

Table 9-2 Observer gain schedule from Lipschitz observer

$r_{eff}\omega$	$r_{eff}\omega_0$	L
$24 \leq r_{eff}\omega \leq 28$	26	$[43.7700 \quad 125.9678]^T$
$28 \leq r_{eff}\omega \leq 32$	30	$[51.4416 \quad 140.5622]^T$
$32 \leq r_{eff}\omega \leq 26$	34	$[51.5478 \quad 138.2755]^T$

9.5. Simulation Results

Assume: the statistic error of angular velocity of wheel is normal distribution with 0 mean and 0.23 standard division.

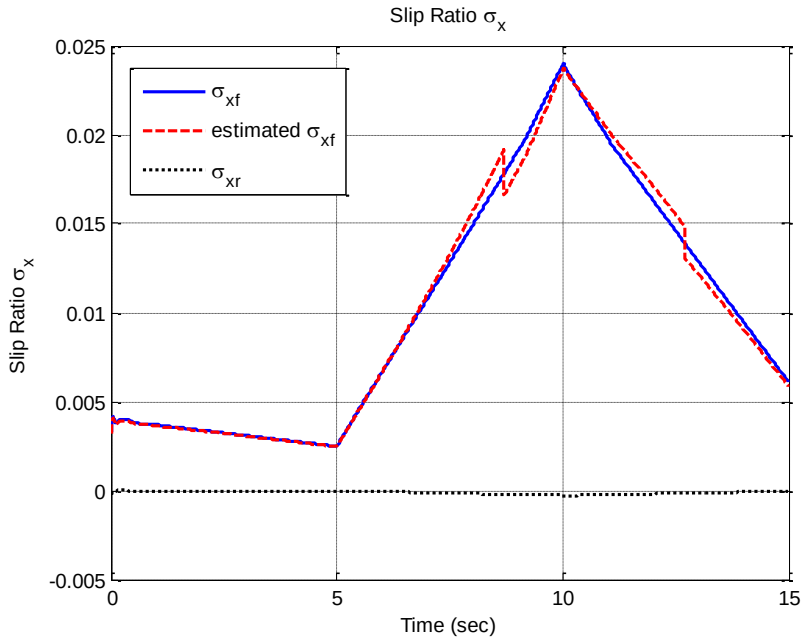

Figure 9-1 Slip ratio σ_x.

Figure 9-1 shows the slip ratio and the estimated slip ratio when the vehicle acceleration is positive. During the time 0 to 5 seconds, there are few changes in the slip ratio of front wheels because the engine torque is kept near constant. Then, the slip ratio of front wheels is increased during 5 to 10 seconds and decreased during 10 to 15 second because the engine torque is increased and decreased, respectively.

Also, Figure 9-1 shows that the estimate slip ratio of front wheel is close to the true slip ratio. Likewise, the slip ratio of rear wheels is approximately zero. This is because rear wheel speed is very close to the vehicle speed during acceleration of a front wheel drive vehicle.

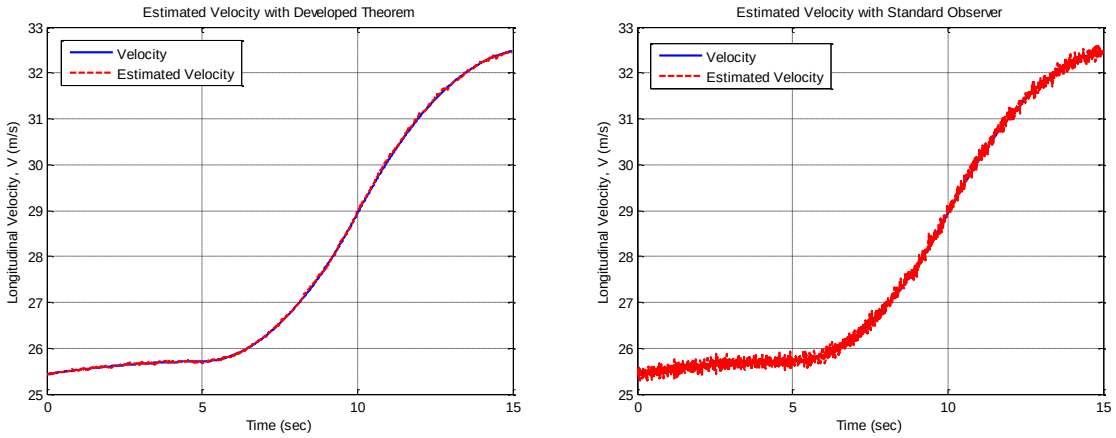

a) Develop theorem observer b) Standard observer

Figure 9-2 Velocity estimation.

Figure 9-2 presents the longitudinal velocity and the estimated longitudinal velocity when the vehicle acceleration is positive.

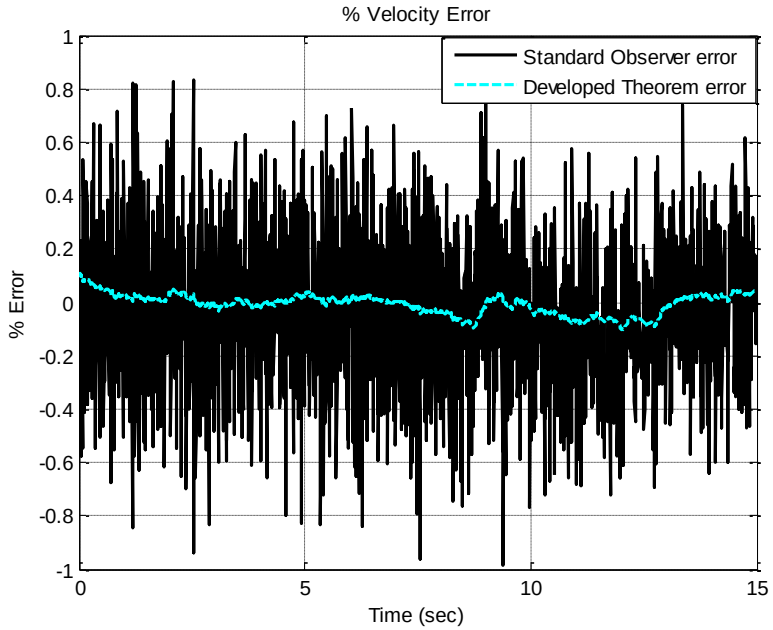

Figure 9-3 Percentage velocity error.

Figure 9-3 shows percentage velocity error from each observer. The percentage velocity error from the developed theorem is smaller than that from the standard observer.

Table 9-3 Comparison of observer gains

$r_{eff}\omega_0$	Observer Desgin	Standard Lipschitz Based Observer
26	$[0.5149 \quad 2.8749]^T$	$[43.7700 \quad 125.9678]^T$
30	$[0.5556 \quad 2.9409]^T$	$[51.4416 \quad 140.5622]^T$
34	$[0.4810 \quad 2.6522]^T$	$[51.5478 \quad 138.2755]^T$

9.6. Conclusions

The results show that both the new and standard Lipschitz based observers can estimate the longitudinal velocity. However, the developed new observer is the more appropriate observer for this problem. This is because the aerodynamic force term, $-D_a\dot{x}^2$, is not Lipschitz. By using the developed theorem, it is possible to obtain observer gains which are smaller than those from a Lipschitz based observer. The small gains of the observer are good for estimating parameters because they will not enhance noise unlike the Lipshitz based observer. The performance of the new observer is clearly better than that of the standard Lipshitz observer.

Chapter 10

10. APPLICATION OF NONLINEAR OBSERVER TO SLIP ANGLE ESTIMATION

10.1. Summary

Real-time knowledge of the slip angle in a vehicle is useful in many active vehicle safety applications, including yaw stability control, rollover prevention, and lane departure avoidance. Sensors that can directly measure slip angle are too expensive for ordinary automotive applications. This section uses a new nonlinear observer design technique for estimation of slip angle using inexpensive sensors normally available for yaw stability control applications. The approach utilized is to use the mean value theorem to express the nonlinear error dynamics as a convex combination of known matrices with time varying coefficients. A modified form of the mean value theorem for vector nonlinear systems is presented. The observer gains are then obtained by solving linear matrix inequalities (LMIs). The developed approach also can enable observer design for a large class of differentiable nonlinear systems with a globally (or locally) bounded Jacobian. The developed nonlinear observer is evaluated through experimental tests on a Volvo XC90 sport utility vehicle. Detailed experimental results show that the developed nonlinear observer can reliably estimate slip angle for a variety of test maneuvers on road surfaces with different friction coefficients.

10.2. Introduction

Electronic stability control (ESC) systems that prevent vehicles from spinning, drifting out, and rolling over have been developed and recently commercialized by several automotive manufacturers [**3**], [**4**], [**13**]. Many electronic stability control systems focus on yaw rate feedback for enhancing stability performance. In such cases, the control system attempts to ensure that the actual yaw rate of the vehicle tracks a desired yaw rate determined by the driver's steering input [1]. However, in situations on low-friction road surfaces, it is also beneficial to control the vehicle slip angle and prevent it from

becoming too large, in addition to controlling yaw rate [**3**], [**4**], [**13**]. Slip angle control is necessary because too high a slip angle can reduce the ability of the tires to generate lateral forces and can significantly compromise the performance of the vehicle control system. Hence, both yaw rate and slip angle are variables needed for vehicle stability control.

This dissertation focuses on methods of slip angle estimation for real-time yaw stability control. To begin with, let us review the formal definition of slip angle. The slip angle of a vehicle β is the angle its velocity vector at the center of gravity (c.g.) makes with the longitudinal axis of the vehicle. The slip angle of a tire α is the angle of the velocity vector at the tire with the orientation of the tire [**3**]. Both of these definitions are illustrated in Figure 10-1.

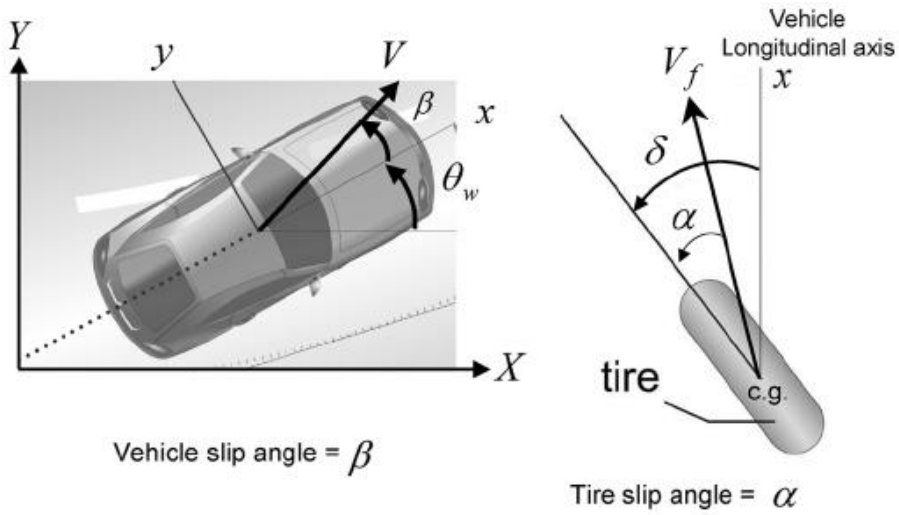

Figure 10-1 Vehicle and tire slip angles.

10.3. Review of Slip Angle Estimation Methods

10.3.1. One-Antenna and Two-Antenna GPS Systems

One-antenna carrier-phase GPS systems can measure vehicle velocity quite accurately even without the use of local differential correction signals. For example, GPS systems such as the Novatel Superstar are relatively inexpensive and have a cost in the range of about $300. The Novatel Superstar can provide a horizontal position accuracy of 5–10 m

and a velocity accuracy of 0.05 m/s. The velocity accuracy obtained is far superior to the position accuracy due to the use of carrier phase signals [**32**]. By using velocity measurements in the absolute (inertial) earth coordinates, the orientation of the velocity vector in the horizontal plane of the vehicle can be obtained as

$$\theta_w = \tan^{-1}\left(\frac{\dot{Y}}{\dot{X}}\right) \tag{10.1}$$

where θ_w is the orientation of the velocity vector of the vehicle in absolute coordinates. In order to obtain slip angle, one further needs to obtain the absolute orientation angle of the vehicle itself, since slip angle is the angle between the vehicle longitudinal axis and its velocity vector. A two-antenna GPS system can be used to obtain absolute orientation of the vehicle. A two-antenna system provides real time position information at two points along the vehicle – the two points being those corresponding to the antenna locations. While these position values are themselves inaccurate (with accuracy of the order of 5–10 m), the fact that the relative distance between these two points is fixed and known can be used to obtain accurate estimates of vehicle orientation [**32**]. Algorithms and results on obtaining orientation with inexpensive two-antenna systems for satellites are presented in [**32**] and could potentially be extended to obtain similar results for automotive systems.

It should be noted that two-antenna GPS systems are likely to cost as much as $600 and will be considered expensive for passenger sedans by automotive manufacturers.

A one-antenna GPS system cannot by itself measure slip angle, as explained earlier. However, several researchers have developed systems for slip angle measurement based on the use of an inertial measurement unit together with a one-antenna GPS system [**33**], [**34**]. In the case of such systems, the inertial measurement unit provides lateral and longitudinal acceleration measurements, which can be integrated to obtain lateral and longitudinal velocities. The ratio of these body-fixed velocities can then be used to obtain slip angle. The major problem with this integration approach is that bias errors in the acceleration measurements will cause serious drift in the velocity estimates. The bias

errors can be estimated in real time using a Kalman filter that combines the use of inertial sensors with a single-antenna GPS system.

The disadvantage of the GPS-inertial measurement unit approach is that the inertial sensors often have to be of very high quality in order to obtain accurate drift-free estimates. High quality inertial measurements can be extremely expensive. For example, the RT3000 system sold by Oxford Technical Solutions costs over $50,000 [**35**]! To the best of the authors' knowledge, there are no inexpensive single-antenna slip angle estimation systems currently being sold on the market.

Another disadvantage of GPS-based systems in general is that they are unreliable in urban environments where tall buildings and urban canyons can prevent access to GPS satellite signals.

10.3.2. Optical Sensors for Slip Angle Measurement

Noncontact optical sensors for slip angle measurement have been developed by Corrsys–Datron [**36**] and others. These sensors use optical means to capture planar road texture and evaluate the motion of the vehicle by measuring the direction and magnitude of change with respect to the road texture. Such optical sensors can provide very accurate slip angle measurements. However, they are very expensive. For example, the sensors by Corrsys–Datron cost over $30,000!

10.3.3. Dynamic Model-Based Estimation

A more cost-effective solution compared with optical sensors and GPS-based systems is to estimate slip angle from typical on-board sensors already available for use by the vehicle stability control system. For example, accelerometers that measure lateral and longitudinal acceleration, a gyroscope that measures yaw rate and a steering angle sensor are typically used by all stability control systems. A slip-angle estimation system that relies only on these sensors would not add any cost to the stability control system and would therefore be valuable. It should also be noted that accelerometers in general cost as little as $5–$10 a piece and are extremely viable for automotive applications. Several researchers have proposed different slip angle estimation methodologies based on use of

the above stability control system sensors. Most methods can be categorized in two groups: kinematics-based methods [**4**], [**5**], [**37**] and vehicle-model-based methods [**38**], [**39**], [**40**], [**41**], [**42**], [**43**]. The kinematics-based methods (or integration methods) are robust against vehicle parameters, changes in tire-road conditions, and changes in driving maneuvers. However, such methods are very sensitive to sensor error especially sensor bias error, which causes a drift, and sensor error caused by road bank angle. The model-based methods, on the other hand, are relatively robust against sensor errors. However, they depend heavily on the accuracy of the vehicle and tire parameters and knowledge of road conditions. Most slip angle estimation methods rely on a linear vehicle model that can work effectively only under normal vehicle operating condition. When the vehicle is skidding and the slip angle becomes large, these estimation methods can no longer provide slip angle estimation reliably.

In this dissertation, we present a method of estimating vehicle slip angle based on a nonlinear vehicle model. The method is suitable for a large range of operating conditions. The developed estimation algorithm was validated with experimental measurements on a test vehicle. It was verified that this slip angle estimation provides reliable slip angle and can be potentially used effectively in vehicle stability controllers.

10.4. Vehicle Lateral Dynamics

Consider the two-degrees-of-freedom (2-DOF) model used to represent the vehicle lateral dynamics as shown in Figure 10-2. The 2 DOF are the lateral translation of the vehicle y and the yaw rate r of the vehicle. The nonlinear vehicle lateral dynamics when the steering angle is assumed to be small can be formulated as

$$ma_y = m(\ddot{y} + ru_x) = F_{yf} + F_{yr} \tag{10.2}$$

$$I_z\dot{r} = aF_{yf} - bF_{yr} \tag{10.3}$$

where F_{yf} and F_{yr} are the lateral tire forces of the front and rear wheels respectively, u_x is longitudinal velocity and a and b are the distances of the front and rear tires respectively from the c.g. of the vehicle.

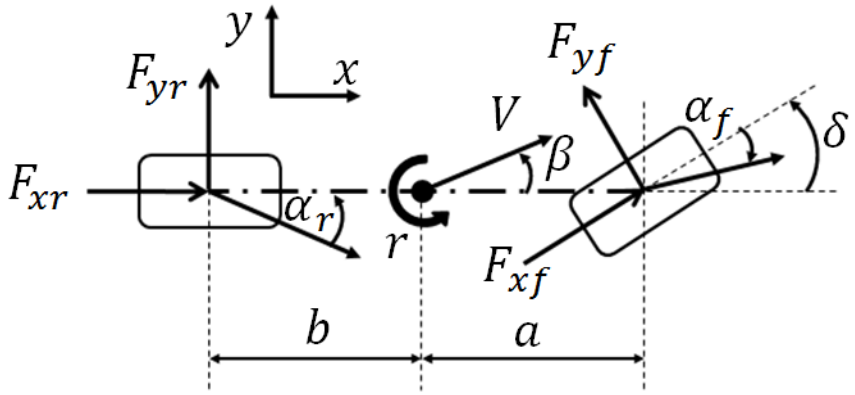

Figure 10-2 Single track model for vehicle lateral dynamics.

It should be noted that in the presence of road bank angle, the lateral translational equation (10.2) is modified to $m(\ddot{y} + ru_x) = F_{yf} + F_{yr} - mgsin(\varphi_r)$, where φ_r is the road bank angle. Since the measured lateral acceleration includes the influence of the gravity component due to the road bank angle, the lateral acceleration measurement is given by $a_y = \ddot{y} + ru_x + gsin(\varphi_r)$. Hence, the equation $ma_y = F_{yf} + F_{yr}$ holds even in the presence of road bank angle. Road bank angle also does not affect equation (10.3).

The lateral tire force for each of the front and rear tires is computed from a lateral tire model for parabolic normal pressure distribution [**3**]:

$$F_y = \mu F_z\,(3\theta\alpha - 3\theta^2\alpha^2 sgn(\alpha) + \theta^3\alpha^3), \qquad \theta = \frac{4a_c^2 b_c k}{3\mu F_z} \tag{10.4}$$

where μ is tire-road friction coefficient, F_z is the vertical force on the tire, a_c is half-length of contact patch, b_c is half-width of contact patch, and k is isotropic stiffness of tire elements per unit area of the belt surface. Assume that the variables $\mu, F_z,$ and θ are known and that they change slowly. This is a reasonable assumption. The variable θ is indeed a constant dependent only on tire parameters. While the variable F_z does change somewhat with longitudinal acceleration and deceleration, this change is slow and can be estimated quite easily. The friction coefficient μ can be estimated from the longitudinal dynamics of the vehicle [**3**], [**31**]. The equation (10.4) can then be simplified as

$$F_y = c_1\alpha - c_2\alpha^2 sgn(\alpha) + c_3\alpha^3. \tag{10.5}$$

Note: It is also possible to use other nonlinear lateral tire models for the problem, such as the Pacejka Magic Formula tire model [**3**].

The lateral tire forces described by equation (10.4) are presented in Figure 10-3.

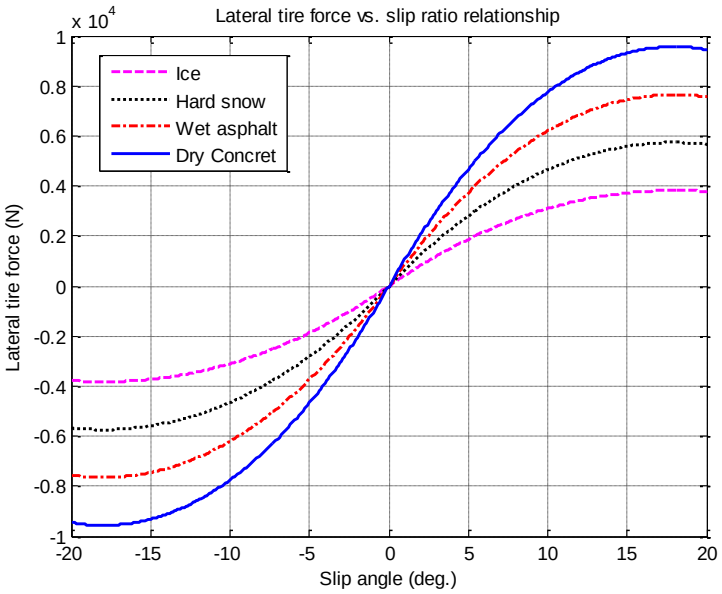

Figure 10-3 Lateral tire force described by equation (10.4).

The slip angles at the front and rear tires can be related to the body slip angle and the yaw rate using the following linear approximations:

$$\alpha_f = \delta - \left(\beta + \frac{ra}{u_x}\right), \qquad \alpha_r = \frac{rb}{u_x} - \beta \tag{10.6}$$

where α_f and α_r are slip angles of the front and rear wheels respectively and β is vehicle body slip angle.

Including the tire model, the vehicle dynamic model can be written as

$$\begin{aligned} ma_y &= m(\ddot{y} + ru_x) = c_{1f}\alpha_f + c_{1r}\alpha_r + \eta(\alpha_f) + \eta(\alpha_r) \\ I_z\dot{r} &= ac_{1f}\alpha_f - bc_{1r}\alpha_r + a\eta(\alpha_f) - b\eta(\alpha_r) \end{aligned} \tag{10.7}$$

where $\eta(\alpha_f) = -c_{2f}\alpha_f^2 sgn(\alpha_f) + c_{3f}\alpha_f^3$ and $\eta(\alpha_r) = -c_{2r}\alpha_r^2 sgn(\alpha_r) + c_{3r}\alpha_r^3$.

We need to rewrite equation (10.7) in the standard system dynamics format described by

$$\begin{aligned} \dot{x} &= Ax + \Phi(x) + g(y,u) \\ y &= Cx + \Psi(x) \end{aligned} \tag{10.8}$$

where $x \in R^n$ is the state vector, $u \in R^p$ is the input vector, and $y \in R^m$ is the output measurement vector. $A \in R^{n\times n}$ and $C \in R^{m\times n}$are appropriate matrices. The functions $\Phi(x)\colon R^n \to R^n$, $\Psi(x)\colon R^n \to R^m$, and $g(y,u)\colon R^m \times R^p \to R^n$ are nonlinear.

It is possible to choose β and r as the state vector and write equation (10.7) in the form of equation (10.8). However, the nonlinearities of the system as shown in equation (10.9) will become too complicated, if these state variables are chosen.

$$\begin{aligned} m(\ddot{y} + ru) &= c_1\left(\delta - \left(\beta + \frac{ra}{u}\right)\right) + c_2\left(\frac{rb}{u} - \beta\right) + \eta\left(\delta - \left(\beta + \frac{ra}{u}\right)\right) + \eta\left(\frac{rb}{u} - \beta\right) \\ I\dot{r} &= ac_1\left(\delta - \left(\beta + \frac{ra}{u}\right)\right) - bc_2\left(\frac{rb}{u} - \beta\right) + a\eta\left(\delta - \left(\beta + \frac{ra}{u}\right)\right) - b\eta\left(\frac{rb}{u} - \beta\right) \end{aligned} \tag{10.9}$$

where $\eta(\alpha_f) = -c_{2f}\alpha_f^2 sgn(\alpha_f) + c_{3f}\alpha_f^3$ and $\eta(\alpha_r) = -c_{2r}\alpha_r^2 sgn(\alpha_r) + c_{3r}\alpha_r^3$.

To overcome this problem, we choose the slip angles at the front and rear tires α_f and α_r as the states. Then, the system equations can be written as

$$\begin{aligned} \begin{bmatrix} \dot{\alpha}_f \\ \dot{\alpha}_r \end{bmatrix} &= \begin{bmatrix} -\left(\frac{u_x}{a+b} + \frac{a^2 c_{1f}}{I_z u_x}\right) & \left(\frac{u_x}{a+b} + \frac{abc_{1r}}{I_z u_x}\right) \\ -\left(\frac{u_x}{a+b} - \frac{abc_{1f}}{I_z u_x}\right) & \left(\frac{u_x}{a+b} - \frac{b^2 c_{1r}}{I_z u_x}\right) \end{bmatrix} \begin{bmatrix} \alpha_f \\ \alpha_r \end{bmatrix} \\ &+ \begin{bmatrix} \left(\frac{u_x}{a+b}\right) & 1 & -\frac{1}{u_x} \\ \left(\frac{u_x}{a+b}\right) & 0 & -\frac{1}{u_x} \end{bmatrix} \begin{bmatrix} \delta \\ \dot{\delta} \\ a_y \end{bmatrix} + \begin{bmatrix} -\frac{a^2}{I_z u_x}\eta(\alpha_f) + \frac{ab}{I_z u_x}\eta(\alpha_r) \\ +\frac{ab}{I_z u_x}\eta(\alpha_f) - \frac{b^2}{I_z u_x}\eta(\alpha_r) \end{bmatrix}. \end{aligned} \tag{10.10}$$

For the output, we can measure a_y using an accelerometer and r by a gyroscope. Also, we know the steering input, δ, and the steering rate input, $\dot{\delta}$. These are known inputs. Then, the output equation can be written as

$$\begin{bmatrix} y_1 \\ y_2 \end{bmatrix} = \begin{bmatrix} r - \left(\frac{u_x}{a+b}\right)\delta \\ a_y \end{bmatrix} = \begin{bmatrix} -\left(\frac{u_x}{a+b}\right) & \left(\frac{u_x}{a+b}\right) \\ \frac{c_{1f}}{m} & \frac{c_{1r}}{m} \end{bmatrix} \begin{bmatrix} \alpha_f \\ \alpha_r \end{bmatrix} + \begin{bmatrix} 0 \\ \frac{\eta(\alpha_f)}{m} + \frac{\eta(\alpha_r)}{m} \end{bmatrix}. \tag{10.11}$$

Then, the slip angle of the vehicle can be computed from the slip angle of the front or rear tire as

$$\beta = \delta - \left(\alpha_f + \frac{ra}{u_x}\right) \; or \; \beta = \frac{rb}{u_x} - \alpha_r. \tag{10.12}$$

It is desired to use a nonlinear observer based on the above nonlinear vehicle model (10.10)-(10.11) to estimate slip angle. However, most available nonlinear observers in literature are designed for a nonlinear system with linear measurement equations. Moreover, the most commonly used techniques and applicable observer design methods are based on either linearization or on the assumption that the nonlinear system is Lipschitz. A major limitation of the existing results for Lipschitz nonlinear systems is that they work only for adequately small values of the Lipschitz constant. When the equivalent Lipschitz constant has to be chosen large due to the inherent non-Lipschitz nature of the nonlinearity (such as in the case of vehicle systems), most existing observer design results fail to provide a solution. Hence, we use the corollary to theorem 3 in Chapter 7 to design the nonlinear observer.

10.5. Observer Design for Slip Angle Estimation

For the dynamic equations, the scaling factor $\bar{z}_H$ is 4. ($\bar{z}_H = n \times n - w_H = 2 \times 2 - 0 = 4$). The term $\Phi(x)$ is

$$\Phi(x) = \begin{bmatrix} -\frac{a^2}{I_z u_x}\eta(\alpha_f) + \frac{ab}{I_z u_x}\eta(\alpha_r) \\ +\frac{ab}{I_z u_x}\eta(\alpha_f) - \frac{b^2}{I_z u_x}\eta(\alpha_r) \end{bmatrix} \tag{10.13}$$

where $\eta(\alpha_f) = -c_{2f}\alpha_f^2 sgn(\alpha_f) + c_{3f}\alpha_f^3$ and $\eta(\alpha_r) = -c_{2r}\alpha_r^2 sgn(\alpha_r) + c_{3r}\alpha_r^3$.

The jacobian of the nonlinear function $\Phi(x)$ is computed to find $\bar{H}_{ij}^{max}$ and $\bar{H}_{ij}^{min}$.

$$\frac{\partial \Phi_1}{\partial \alpha_f} = -\frac{a^2}{I_z u_x}\frac{\partial \eta(\alpha_f)}{\partial \alpha_f} = -\frac{a^2}{I_z u_x}(-2c_2\alpha_f sgn(\alpha_f) + 3c_3\alpha_f^2) \tag{10.14}$$

$$\frac{\partial \Phi_1}{\partial \alpha_r} = -\frac{ab}{I_z u_x}\frac{\partial \eta(\alpha_r)}{\partial \alpha_r} = -\frac{ab}{I_z u_x}(-2c_2\alpha_r sgn(\alpha_r) + 3c_3\alpha_r^2) \tag{10.15}$$

$$\frac{\partial \Phi_2}{\partial \alpha_f} = -\frac{ab}{I_z u_x}\frac{\partial \eta(\alpha_f)}{\partial \alpha_f} = -\frac{ab}{I_z u_x}(-2c_2\alpha_f sgn(\alpha_f) + 3c_3\alpha_f^2) \tag{10.16}$$

$$\frac{\partial \Phi_2}{\partial \alpha_r} = -\frac{b^2}{I_z u_x}\frac{\partial \eta(\alpha_r)}{\partial \alpha_r} = -\frac{b^2}{I_z u_x}(-2c_2\alpha_r sgn(\alpha_r) + 3c_3\alpha_r^2) \tag{10.17}$$

Then $\bar{H}_{ij}^{max}$ and $\bar{H}_{ij}^{min}$ are

$$\bar{H}_{11}^{max} = 4\begin{bmatrix} \max\left(-\frac{a^2}{I_z u_x}(-2c_2\alpha_f sgn(\alpha_f) + 3c_3\alpha_f^2)\right) & 0 \\ 0 & 0 \end{bmatrix} \tag{10.18}$$

$$\bar{H}_{12}^{max} = 4\begin{bmatrix} 0 & max\left(-\frac{ab}{I_z u_x}(-2c_2\alpha_r sgn(\alpha_r) + 3c_3\alpha_r^2)\right) \\ 0 & 0 \end{bmatrix} \tag{10.19}$$

$$\bar{H}_{21}^{max} = 4\begin{bmatrix} 0 & 0 \\ max\left(-\frac{ab}{I_z u_x}(-2c_2\alpha_f sgn(\alpha_f) + 3c_3\alpha_f^2)\right) & 0 \end{bmatrix} \tag{10.20}$$

$$\bar{H}_{22}^{max} = 4\begin{bmatrix} 0 & 0 \\ 0 & max\left(-\frac{b^2}{I_z u_x}(-2c_2\alpha_r sgn(\alpha_r) + 3c_3\alpha_r^2)\right) \end{bmatrix} \tag{10.21}$$

$$\bar{H}_{11}^{min} = \bar{H}_{12}^{min} = \bar{H}_{21}^{min} = \bar{H}_{22}^{min} = 0. \tag{10.22}$$

For the measurement equation, the scaling factor $\bar{z}_G$ is 2. Since $\Psi_1(x) = 0$, the scaling factor $\bar{z}_G$ is less than $m \times n$. ($\bar{z}_G = m \times n - w_G = 2 \times 2 - 2 = 2$). The nonlinear function $\Psi(x)$ is

$$\Psi(x) = \begin{bmatrix} 0 \\ \frac{\eta(\alpha_f)}{m} + \frac{\eta(\alpha_r)}{m} \end{bmatrix}. \tag{10.23}$$

where $\eta(\alpha_f) = -c_{2f}\alpha_f^2 sgn(\alpha_f) + c_{3f}\alpha_f^3$ and $\eta(\alpha_r) = -c_{2r}\alpha_r^2 sgn(\alpha_r) + c_{3r}\alpha_r^3$.

The jacobian of the nonlinear function $\Psi(x)$ is computed to find $\bar{G}_{kj}^{max}$ and $\bar{G}_{kj}^{min}$.

$$\frac{\partial \Psi_1}{\partial \alpha_f} = 0, \qquad \frac{\partial \Psi_1}{\partial \alpha_r} = 0 \tag{10.24}$$

$$\frac{\partial \Psi_2}{\partial \alpha_f} = \frac{\partial \eta(\alpha_f)}{m\partial \alpha_f} = \frac{1}{m}(-2c_2\alpha_f sgn(\alpha_f) + 3c_3\alpha_f^2) \tag{10.25}$$

$$\frac{\partial \Psi_2}{\partial \alpha_r} = \frac{\partial \eta(\alpha_r)}{m \partial \alpha_r} = \frac{1}{m}(-2c_2\alpha_r sgn(\alpha_r) + 3c_3\alpha_r^2) \tag{10.26}$$

Then $\bar{G}_{kj}^{max}$ and $\bar{G}_{kj}^{min}$ are

$$\bar{G}_{11}^{max} = \bar{G}_{12}^{max} = 0 \tag{10.27}$$

$$\bar{G}_{21}^{max} = 2\begin{bmatrix} 0 & 0 \\ \max\left(\frac{1}{m}\left(-2c_2\alpha_f sgn\left(\alpha_f\right) + 3c_3\alpha_f^2\right)\right) & 0 \end{bmatrix} \tag{10.28}$$

$$\bar{G}_{22}^{max} = 2\begin{bmatrix} 0 & 0 \\ \max\left(\frac{1}{m}(-2c_2\alpha_r sgn(\alpha_r) + 3c_3\alpha_r^2)\right) & 0 \end{bmatrix} \tag{10.29}$$

$$\bar{G}_{11}^{min} = \bar{G}_{12}^{min} = \bar{G}_{21}^{min} = \bar{G}_{22}^{min} = 0 \tag{10.30}$$

Next, we solve equations (7.27) for the observer gain. Using the LMI toolbox in Matlab, the example of observer gain for high friction surface is found to be $L = \begin{bmatrix} -40.8224 & 1.6749 \\ 44.9540 & 2.9837 \end{bmatrix}$. (Note: The LMI toolbox in Matlab provides only one gain, though theoretically many solutions can exist to the LMI (7.27). If a faster convergence rate is desired, the RHS in equation (7.27) could be replaced by a negative definite matrix instead of zero.)

10.6. Experimental Set Up

The test vehicle used for the experimental evaluation is a Volvo XC90 sport utility vehicle. Vehicle testing was conducted at the Eaton Proving Ground in Marshall, Michigan. A MicroAutoBox from dSPACE was used for real-time data acquisition. A real-time GPS system, RT3000, from Oxford Technical Solutions was used for these tests to accurately measure the vehicle slip angle for comparison with the performance of the slip angle estimation algorithm. The specification of slip angle estimates from this system according to the manufacturer is 0.15 degrees [**35**]. The GPS outputs were connected to the MicroAutoBox via CAN communication at the baud rate of 0.5 Mbits/sec. To obtain objective test results, the vehicle was instrumented to record the relevant values from

both CAN network and GPS. The sampling time is set at 2 milliseconds. A photograph of the test vehicle is shown in Figure 10-4.

Figure 10-4 The Volvo XC90 test vehicle with GPS system.

The signals required by the observer (7.2) are the lateral acceleration, longitudinal velocity, yaw rate, steering angle and steering rate. The steering angle was obtained over the CAN network bus of the Volvo XC90. The steering rate was obtained by differentiating the steering angle. The other variables were obtained from the RT3000 system. While the RT3000 system is an expensive 6 axis inertial system combined with GPS, the observer developed in this dissertation utilized only raw lateral acceleration, longitudinal velocity and yaw rate signals.

10.7. Experimental Evaluation of Slip Angle Estimation

The maneuvers that were chosen to evaluate the observer are a standard double lane-change on high friction road, standard double lane-change on low friction road, and a random maneuver on a dirt surface. The estimated slip angle was compared with the slip angle detected using the accurate GPS-INS system.

Figure 10-5 shows the experimental results of a double lane-change maneuver on a high friction road with the vehicle speed at 70 mph. The figure shows that the estimated slip angle is able to match the slip angle obtained from the GPS system very well. Figure 10-6 shows the experimental results of a random driving maneuver on a high friction road surface. It can be seen again that the nonlinear observer provides accurate and drift-free estimates of the slip angle.

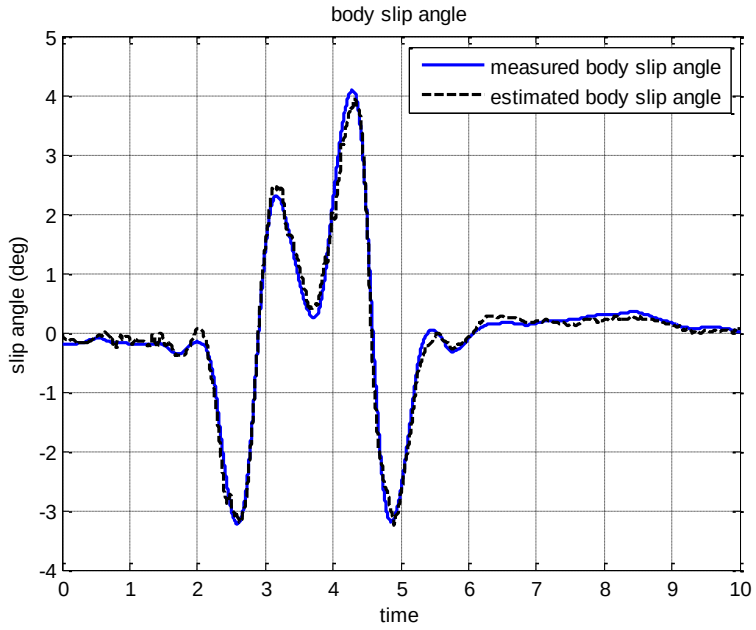

Figure 10-5 Slip angle estimation result in double lane change test on high friction road surface.

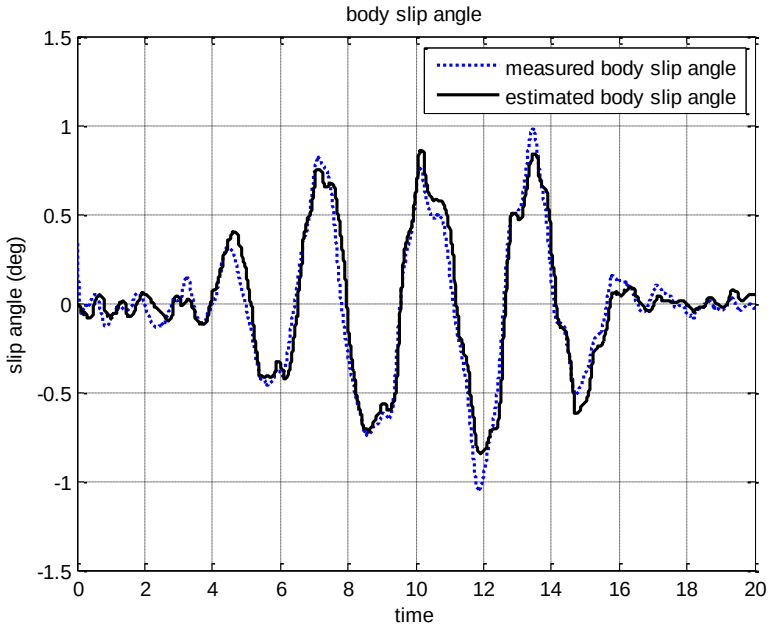

Figure 10-6 Slip angle estimation result in random driving test.

Figure 10-7 and Figure 10-8 show the experimental results of a double lane-change maneuver on a low friction road surface ($\mu = 0.35$) with the vehicle speed at 35 mph.

Figure 6 shows the relation between rear slip angle and total lateral force of the vehicle. The figure indicates that the total lateral force is proportional to the slip angle when the slip angle is small ($\alpha < 0.07$). The maximum lateral force is 9000 N. After $\alpha \geq 0.07$, the lateral fire force saturates. In this case, it implies that a linear tire force model cannot be used for this problem. If the model is described by a linear tire force model, it will cause large errors in the slip angle estimation. Figure 10-8 shows the estimated slip angle on the low friction road.

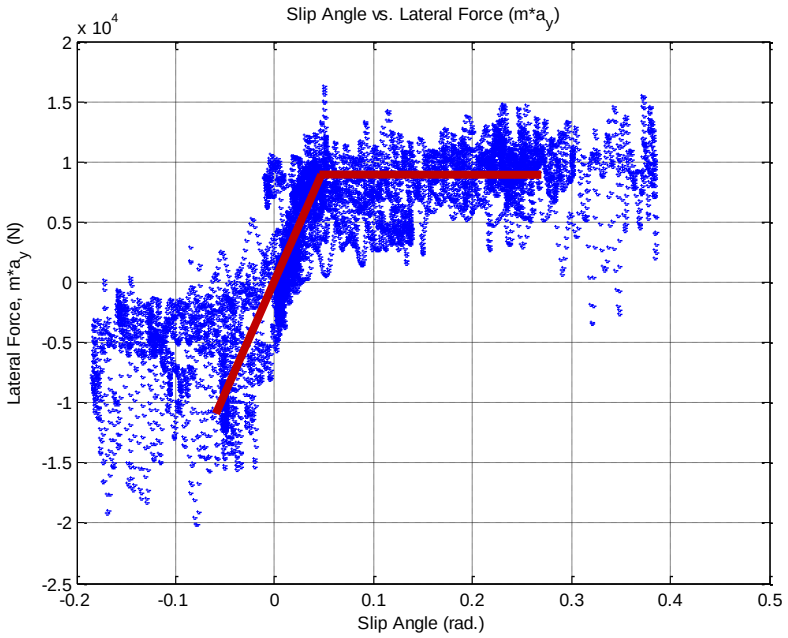

Figure 10-7 Rear slip angle vs. total lateral force (ma_y) result in double lane change test on low friction road surface.

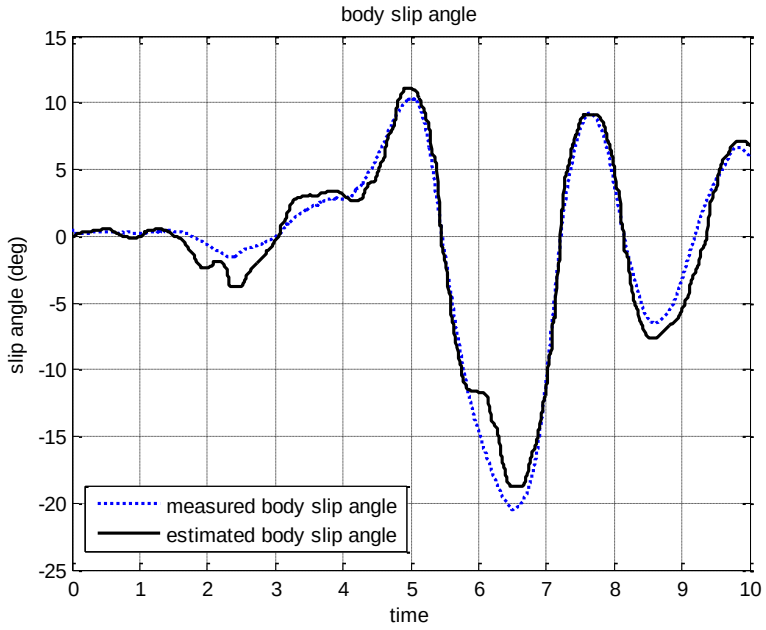

Figure 10-8 Slip angle estimation result in double lane change test on low friction road surface.

The estimation errors for slip angle in the 3 different maneuvers are shown in Table 1. The table shows that the RMS errors are less than 0.15 degrees on high friction road and approximatly 1.4 degrees on icy road. It should be noted that the slip angle values are far higher on the icy road and hence the RMS error as a percentage of slip angle range is of the same order as on the high friction road.

Table 10-1 Estimation errors for experimental tests.

	Double lane-change on high friction surface	**Random driving on high friction surface**	**Double lane-change on low friction surface**
Maximum error (deg)	**0.6588**	**0.3791**	**4.7024**
RMS error (deg)	**0.1421**	**0.1015**	**1.3217**
$\frac{maximum\ error}{maximum\ \beta}$	**0.1624**	**0.3602**	**0.2273**
R^2	**0.98700**	**0.9259**	**0.9662**

The extended Kalman filter (EKF) is an observer that involves a copy of the plant and output injection to the observer. It is used to design observers for nonlinear problems. However, there are few theoretical results to show when an observer design will be

successful. In references [**44**], [**45**], they have shown conditions that the EKF will be a locally asymptotic stable. However, their conditions are not easy to verify. In order to compare the EKF and the new observer design, it seems that the new observer design is easier to guarantee the stability of the system. Also, the computation cost of the new observer is less than the EKF.

10.8. Conclusions

This dissertation developed a new nonlinear observer design technique for estimation of slip angle using inexpensive sensors normally available for yaw stability control applications. The approach utilized is to use the mean value theorem to express the nonlinear error dynamics as a convex combination of known matrices with time varying coefficients. The observer gains are then obtained by solving linear matrix inequalities (LMIs). The developed approach can enable observer design for a large class of differentiable nonlinear systems with a globally (or locally) bounded Jacobian. The developed nonlinear observer for slip angle estimation is evaluated through experimental tests on a Volvo XC90 sport utility. The experimental results show that the developed nonlinear observer can reliably estimate slip angle for a variety of test maneuvers.

Chapter 11

11. APPLICATION OF NONLINEAR OBSERVER TO AUTOMOTIVE ROLL ANGLE ESTIMATION

11.1. Summary

Roll Angle is an important variable that play a critical role in the calculation of real-time rollover index for a vehicle. The rollover index predicts the real-time propensity for rollover and is used in activation of rollover prevention systems such as differential braking based stability control systems. Sensors to measure roll angle are expensive. Thus this chapter utilized the previously developed nonlinear observer design technique in Chapter 6 for estimation of roll angle using inexpensive sensors, a gyroscope and a lateral accelerometer. The performance of the developed algorithms is investigated using experimental tests. Experimental data confirm that the developed algorithms perform reliably in a number of different maneuvers that include constant steering, ramp steering, double lane change, and sine with dwell steering tests.

11.2. Introduction

Vehicles rollovers account for a significant fraction of highway traffic fatalities. According to NHTSA's records (http://www.safercar.gov), although there were nearly 11 million crashes in 2002, only 3% involved a rollover. However, there were more than 10,000 deaths in rollover crashes in 2002. Thus, rollovers caused nearly 33% of all deaths from passenger vehicle crashes [**8**]. Hence there is significant research being conducted on development of active rollover prevention systems. An active rollover prevention system typically utilizes differential braking to reduce the yaw rate of the vehicle and to slow down the vehicle speed. This factor contributes to reducing the propensity of the vehicle to rollover.

An important challenge in the design of an active rollover prevention system is the calculation of the rollover index which indicates the likelihood of the vehicle to rollover

and is used to trigger differential braking to prevent rollover. Accurate calculation of the rollover index is important in order to ensure that rollovers can be prevented in time while at the same ensuring that active rollover prevention is not triggered unnecessarily.

One method of defining the rollover index is based on the use of the real-time difference in vertical tire loads between left and right sides of the vehicle. Figure 11-1 shows a schematic of a vehicle with a sprung mass that undergoes roll motion. The difference between the vertical tire forces F_{zl} and F_{zr} caused by the roll motion of the vehicle is used to define the rollover index R [**46**]:

$$R = \frac{F_{zl} - F_{zr}}{F_{zl} + F_{zr}}, \qquad -1 \leq R \leq 1 \tag{11.1}$$

F_{zr} and F_{zl} are the right and left vertical tire forces of a vehicle respectively. A vehicle is considered to roll over when R is more than 1 or less than -1. It should be noted that when a vehicle is traveling straight, F_{zr} equals to F_{zl} and $R = 0$.

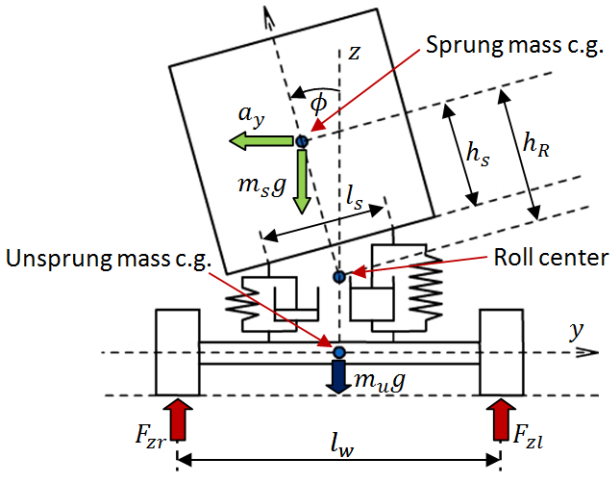

Figure 11-1 Rollover index using lateral load transfer.

If we assume that the roll motion of the sprung mass is caused entirely by the lateral acceleration of the vehicle (ignoring road and other external inputs), then it can be shown that the rollover index of equation (11.1) can be represented as [**20**]

$$R = \frac{2h_R a_y cos\phi + 2h_R sin\phi}{l_w g cos\phi} \tag{11.2}$$

where h_R is the height of the center-of-gravity (c.g.) of the vehicle from the roll center of the sprung mass, l_w is track width of the vehicle, and a_y is the lateral acceleration of the vehicle measured on the unsprung mass.

It should be noted that the rollover index of equation (11.2) needs measurement of lateral acceleration a_y, roll angle ϕ. However, roll angle cannot be measured easily in a vehicle. Suspension deflection measurements on the left and right sides of the vehicle are required in order to calculate roll angle. Since suspension deflection sensors are expensive, real-time measurement of roll angle is typically not available on a passenger vehicle.

Hence the rollover index of equation (11.2) is typically approximated by

$$R_{approx} = \frac{2h_R a_y}{l_w g} \tag{11.3}$$

This dissertation focuses on the accurate estimation of roll angle of the vehicle so as to enable implementation of the original rollover index calculation of equation (11.2).

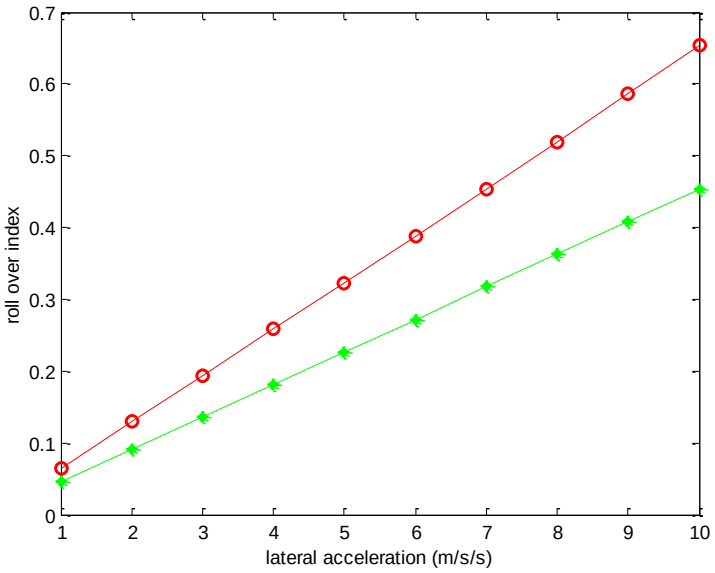

Figure 11-2 Rollover indices *R* (circles) and R_{approx} (stars) as a function of lateral acceleration.

Figure 11-2 shows the original rollover index R and its approximation R_{approx} as a function of lateral acceleration during steady state cornering around a circular track for a Volvo XC 90 SUV. It can be seen that the difference between the two curves increases as lateral acceleration increases, resulting in higher error during tight cornering maneuvers. Further, the error increases with increase in height of the c.g. This motivates the need to estimate roll angle so as use a more accurate calculation of the rollover index.

In this dissertation, we present a method of estimating vehicle roll angle based on a nonlinear vehicle model. The method is suitable for a large range of operating conditions. The developed estimation algorithm was validated with experimental measurements on a test vehicle. They confirm that the developed algorithms perform reliably in a number of different maneuvers.

11.3. Vehicle Roll Dynamics

The approach to estimation of roll angle is to use an observer based on a dynamic model of the vehicle roll dynamics, using only the lateral acceleration and a roll rate gyroscope as the measurements for the observer. Since a lateral accelerometer is anyway required for the rollover index calculation, the only additional sensor being used here then is the roll rate gyroscope.

To develop a dynamic model for the roll dynamics of the vehicle, consider the free body diagram in Figure 11-3.

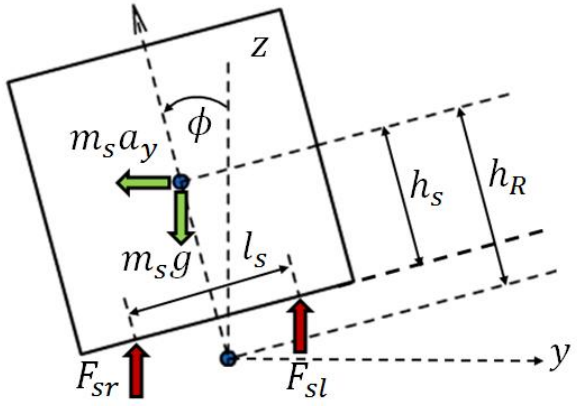

Figure 11-3 Roll dynamics and free body diagram.

Taking moments about the roll center, the roll dynamics equation can be written as

$$\begin{aligned}(I_{xx}+m_s h_R^2)\ddot{\phi} &= \sum M_x \\ (I_{xx}+m_s h_R^2)\ddot{\phi} &= \frac{l_s}{2}(F_{sl}-F_{sr}) + m_s a_y h_R cos\phi + m_s g h_R sin\phi\end{aligned} \tag{11.4}$$

where I_{xx} is moment inertia, l_s is distance between left and right suspension, and m_s is mass of a sprung mass.

The suspension forces are given by

$$F_{sr} = k\frac{l_s}{2}sin\phi + d\frac{l_s}{2}\dot{\phi}cos\phi, \tag{11.5}$$

$$F_{sl} = -k\frac{l_s}{2}sin\phi - d\frac{l_s}{2}\dot{\phi}cos\phi \tag{11.6}$$

where k is suspension stiffness, d is suspension damping.

Substituting equations (11.5) and (11.6) into (11.4). Then the roll dynamics can finally be written down as

$$(I_{xx}+m_s h_R^2)\ddot{\phi} = m_s a_y h_R cos\phi + m_s g h_R sin\phi - k\frac{l_s^2}{2}sin\phi - d\frac{l_s^2}{2}\dot{\phi}cos\phi \tag{11.7}$$

It should be noted that the roll dynamics depend on the lateral dynamics through the lateral acceleration term a_y. By avoiding further expansion of this term in terms of lateral tire forces and lateral dynamic states, a complicated coupled set of equations between roll and lateral dynamics is avoided. Instead, the variable a_y is assumed to be measured.

The state space form of equation (11.7) and measurement equation can be written as

$$\begin{bmatrix}\dot{\phi}\\ \ddot{\phi}\end{bmatrix} = \begin{bmatrix}0 & 1\\ 0 & 0\end{bmatrix}\begin{bmatrix}\phi\\ \dot{\phi}\end{bmatrix} + \begin{bmatrix}0\\ \dfrac{\left(m_s g h_R - k\frac{l_s^2}{2}\right)}{(I_{xx}+m_s h_R^2)}sin\phi - \dfrac{\left(d\frac{l_s^2}{2}\right)}{(I_{xx}+m_s h_R^2)}\dot{\phi}cos\phi + \dfrac{m_s h_R}{(I_{xx}+m_s h_R^2)}a_y cos\phi\end{bmatrix} \tag{11.8}$$

$$y = [0 \quad 1]\begin{bmatrix}\phi \\ \dot{\phi}\end{bmatrix} \tag{11.9}$$

It is desired to use a nonlinear observer based on the above nonlinear vehicle model to estimate roll angle. Hence, we use the corollary to theorem 2 in Chapter 6 to design the nonlinear observer.

11.4. Observer Design for Roll Angle Estimation

The equations (11.8) and (11.9) show that the pair of (A, C) is unobservable. With this system, we cannot design an observer for this problem. We need to modify the equation (11.8).

The modified model is given by

$$\begin{bmatrix}\dot{\phi} \\ \ddot{\phi}\end{bmatrix} = \begin{bmatrix}0 & 1 \\ -A_{21} & -A_{22}\end{bmatrix}\begin{bmatrix}\phi \\ \dot{\phi}\end{bmatrix} + \begin{bmatrix} 0 \\ \left(\frac{\left(m_s g h_R - k\frac{l_S^2}{2}\right)}{(I_{xx} + m_s h_R^2)} sin\phi - \frac{\left(d\frac{l_S^2}{2}\right)}{(I_{xx} + m_s h_R^2)}\dot{\phi}cos\phi + \frac{m_s h_R}{(I_{xx} + m_s h_R^2)} a_y cos\phi + A_{21}\phi + A_{22}\dot{\phi}\right) \end{bmatrix}. \tag{11.10}$$

where $A_{21} > 0$ and $A_{22} > 0$. The modified model is valid for designing an observer since the original model include stabilized terms, $\frac{\left(m_s g h_R - k\frac{l_S^2}{2}\right)}{(I_{xx}+m_s h_R^2)} sin\phi$ and $-\frac{\left(d\frac{l_S^2}{2}\right)}{(I_{xx}+m_s h_R^2)}\dot{\phi}cos\phi$. Also, the modified model will be unobservable only when $\phi = 0$.

11.4.1. Observer Design Using Corollary to Theorem 2

Apply corollary to theorem 2 in the chapter 6 for the problem.

For the dynamic equation (11.10), the scaling factor $\bar{z}_H$ is 2. Since Φ_1=0, then $w_H = 2$ and the scaling factor $\bar{z}_H$ is $n \times n - w_H$. ($\bar{z}_H = 2 \times 2 - 2 = 2$). The nonlinear function Φ is

$$\Phi = \begin{bmatrix} 0 \\ \left(\frac{\left(m_s g h_R - k\frac{l_s^2}{2}\right)}{(I_{xx} + m_s h_R^2)} sin\phi - \frac{\left(d\frac{l_s^2}{2}\right)}{(I_{xx} + m_s h_R^2)} \dot{\phi} cos\phi \right. \\ \left. + \frac{m_s h_R}{(I_{xx} + m_s h_R^2)} a_y cos\phi + A_{21}\phi + A_{22}\dot{\phi} \right) \end{bmatrix} \tag{11.11}$$

Then the jacobian of the nonlinear function $\Phi(x)$ is computed to find $\bar{H}_{ij}^{max}$ and $\bar{H}_{ij}^{min}$.

$$\frac{\partial \Phi_1}{\partial \phi} = 0, \qquad \frac{\partial \Phi_1}{\partial \dot{\phi}} = 0 \tag{11.12}$$

$$\frac{\partial \Phi_2}{\partial \phi} = \begin{pmatrix} \frac{\left(m_s g h_R - k\frac{l_s^2}{2}\right)}{(I_{xx} + m_s h_R^2)} cos\phi + \frac{\left(d\frac{l_s^2}{2}\right)}{(I_{xx} + m_s h_R^2)} \dot{\phi} sin\phi \\ - \frac{m_s h_R}{(I_{xx} + m_s h_R^2)} a_y sin\phi + A_{21} \end{pmatrix} \tag{11.13}$$

$$\frac{\partial \Phi_2}{\partial \phi} = -\frac{\left(d\frac{l_s^2}{2}\right)}{(I_{xx} + m_s h_R^2)} cos\phi + A_{22} \tag{11.14}$$

The $\bar{H}_{ij}^{max}$ and $\bar{H}_{ij}^{min}$ are given by

$$\bar{H}_{11}^{max} = \bar{H}_{12}^{max} = \bar{H}_{11}^{min} = \bar{H}_{12}^{min} = 0 \tag{11.15}$$

$$\bar{H}_{21}^{max} = 2\begin{bmatrix} 0 & 0 \\ \max(\partial\Phi_2/\phi) & 0 \end{bmatrix}, \bar{H}_{21}^{min} = 2\begin{bmatrix} 0 & 0 \\ \min(\partial\Phi_2/\phi) & 0 \end{bmatrix} \tag{11.16}$$

$$\bar{H}_{22}^{max} = 2\begin{bmatrix} 0 & 0 \\ 0 & \max(\partial\Phi_2/\dot{\phi}) \end{bmatrix}, \bar{H}_{22}^{min} = 2\begin{bmatrix} 0 & 0 \\ 0 & \min(\partial\Phi_2/\dot{\phi}) \end{bmatrix} \tag{11.17}$$

Next, we solve equations (6.35) for the observer gain. Using the LMI toolbox in Matlab. (Note: The LMI toolbox in Matlab provides only one gain, though theoretically many solutions can exist to the LMI (6.35). If a faster convergence rate is desired, the RHS in equation (6.35) could be replaced by a negative definite matrix instead of zero.)

11.5. Experimental Evaluation of Roll Angle Estimation

11.5.1.Experimental Set Up

The test vehicle used for the experimental evaluation is a Volvo XC90 sport utility vehicle. A MicroAutoBox from dSPACE was used for real-time data acquisition. The vehicle had been installed with a gyroscope, a lateral accelerometer, and a tilt angle

sensor to estimate the roll angle of the vehicle. The tilt angle sensor consisting of the Crossbow CXTD02 inertial angle sensor can be used to supplement the gyroscope. The Crossbow tilt angle sensor consist of two axis in-built accelerometer and signal processing algorithms that enable static tilt angle to be calculated from the accelerometer measurements. An example of an algorithm that can be used for this purpose can be found in [**47**].

Figure 11-4 The test vehicle, Volvo XC90 sport utility vehicle

In order to compare the performance of the new observer design, we will compare the results of the new observer and the results of a standard observer [**24**] based on Lipschitz system based design.

The standard observer has the same form of the observer equation as shown in equation (6.2). However, there is a different method to select the observer gain L. The details of the standard observer is in section 9.4.2 of chapter 9.

For designing an observer for this problem, we assume that

1.$-25 \leq \phi \leq 25\ deg.$,

2. $-1 \leq \dot{\phi} \leq 1$ rad./sec. or $-57.3 \leq \dot{\phi} \leq 57.3$ deg./sec.,

3.$-10 \leq a_y \leq 10$ m/s^2,

4. $\dot{a}_y$ is small.

Then the local bound of the nonlinear function can be found and can be used as the Lipschitz constant.

11.5.2.Experimental Results

The observer gain found by using the new observer is $L = [-3.3628 \quad 27.9208]^T$. Also, the observer gain found by using the standard observer is $L = [-184.8724 \quad 48.0296]^T$

The comparison results between the new observer and the standard observer is shown in Figure 11-5. In this case, the maneuver is created by a constant steering.

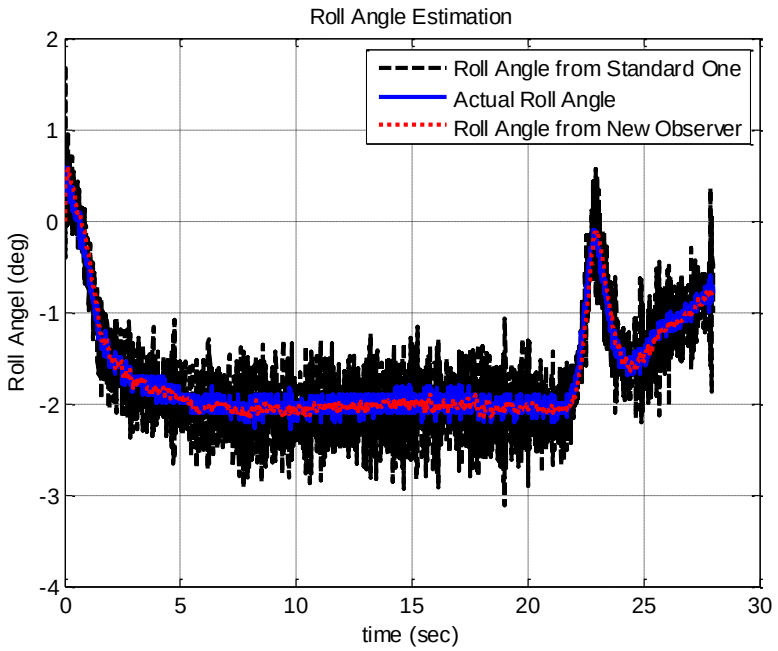

Figure 11-5 Roll angle estimation from constant steering.

Figure 11-5 shows that the developed new observer is the more appropriate observer for this problem. This is because the Lipschitz constant for this problem is very large. By using the developed theorem, it is possible to obtain observer gains which are smaller than those from a Lipschitz based observer. The small gains of the observer are good for estimating parameters because they will not enhance noise unlike the Lipshitz based observer. The performance of the new observer is clearly better than that of the standard Lipshitz observer.

To confirm the results, we also evaluate the algorithm with other maneuvers, ramp steering and double lane change. The results on Figure 11-6 and Figure 11-7 show that the estimated roll angle is able to match the measurement roll angle.

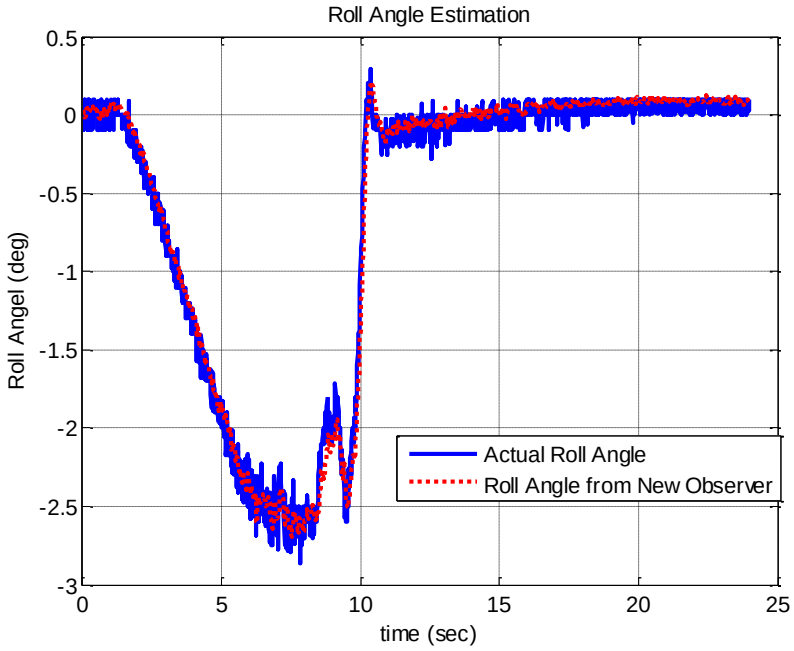

Figure 11-6 Roll angle estimation from ramp steering.

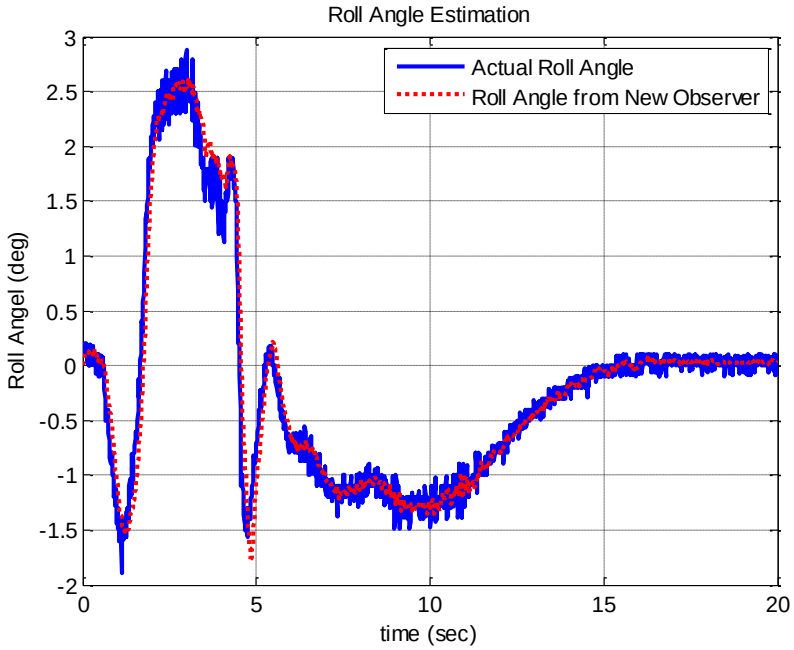

Figure 11-7 Roll angle estimation from double lane change.

11.6. Conclusions

Roll angle is an important variable that play a critical role in the calculation of real-time rollover index for a vehicle. Sensors to measure roll angle are expensive.

This dissertation developed a new nonlinear observer design technique for estimation of roll angle using inexpensive sensors, a gyroscope and a lateral accelerometer. The approach utilized is to use the mean value theorem to express the nonlinear error dynamics as a convex combination of known matrices with time varying coefficients. The observer gains are then obtained by solving linear matrix inequalities (LMIs). The developed approach can enable observer design for a large class of differentiable nonlinear systems with a globally (or locally) bounded Jacobian. The performance of the developed algorithms was investigated using simulation and experimental tests on a large SUV. Experimental data confirm that the developed algorithms performed reliably in a number of different maneuvers that include constant steering, ramp steering, and sine with dwell steering tests. The results in the dissertation provide solutions that will enable accurate calculation of rollover index, thus enabling better rollover prevention systems to be developed.

Chapter 12

12. APPLICATION OF NONLINEAR OBSERVER TO ROLLOVER INDEX ESTIMATION FOR TRIPPED AND UN-TRIPPED ROLLOVERS

In order to predict tripped and un-tripped rollovers as described in section 2.3, many variables need to be measured. However, some variables such as unknown road inputs, vertical displacements of unsprung masses and sprung mass, and the unknown lateral force input cannot be directly measured by sensors. Therefore, two different algorithms to estimate rollover index for tripped and un-tripped rollovers have been developed.

The first algorithm is an approach to estimate unknown disturbance inputs in a nonlinear system using dynamic model inversion and a modified version of the mean value theorem. The developed theory is used to estimate vertical tire forces and predict tripped rollovers in situations involving road bumps, potholes, and lateral unknown force inputs.

The second algorithm utilizes a new algebraic formulation of the new rollover index. This algorithm is simple and convenient but can be used only if the roll angle and vertical accelerations on the vehicle body are available as measurments.

12.1. Summary

Accurate detection of the danger of an impending rollover is necessary for active vehicle rollover prevention systems. A real-time rollover index is an indicator used for this purpose. A traditional rollover index utilizes lateral acceleration measurements and can detect only un-tripped rollovers that happen due to high lateral acceleration from a sharp turn. It fails to detect tripped rollovers that happen due to tripping from external inputs such as forces when a vehicle strikes a curb or a road bump. Therefore, this dissertation develops a new rollover index that can detect both tripped and un-tripped rollovers. A methodology is developed for estimation of unknown inputs in a class of nonlinear systems. The methodology is based on dynamic model inversion and nonlinear observer

design to compute the unknown inputs from output measurements. The observer design utilizes the mean value theorem to express the nonlinear error dynamics as a convex combination of known matrices with time varying coefficients. The observer gains are then obtained by solving linear matrix inequalities (LMIs). The developed approach can enable observer design for a large class of differentiable nonlinear systems with a globally (or locally) bounded Jacobian. The developed nonlinear observer is then applied for rollover index estimation. The developed rollover index is also evaluated through simulations with an industry standard software, CARSIM, and with experimental tests on a $1/8^{th}$ scaled vehicle. In order to verify that the scaled vehicle experiments can represent a full-sized vehicle, the Buckingham π theorem is used to show dynamic similarity. The simulation and experimental results show that the developed nonlinear observer can reliably estimate vehicle states, unknown normal tire forces, and rollover index for predicting both un-tripped and tripped rollovers.

12.2. Introduction

Vehicles with increased dimensions and weights are known to be at higher risk of rollover. Normally, rollovers occur in one of two ways, tripped and un-tripped [**48**]. The two types of rollovers are shown in Figure 12-1. A tripped rollover happens due to tripping from external inputs. An example of this rollover happens when a vehicle leaves the roadway and slides sideways, digging its tires into soft soil or striking an object such as a curb or guardrail. An un-tripped rollover, on the other hand, happens due to high lateral acceleration from a sharp turn and not due to external inputs. An example of an un-tripped rollover is when a vehicle makes a sharp collision avoidance lane change maneuver or a cornering maneuver at high speed, and consequently rolls over.

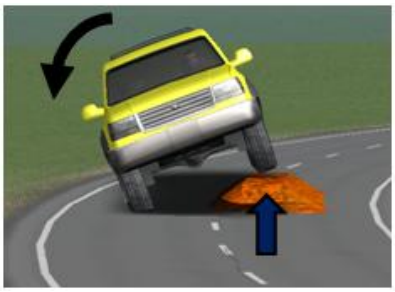

a) Tripped Rollver

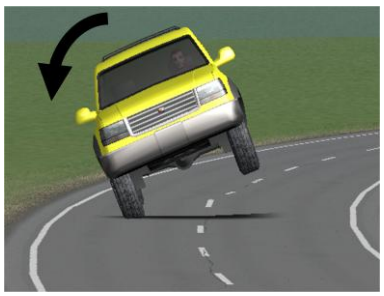

b) Un-tripped Rollover

Figure 12-1 Type of rollover.

An active rollover prevention system is a vehicle stability control system that prevents vehicles from un-tripped rollovers. It has been developed by several automotive manufacturers [**49**], [**9**], e.g. Ford and Volvo. To the best of the authors' knowledge, there are no assistance systems currently available that directly address tripped rollovers. Several types of actuation systems can be used in rollover prevention. A differential braking system has received the most attention from researchers [**50**], [**51**], [**52**] and is used for preventing rollovers by reducing the yaw rate of a vehicle and its speed. Also, steer-by-wire and active suspension systems can be potentially used to prevent rollovers [**19**], [**53**].

In order to make these systems effective in their tasks, accurate detection of the danger of un-tripped and tripped vehicle rollovers is necessary [**9**]. To detect a vehicle rollover, many researchers have developed a real-time index that provides an indication of the danger of rollover. However, they have focused on developing an indicator only for un-tripped rollovers. There are no currently published papers that have studied how to detect tripped vehicle rollovers with unknown external inputs.

In this dissertation, we present a method of estimating vehicle states based on a nonlinear vehicle model. The estimated vehicle states are used to calculate unknown normal tire forces, and a rollover index that can detect both un-tripped and tripped rollovers. The method is suitable for a large range of operating conditions. To begin with, we will introduce the vehicle rollover index in section 12.3. Then the vehicle dynamic model is presented in section 12.4. In section 12.5, we apply the new observer design in chapter 8 to the vehicle problem. After that, in section 12.6, we evaluate the developed estimation algorithm by implementing them in CARSIM, an industry standard vehicle dynamics simulation software. Moreover, we evaluate the estimation algorithm with experimental tests on a $1/8^{th}$ scaled vehicle in section 12.7. Alternate rollover Index with additional measurements will be presented in section 12.8. Finally, the conclusions are presented in section 12.9.

12.3. Vehicle Rollover Index

Accurate detection of the danger of a vehicle rollover is important. Initially, the concept of a static rollover threshold called the static stability factor (SSF) [**15**], [**54**] was studied to detect vehicle rollovers. However, the SSF by itself is not adequate for rollover prediction in dynamic situations. After that the concept of a rollover index has been introduced. A rollover index has also been known by other names such as Roll Safety Factor (RSF) and Load Transfer Ratio (LTR). A rollover index is a real-time variable used for this propose. A simple method of defining the rollover index is based on the use of the real-time difference in vertical tire loads between left and right sides of the vehicle. The formula of the rollover index is described by equation (12.1) [**46**].

$$R = \frac{F_{zr} - F_{zl}}{F_{zr} + F_{zl}}, \qquad -1 \le R \le 1 \tag{12.1}$$

where F_{zr} and F_{zl} are the right and left vertical tire forces of a vehicle respectively. When $R = 1$ ($F_{zl} = 0$) or $R = -1$ ($F_{zr} = 0$), the left or right wheels lift off. Thus R should be prevented from approaching 1 or -1. It should be noted that when a vehicle is traveling straight, F_{zr} equals to F_{zl} and $R = 0$.

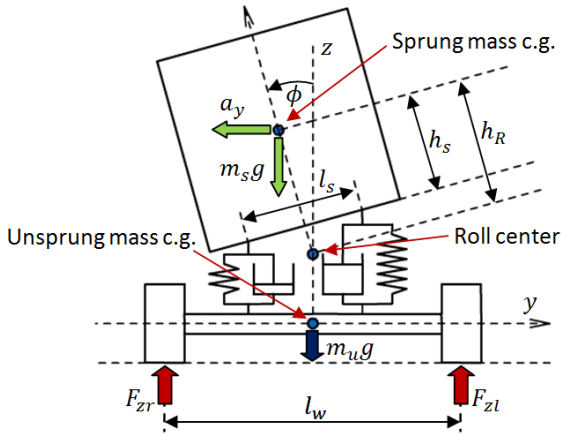

Figure 12-2 Vehicle model for un-tripped rollovers.

The definition of R in equation (12.1) cannot be easily implemented in real-time because the vertical tire forces F_{zr} and F_{zl} cannot be directly measured. Thus, many researchers have tried to derive an estimation of the rollover index based on a 1-degree of freedom

model as shown in Figure 12-2. The 1-degree of freedom is the roll angle ϕ of the vehicle body. Such an example of a traditional rollover index calculated using a one degree of freedom is shown below in equation (12.2):

$$R = \frac{F_{zr} - F_{zl}}{F_{zr} + F_{zl}} = \frac{2m_s a_y h_R}{mgl_w} + \frac{2m_s h_R tan\phi}{ml_w} \tag{12.2}$$

where $m = m_s + m_u$, h_R is c.g. height, l_w is track width, m_u is unsprung mass, m_s is spung mass, a_y is lateral acceleration, and ϕ is roll angle.

This type of rollover index is used for detecting un-tripped rollovers only. It is a function of lateral acceleration and roll angle. Some papers have proposed a rollover index that uses only lateral acceleration [**20**], [**21**] since roll angle is expensive to measure. The stability control with this rollover index may arbitrarily reduce the lateral acceleration capability of the vehicle. Also, as we shall show, it still fails to detect rollovers when rollovers are induced by vertical road inputs or other external inputs.

In order to detect tripped rollovers, which happen due to tripping from external inputs, a new rollover index should include the influence of road and other external inputs. Figure 12-3 shows a vehicle rollover model that includes the influence of road inputs, z_{rr} and z_{rl}. The figure also shows the normal forces on the vehicle, F_{zr} and F_{zl}.

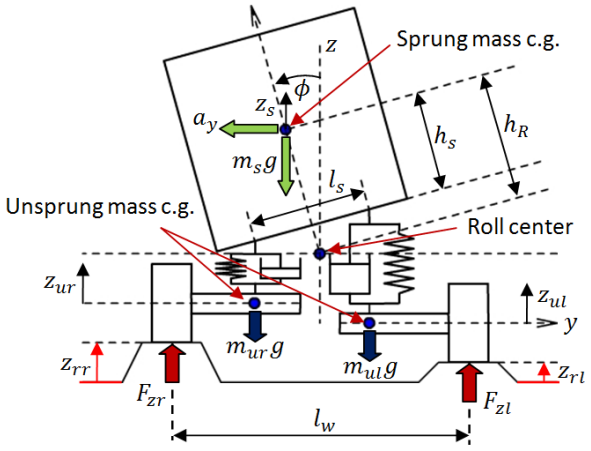

Figure 12-3 Vehicle model for un-tripped and tripped rollovers.

To derive a rollover index in this case, four-degrees of freedom in the model are needed as described in section 12.4. When the influence of road inputs is included, the normal forces on the vehicle, F_{zr} and F_{zl}, are defined by

$$F_{zr} = -F_{tr} + m_{ur}g + \frac{m_s}{2}g, \tag{12.3}$$

$$F_{zl} = -F_{tl} + m_{ul}g + \frac{m_s}{2}g \tag{12.4}$$

where F_{tr} and F_{tl} are the right and left dynamic vertical tire forces, and m_{ur} and m_{ul}, are right and left unsprung masses.

The right and left dynamic vertical tire forces, F_{tr} and F_{tl}, can be calculated by

$$F_{tr} = k_t(z_{ur} - z_{rr}), \tag{12.5}$$

$$F_{tl} = k_t(z_{ul} - z_{rl}) \tag{12.6}$$

where k_t is vertical tire stiffness, z_{rr} and z_{rl} are right and left unknown road profile inputs, z_{ur} and z_{ul} are right and left unsprung mass positions.

It should be noted that the right and left unsprung mass positions, z_{ur} and z_{ul}, depend on the dynamic motions of the heave z_s (sprung mass position), roll angle ϕ of the vehicle body, and the vertical motion of each side of the unsprung masses, z_{ur} and z_{ul}. Therefore, the measurements of roll angle, ϕ, and lateral acceleration, a_y, alone are not enough to calculate the rollover index for predicting tripped rollover. A lot of variables need to be measured or estimated. Moreover, some variables such as unknown road inputs, z_{rr} and z_{rl}, vertical displacements of unsprung masses, and sprung mass, cannot be directly measured by sensors. Therefore, it is necessary to develop an approach for estimating the normal forces of a vehicle, F_{zr} and F_{zl} using available sensors only.

In the next section, we will present the vehicle dynamic model for un-tripped and tripped rollovers. We will write the model in a form that is suitable for estimating the unknown normal forces of a vehicle, F_{zr} and F_{zl}. Subsequently the rollover index can be calculated.

12.4. Vehicle Dynamics Model [3]

In order to obtain the rollover index for predicting tripped rollovers, a model of a vehicle with 4-degrees of freedom is needed as shown in Figure 12-4. The vehicle body is

represented by the sprung mass m_s while the mass due to the axles and tires are represented by unsprung masses m_{ul} and m_{ur}. The springs and dampers between the sprung and unsprung masses represent the vehicle suspension. The vertical tire stiffness of each side of the vehicle is represented by the spring k_t.

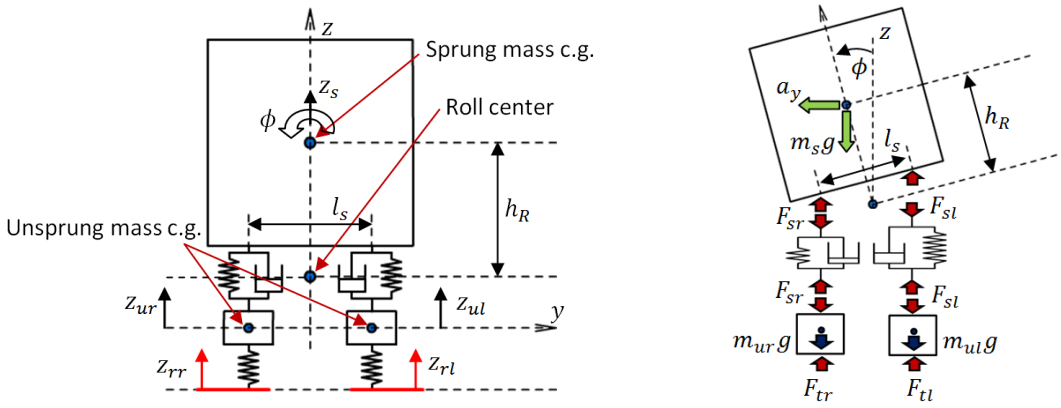

Figure 12-4 Four-degrees of freedom vehicle model.

The 4-degrees of freedom of the model are the heave z_s, roll angle ϕ of the vehicle body, and the vertical motion of each side of the unsprung masses, z_{ur} and z_{ul}. The variables z_{rr} and z_{rl} are the road profile inputs that excite the system.

The dynamic suspension forces are given by

$$F_{sr} = -k(z_s - z_{ur}) + k\frac{l_s}{2}sin\phi - d(\dot{z}_s - \dot{z}_{ur}) + d\frac{l_s}{2}\dot{\phi}cos\phi, \tag{12.7}$$

$$F_{sl} = -k(z_s - z_{ul}) - k\frac{l_s}{2}sin\phi - d(\dot{z}_s - \dot{z}_{ul}) - d\frac{l_s}{2}\dot{\phi}cos\phi \tag{12.8}$$

where k is suspension stiffness, d is suspension damping. z_s, z_{ur}, and z_{ul} are measured from their equilibrium points.

Then, the dynamic equations of sprung mass heave and sprung mass roll motions are given by (12.9) and (12.10).

$$\ddot{z}_s = -\frac{k}{m_s}(z_s - z_{ur}) - \frac{d}{m_s}(\dot{z}_s - \dot{z}_{ur}) - \frac{k}{m_s}(z_s - z_{ul}) - \frac{d}{m_s}(\dot{z}_s - \dot{z}_{ul}) \tag{12.9}$$

$$\ddot{\phi} = \frac{kl_s}{2I}(z_s - z_{ur}) + \frac{dl_s}{2I}(\dot{z}_s - \dot{z}_{ur}) - \frac{kl_s}{2I}(z_s - z_{ul}) - \frac{dl_s}{2I}(\dot{z}_s - \dot{z}_{ul}) + \left(\frac{m_s g h_R}{I} - \frac{kl_s^2}{2I}\right) sin\phi - \frac{dl_s^2}{2I}\dot{\phi}cos\phi + \frac{m_s a_y h_R}{I} cos\phi \quad (12.10)$$

where I is moment of inertia, and l_s is distance between right and left suspension. It should be noted that the roll dynamics depend on the lateral dynamics through the lateral acceleration term a_y. By avoiding further expansion of this term in terms of lateral tire forces and lateral dynamic states, a complicated coupled set of equations between roll and lateral dynamics is avoided. Instead, the variable a_y is assumed to be measured.

Assume that $m_{ur} = m_{ul} = m_u$. Then, the dynamic models of the right and left unsprung mass motions are given by

$$\ddot{z}_{ur} = \frac{k}{m_u}(z_s - z_{ur}) - \frac{d}{m_u}(\dot{z}_s - \dot{z}_{ur}) - \frac{kl_s}{2m_u} sin\phi - \frac{dl_s}{2m_u}\dot{\phi}cos\phi - \frac{F_{tr}}{m_u}, \quad (12.11)$$

$$\ddot{z}_{ul} = \frac{k}{m_u}(z_s - z_{ul}) - \frac{d}{m_u}(\dot{z}_s - \dot{z}_{ul}) + \frac{kl_s}{2m_u} sin\phi + \frac{dl_s}{2m_u}\dot{\phi}cos\phi - \frac{F_{tl}}{m_u}. \quad (12.12)$$

The equations (12.3) and (12.4) show that the normal forces on the vehicle, F_{zr} and F_{zl}, can be computed if we know the right and left vertical tire forces, F_{tr} and F_{tl}.

In order to design an observer to estimate the variables used to calculate the rollover index, we need to rewrite equations (12.9)-(12.12) into a state space form. The state space form of equations (12.9)-(12.12) is shown in equation (12.13).

$$\dot{x} = \bar{A}x + \eta(x, u) + \bar{B}\mu \quad (12.13)$$

where u is the vector of known inputs, μ is the vector of unknown inputs,

$$x = [z_s - z_{ur} \quad \dot{z}_s - \dot{z}_{ur} \quad z_s - z_{ul} \quad \dot{z}_s - \dot{z}_{ul} \quad \phi \quad \dot{\phi}]^T, \quad (12.14)$$

$$\bar{A} = \begin{bmatrix} 0 & 1 & 0 & 0 & 0 & 0 \\ -\frac{k}{m_s} - \frac{k}{m_u} & -\frac{d}{m_s} - \frac{d}{m_u} & -\frac{k}{m_s} & -\frac{d}{m_s} & 0 & 0 \\ 0 & 0 & 0 & 1 & 0 & 0 \\ -\frac{k}{m_s} & -\frac{d}{m_s} & -\frac{k}{m_s} - \frac{k}{m_u} & -\frac{d}{m_s} - \frac{d}{m_u} & 0 & 0 \\ 0 & 0 & 0 & 0 & 0 & 1 \\ \frac{kl_s}{2I} & \frac{dl_s}{2I} & -\frac{kl_s}{2I} & -\frac{dl_s}{2I} & 0 & 0 \end{bmatrix},$$

$$\eta(x,u) = \begin{bmatrix} 0 \\ +\frac{kl_s}{2m_u} sin\phi + \frac{dl_s}{2m_u} \dot{\phi} cos\phi \\ 0 \\ -\frac{kl_s}{2m_u} sin\phi - \frac{dl_s}{2m_u} \dot{\phi} cos\phi \\ 0 \\ +\frac{m_s a_y h_R}{I} cos\phi + \left(\frac{m_s g h_R}{I} - \frac{kl_s^2}{2I}\right) sin\phi - \frac{dl_s^2}{2I} \dot{\phi} cos\phi \end{bmatrix},$$

$$\bar{B} = \begin{bmatrix} 0 & 0 \\ \frac{1}{m_u} & 0 \\ 0 & 0 \\ 0 & \frac{1}{m_u} \\ 0 & 0 \\ 0 & 0 \end{bmatrix}, \mu = \begin{bmatrix} F_{tr} \\ F_{tl} \end{bmatrix}.$$

The available measurements used to estimate variables is shown in equation (12.15) and (12.17).

$$z = Ex + \beta(x,u) + b\mu \tag{12.15}$$

where

$$z = \begin{bmatrix} \ddot{z}_{ur} \\ \ddot{z}_{ul} \end{bmatrix}, E = \begin{bmatrix} \frac{k}{m_u} & \frac{d}{m_u} & 0 & 0 & 0 & 0 \\ 0 & 0 & \frac{k}{m_u} & \frac{d}{m_u} & 0 & 0 \end{bmatrix},$$
$$\beta = \begin{bmatrix} -\frac{kl_s}{2m_u} sin\phi - \frac{dl_s}{2m_u} \dot{\phi} cos\phi \\ +\frac{kl_s}{2m_u} sin\phi + \frac{dl_s}{2m_u} \dot{\phi} cos\phi \end{bmatrix}, b = \begin{bmatrix} -\frac{1}{m_u} & 0 \\ 0 & -\frac{1}{m_u} \end{bmatrix}. \tag{12.16}$$

$$y = Cx + \Psi(x) \tag{12.17}$$

where

$$y = \begin{bmatrix} z_s - z_{ur} - \frac{l_s}{2} sin\phi \\ \dot{\phi} \end{bmatrix}, C = \begin{bmatrix} 1 & 0 & 0 & 0 & 0 & 0 \\ 0 & 0 & 0 & 0 & 0 & 1 \end{bmatrix}, \Psi = \begin{bmatrix} -\frac{l_s}{2} sin\phi \\ 0 \end{bmatrix}. \quad (12.18)$$

It is desired to use an observer based on the above vehicle model to estimate variables. The equations (12.13) and (12.17) show that we have the nonlinear terms, η and Ψ, and the unknown inputs μ included in the dynamic and measurement equations. Also, the relative degree for this problem is zero, $r_\mu = 0$. We do not have to differentiate the equation (12.15). The measurements, z, directly relate to the unknown inputs, μ. Thus, the dynamic and measurement equations of this problem are in the appropriate state space form for applying the nonlinear observer described in chapter 8 to solve the problem.

The form of equations (12.13), (12.15), and (12.17) is the same as the form of equations (8.1)-(8.3). So, we can design a nonlinear observer for this problem.

12.5. Observer Design for the Vehicle Problem

In this section, we will apply Theorem 7 and Corollary to Theorem 5 for the problem. To apply them, first, we need to calculate the matrix A. Then, the observability of the pair of (A, C) needs to be examined. If the pair of (A, C) is detectable, we can apply Corollary to Theorem 5 for observer gains.

Using Theorem 7, the unknown inputs, μ, can be computed by

$$\mu = b^{-1}[z - Ex - \beta(x, u)] \quad (12.19)$$

Substitute equation (12.19) into (12.13).

$$\dot{x} = \bar{A}x + \eta(x, u) + \bar{B}b^{-1}[z - Ex - \beta(x, u)] \quad (12.20)$$

$$\dot{x} = (\bar{A} - \bar{B}b^{-1}E)x + \eta(x, u) - \bar{B}b^{-1}\beta(x, u) + \bar{B}b^{-1}z \quad (12.21)$$

Then, $A, \Phi, g(z_f)$ are given by

$$A = (\bar{A} - \bar{B}b^{-1}E), \qquad \Phi = \eta(x, u) - \bar{B}b^{-1}\beta(x, u), \qquad g(z_f) = \bar{B}b^{-1}z \quad (12.22)$$

However, we found that the pair (A, C) is unobservable. With this system, we cannot design an observer for this problem. We need to modify the equations (12.13) and (12.14)

.

The modified model is given by

$$\dot{x} = \bar{A}x + \eta(x,u) + \bar{B}\mu \tag{12.23}$$

$$x = [z_s - z_{ur} \quad \dot{z}_s - \dot{z}_{ur} \quad z_s - z_{ul} \quad \dot{z}_s - \dot{z}_{ul} \quad \phi \quad \dot{\phi}]^T, \tag{12.24}$$

$$\bar{A} = \begin{bmatrix} 0 & 1 & 0 & 0 & 0 & 0 \\ -\frac{k}{m_s} - \frac{k}{m_u} & -\frac{d}{m_s} - \frac{d}{m_u} & -\frac{k}{m_s} & -\frac{d}{m_s} & 0 & 0 \\ 0 & 0 & 0 & 1 & 0 & 0 \\ -\frac{k}{m_s} & -\frac{d}{m_s} & -\frac{k}{m_s} - \frac{k}{m_u} & -\frac{d}{m_s} - \frac{d}{m_u} & 0 & 0 \\ 0 & 0 & 0 & 0 & 0 & 1 \\ \frac{kl_s}{2I} & \frac{dl_s}{2I} & -\frac{kl_s}{2I} & -\frac{dl_s}{2I} & -a_{65} & -a_{66} \end{bmatrix},$$

$$\eta(x,u)$$

$$= \begin{bmatrix} 0 \\ +\frac{kl_s}{2m_u} sin\phi + \frac{dl_s}{2m_u}\dot{\phi}cos\phi \\ 0 \\ -\frac{kl_s}{2m_u} sin\phi - \frac{dl_s}{2m_u}\dot{\phi}cos\phi \\ 0 \\ +\frac{m_s a_y h_R}{I} cos\phi + \left(\frac{m_s g h_R}{I} - \frac{kl_s^2}{2I}\right) sin\phi - \frac{dl_s^2}{2I}\dot{\phi}cos\phi + a_{65}\phi + a_{66}\dot{\phi} \end{bmatrix}, \tag{12.25}$$

$$\bar{B} = \begin{bmatrix} 0 & 0 \\ \frac{1}{m_u} & 0 \\ 0 & 0 \\ 0 & \frac{1}{m_u} \\ 0 & 0 \\ 0 & 0 \end{bmatrix}, \mu = \begin{bmatrix} F_{tr} \\ F_{tl} \end{bmatrix}$$

where $a_{65} > 0$, $a_{66} > 0$.

The modified model is valid for designing an observer since the original model includes stabilized terms, $\left(\frac{m_s g h_R}{I} - \frac{kl_s^2}{2I}\right) sin\phi$ and $-\frac{dl_s^2}{2I}\dot{\phi}cos\phi$. Now, the modified model will be unobservable only when $\phi = 0$.

To make the problem easy to solve, the measurement model is given by

$$y = \begin{bmatrix} z_s - z_{ur} - \frac{l_s}{2} sin\phi \\ \dot{\phi} \end{bmatrix} = \begin{bmatrix} 1 & 0 & 0 & 0 & -c_{15} & 0 \\ 0 & 0 & 0 & 0 & 0 & 1 \end{bmatrix} x + \begin{bmatrix} -\frac{l_s}{2} sin\phi + c_{15}\phi \\ 0 \end{bmatrix}. \quad (12.26)$$

where $c_{15} > 0$. With this modification, bounds on the Jacobian of the nonlinear function are decreased.

12.5.1. Observer Design Using Corollary to Theorem 5 in Chapter 8

Apply Corollary to Theorem 5 for the problem.

The nonlinear function Φ is

$$\Phi = \eta(x,u) - \bar{B} b^{-1} \beta(x,u)$$

$$= \begin{bmatrix} 0 \\ 0 \\ 0 \\ 0 \\ 0 \\ +\frac{m_s a_y h_R}{I} cos\phi + \left(\frac{m_s g h_R}{I} - \frac{k l_s^2}{2I}\right) sin\phi - \frac{d l_s^2}{2I} \dot{\phi} cos\phi + a_{65}\phi + a_{66}\dot{\phi} \end{bmatrix} \quad (12.27)$$

For the nonlinear function in equations (12.27), the scaling factor $\bar{z}_H$ is 2. Since $\Phi_1, \Phi_2, \dots, \Phi_5 = 0$, and $\frac{\partial \Phi_6}{\partial x_{i=1:4}} = 0$ then $w_H = 34$ and the scaling factor $\bar{z}_H$ is $n \times n - w_H$. ($\bar{z}_H = 6 \times 6 - 34 = 2$). Then, the jacobian of the nonlinear function Φ is computed to find $\bar{H}_{65}^{max}, \bar{H}_{66}^{max}$ and $\bar{H}_{65}^{min}, \bar{H}_{66}^{min}$. (Note: we can choose a_{65}, a_{66} such that $|\bar{H}_{ij}^{max}|$ and $|\bar{H}_{ij}^{min}|$ are small.)

$$\frac{\partial \Phi_6}{\partial \phi} = -\frac{m_s a_y h_R}{I} sin\phi + \left(\frac{m_s g h_R}{I} - \frac{k l_s^2}{2I}\right) cos\phi + \frac{d l_s^2}{2I} \dot{\phi} sin\phi + a_{65} \quad (12.28)$$

$$\frac{\partial \Phi_6}{\partial \dot{\phi}} = -\frac{d l_s^2}{2I} cos\phi + a_{66} \quad (12.29)$$

$$\bar{H}_{65}^{max}(6,5) = 2 \times \max\left(\frac{\partial \Phi_6}{\partial \phi}\right), \qquad \bar{H}_{65}^{min}(6,5) = 2 \times \min\left(\frac{\partial \Phi_6}{\partial \phi}\right) \quad (12.30)$$

$$\bar{H}_{66}^{max}(6,6) = 2 \times \max\left(\frac{\partial \Phi_6}{\partial \dot{\phi}}\right), \qquad \bar{H}_{66}^{min}(6,6) = 2 \times \min\left(\frac{\partial \Phi_6}{\partial \dot{\phi}}\right) \quad (12.31)$$

(The other elements of $\bar{H}^{max}$ and $\bar{H}^{min}$ are zeros.)

The nonlinear function Ψ is

$$\Psi = \begin{bmatrix} -\frac{l_s}{2} sin\phi + c_{15}\phi \\ 0 \end{bmatrix}. \tag{12.32}$$

For the nonlinear function in equation (12.32), the scaling factor $\bar{z}_G$ is 1. Since $\Psi_2 = 0$ and $\frac{\partial \Psi_1}{\partial x_{i=1:4,6}} = 0$ the scaling factor $\bar{z}_G$ is $m \times n - w_G$. ($\bar{z}_G = 2 \times 6 - 11 = 1$). Then, the jacobian of the nonlinear function Ψ is computed to find $\bar{G}_{15}^{max}$ and $\bar{G}_{16}^{min}$. (Note: we can choose a_{65}, a_{66} such that $|\bar{G}_{ij}^{max}|$ and $|\bar{G}_{ij}^{min}|$ are small.)

$$\frac{\partial \Psi_1}{\partial \phi} = -\frac{l_s}{2} + c_{15} \tag{12.33}$$

$$\bar{G}_{15}^{max}(1,5) = 1 \times \max\left(\frac{\partial \Psi_1}{\partial \phi}\right), \qquad \bar{G}_{15}^{min}(1,5) = 1 \times \min\left(\frac{\partial \Psi_1}{\partial \phi}\right) \tag{12.34}$$

(The other elements of $\bar{G}^{max}$ and $\bar{G}^{min}$ are zeros.)

Next, we solve equations (8.22) for the observer gain using the LMI toolbox in Matlab. (Note: The LMI toolbox in Matlab provides only one gain, though theoretically many solutions can exist to the LMI (8.22). If a faster convergence rate is desired, the RHS in equation (8.22) could be replaced by a negative definite matrix instead of zero.)

12.6. Simulation and Simulation Results

12.6.1. Simulation Setup

In this section, we will evaluate the algorithm described in the previous section in simulations by implementing it in CARSIM, industry standard vehicle dynamics simulation software. The vehicle model from CARSIM chosen for this simulation is a standard SUV.

In the simulation, we simulate the case that the SUV vehicle strikes road bumps during cornering. The curvature of the road is shown on Figure 12-5 and the road bumps are shown on the second row of Figure 12-5. The first bump is applied to the right wheels of the vehicle and the second bump is applied to the left wheels of the vehicle. The magnitude of the first bump is larger than that of the second bump but the displacement

rate of the first bump is slower than that of the second bump. The fast displacement rate of the road input causes a lot of change in normal tire forces. The vehicle is set up to make cornering with vehicle speed of 100 kph. It should be noted that when the vehicle strikes a bump, the wheels of the vehicle still do not lift off the road surface. The lateral acceleration in this case is shown on the first row of Figure 12-6.

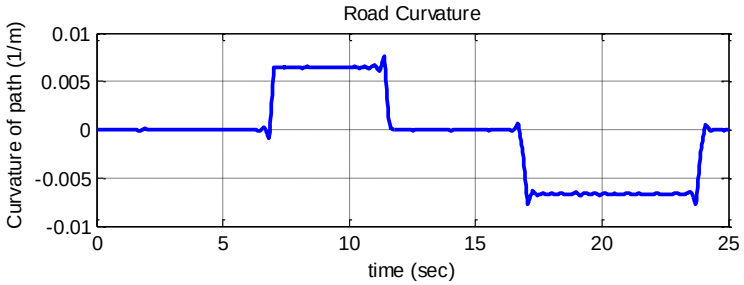

Figure 12-5 Road curvature.

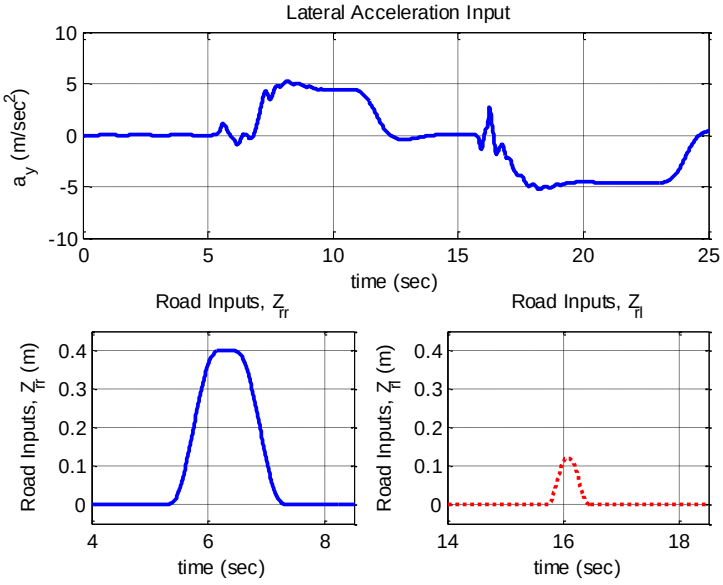

Figure 12-6 Lateral acceleration and road inputs.

12.6.2. Simulation Results

For designing an observer for this problem, we assume that

1. $-45 \leq \phi \leq 45\ deg.$,
2. $-1 \leq \dot{\phi} \leq 1$ rad./sec. or $-57.3 \leq \dot{\phi} \leq 57.3$ deg./sec.,
3. $-15 \leq a_y \leq 15$ m/s^2,

4. $\dot{a}_y$ is small.

The measurements that we need to feed to the observer are 1. Lateral acceleration, a_y, 2. Right unsprung mass vertical acceleration, $\ddot{z}_{ur}$, 3. Left unsprung mass vertical acceleration, $\ddot{z}_{ul}$, 4. Right suspension compression, $(z_s - z_{ur} + \frac{l_s}{2} sin\phi)$, and 5. roll rate, $\dot{\phi}$.

Then the local bound of the nonlinearity can be found. The observer gain found by using the new observer is

$$L = \begin{bmatrix} 1.4320 & -109.8388 & 0.8108 & -20.0510 & -0.2167 & 5.2887 \\ 13.5762 & 440.6767 & -13.5380 & -432.6672 & 8.1034 & 113.1697 \end{bmatrix}^T.$$

The estimation results are shown on Figure 12-7-Figure 12-10. The results show that the estimated states are very close to the actual values. The estimated states are not exactly equal to the actual values because the vehicle model in CARSIM has many degrees of freedom but our model is only a 4-degrees of freedom model. Also, there is a time delay in CARSIM between the front and rear wheels of the vehicle when the vehicle strikes a bump.

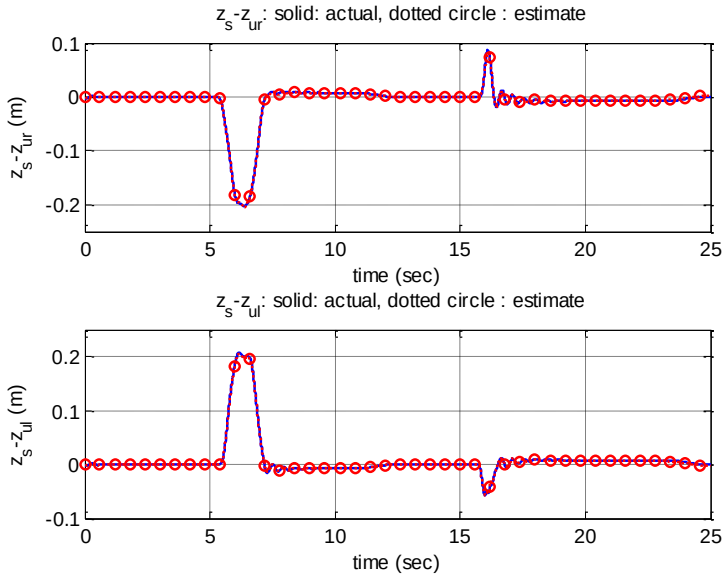

Figure 12-7 Estimation of right and left suspension compressions.

Note: the outputs of the Carsim are right and left suspension compressions, $(z_s - z_{ur} + \frac{l_s}{2} sin\phi)$ and $(z_s - z_{ul} - \frac{l_s}{2} sin\phi)$. However, on Figure 12-7, we compute the actual value of $(z_s - z_{ur})$ and $(z_s - z_{ul})$ and compare the value of them.

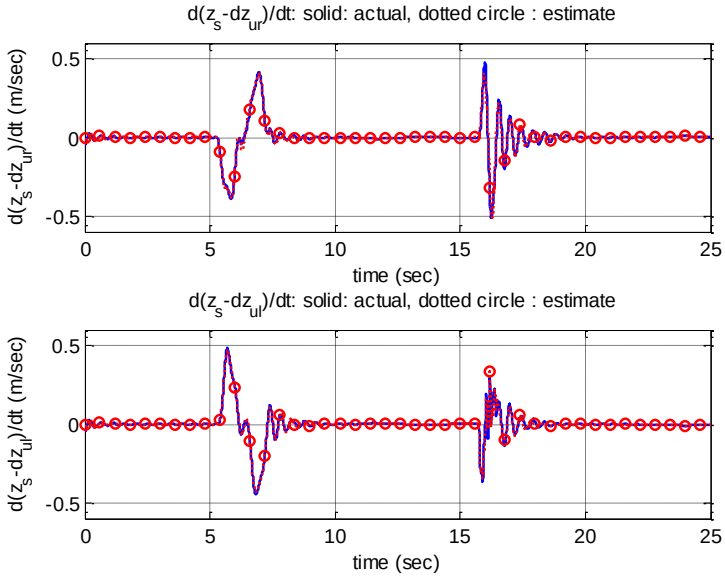

Figure 12-8 Estimation of right and left suspension compression rate.

Note: the outputs of the Carsim are right and left suspension compression rates, $(\dot{z}_s - \dot{z}_{ur} + \frac{l_s}{2}\dot{\phi}cos\phi)$ and $(\dot{z}_s - \dot{z}_{ul} + \frac{l_s}{2}\dot{\phi}cos\phi)$. However, on Figure 12-8, we compute the actual value of $(\dot{z}_s - \dot{z}_{ur})$ and $(\dot{z}_s - \dot{z}_{ul})$ and compare these values.

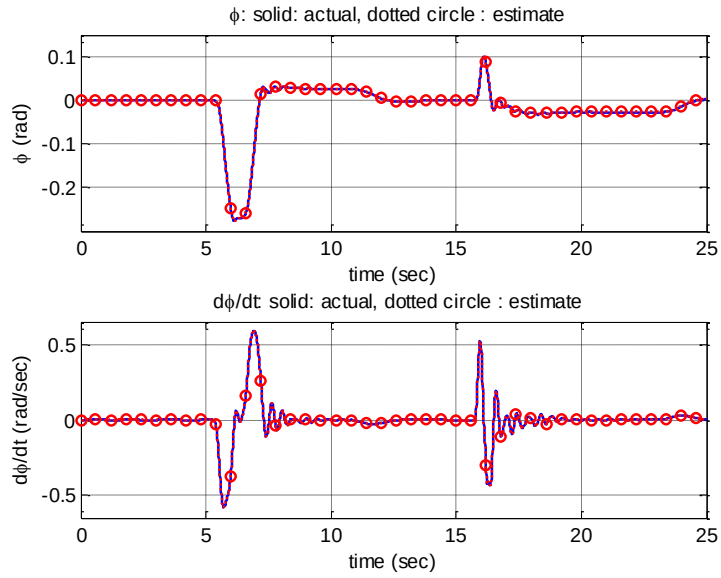

Figure 12-9 Roll angle and roll rate estimation.

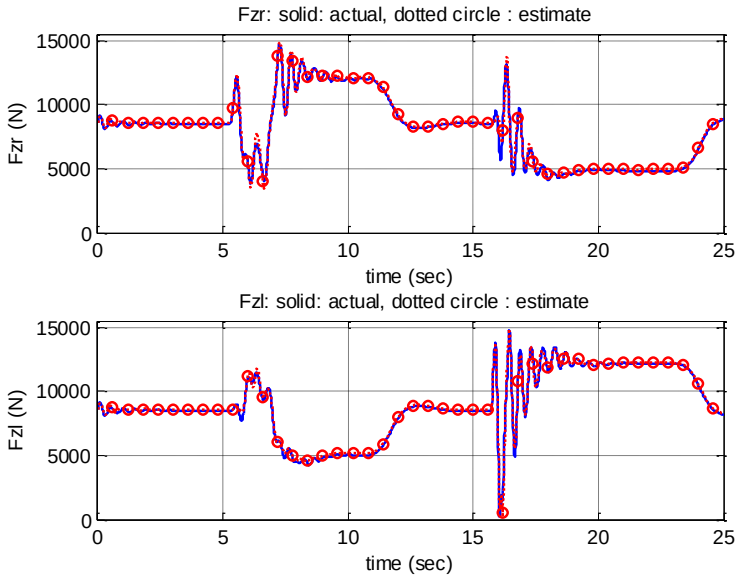

Figure 12-10 Normal tire forces estimation, F_{zr} and F_{zl}

The estimated rollover index is shown on Figure 12-11. The result shows that the estimated and actual rollover indices are extremely close. There are very small errors and these happen because there is a time delay between the front and rear wheels of the vehicle when the vehicle strikes a bump. Since we use only 4-degrees of freedom for

observer design, we cannot handle this time delay. However, if we carefully look at the result, we will see that the estimated rollover is good enough to predict un-tripped and tripped rollovers.

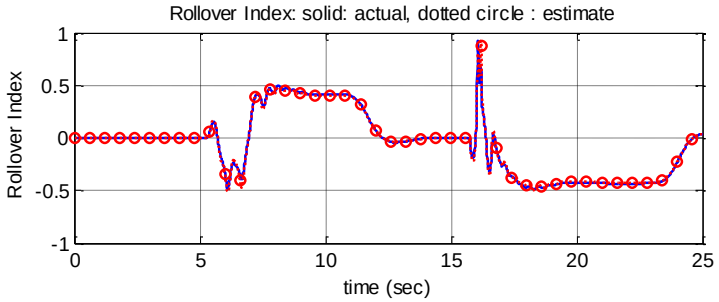

Figure 12-11 Rollover index estimation.

12.7. The Scaled Vehicle for Experiments

The simulation results in the previous section show that the new rollover index can detect both tripped and un-tripped rollovers. However, we still need to confirm the approach with a test vehicle.

The use of a full-sized vehicle for testing of a control system in this rollover application is challenging due to cost limitations and safety issues. It is estimated that the cost of developing a full-sized instrumented vehicle for testing is more than $100,000 [**55**]. Most of this cost goes for equipment and instrumentation development. Also, a full-sized vehicle is difficult to operate and involves significant safety issues in this application which involves vehicle rollover.

It is more convenient to use a scaled vehicle to test the roll control system. A scaled radio controlled vehicle is inexpensive and safe for evaluation of rollover maneuvers. Many researchers have studied scaled vehicles for testing of vehicle dynamics and control systems. For instance, references [**55**], [**56**], [**57**], and [**58**] developed a $1/10^{th}$ scaled vehicle to study lateral vehicle dynamics. Reference [**59**] developed a $1/8^{th}$ scaled vehicle to study longitudinal vehicle dynamics. References [**60**], [**61**], [**62**] and [**63**] studied stability control algorithms with a scaled vehicle. Reference [**64**] studied tire characteristics with scaled tries.

In order to use a scaled vehicle to describe the behavior of a full-sized vehicle, we need to show that they have dynamic similarity. In the next section, we will show that the scaled vehicle we use has dynamic similarity to a full-sized vehicle. Then, we describe the experimental setup to test rollover scenarios and present the experimental results in the following section.

12.7.1.Dynamic Similitude Analysis

Two systems of different size scales are dynamically similar if the solutions to their governing differential equations are identical after accounting for the dimensional scaling of parameters in the equations of motion. There are many approaches to evaluate dynamic similarity. The Buckingham π theorem is a tool that provides us an easy approach to show dynamic similarity. The details of the Buckingham π theorem are discussed in [**59**], and [**65**].

This theorem is convenient to apply. It can show dynamic similarity without explicitly knowing the accurate dynamic equations of both systems. We need only to know the list of all variables and parameters associated with the system. References [**55**], [**56**], [**58**], and [**64**] used the Buckingham π theorem to show the lateral dynamic similarity between a full-sized vehicle and a $1/10^{th}$ scaled vehicle. Also, reference [**59**] showed the longitudinal dynamic similarity between a full-sized vehicle and a $1/13^{th}$ scaled vehicle. Therefore, we use the Buckingham π theorem to show the roll and vertical vehicle dynamics similarity between our scaled vehicle and a full-sized vehicle.

The Buckingham π theorem shows that if the dimensionless π groups of variables and parameters are maintained, then the solution to any differential equation, regardless of its order or nonlinearity, can be made invariant with respect to dimensional scaling [**58**]. To apply the Buckingham π theorem to the roll and vertical vehicle dynamics, we need the list of all variables and parameters associated with these dynamics. We limit the number of variables and parameters to those used in the 4-degrees of freedom model as described in section 12.4. Therefore, the roll angle will be a function primarily dependent on the scaled parameters,

$$\phi = F\left(m_s, m_u, I_{xx}, k, d, l_s, h_R, k_t, a_y, \ddot{z}_s, \ddot{z}_{ul}, \ddot{z}_{ur}\right). \quad (12.35)$$

The parameters and variables of the vehicle dynamic model in equation (12.35) and their units are given in Table 12-1.

Table 12-1 Summary of parameters associated with the vehicle dynamics.

		Mass	Length	Time
ϕ, roll angle	dimensionless	0	0	0
m_s, sprung mass	kg	1	0	0
m_u, unsprung mass	kg	1	0	0
I_{xx}, moment of inertia	kg.m^2	1	2	0
k, spring stiffness	kg/sec^2	1	0	-2
d, damper	kg/sec	1	0	-1
l_s, distance between left and right suspensions	m	0	1	0
h_R, c.g. height	m	0	1	0
k_t, tire stiffness	kg/sec^2	1	0	-2
a_y, lateral acceleration	m/sec^2	0	1	-2
$\ddot{z}_s$, sprung mass vertical acceleration	m/sec^2	0	1	-2
$\ddot{z}_{ul}$, left unsprung mass vertical acceleration	m/sec^2	0	1	-2
$\ddot{z}_{ur}$, right unsprung mass vertical acceleration	m/sec^2	0	1	-2

There are 13 parameters ($n = 13$) to represent the vehicle dynamics and 3 basic unit dimensions (j=3): mass (M), length (L), and time (T). We choose the sprung mass (m_s), c.g. height (h_R), and lateral acceleration (a_y) to represent repeating fundamental units in the three-dimensional spaces. So, the remaining 10 unused parameters (k=n-j=10) can be formed as dimensionless π groups by appropriate division or multiplication of the repeating variables m_s, h_R, and a_y. The list of all the π groups is given in Table 12-2.

Table 12-2 π groups

$(m_s, h_R, a_y, \phi) \rightarrow$	$[M]^0[L]^0[LT^{-2}]^0[] \rightarrow$	$\pi_1 = \phi$
$(m_s, h_R, a_y, m_u) \rightarrow$	$[M]^1[L]^0[LT^{-2}]^0[M]^{-1} \rightarrow$	$\pi_2 = \frac{m_s}{m_u}$
$(m_s, h_R, a_y, I_{xx}) \rightarrow$	$[M]^{-1}[L]^{-2}[LT^{-2}]^0[ML^2]^1 \rightarrow$	$\pi_3 = \frac{I_{xx}}{m_s h_R^2}$
$(m_s, h_R, a_y, k) \rightarrow$	$[M]^{-1}[L]^1[LT^{-2}]^{-1}[MT^{-2}]^1 \rightarrow$	$\pi_4 = \frac{k h_R}{a_y m_s}$

$(m_s, h_R,\ a_y, d) \rightarrow$	$[M]^{-2}[L]^{1}[LT^{-2}]^{-1}[MT^{-1}]^{2}\rightarrow$	$\pi_5 = \frac{d^2 h_R}{a_y {m_s}^2}$
$(m_s, h_R,\ a_y, l_s) \rightarrow$	$[M]^{0}[L]^{-1}[LT^{-2}]^{0}[L]^{1}\rightarrow$	$\pi_6 = \frac{l_s}{h_R}$
$(m_s, h_R,\ a_y, k_t) \rightarrow$	$[M]^{-1}[L]^{1}[LT^{-2}]^{-1}[MT^{-2}]^{1}\rightarrow$	$\pi_7 = \frac{k_t h_R}{a_y m_s}$
$(m_s, h_R,\ a_y, \ddot{z}_s) \rightarrow$	$[M]^{0}[L]^{0}[LT^{-2}]^{-1}[LT^{-2}]^{1}\rightarrow$	$\pi_8 = \frac{\ddot{z}_s}{a_y}$
$(m_s, h_R,\ a_y, \ddot{z}_{ul}) \rightarrow$	$[M]^{0}[L]^{0}[LT^{-2}]^{-1}[LT^{-2}]^{1}\rightarrow$	$\pi_9 = \frac{\ddot{z}_{ul}}{a_y}$
$(m_s, h_R,\ a_y, \ddot{z}_{ur}) \rightarrow$	$[M]^{0}[L]^{0}[LT^{-2}]^{-1}[LT^{-2}]^{1}\rightarrow$	$\pi_{10} = \frac{\ddot{z}_{ur}}{a_y}$

Note: All of the dimensionless parameters, such as angles form their own π group.

To have the roll and vertical vehicle dynamics of the scaled vehicle the same as those of a full-sized vehicle, we need to tune the scaled vehicle until the values of π groups of the scaled vehicle are close to the values of π groups of a full-sized vehicle. The variables and parameters of the full-sized and scaled vehicle are shown in Table 12-3 and the π groups of them are shown in Table 12-4. The photographs of the scaled vehicle are shown in Figure 12-12.

Figure 12-12 Scaled test vehicle: 1:8 (30.5 x 58.5 cm).

Table 12-3 Vehicle variables and parameters.

Variables and Parameter	Scaled Vehicle	Full-Sized vehicle
m_s (kg)	3	1600
m_u (kg)	0.2	135
I_{xx} (kg.m^2)	0.04	600
k (N/m)	900	90000
d (N.sec/m)	15	3000

l_s (m)	0.2	1.11
h_R (m)	0.18	1
k_t(N/m)	4000	400000

Note: The parameters of the full-sized vehicle are obtained from the software CARSIM.

Table 12-4 Comparison of π groups.

π	Scaled Vehicle	Full-Sized vehicle
π_1	ϕ_s	ϕ_f
π_2	15	11.9
π_3	0.41	0.375
π_4	$54/a_{ys}$	$56.25/a_{yf}$
π_5	$4.5/a_{ys}$	$3.5/a_{yf}$
π_6	1.11	1.11
π_7	$240/a_{ys}$	$250/a_{yf}$
π_8	$\ddot{z}_{ss}/a_{ys}$	$\ddot{z}_{sf}/a_{yf}$
π_9	$\ddot{z}_{uls}/a_{ys}$	$\ddot{z}_{ulf}/a_{yf}$
π_{10}	$\ddot{z}_{urs}/a_{ys}$	$\ddot{z}_{urf}/a_{yf}$

Table 12-4 shows that if the lateral accelerations (a_{ys} and a_{yf}) that cause the scaled and full-sized vehicle to roll over have the same order, then the π group values of the scaled vehicle are close to those of the full-sized vehicle. Also, the vertical accelerations will have the same order.

Based on experiments on the scaled vehicle and simulations of the full-sized vehicle, the lateral accelerations that cause them to roll over are both approximately 7 m/s^2. Then, the dimensionless π groups of them are of the same order and it is reasonable to use the scaled vehicle to study the roll and vertical dynamics of the vehicle.

Note: The dimensional analysis will be correct, only if all variables and parameters associated with the system are involved. In this problem, we assume that only the variables and parameters shown in equation (12.35) are associated with the dynamics.

Then, the π groups are shown on Table 12-4. However, un-modeled dynamics between the full-sized and scaled vehicles could be different and might lead to errors. For example, the scaled vehicle could have significant friction forces which are large compared to other forces on the system. On the full-sized vehicle, on the other hand, the friction could be negligible. For purposes of this dissertation, we ignore the unmodeled dynamics of the scaled and full vehicles.

12.7.2.Experimental Set Up

The developed rollover index will be validated with the scaled vehicle since the roll and vertical dynamics of it are similar to those of a full-size vehicle. A microcontroller (EM430F6137RF900) from Texas Instruments is used for real-time data acquisition and control of the scaled vehicle speed and steering. The microcontroller is installed on the test vehicle. It samples the data from sensors and wirelessly sends them to a receiver connected to a computer at the baud rate of 66 Hz. Four 3-axis accelerometers (MMA7260Q) from Freescale Semiconductor and a dual axis gyroscope (LPY530AL) from STMicroelectronics are used for this test to measure acceleration and angle rate, respectively. Two accelerometers installed on the left and right size of the sprung mass are used to measure the left and right vertical accelerations. Another two accelerometers are placed on the front left and front right wheels, unsprung masses, for measuring longitudinal, lateral, and left and right vertical accelerations. Also, the dual axis gyroscope placed near the c.g. of the vehicle is used to measure yaw rate and roll rate. In order to measure the suspension defection of the scaled vehicle, a linear potentiometer (LCP12Y-25-10K) from ETI systems is installed parallel to the front right suspension of the scaled vehicle. The photographs of the microcontroller and the sensors are shown in Figure 12-13.

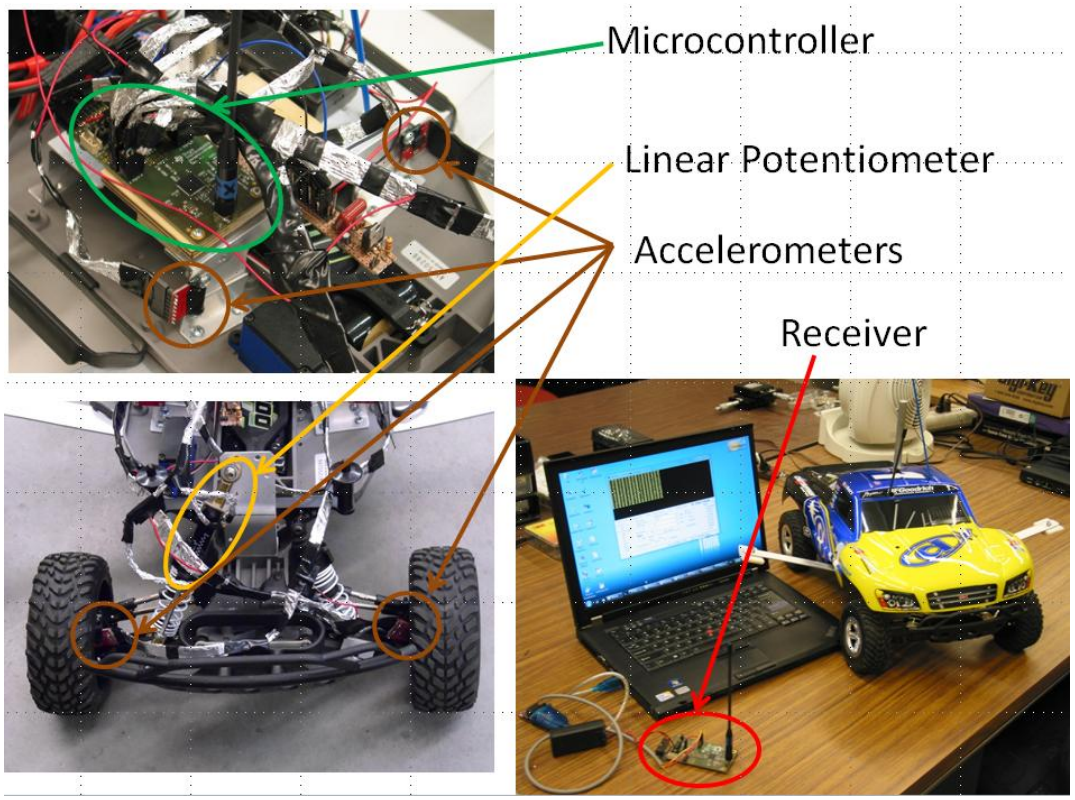

Figure 12-13 Microcontroller and Sensors.

To evaluate the rollover index, the scaled vehicle speed and steering inputs are programmed in the microcontroller. So, the identical experiment can be repeated many times. For the first experiment, we set the vehicle to follow the path as shown in Figure 12-14a at a speed of approximately 2.4 meter per second. In this case, the right wheels of the scaled vehicle come close to lifting off from the ground.

For the second experiment, we put an obstacle on the route of the vehicle as shown in Figure 12-14b. The size of the obstacle is 2.54 centimeters in height and 2.54 centimeters in width. Then, we set the vehicle to follow the path at a speed of approximately 2.4 meter per second. In this case, the right wheels of the scaled vehicle fully lift off.

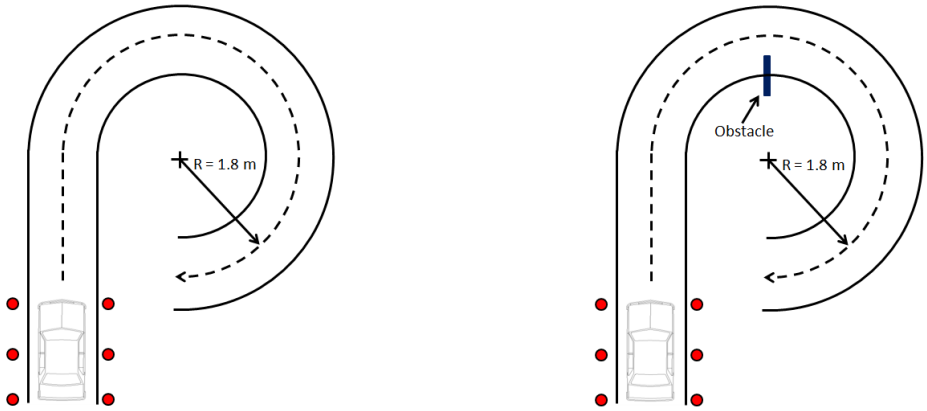

a) 1st experiment b) 2nd experiment

Figure 12-14 The scaled vehicle path.

12.7.3.Experimental Results

The measurements of the vehicle longitudinal and lateral accelerations are presented in Figure 12-15. The longitudinal and lateral accelerations in all experiments are similar and of the same order because of the same setting in all experiments. The scaled vehicle starts to accelerate after $t > 7$ sec. Then it starts to bend to the right after $t > 8.5$. The scaled vehicle completes the maneuver after $t > 12.5$ sec.

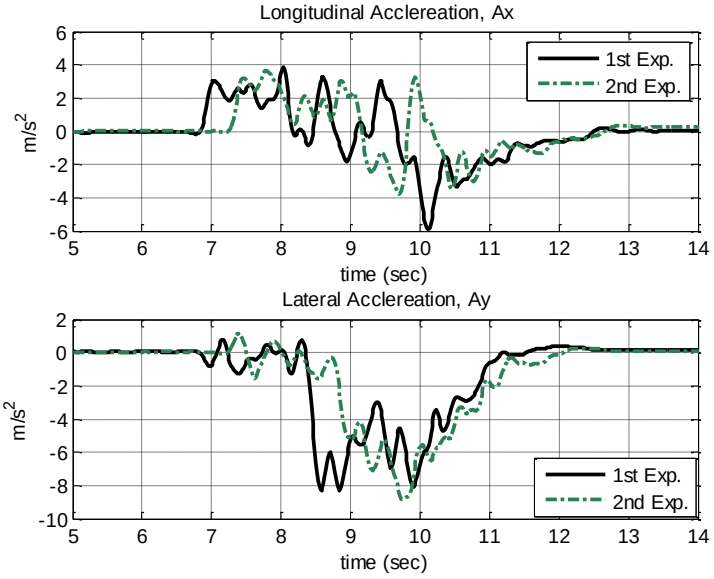

Figure 12-15 Longitudinal and lateral acceleration of the scaled vehicle.

Now, we apply the Corollary to Theorem 5 for the problem. The signals required for the designed observer are 1. lateral acceleration, 2. left and right vertical accelerations of

unsprung masses, 3. roll rate, and 4. front right suspension defection. Then, vehicle states and unknown vertical tire forces can be estimated. The results of the experiments are shown in Figure 12-16-Figure 12-19.

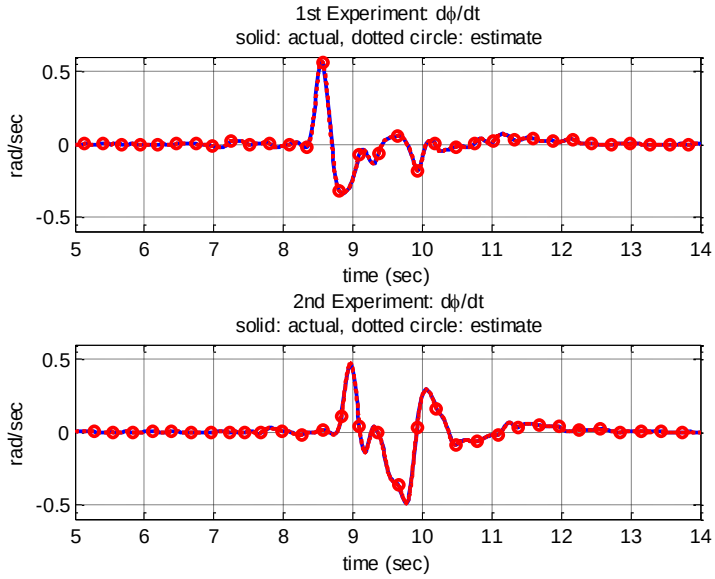

Figure 12-16 Estimation of Roll Rate.

Figure 12-16 shows the estimation of roll rate. The figure shows that the estimated roll rates from the first and second experiments match well with the actual roll rates. The magnitude and shape of roll angle and roll rate are reasonable since they look similar to the results that we obtained when we simulate with CARSIM.

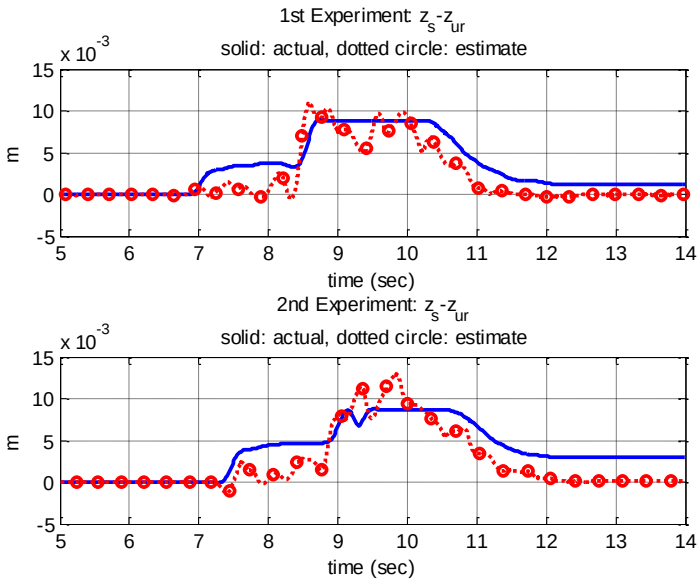

Figure 12-17 Estimation of Right Suspension Defection (z_s-z_{ur}-$l_s sin\phi/2$)

The estimations of front right suspension defection of the first and second experiments are shown in Figure 12-17. The suspension defections from the linear potentiometer needs to be scaled before using it because the suspension of the scaled vehicle are not perpendicular to the sprung mass and unsprung masses. Also, we did not measure the rear right suspension defections. Thus we assume that the rear right suspension defection is proportional to the front right suspension for calculation.

The measurements of front right suspension defection in Figure 12-17 show that the suspensions of the scaled vehicle are nonlinear suspensions. There is a saturation point. Moreover, due to the coulomb friction, there are more than one equilibrium points. When the scaled vehicle rested at the start point ($t < 7sec$), the equilibrium point of the suspension defection was 0 m. During the scaled vehicle acceleration on the straight route ($7 < t < 8.5$), the equilibrium point converged to another value ($\approx 4 \times 10^{-4} m$). During the scaled vehicle making a turn, the suspension defection saturated at about $8.8 \times 10^{-4} m$. After the scaled vehicle completed the maneuver, the equilibrium point moved to another value ($\approx 3 \times 10^{-4} m$). In order to make the computation simple, we ignore the unmodeled dynamics of the friction of the scaled vehicle.

Note: For the second experiment, the second row of Figure 12-17 shows the vehicle strikes the obstacle at $t \approx 9.1$ seconds. This makes the right vertical acceleration larger than the left vertical acceleration. It should be noted that when the right wheels of the scaled vehicle lift off during the time, $t \approx 9.7 - 10$ seconds, the measurements during this period may not be accurate.

Even though the estimations of right suspension defection in Figure 12-17 do not perfectly match to the actual value, the magnitude and shape of them seem reasonable. They try to track the actual value.

Now we need to examine the rollover index. Since, the unknown vertical tire forces can be estimated, the rollover index can be directly calculated from equation (12.1). In order to examine the rollover index from the designed observer, we will compare it with the traditional rollover index as shown in equation (12.2). However, we do not know the actual roll angle of the scaled vehicle since the measurement of roll angle is expensive. So, we assume that the roll angle is small. (Figure 12-18 also confirms that the roll angle is small.) Then, it is appropriate to use rollover index given by equation (12.36) instead of equation (12.2).

$$R_t = \frac{2m_s a_y h_R}{mgl_w} + \frac{2m_s h_R tan\phi}{ml_w} \approx \frac{2m_s a_y h_R}{mgl_w} \tag{12.36}$$

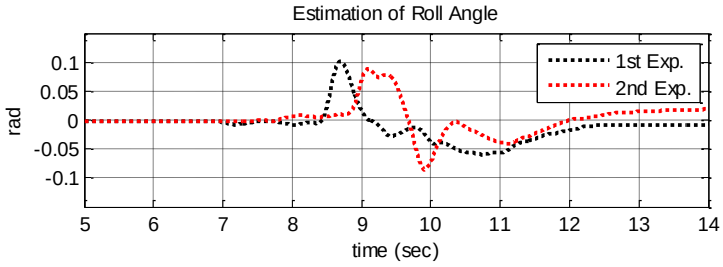

Figure 12-18 Estimation of Roll Angle

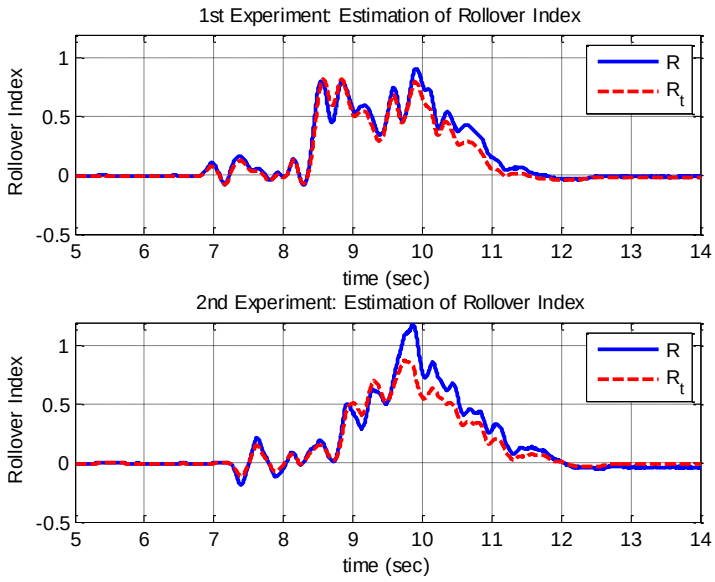

Figure 12-19 Comparison of rollover indices of the scaled vehicle.

The first row of Figure 12-19 shows the rollover indices from the first experiment. In this experiment, the external road input is not applied to the vehicle. So, the difference of vertical accelerations is small between the two cases. Then, the rollover indices from the equations (12.1) and (12.36) are almost the same. Both rollover indices show that the wheels of the vehicle do not lift off.

Likewise, the second row of Figure 12-19 shows the rollover indices from the second experiment. The scaled vehicle strike the obstacle and its right wheels fully lift off in this case. Thus, there is a difference of vertical accelerations. The traditional rollover index R_t in equation (12.36) shows that the wheels of the vehicle come close to lift off. That fails to detect the wheel lift off condition. However, the rollover index R that is computed by using the developed nonlinear observer shows that the right wheels of the vehicle do lift off. Therefore, the develop rollover index is able to detect both tripped and un-tripped rollovers.

12.8. Alternate Rollover Index with Additional Measurements

If the roll angle, ϕ, and vertical accelerations on the vehicle body (sprung mass) are measured and available, then the rollover R for tripped and un-tripped rollovers can be computed algebraically without needing to use an observer.

12.8.1.New Rollover Index for Tripped and Un-Tripped Rollovers

In this section, a new version of the rollover index computed algebraically from available measurements is presented. The new rollover index can be computed without knowing any of the following variables: the road input disturbances, z_{rr} and z_{rl}, the vertical displacements of unsprung masses, z_{ur} and z_{ul}, the vertical displacement of sprung mass, z_s, and the unknown lateral force input, F_{lat}.

In order to obtain the rollover index for predicting tripped rollovers, we need a model of a vehicle with 4-degrees of freedom which is shown in Figure 12-20. The vehicle body is represented by the sprung mass m_s while the mass due to the axles and tires are represented by unsprung masses m_{ul} and m_{ur}. The springs and dampers between the sprung and unsprung masses represent the vehicle suspension. The vertical tire stiffness of each side of the vehicle are represented by the springs k_{tr} and k_{tl}.

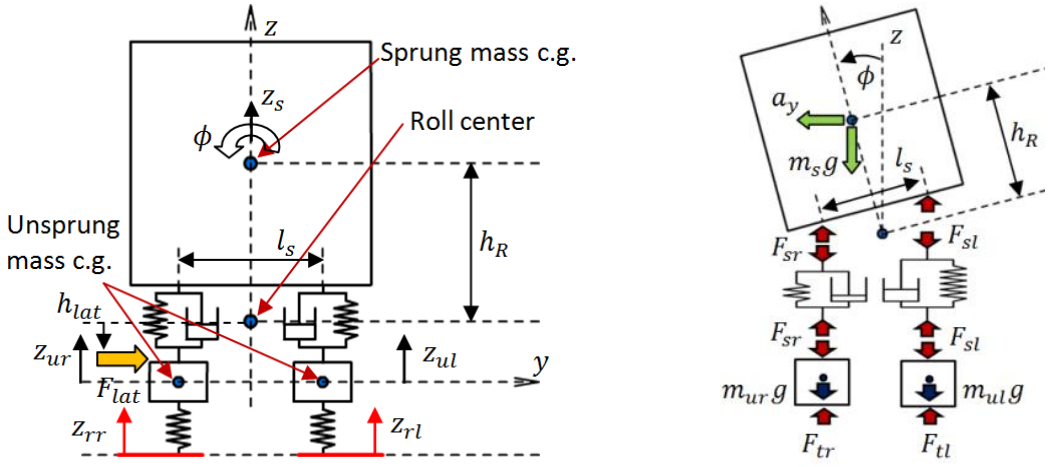

Figure 12-20 Four-degrees of freedom vehicle model.

The 4-degrees of freedom of the model are the heave z_s, roll angle ϕ of the vehicle body, and the vertical motion of each side of the unsprung masses, z_{ur} and z_{ul}. The variables z_{rr} and z_{rl} are the road profile inputs that excite the system.

The external inputs z_{rl}, z_{rr}, and F_{lat} cannot be measured and are unknown. However, outputs that depend on these unknown inputs are available for measurement. For example, vertical and lateral accelerations of the vehicle can be measured using accelerometers placed on the vehicle body. These vertical and lateral accelerations can be related to the unknown inputs and to the states of the system using algebraic equations. This section develops equations for the external disturbance inputs z_{rl}, z_{rr}, and F_{lat} using measured accelerometers signals and measured states of the vehicle model.

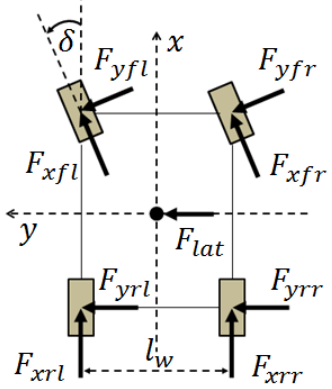

Figure 12-21 Lateral vehicle dynamics.

Consider the vehicle lateral dynamics as shown in Figure 12-21. The measurement of lateral acceleration a_y involves the influence of the lateral tire forces and the unknown external lateral force F_{lat}. The measured lateral acceleration a_y is given by

$$a_y = \frac{(F_{yr} + F_{xf}\sin(\delta) + F_{yf}\cos(\delta) + F_{lat})}{m} \tag{12.37}$$

where $m = m_s + m_u$, F_{xf} is the longitudinal tire forces of the front wheels, F_{yf} and F_{yr} are the lateral tire forces of the front and rear wheels respectively, δ is steering angle, and F_{lat} is the unknown external lateral force.

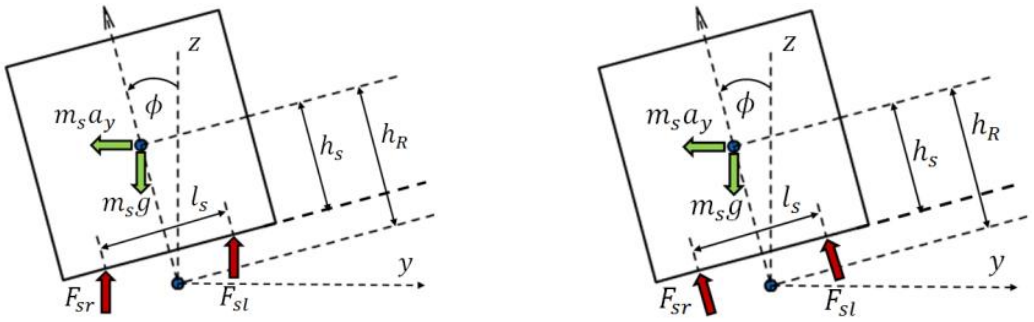

a) Suspension forces are always vertical.

b) Suspension forces are perpendicular to the sprung mass.

Figure 12-22 Suspension forces direction.

Derivation of Rollover Index

Assume that the suspension forces always act vertically. Then, the sprung mass roll motion is given by equation (12.38)

$$\begin{aligned}&(I_{xx} + m_s h_R^2)\ddot{\phi} \\ &= \frac{l_s}{2}(F_{sl} - F_{sr}) + m_s a_y h_R cos\phi + m_s g h_R sin\phi \\ &- (F_{sl} + F_{sr})(h_R - h_s) sin\phi\end{aligned} \tag{12.38}$$

which leads to

$$(I_{xx} + m_s h_R^2)\ddot{\phi} = \frac{l_s}{2}(F_{sl} - F_{sr}) + m_s a_y h_R cos\phi + m_s g h_s sin\phi. \tag{12.39}$$

where I_{xx} is roll moment of inertia.

However, if we assume that the suspension forces always act perpendicular to the sprung mass. The sprung mass roll motion is then given by equation (12.40)

$$(I_{xx} + m_s h_R^2)\ddot{\phi} = \frac{l_s}{2}(F_{sl} - F_{sr}) + m_s a_y h_R cos\phi + m_s g h_R sin\phi \tag{12.40}$$

Thus the major difference between equations (12.39) and (12.40) is the coefficient h_s instead of h_R in the gravity term. Both models are quite similar. Since h_s and h_R will be never be perfectly known, the difference between the 2 models is not great importance. To keep the presentation simple, we will use the sprung mass roll motion as described by equation (12.40).

In this case, the vertical dynamics of sprung mass translation is given by equation (12.41)

.

$$m_s\ddot{z}_s = F_{sr} + F_{sl} - m_s g, \tag{12.41}$$

The dynamic models of the unsprung mass motions are given by

$$m_{ur}\ddot{z}_{ur} = -F_{sr} + F_{tr} - m_{ur}g, \tag{12.42}$$

$$m_{ul}\ddot{z}_{ul} = -F_{sl} + F_{tl} - m_{ul}g \tag{12.43}$$

where F_{tr} and F_{tl} are left and right vertical tire forces respectively.

From unsprung mass equations, the vertical tire forces are seen to be given by

$$F_{tr} = m_{ur}\ddot{z}_{ur} + F_{sr} + m_{ur}g, \tag{12.44}$$

$$F_{tl} = m_{ul}\ddot{z}_{ul} + F_{sl} + m_{ul}g \tag{12.45}$$

Since the vertical tire forces F_{tr} and F_{tl} equal to the normal forces F_{zr} and F_{zl}, the rollover index can be written as

$$R = \frac{F_{zr} - F_{zl}}{F_{zr} + F_{zl}} = \frac{F_{tr} - F_{tl}}{F_{tr} + F_{tl}} = \frac{m_{ur}\ddot{z}_{ur} + F_{sr} + m_{ur}g - m_{ul}\ddot{z}_{ul} - F_{sl} - m_{ul}g}{m_{ur}\ddot{z}_{ur} + F_{sr} + m_{ur}g + m_{ul}\ddot{z}_{ul} + F_{sl} + m_{ul}g}. \tag{12.46}$$

If $m_{ur} = m_{ul} = m_u$, then the rollover index becomes

$$R = \frac{m_u(\ddot{z}_{ur} - \ddot{z}_{ul}) + F_{sr} - F_{sl}}{m_u(\ddot{z}_{ur} + \ddot{z}_{ul}) + F_{sr} + F_{sl} + 2m_u g} \tag{12.47}$$

where F_{sr} and F_{sl} are computed from equations (12.7) and (12.8). However, F_{sr} and F_{sl} are unknown and cannot measured or easily estimated. We need to eliminate these unknown parameters.

To determine suspension forces F_{sr} and F_{sl}, we consider equations (12.40) and (12.41).

$$\begin{gathered} m_s\ddot{z}_s = F_{sr} + F_{sl} - m_s g \\ (F_{sr} + F_{sl}) = m_s\ddot{z}_s + m_s g \end{gathered} \tag{12.48}$$

$$\begin{gathered} (I_{xx} + m_s h_R^2)\ddot{\phi} = \frac{l_s}{2}(F_{sl} - F_{sr}) + m_s a_y h_R cos\phi + m_s g h_R sin\phi \\ (F_{sl} - F_{sr}) = \frac{2}{l_s}\left[(I_{xx} + m_s h_R^2)\ddot{\phi} - m_s a_y h_R cos\phi - m_s g h_R sin\phi\right] \end{gathered} \tag{12.49}$$

$\ddot{z}_s$ can be measured by using an accelerometer and ϕ can be obtained by a tilt angle sensor. An example of a tilt angle sensor is the Crossbow CXTD02. The Crossbow tilt angle sensor consists of two axis in-built accelerometers and signal processing algorithms that enable static tilt angle to be calculated from the accelerometer measurements. An example of an algorithm that can be used for this purpose can be found in [**47**]. However, $\ddot{\phi}$ is still unknown and cannot be measured.

To measure $\ddot{\phi}$, we need to place two extra accelerometers at the right and left ends on a vehicle sprung mass. The locations of the extra accelerometers are shown on Figure 12-23.

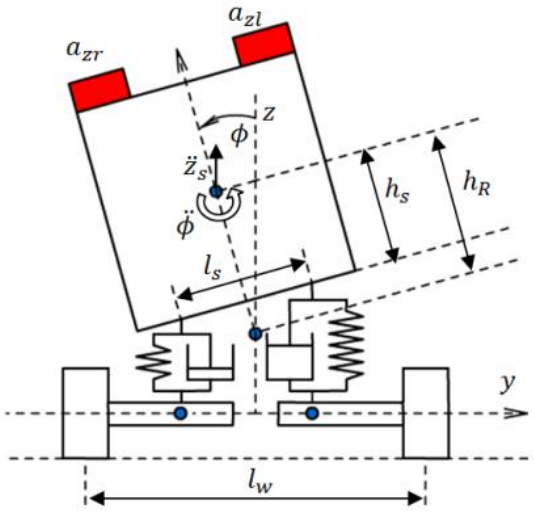

Figure 12-23 Extra accelerometer locations.

The right accelerometer measurement a_{zr} is given by

$$a_{zr} = \ddot{z}_s cos\phi - \frac{l_s}{2}\ddot{\phi} + (\ddot{y} + v_x r) sin\phi + g cos\phi. \tag{12.50}$$

The left accelerometer measurement a_{zl} is given by

$$a_{zl} = \ddot{z}_s cos\phi + \frac{l_s}{2}\ddot{\phi} + (\ddot{y} + v_x r) sin\phi + g cos\phi. \tag{12.51}$$

It should be noted that the term $(\ddot{y} + v_x r)$ includes the influence of the unknown lateral force F_{lat}.

Subtract equation (12.50) from (12.51).

$$a_{zl} - a_{zr} = l_s\ddot{\phi} \tag{12.52}$$

$$\ddot{\phi} = \frac{a_{zl} - a_{zr}}{l_s} \tag{12.53}$$

With equation (12.53), the equation (12.49) can be rewritten as

$$(F_{sl} - F_{sr}) = \frac{2}{l_s}\left[(I_{xx} + m_s h_R^2)\left(\frac{a_{zr} - a_{zl}}{l_s}\right) - m_s a_y h_R cos\phi - m_s g h_R sin\phi\right]. \tag{12.54}$$

Place equations (12.48) and (12.54) into (12.47).

$$R = \frac{m_u(\ddot{z}_{ur} - \ddot{z}_{ul}) - \frac{2}{l_s^2}(I_{xx} + m_s h_R^2)(a_{zl} - a_{zr})}{m_u(\ddot{z}_{ur} + \ddot{z}_{ul}) + m_s\ddot{z}_s + m_s g + 2m_u g} + \frac{\frac{2}{l_s} m_s a_y h_R cos\phi + \frac{2}{l_s} m_s g h_R sin\phi}{m_u(\ddot{z}_{ur} + \ddot{z}_{ul}) + m_s\ddot{z}_s + m_s g + 2m_u g} \tag{12.55}$$

Then, the rollover index for this case is

$$R = \frac{m_u(\ddot{z}_{ur} - \ddot{z}_{ul}) - \frac{2}{l_s^2}(I_{xx} + m_s h_R^2)(a_{zl} - a_{zr})}{m_u(\ddot{z}_{ur} + \ddot{z}_{ul}) + m_s\ddot{z}_s + mg} + \frac{\frac{2}{l_s} m_s a_y h_R cos\phi + \frac{2}{l_s} m_s g h_R sin\phi}{m_u(\ddot{z}_{ur} + \ddot{z}_{ul}) + m_s\ddot{z}_s + mg} \tag{12.56}$$

where $m = m_s + 2m_u$, $(\ddot{z}_{ur} - \ddot{z}_{ul})$ is difference between unsprung mass accelerations, $(a_{zl} - a_{zr})$ is difference between sprung mass accelerations, a_y is lateral acceleration, ϕ is roll angle. These parameters can be measured and estimated. Since the new rollover index involves the term $(a_{zl} - a_{zr})$ or $\ddot{\phi}$, the new rollover index can handle both unknown external lateral force inputs and unknown road inputs with the same algorithm.

Note: 1. The term involving $sin\phi$ can be ignored at small roll angles. However, it becomes important at large roll angles. In particular, if roll angle is higher for a given lateral acceleration (e.g. for higher c.g. vehicles), then the term $sin\phi$ is important and must be considered in the rollover index calculation. The roll angle may be obtained from a Crossbow tilt angle sensor or a fusion of a tilt sensor and a gyroscope with a simple first order observer [**47**].

2. Since tripped rollovers happen due to external inputs, rollover can happen, even if the roll angle is small. Thus, only lateral acceleration and roll angle measurements cannot by themselves be used to predict tripped rollovers.

12.8.1.1. Sensitivity Analysis to Mass Change

The vehicle mass changes due to the increase or decrease of passengers or goods in the vehicle. In this section, we show that the rollover index of equation (12.56) has very little sensitivity to mass change.

In general, the sprung mass is significantly larger than the unsprung mass ($m_s \gg m_u$). For purposes of rough analysis, we can neglect the unsprung mass and also assume that $m_s \approx m$. The equation (12.56) can then be rewritten as

$$R = \frac{-m\frac{2}{l_s^2}\left(\frac{(h_R^2 + l_w^2)}{12} + h_R^2\right)(a_{zl} - a_{zr})}{m(\ddot{z}_s + g)} + \frac{m\left(\frac{2}{l_s}a_y h_R cos\phi + \frac{2}{l_s}g h_R sin\phi\right)}{m(\ddot{z}_s + g)} \tag{12.57}$$

where $I_{xx} = m(h_R^2 + l_w^2)/12$.

Equation (12.57) shows that the rollover index is roughly independent of the vehicle mass, m, since it appears in both the numerator and denominator as a factor. Thus, the developed rollover index has low sensitivity to mass change.

Note: While the rollover index is not sensitive to mass, the equation (12.57) clearly shows that the rollover index is sensitive to the c.g. height, h_R. The c.g. height , h_R, can be estimated by an algorithm, as suggested in [**66**].

12.8.2. Simulation and Simulation Results

In this section, the rollover indices that are described in the previous section are evaluated in simulations by implementing them in CARSIM, industry standard vehicle dynamics simulation software. The vehicle model from CARSIM chosen for this simulation is a standard SUV. The rollover indices evaluated are

1. The traditional rollover index given by

$$R_1 = \frac{2m_s a_y h_R}{mgl_w} + \frac{2m_s h_R tan\phi}{ml_w}. \tag{12.58}$$

2. The traditional rollover index plus the difference of unsprung mass accelerations given by

$$R_2 = \frac{2m_s a_y h_R}{mgl_w} + \frac{2m_s h_R tan\phi}{ml_w} + \frac{m_u(\ddot{z}_{ur} - \ddot{z}_{ul})}{mg}. \tag{12.59}$$

3. The new rollover index given by

$$R_3 = \frac{m_u(\ddot{z}_{ur} - \ddot{z}_{ul}) - \frac{2}{l_s^2}(I_{xx} + m_s h_R^2)(a_{zl} - a_{zr})}{m_u(\ddot{z}_{ur} + \ddot{z}_{ul}) + m_s\ddot{z}_s + mg} + \frac{\frac{2}{l_s}m_s a_y h_R cos\phi + \frac{2}{l_s}m_s g h_R sin\phi}{m_u(\ddot{z}_{ur} + \ddot{z}_{ul}) + m_s\ddot{z}_s + mg} \tag{12.60}$$

These rollover indices are compared with the actual unimplementable rollover index given by equation (12.1) and denoted by R.

In the first two simulations, we simulate the case that the wheels of the vehicle do not lift off. The first simulation evaluates the case that the input is a step road input. The step road input, $z_{rl} = 0.15\,m$, is applied to the left wheels of the vehicle. The vehicle speed is set at 80 kph. The rollover indices of this simulation are shown in Figure 12-24a.

The next simulation evaluates the event that the inputs are a simultaneous step road input and step steering input. The step steering input, $\delta = 1.2\,deg.$, is applied starting at the 1st second. Then, the step road input, $z_{rl} = 0.15\,m$, is applied to the left wheels of the vehicle at the 3rd second. The vehicle speed is set at 80 kph. The rollover indices of this case are shown in Figure 12-24b.

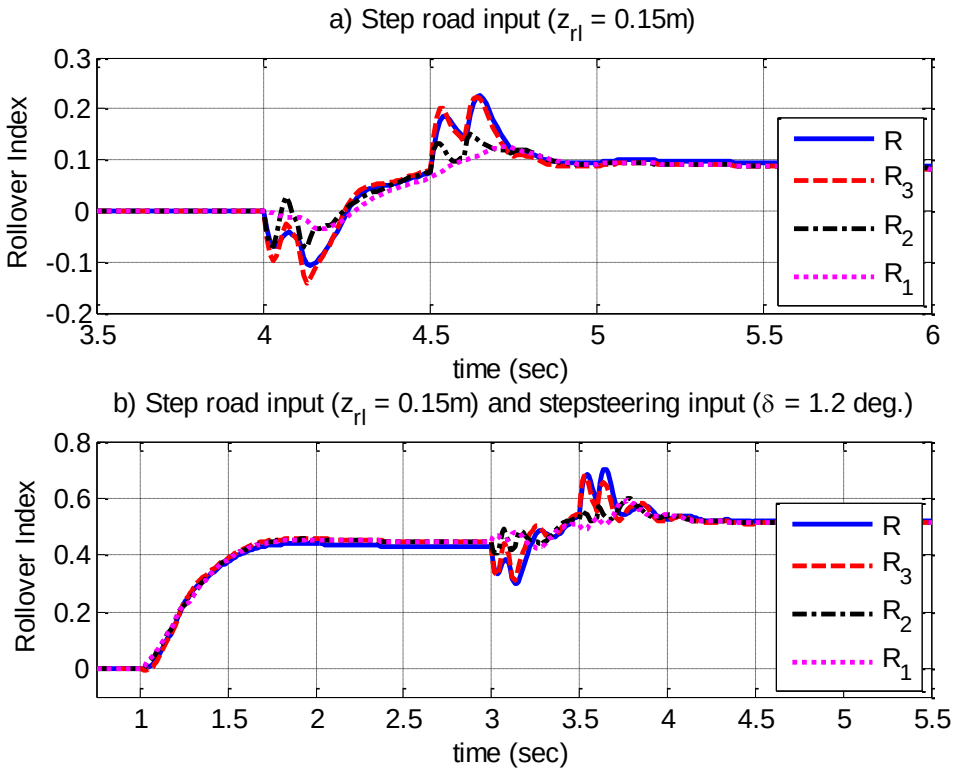

Figure 12-24 Comparison of rollover Indices.

For the last simulation, we simulate the case that the wheels of the vehicle lift off. The vehicle speed is set at 100 kph. The step steering input, $\delta = 1.2\ deg.$, is started to apply at the 1st second. Then the left wheels of the vehicle strike a bump at approximately the 2nd second. This cause the left wheels of the vehicle to lift off for a few seconds. The results of this simulation are shown in Figure 12-25.

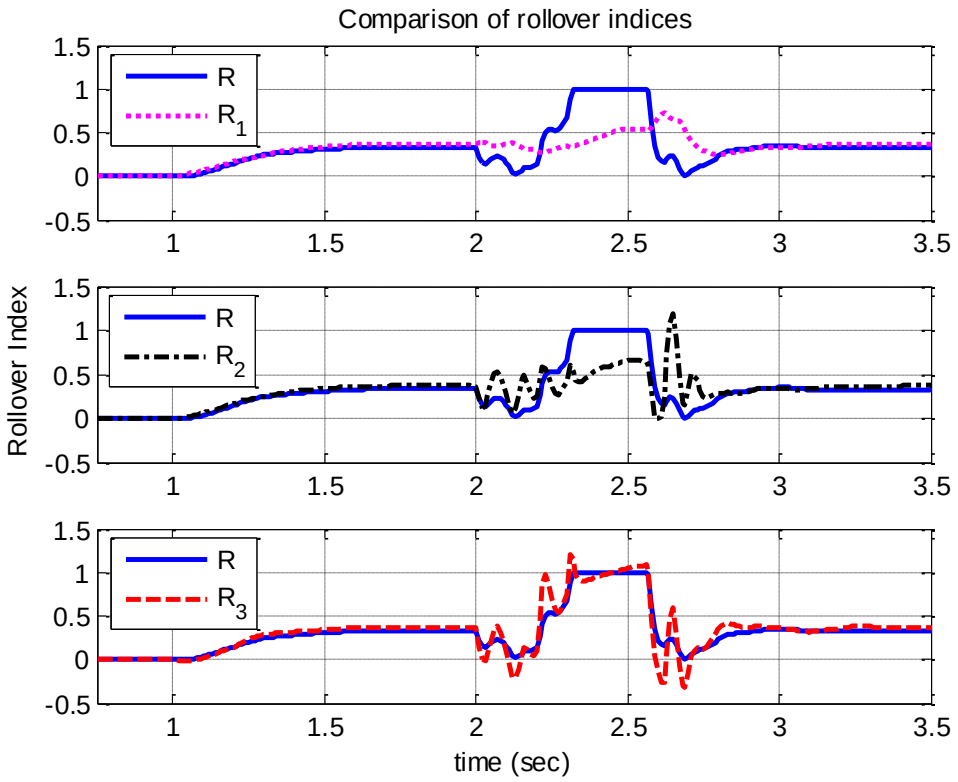

Figure 12-25 Rollover Indices with step steering input (δ=1.2 deg.) and road bump (z_{rl}=0.15 m).

Figure 12-24b and Figure 12-25 show that if a vehicle experiences only lateral acceleration, then the rollover indices R_1, R_2, and R_3 can all be used to detect rollovers. However, if a rollover happens due to tripping from external inputs, all the results show that the rollover indices R_1 and R_2 fail to estimate the actual (unimplementable) rollover index. (Only lateral acceleration and roll angle measurements by themselves cannot predict tripped rollover.) The values of the rollover index R_3 are close to the value of the actual rollover index R in all cases. Therefore, the results show that the developed rollover index is able to predict both tripped and un-tripped rollovers very well.

12.8.3.Experimental Set Up

We use the scaled vehicle as described in section 12.7.

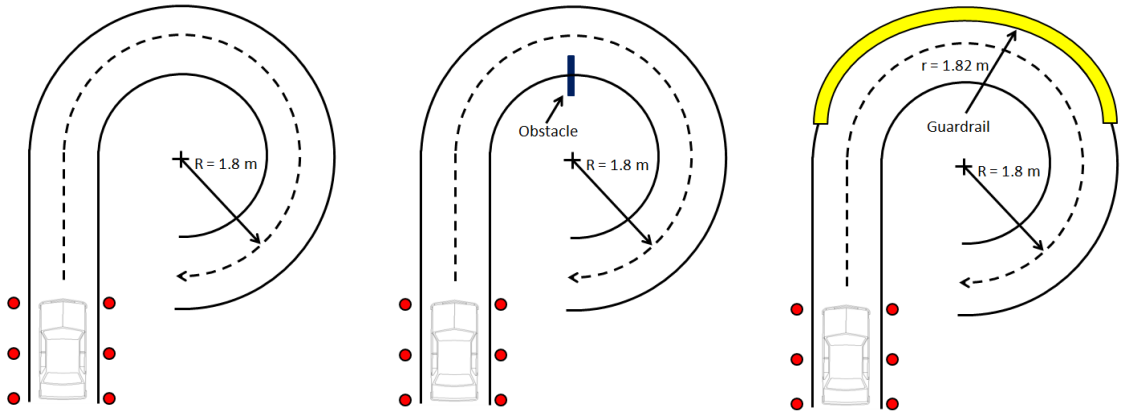

a) 1st experiment b) 2nd experiment c) 3rd experiment

Figure 12-26 The scaled vehicle path.

To evaluate the rollover index, the scaled vehicle speed and steering inputs are programmed in the microcontroller. So, the identical experiment can be repeated many times. For the first experiment, we set the vehicle to follow the path as shown in Figure 12-26a at a speed of approximately 2.4 meter per second.

In this case, the wheels of the scaled vehicle come close to lifting off from the ground.

For the second experiment, we put an obstacle on the route of the vehicle as shown in Figure 12-26b. The size of the obstacle is 2.54 centimeters in height and 2.54 centimeters in width. Then, we set the vehicle to follow the path at a speed of approximately 2.4 meter per second. In this case, the right wheels of the scaled vehicle fully lift off.

For the third experiment, we want to evaluate the developed rollover index in the case that the vehicle is confronted with unknown lateral forces. We set a guardrail on the route of the vehicle as shown in Figure 12-26c. The size of the guardrail is 3.9 centimeters in height and 1.82 meters in radius. Then, we set the vehicle to follow the path at a speed of approximately 2.4 meter per second. However, it is difficult to experimentally have only unknown lateral forces applied to the vehicle. When the vehicle strikes the guardrail, the front left wheel of the vehicle confronts with both unknown lateral forces and unknown vertical forces. Therefore, in this experiment, when the vehicle strikes the guardrail, the vehicle firstly leans toward the inside of the curve because of the vertical forces. After

that, the vehicle leans back toward the outside of the curve and fully rolls over because of the lateral forces and lateral acceleration.

12.8.4.Experimental Results

The signals required for computing the new rollover index are the lateral acceleration, the left and right vertical accelerations of sprung mass and unsprung masses, and roll angle. Since the mass of unsprung masses of the scaled vehicle is very small, it is reasonable to neglect the left and right vertical accelerations of unsprung masses. Also, the road input is a bump. The roll angle can be assumed to be small for the scaled vehicle. (With the linear potentiometer, we can approximate roll angle of the scaled vehicle. When the scaled vehicle rolls over, the roll angle seems to be less than 0.1 rad.) Then, the simplified rollover indices we examine are shown in equations (12.61) and (12.62).

$$R_4 = \frac{2m_s a_y h_R}{mgl_w} \tag{12.61}$$

$$R_5 = \frac{-\frac{2}{l_s^2}(I_{xx} + m_s h_R^2)(a_{zl} - a_{zr}) + \frac{2}{l_s} m_s a_y h_R}{mg} \tag{12.62}$$

The results of the experiments are shown in Figure 12-27-Figure 12-30. The longitudinal and lateral accelerations in all experiments are similar and of the same order because of the same setting in all experiments. For the first and second experiments, the left vertical accelerations are close to zero. However, the right vertical acceleration from the second experiment is larger than that from the first experiment.

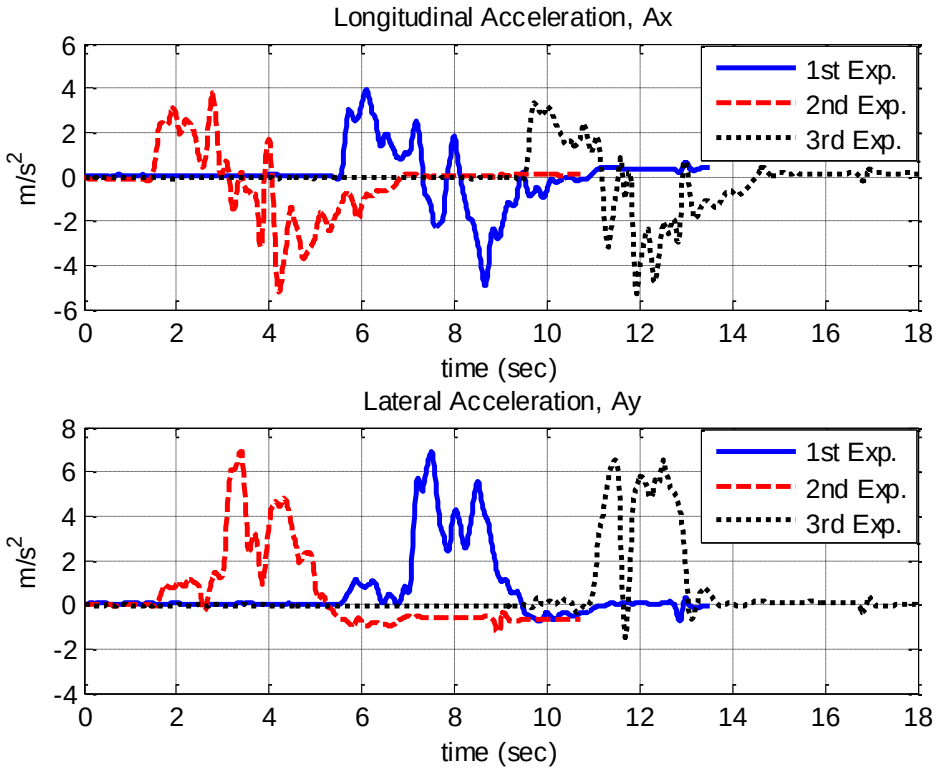

Figure 12-27 Longitudinal and lateral acceleration of the scaled vehicle.

The left and right vertical accelerations of the third experiment are shown in Figure 12-28. When the vehicle strikes the guardrail during the time, $t \approx 11.4 - 11.7$ seconds, the vertical forces apply to the left side of the vehicle. This makes the left vertical acceleration larger than the right vertical acceleration. During the time, $t \approx 11.7 - 12$ seconds, the left vertical acceleration decreases and the right acceleration increases since the vehicle leans back toward the outside of the curve and fully rolls over after the time, $t > 12$ seconds. It should be noted that roll angle during the time, $t \approx 12 - 13$ seconds, is very large. So the measurements during this period may not be accurate.

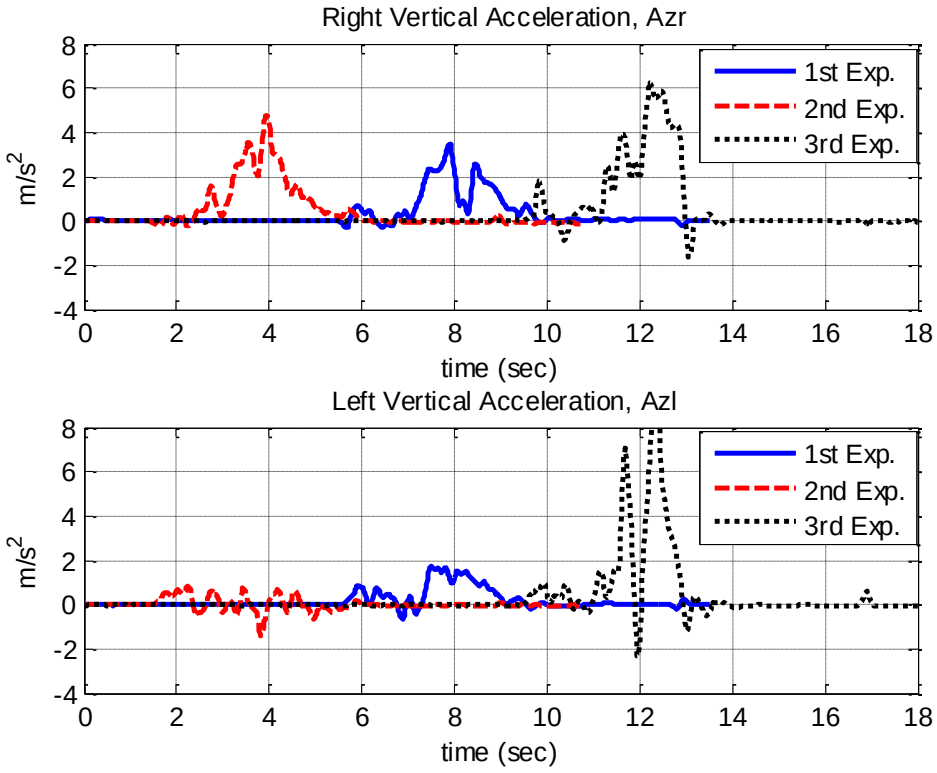

Figure 12-28 Right and left vertical acceleration of the scaled vehicle.

The first row of Figure 12-29 shows the rollover indices from the first experiment. In this experiment, the external input is not applied to the vehicle. So, the difference of vertical accelerations is small. Then, the rollover indices from the equations (12.61) and (12.62) are almost the same. Both rollover indices show that the wheels of the vehicle are close to lift off.

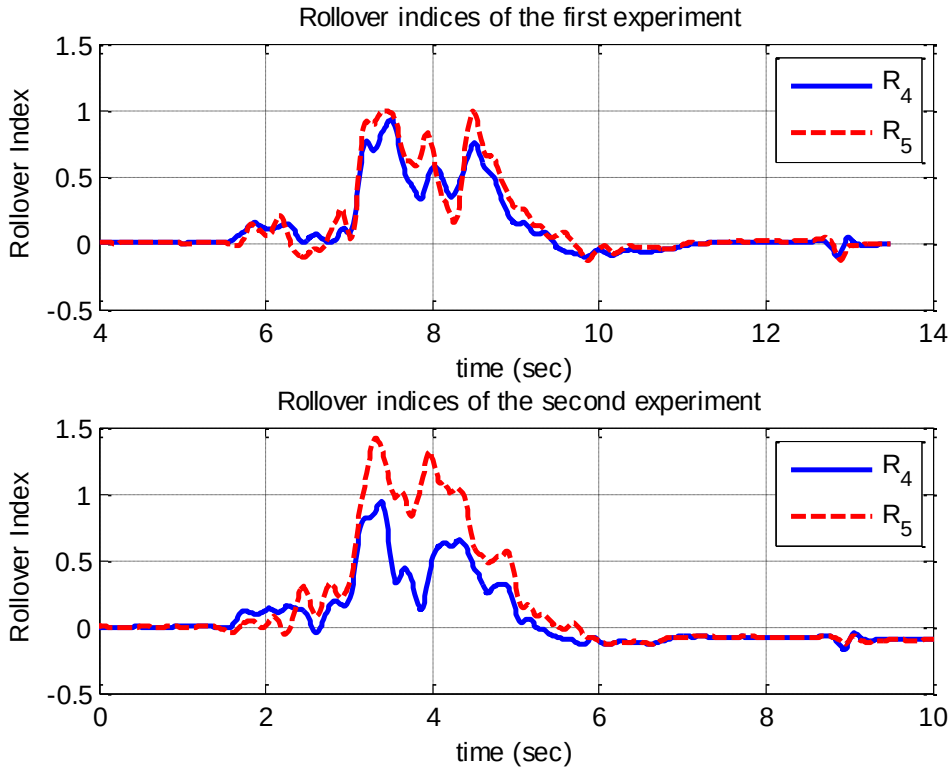

Figure 12-29 Comparison of rollover indices of the scaled vehicle.

Likewise, the second row of Figure 12-29 shows the rollover indices from the second experiment. The scaled vehicle strike the obstacle and its right wheels lift off in this case. Thus, there is a difference of vertical accelerations. The traditional rollover index R_4 in equation (12.61) shows that the wheels of the vehicle come close to lift off. That fails to detect the wheel lift off condition. However, the new rollover index R_5 of equation (12.62) shows that the wheels of the vehicle do lift off. Therefore, the develop rollover index is able to detect both tripped and un-tripped rollovers.

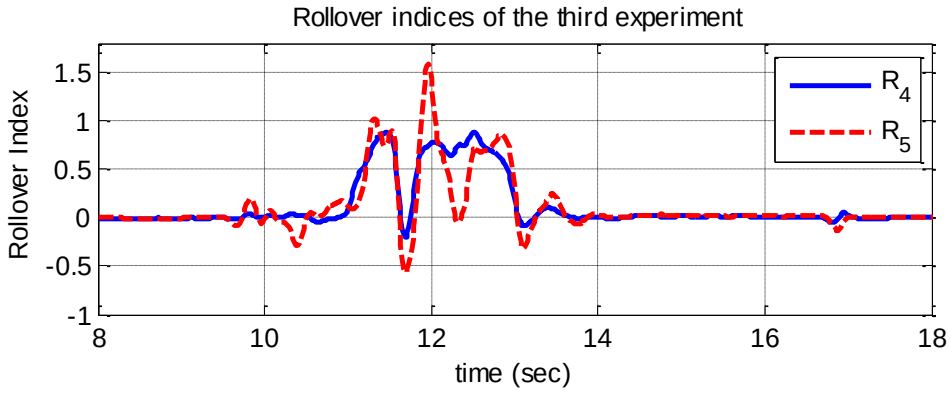

Figure 12-30 Comparison of rollover indices of the third experiment.

Figure 12-30 shows the rollover indices from the third experiment. In this case, the vehicle leans toward the inside of the curve. Then the vehicle leans back toward the outside of the curve and fully rolls over. The results show that the traditional rollover index R_4 fails to detect the wheel lift off condition. However, the new rollover index R_5 shows that the wheels of the vehicle do lift off. Therefore, the new rollover index can also handle unknown external lateral force inputs with the same algorithm.

12.9. Conclusions

Rollover index is an important real-time variable that is used to predict un-tripped and tripped rollovers. This dissertation develops a methodology for estimation of unknown inputs in a class of nonlinear systems. The approach utilized is to use the mean value theorem to express the nonlinear error dynamics as a convex combination of known matrices with time varying coefficients. The observer gains are then obtained by solving linear matrix inequalities (LMIs). The developed approach can enable observer design for a large class of differentiable nonlinear systems with a globally (or locally) bounded Jacobian. The developed nonlinear observer can be applied for rollover index estimation. The approach is evaluated through simulation with software CARSIM and with experimental tests on a $1/8^{th}$ scaled vehicle. In order to show that the scaled vehicle experiments can represent a full-sized vehicle, the Buckingham π theorem is used to show dynamic similarity. The simulation and experimental results show that the developed nonlinear observer can reliably estimate vehicle variables, unknown normal

tire forces, and rollover index for predicting un-tripped and tripped rollovers. This is the first ever publication on a rollover index that can handle tripped rollovers.

Chapter 13

13. THESIS SUMMARY

The increasing worldwide use of automobiles has brought about a dramatic increase in numbers of accidents. The high number of accidents and their root cause in human error has motivated the need to develop driver assistance systems. A variety of active safety control systems such as traction control, electronic stability control (ESC), rollover prevention, lane departure avoidance systems, collision avoidance systems, and adaptive cruise control (ACC) are being developed to reduce driver burden, partially automate normal driving operations, and reduce accidents.

The effectiveness of these driver assistance systems can be significant enhanced if the real-time values of several vehicle parameters and state variables, namely tire-road friction coefficient, slip angle, roll angle, and rollover index can be known. Since there are no inexpensive sensors available to measure these variables, it is necessary to estimate them. However, due to the significant nonlinear dynamics in a vehicle, due to unknown and changing plant parameters, and due to the presence of unknown input disturbances, the design of estimation algorithms for this application is challenging.

This dissertation develops a variety of nonlinear observers to deal with nonlinear systems. The developed nonlinear observer design techniques are a nonlinear observer for Lipschitz nonlinear systems, nonlinear observer using a bounded Jacobian approach, nonlinear observer for systems with a nonlinear function in the measurement equation, and nonlinear observer and unknown input estimation for bounded Jacobian nonlinear systems with unknown disturbance inputs. A number of illustrative examples are presented to show that the developed bounded Jacobian approach is less conservative and more useful than the standard Lipschitz assumption based nonlinear observer. The developed nonlinear observers are utilized for estimation of longitudinal vehicle velocity, vehicle slip angle, vehicle roll angle, and vehicle rollover index.

The developed nonlinear observer using a bounded Jacobian approach is a new approach to observer design for nonlinear systems in which the nonlinearity has a globally (or locally) bounded Jacobian. The developed approach presents a modified version of the mean value theorem and utilizes it to express the nonlinearity in the estimation error dynamics as a convex combination of known matrices with time varying coefficients. The observer gains are then obtained by solving linear matrix inequalities (LMIs). The developed approach can enable observer design for a large class of differentiable nonlinear systems with a globally (or locally) bounded Jacobian. This observer is utilized for longitudinal vehicle velocity, and vehicle roll angle estimation.

The nonlinear observer with a nonlinear function in the measurement equation is an extended result of the previous bounded Jacobian nonlinear observer. This observer is utilized for vehicle slip angle estimation.

The nonlinear observer and unknown input estimation algorithm for nonlinear systems with unknown disturbance inputs can be applied for an unknown inputs nonlinear system with a nonlinear measurement equation. The approach utilized is to express the unknown inputs as a function of the measurements and states and to use the mean value theorem to express the nonlinear error dynamics as a convex combination of known matrices with time varying coefficients.

In order to predict and prevent vehicle rollovers in tripped and un-tripped situations, an algorithm to estimate rollover index for tripped and un-tripped rollovers is developed. The algorithm utilizes the developed theory for unknown input estimation in bounded Jacobian nonlinear systems. The algorithm is used to estimate vertical tire forces and predict tripped rollovers in situations involving road bumps, potholes, and lateral unknown force inputs. This estimation algorithm provides accurate estimation of the rollover index, roll angle, and state variables of the vehicle.

To estimate the tire-road friction coefficients at each individual tire of the vehicle, algorithms to estimate longitudinal forces and slip ratios at each tire are proposed. Subsequently, tire-road friction coefficients are obtained using recursive least squares

parameter estimators that exploit the relationship between longitudinal force and slip ratio at each tire.

Three different algorithms are proposed for estimation of longitudinal tire force and slip ratio based on the types of sensors available – one that utilizes engine torque, brake torque and GPS measurements, one that utilizes torque measurements and an accelerometer and one that utilizes GPS measurements and an accelerometer. While GPS measurements are subject to long-time drop outs in urban environments, brake torque and engine torque signals may not be available on all cars. Thus, each of the three friction coefficient estimation algorithms has different application domains.

The developed approaches are evaluated through simulations with industry standard software, CARSIM, and with experimental tests on a Volvo XC90 sport utility vehicle and on a $1/8^{th}$ scaled vehicle.

The simulation and experimental results show that the developed approaches can reliably estimate the vehicle parameters and variables needed for effective ESC and rollover prevention applications.

Bibliography

[1] NHTSA, "Federal Motor Vehicle Safety Standards; Electronic Stability Control Systems," DEPARTMENT OF TRANSPORTATION, National Highway Traffic Safety Administration, NHTSA–200727662, 2007.

[2] M. Peden et al., *World Report on Road Traffic Injury Prevention*.: World Health Organization, Nonserial Publication, 2004.

[3] R. Rajamani, *Vehicle Dynamics and Control*. New York: Springer Verlag, 2005.

[4] A.T. van Zanten, "Bosch ESP Systems: 5 Years of experience," in *Proc. SAE Automotive Dynamics and Stability Conf., SAE 2000-01-1633*, Troy, MI, May 2000.

[5] H. E. Tseng, D. Madau, B. Ashrafi, T. Brown, and D. Recker, "Technical Challenges in the Development of Vehicle Stability Control System," *Proc. of the 1999 IEEE Int. Conf. on Control Applications*, vol. 2, pp. 1660-1666, August 1999.

[6] D. Piyabongkarn, R. Rajamani, Jae Y. Lew, and Hai Yu, "On the Use of Torque-Biasing Devices for Vehicle Stability Control," in *Proc. of the 2006 American Control Conference*, Minneapolis, MN, June 2006, pp. 5360 -5365.

[7] M. Eslamian, G. Alizadeh, and M. Mirzaei, "Optimization-based Non-linear Yaw Moment Control Law for Stabilizing Vehicle Lateral Dynamics," *Proceedings of the Institution of Mechanical Engineers, Part D: Journal of Automobile Engineering*, vol. 221, no. 12, pp. 1513-1523, December 2007.

[8] National Highway Traffic Safety Administration (NHTSA), "Types of Rollovers," National Highway Traffic Safety Administration, Available: http://www.safercar.gov 06/01/2011.

[9] A. Hac, T. Brown, and J. Martens, "Detection of Vehicle Rollover," *SAE*

International, no. 0-7680-1319-4, 2004.

[10] R. Rajamani, D. Piyabongkarn, J.Y. Lew, K. Yi, and G. Phanomchoeng, "Algorithms for Real-Time Estimation of Individual Wheel Tire-Road Friction Coefficients," *IEEE/ASME Transactions on Mehatronics*, 2011.

[11] H.B. Pacejka and E. Bakker, "The Magic Formula Tyre Model," *Vehicle System Dynamics v21. Supplement, Tyre Models for Vehicle Dynamics Analysis*, vol. 21, no. S1, pp. 1-18, 1993.

[12] H. Dugoff, P.S. Fancher, and L. Segal, "Tire Performance Characteristics Affecting Vehicle Response to Steering and Braking Control Inputs," Office of Vehicle System Research, US National Bureau of Standards, Final Report, Contract CST-460 1969.

[13] H.E. Tseng, B. Ashrafi, D. Madau, T.A. Brown, and D. Recker, "The Development of Vehicle Stability Control at Ford," *IEEE/ASME Transactions on Mechatronics*, vol. 4, no. 3, pp. 223-234, 1999.

[14] A.T. Van Zanten et al., "Control Aspects of the Bosch-VDC," *Proceedings of the Int. Symposium on Advanced Vehicle Control*, vol. 1, pp. 573-608, 1996.

[15] Desmond N. Penny, "Rollover of Sport Utility Vehicles," *THE PHYSICS TEACHER*, vol. 42, February 2004.

[16] B.C. Chen and H. Peng, "Rollover Warning for Articulated Heavy Vehicles Based on a Time-to-Rollover Metric," in *Proceedings of the 1999 ASME International Congress and Exposition*, Knoxville, TN, November, 1999.

[17] J. Yoon, D. Kim, and K. Yi, "Design of a Rollover Index-Based Vehicle Stability Control Scheme," *Vehicle System Dynamics*, vol. 45, no. 5, pp. 459-479, May 2007.

[18] K. Yi, J. Yoon, and D. Kim, "Model-based Estimation of Vehicle Roll State for Detection of Impending Vehicle Rollover," in *Proceedings of the 2007 American Control Conference*, New York City, USA, July, 2007.

[19] Yang Hanlong and Liu Louis Yizhang, "A Robust Active Suspension Controller with Rollover Prevention," *Society of Automotive Engineers*, vol. 112, no. 6, pp. 992-997, 2003.

[20] D. Odenthal, T. Bunte, and J. Ackermann, "Nonlinear Steering and Braking Control for Vehcile Rollover Avoidance," DLR, German Aerospace Center, Institute of Robotics ans System Dynamics, Oberpfaenhofen, D-82230 Wessling, Germany,.

[21] S. Solmaz, M.J. Corless, and R. Shorten, "A Methodology for the Design of Robust Rollover Prevention Controllers for Automotive Vehicles: Part 1 - Differential Braking," in *45th IEEE Conference on Decision and Control*, San Diego, CA, 2006, pp. 1739-1744.

[22] G. Phanomchoeng and R. Rajamani, "The Bounded Jacobian Approach to Nonlinear Observer Design," in *Proc. ot the 2010 American Control Conference*, Baltimore, MD, 2010.

[23] J. Wang, L. Alexander, and R. Rajamani, "Friction Estimation on Highway Vehicles Using Longitudinal Measurements," *ASME Journal of Dynamic Systems, Measurement and Control, Special Issue on Sensors*, vol. 126, no. 2, pp. 265-275, June 2004.

[24] S. Boyd, L.E. Ghaoui, E. Feron, and V. Balakrishnan, "Linear Matrix Inequalities in Systems and Control Theory," *Society for Industrial and Applied Mathematics, SIAM Studies in Applied Mathematics*, 1994.

[25] M. Spong, "Modeling and Control of Elastic Joint Robots," *ASME Journal of*

Dynamic Systems, Measurement and Control, vol. 109, pp. 310-319, 1987.

[26] P.K. Sahoo and T. Riedel, *Mean Value Theorems and Functional Equations*, 1st ed.: World Scientific Publishing Company, 1999.

[27] K. Eriksson, D. Estep, and C. Johnson, *Applied Mathematics: Body and Soul*, 1st ed.: Springer Berlin Heidelberg, 2010.

[28] A. Zemouche, M. Boutayeb, and G.I. Bara, "Observer Design for Nonlinear Systems: An Approach Based on the Differential Mean Value Theorem," in *Proceedings of the 44th IEEE Conference on Decision and Control, and the European Control Conference 2005*, Seville, Spain, 2005, pp. 12-15.

[29] K. Vijayaraghaven, R. Rajamani, and and J. Bokor, "Quantitative fault estimation for a class of non-linear systems," *International Journal of Control*, vol. 80, no. 1, pp. 64-67, January 2007.

[30] K. Vijayaraghaven, R. Rajamani, and and J. Bokor, "Quantitative Fault Estimation for a Class of Non-linear Systems," *International Journal of Control*, vol. 80, no. 1, pp. 64-67, January 2007.

[31] R. Rajamani, D. Piyabongkarn, J.Y. Lew, K. Yi, and G. Phanomchoeng, "Tire Road Friction Coefficient Estimation – Real-Time Estimation Methods for Active Automotive Safety Applications," *IEEE Control Systems Magazine*, vol. 30, no. 4, pp. 54-69, August 2010.

[32] P. Misra and P. Enge, *Global Positioning System, Signals, Measurements and Performance*. Lincoln, MA: Ganga-Jamuna Press, 2004.

[33] R. Daily and D. M. Bevly, "The Use of GPS for Vehicle Stability Control Systems," *IEEE TRANSACTIONS ON INDUSTRIAL ELECTRONICS*, vol. 51, no. 2, pp. 270-277, April 2004.

[34] J. Ryu and J. C. Gerdes, "Integrating Inertial Sensors with GPS for Vehicle Dynamics Control," *Journal of Dynamic Systems, Measurement, and Control*, vol. 126, no. 2, pp. 243–254, June 2004.

[35] "RT3000 Inertial and Measurement System User Manual," Oxford Technical Solutions, 2004.

[36] "Corrsys-Datron Optical Sensors," Available: http://www.corrsys-datron.com/optical_sensors.htm 06/01/11.

[37] J. Farrelly and P. Wellstead, "Estimation of Vehicle Lateral Velocity," in *Proceedings of the 1996 IEEE International Conference on Control Applications*, Dearborn, MI, USA, Sep. 1996, pp. 552–557.

[38] A. Hac and M. D. Simpson, "Estimation of Vehicle Side Slip Angle and Yaw Rate," *Proc. SAE*, vol. 2000-10-0696, p. 1, 2000.

[39] M. Hiemer, A. V. Vietinghoff, U. Kiencke, and T. Matsunaga, "Determination of the Vehicle Body Side Slip Angle with Non-linear Observer Strategies," *Proc. SAE*, vol. 2005-01-0400, no. 1, 2005.

[40] C. Liu and H. Peng, "A State and Parameter Identification Scheme for Linearly Parameterized Systems," *ASME Journal of Dynamic Systems, Measurement and Control*, vol. 120, no. 4, pp. 524–528, December 1998.

[41] A. Nishio, K. Tozu, H. Yamaguchi, K. Asano, and Y. Amano, "Development of Vehicle Stability Control System Based on Vehicle Side Slip Angle Estimation," *Proc. SAE*, vol. 2001-01-0137, p. 1, 2001.

[42] A. Y. Ungoren, H. Peng, and H. E. Tseng, "A Study on Lateral Speed Estimation Methods," *Int. J. Vehicle Autonomous Systems*, vol. 2, no. 1/2, pp. 126–144, 2004.

[43] J. Zuurbier and P. Bremmer, "State Estimation for Integrated Vehicle Dynamics

Control," in *Proc. AVEC 6th Int. Symp. Adv. Vehicle Control*, Hiroshima, Japan, 2002, pp. 379–384.

[44] J. S. Baras, A. Bensoussan, and M. R. James, "Dynamic Observers as Asymptotic Limits of Recursive Filters: Special Cases," *SIAM Jounal on Applied Mathematics*, vol. 48, no. 5, pp. 1147-1158, 1988.

[45] Y. Song and J. W. Grizzle, "The Extended Kalman Filter as a Local Asymptotic Observer for Nonlinear Discrete-time Systems," *Journal of Mathematical Systems, Estimation, and Control*, vol. 5, no. 1, pp. 59-78, 1995.

[46] P.J. Liu, S. Rakheja, and A.K.W. Ahmed, "Detection of Dynamic Roll Instability of Heavy Vehicles for Open-Loop Rollover Control," *Society of Automotive Engineers, Inc*, pp. 105-112, November 1997.

[47] D. Piyabongkarn, R. Rajamani, J. Grogg, and J. Lew, "Development and Experimental Evaluation of a Slip Angle Estimator for Vehicle Stability Control," *IEEE Transactions on Control Systems Technology*, vol. 17, no. 1, pp. 78-88, January 2009.

[48] National Highway Traffic Safety Administration (NHTSA), "Types of Rollovers," National Highway Traffic Safety Administration, Available: http://www.safercar.gov 03/01/2011.

[49] J. Lu, D. Messih, and A. Salib, "Roll Rate Based Stability Control-The Roll Stability Control System," in *Proceedings of the 20th Enhanced Safety of Vehicles Conference*, 2007.

[50] C. Geng, L. Mostefai, M. Denaï, and Y. Hori, "Direct Yaw-Moment Control of an In-Wheel-Motored Electric Vehicle Based on Body Slip Angle Fuzzy Observer," *IEEE Transactions on Industrial Electronics*, vol. 56, no. 5, pp. 1411-1419, May 2009.

[51] C.R. Carlson and and J.C. Gerdes, "Optimal Rollover Prevention with Steer by Wire and Differential Braking," *ASME International Mechanical Engineering Congress and Exposition*, pp. 345-355, November 2003.

[52] S. Takano and M. Nagai, "Dynamic Control of Large Vehicles for Rollover Prevention," *IEEE IVEC*, pp. 85-89, 2001.

[53] M. Akar and J.C. Kalkkuhl, "Design and Evaluation of an Integrated Chassis Controller for Automated Vehicle Emulation," *IEEE Transactions on industrial Electronics*, vol. 56, no. 9, pp. 3571-3579, September 2009.

[54] Marie C. Walz, "Trends in the Static Stability Factor of Passenger Cars, Light Trucks, and Vans," National Highway Traffic Safety Administration, Washington, DC 20590, NHTSA Technical Report DOT HS 809 868, June 2005.

[55] S.N. Brennan, "Modeling and Control Issues Associated with Scaled Vehicles," University of Illinois at Urbana-Champaign, Thesis 1999.

[56] S. Brennan and A. Alleyne, "A Scaled Testbed for Vehicle Control: The IRS," in *Proceedings of the 1999 IEEE*, Kohala Coast-lsland of Hawaii, Hawaii, USA, 1999, pp. 327 - 332.

[57] R.T. O'Brien, J.A. Piepmeier, P.C. Hoblet, S.R. Burns, and C.E. George, "Scale-Model Vehicle Analysis Using an Off-the-Shelf Scale-Model Testing Apparatus," in *Proceeding of the 2004 American Control Conference*, Boston, Massachusetts, 2004, pp. 3387 - 3392.

[58] S. Brennan and A. Alleyne, "Using a Scale Testbed: Controller Design and Evaluation," *IEEE Control Systems Magazine*, vol. 21, no. 3, pp. 15-26, June 2001.

[59] R. Verma, D. D. Vecchio, and H.K. Fathy, "Development of a Scaled Vehicle With Longitudinal Dynamics of an HMMWV for an ITS Testbed," *IEEE/ASME*

TRANSACTIONS ON MECHATRONICS, vol. 13, no. 1, February 2008.

[60] S.J. Hallowell and L.R. Ray, "All-Wheel Driving Using Independent Torque Control of Each Wheel," in *Proceedings of the American Control Conference*, vol. 3, Denver, Colorado, 2003, pp. 2590-2595.

[61] W.E. Travis, R.J. Whitehead, D.M. Bevly, and G.T. Flowers, "Using Scaled Vehicles to Investigate the Influence of Various Properties on Rollover Propensity," in *Proceeding of the 2004 American Control Conference*, Boston, Massachusetts , 2004.

[62] A. Al-Sharif, "Design and Development of a Scaled Test Laboratory for the Study of ABS and other Active Vehicle Systems," The University of Texas at Austin, Thesis 2001.

[63] R. Whitehead et al., "Scaled Vehicle Electronic Stability," ESV International Collegiate Student Safety Technology Design Competition, North American Regional Review 2005.

[64] M. Polley and A.G. Alleyne, "Dimensionless Analysis of Tire Characteristics for Vehicle Dynamics Studies," in *Proceeding of the 2004 American Control Conference*, Boston, Massachusetts, 2004, pp. 3411 - 3416.

[65] F.M.White, *Fluid Mechanics*, 5th ed.: McGraw Hill International, 2003.

[66] R. Rajamani, D. Piyabongkarn, V. Tsourapas, and and J.Y. Lew, "Real-Time Estimation of Roll Angle and CG Hight for Active Rollover Preventioin Applications," in *American Control Conference*, St. Louis, MO, USA, 2009.

[67] J.Y. Lew, D. Piyabongkarn, and and J.A. Grogg, "Minimizing Dynamic Rollover Propensity with Electronic Limited Slip Differentials," *SAE Transactions Journal of Passenger Cars: Mechanical Systems*, vol. 115-6, pp. 1183-1190, 2006.

[68] A. Zemouche, M. Boutayeb, and G.I. Bara, "On Observers Design for Nonlinear Time-Delay Systems," in *Proceeding of the 2006 American Control Conference Minneapolis*, Minnesota, USA, June, 2006.

[69] J.J.E. Slotine and W. Li, *Applied Nonlinear Control*. New Jersey: Prentice-Hall, 1991.

[70] R. Rajamani and Y. Cho, "Observer Design for Nonlinear Systems: Stability and Convergence," *Decision and Control, Proceedings of the 34th IEEE Conference*, vol. 1, pp. 93-94, December 1995.

[71] J. Yoon and K. Yi, "A Rollover Mitigation Control Scheme Based on Rollover Index," in *Proceedings of the 2006 American Control Conference*, Minneapolis, MN, USA, 2006.

[72] C.S. Parenteau et al., "Field Relevance of a Suite of Rollover Tests to Real-World Crashes and Injuries," *Accident Analysis and Prevention*, vol. 35, no. 1, pp. 103-110 , January 2003.

[73] A.J. Krener and A. Isidori, "Linearization by Output Injection and Nonlinear Observers," *Systems & Control Letters*, vol. 3, no. 1, pp. 47-52, June 1983.

[74] A.J. Krener and W. Respondek, "Nonlinear Observers with Linearizable Error Dynamics," *SIAM Journal of Control and Optimization*, vol. 23, pp. 197-216, 1985.

[75] M. Arcak and P. Kokotovic, "Nonlinear Observers: A Circle Criterion Design," in *In Proceedings of the 38th IEEE Conference on Decision and Control*, Phoenix, AZ, 1999, pp. 4872-4876.

[76] M. Arcak and P. Kokotovic, "Observer-based Control of Systems with Slope-restricted Nonlinearities," *IEEE Transactions on Automatic Control*, vol. 46, no. 7, pp. 1146-1151, 2001.

[77] F.E. Thau, "Observing the State of Nonlinear Dynamic Systems," *International Journal of Control*, vol. 17, no. 3, pp. 471 - 479, 1973.

[78] C. Edwards and S.K. Spurgeon, "On the Development of Discontinuous Observers," *International Journal of Control*, vol. 59, no. 5, pp. 1211-1229, 1994.

[79] F. Esfandiari, "Output Feedback Stabilization of Full Linearizable Systems," *International Journal of Control*, vol. 56, no. 5, pp. 1007-1037, 1992.

[80] B. Breuer, U. Eichhorn, and J. Roth, "Measurement of Tyre/Road Friction Ahead of the Car and Inside the Tyre," in *Proceedings of AVEC'92*, 1992, pp. 347–353.

[81] David M. Bevly, J. Christian Gerdes, and Christopher Wilson, "The Use of GPS Based Velocity Measurements for Measurement of Sideslip and Wheel Slip," *Vehicle System Dynamics: International Journal of Vehicle Mechanics and Mobility*, vol. 38, no. 2, pp. 127-147, 2003.

[82] U. Eichhorn and J. Roth, "Prediction and Monitoring of Tyre/Road Friction," in *Proceedings of FISITA*, London, 1992, pp. 67-74.

[83] F. Gustaffson, "Slip-Based Tire-Road Friction Estimation," *Automatica*, vol. 33, no. 6, pp. 1087-1099, June 1997.

[84] J.O. Hahn, R. Rajamani, and L. Alexander, "GPS-Based Real-Time Identification of Tire-Road Friction Coefficient," *IEEE Transactions on Control Systems Technology*, vol. 10, no. 3, May 2002.

[85] W. Hwang and B.S. Song, "Road Condition Monitoring System Using Tire-road Friction Estimation," in *Proceedings of AVEC 2000*, Ann Arbor, Michigan, 2000, pp. 437-442.

[86] S. Müller, M. Uchanski, and Karl Hedrick, "Estimation of the Maximum Tire-Road Friction Coefficient," *ASME Journal of Dynamic Systems*, vol. 125, no. 4, pp. 607-

617, December 2003.

[87] L.R. Ray, "Nonlinear Tire Force Estimation and Road Friction Identification: Simulation and Experiments," *Automatica*, vol. 33, no. 10, pp. 1819-1833, 1997.

[88] K. Yi, J.K. Hedrick, and S.C. Lee, "Estimation of Tire-Road Friction Using Observer Based Identifiers," *Vehicle System Dynamics*, vol. 31, no. 4, pp. 233-261, 1999.

[89] S. Sastry and M. Bodson, *Adaptive Control: Stability, Convergence and Robustness*. Englewood Cliffs, NJ: Prentice-Hall, 1989.

[90] D. Lhomme-Desages, C. Grand, J.-C. Guinot, and F. Ben Amar, "Doppler Based Ground Speed Sensor Fusion and Slip Control for a Wheeled Rover," *IEEE/ASME Transactions on Mechatronics*, vol. 14, no. 4, pp. 484 - 492, Aug 2009.

[91] A.S. Conceicao, A.P. Moreira, and P.J. Costa, "Practical Approavh of Modeling and Parameter Estimation for Omnidorectional Mobile Robots," *IEEE/ASME Transactions on Mechatronics*, vol. 14, no. 3, pp. 377-381, June 2009.

[92] Dongbin Zhao, Xuyue Deng, and Jianqiang Yi, "Motion and Internal Force Control for Omnidirectional Wheeled Mobile Robots," *IEEE/ASME Transactions on Mechatronics*, vol. 14, no. 3, pp. 382-387, June 2009.

[93] "Experimental Determination of Tire Forces and Road Friction," in *Proceedings of the American Control Conference*, June 1998, pp. 1843-1847.

[94] C. Edwards, S.K. Spurgeon, and R.J. Patton, "Sliding Mode Observers for Fault Detection and Isolation," *Automatica*, vol. 36, no. 4, pp. 541-553, 2000.

[95] H.K. Khalil, *Nonlinear Systems*, 3rd ed. New Jersey: Prentice Hall, 2001.

[96] R. Rajamani, "Observers for Lipschitz Nonlinear Systems," *IEEE Transactions on*

Automatic Control, vol. 43, no. 3, pp. 397-401, March 1998.

[97] R. Perla and S. Mukhopadhyay, "Observer Design for Lipschitz Nonlinear Systems with State Dependency and Nonlinearity Distribution," *INDICON, 2005 Annual IEEE*, pp. 437-441, December 2005.

[98] S. Raghavan, "Observers and Compensators for Nonlinear Systems with Application to Flexible-Joint Robots," Ph.D. Dissertation, University of California at Berkeley, Berkeley, CA 94720, U.S.A, 1992.

[99] X. Xiao-Hua and W. Gao, "Nonlinear Observer Design by Observer Error Linearization," *SIAM Journal of Control and Optimization*, vol. 27, no. 1, pp. 199-216, 1989.

[100] K. Reif and R. Unbehauen, "Linearization Along Trajectories and the Extended Kalman Filter," *Proc. 13th IFAC World Congr.*, vol. H, pp. 509–514, 1996.

[101] M. V. Korobkov, "A Generalization of The Mean Value Theorem to The Case of Vector-Valued Mappings," *Siberian Mathematical Journal*, vol. 42, no. 2, pp. 297-300, 2001.

[102] P. R. Pagilla and Y.Zhu, "Controller and Observer Design for Lipschitz Nonlinear Systems," in *Proceeding of the 2004 American Control Conference*, Boston. Massachusetts, 2004.

[103] J. Ryu and J. C. Gerdes, "Integrating Inertial Sensors With Global Positioning System (GPS) for Vehicle Dynamics Control," *Journal of Dynamic Systems, Measurement, and Control*, vol. 126, no. 2, pp. 243–254, June 2004.

[104] E.K. Liebemann, K. Meder, J. Schuh, and G. Nenninger, "Safety and Performance Enhancement: The Bosch Electronic Stability Control (ESP)," in *SAE Convergence 2004 Conference*, Detroit, MI, Oct. 2004.

[105] B. Chen and H. Peng, "Differential Braking Based Rollover Prevention for Sport Utility Vehicles with Human-in-the-loop Evaluations," *Vehicle System Dyanmics*, vol. 36, no. 4-5, pp. 359-389, 2001.

[106] G.J. Forkenbrock, W.R. Garrott, M. Heitz, and B.C. O'Harra, "Experimental Examination of J-Turn and Fishhook Maneuver that may Induce On-Road Untripped Light Vehicle Rollover," *SAE Paper No. 2003-01-1008*, 2003.

[107] G. Phanomchoeng, R. Rajamani, and and D. Piyabongkarn, "Nonlinear Observer for Bounded Jacobian Systems, with Applications to Automotive Slip Angle Estimation," *IEEE Transactions on Automatic Control*, vol. 56, no. 5, pp. 1163-1170, May 2011.